AERODYNAMIC PERFORMANCE EVALUATION OF A NOVEL SAVONIUS-STYLE WIND TURBINE THROUGH UNSTEADY SIMULATIONS AND WIND TUNNEL EXPERIMENTS

A Thesis
Submitted in Partial Fulfillment of the Requirements for
the Award of the Degree of

DOCTOR OF PHILOSOPHY

By

SUKANTA ROY

DEPARTMENT OF MECHANICAL ENGINEERING
INDIAN INSTITUTE OF TECHNOLOGY GUWAHATI
GUWAHATI - 781039, INDIA

July, 2014

To…

My family members

Declaration

I hereby certify that the work compiled in this dissertation entitled '**Aerodynamic Performance Evaluation of a Novel Savonius-Style Wind Turbine through Unsteady Simulations and Wind Tunnel Experiments**' is the outcome of my research work under the guidance of Professor Ujjwal K. Saha in the Department of Mechanical Engineering, Indian Institute of Technology Guwahati, India.

Any part of this work has not earlier been submitted for the award of any degree, diploma, associate-ship, fellowship or its equivalent to any University or Institution.

Date:

(Sukanta Roy)
Registration No. 10610307
Department of Mechanical Engineering
Indian Institute of Technology Guwahati

Department of Mechanical Engineering,
Indian Institute of Technology Guwahati,
Guwahati-781039, India

Certificate

It is certified that the work contained in the thesis entitled '**Aerodynamic Performance Evaluation of a Novel Savonius-Style Wind Turbine through Unsteady Simulations and Wind Tunnel Experiments**' submitted by **Mr. Sukanta Roy** to the Indian Institute of Technology Guwahati for the award of the degree of Doctor of Philosophy has been carried out under my supervision in the Department of Mechanical Engineering, Indian Institute of Technology Guwahati. This work has not been submitted elsewhere for the award of any other degree or diploma.

Date:

(Ujjwal K. Saha)
Professor
Department of Mechanical Engineering
Indian Institute of Technology Guwahati
Guwahati-781039, India

Acknowledgement

It is an honor for me to thank Indian Institute of Technology Guwahati for giving me such an excellent opportunity for undergoing my research. A deep sense of gratitude is extended to Prof. Ujjwal K. Saha for his continuous support, encouragement and active guidance at every stage of this endeavor. His tremendous sense of planning and organization had enabled me to overcome all the difficulties during the entire investigation.

I owe my deepest gratitude to my doctoral committee members Dr. Niranjan Sahoo, Dr. Amaresh Dalal, and Prof. Anugrah Singh for their fruitful discussion and suggestions towards my research findings. It is my pleasure to thank Prof. Anoop K. Dass, Dr. Arnab K. De, Dr. Chandramohan Somayaji, Dr. P. Muthukumar, and Dr. G. Madhusudhana for their excellent teachings during the course work. My sincere acknowledgement goes to Prof. Pinakeswar Mahanta (HOD, Mechanical Engineering Department) and Prof. Debrabrata Chakraborty (Dean, R & D) for providing all the research facilities and financial support.

I would like to thank all the faculty members, staffs, and research scholars of Mechanical Engineering Department for rendering their whole hearted cooperation and pleasurable support in the entire course of work. A word of appreciation goes to the senior technicians of Mechanical Engineering Department Mr. Dilip Chetri, Mr. Mrinal Sarma, Mr. Monoj K. Baishya, and Mr. Dhaneswar Khaklary for their assistance in the fabrication of experimental setup and turbine blades. I am also thankful to my seniors and co-workers Dr. M. Eswaran, Dr. B. K. Debnath, Mr. B. J. Bora, Mr. A. Sarkar, Mr. P. Mukherjee, Mr. K. Biswakarma, and Mr. A. Banerjee for their friendship and unforgettable moments. Special thanks go to my younger brother Mr. Sujit Roy (Assistant Project Engineer, Mechanical Engineering Department) for his immense support during my research activities.

Acknowledgement would be incomplete without giving credit to the authors of many articles/books/proceedings/reports/theses, whose works have formed the framework of the present investigation.

Last but not least, I would like to express my gratitude to my beloved parents for their continuous encouragement and blessings.

July, 2014
Guwahati, India

Sukanta Roy

Abstract

Recent instabilities in the world energy market due to depletion of fossil fuel sources, global warming threats and increasing price of fossil derivatives necessitate the need of harnessing the clean and renewable sources of energy. In this context, research in the field of wind energy is becoming particularly important. Although considerable progress has been achieved in the large-to-medium scale wind turbines, the available technical designs of small scale wind turbines are not yet satisfactory corresponding to the off-grid power generation at low wind speeds.

After going through a detailed literature review, it is perceived that the Savonius-style wind turbines (SSWTs) can be a viable option for off grid energy conversion in certain cases of confined space and low wind speed region, where the counterpart of these turbines cannot work efficiently. However, the existing design is yet a matter of research to make it more useful in particular situations. In view of this, the objective of the present investigation is set to develop and test a novel Savonius-style wind turbine with the intention of improving its performance in terms of power and torque coefficients, and starting characteristics.

Initially, an unsteady two-dimensional computational investigation was carried out for conventional SSWT to study its performance and flow properties at rotating conditions. Further, a series of unsteady simulations are performed on the Bach type SSWT by varying the overlap distance and blade arc angle, and an improved design has been achieved.

Looking at the outcome of the computational study, experimental investigation is planned and executed. The existing experimental set up of low speed wind tunnel is modified and a new test section has been designed to test the performance of SSWTs. Various power and torque measuring devices such as 1-phase and 3-phase alternators, and spring balance dynamometer are installed to measure performance characteristics of SSWTs. However, a better adaptability is achieved with the spring balance dynamometer.

Blockage in the wind tunnel experiments is one of the unavoidable phenomena and thereby this must be taken into account while presenting the experimental results. However, as found in open literature, the investigations related to blockage correction are mostly carried out in closed type test sections, which may not appropriate for open type test sections under

dynamic loading. In this regard, new correlations are developed for blockage corrections in the wind tunnel experiments of SSWTs under an open test section facility, where the blockage correction factor is used to correct the measured parameters such as wind speed, mechanical load applied to the turbine, and rotational speed of the turbine.

Having included the blockage correction, a parametric investigation was carried out on conventional SSWT in terms of overlap ratio, aspect ratio, and tip speed ratio. The obtained geometry of modified Bach type turbine from the 2D unsteady simulations is also tested in comparison with the classical Bach type and conventional semicircular SSWTs.

From the above study, it is observed that a further modification in the blade shape may improve the performance of SSWTs. In view of this, a novel blade shape has been developed by altering the geometric arcs, overlap distances and dimensions of blade profiles. The performance of the newly developed turbine is calculated in terms of torque coefficient, power coefficient, and static torque coefficient. Experiments have also been conducted with other standard blades such as semi-circular, semi-elliptic, Benesh and Bach types in order to have a direct comparison. With the newly developed SSWT, a noticeable improvement in the performance and starting characteristics is achieved maximum over other tested models. With blockage correction, for newly developed SSWT, the maximum power coefficient is found to be 0.31. Further, an attempt is made to improve the efficiency of these SSWTs under concentrated and oriented jets through installation of deflectors at different positions ahead of the turbine.

To study the flow behavior, a 3D unsteady simulation study is executed on the newly developed SSWT, results are validated with the experimental data, and the obtained flow property contours are compared with the other tested SSWTs. The overall efficiency and the payback period are estimated for a wind energy conversion system (WECS) with the newly developed SSWT in comparison to that of modified Bach, Benesh, semi-elliptical, and conventional SSWTs.

Contents

Nomenclature

Notations

A	swept area of the turbine (m^2)
C_D	drag coefficient
C_L	lift coefficient
C_P	power coefficient
C_T	torque coefficient
C_{TS}	static torque coefficient
d	chord length of the blades (m)
D	outer diameter of the turbine (m)
D_o	end plate diameter (m)
e	blade overlap distance (m)
f	blockage correction factor
F	load applied to the turbine (N)
F_D	drag force (N)
F_L	lift force (N)
H	height of the turbine (m)
k	turbulence kinetic energy (m^2/s^2)
n	variable for blockage correction
N	turbine rotational speed (rpm)
$P_{available}$	power available in the wind (W)
$P_{turbine}$	turbine power output (W)
q	dynamic pressure of wind (Pa)
r_p	radius of rotating pulley (m)
R	rotational radius of the turbine (m)
Re	Reynolds number
s	separation gap (m)
S_f	solidity factor of turbine
T	dynamic torque (Nm)
T_S	static torque (Nm)
u	blade tip speed (m/s)
V	free stream wind speed (m/s)
*	blockage corrected data

Greek letters

α	deflector angle for advancing blade (°)
β	deflector angle for returning blade (°)
δ	overlap ratio
ϵ	energy dissipation rate
η_G	generator efficiency
η_O	overall efficiency of WECS
η_T	turbine efficiency
η_{TS}	transmission and storage efficiency
θ	turbine rotational angle (°)
μ	dynamic viscosity (Ns/m^2)
ρ	density of air (kg/m^3)
ϕ	blade arc angle (°)
ω	specific dissipation rate
ω_s	angular speed of the turbine (rad/s)

Abbreviation

ANFIS	adaptive neuro-fuzzy inference system
ANN	artificial neural network
AR	aspect ratio
BR	blockage ratio
CFD	computational fluid dynamics
FIS	fuzzy inference system
HAWT	horizontal-axis wind turbine
RBF	radial basis function
SSWT	Savonius-style wind turbine
TSR	tip speed ratio
VAWT	vertical-axis wind turbine
WECS	wind energy conversion system

List of Figures

List of Tables

CHAPTER –1

Introduction

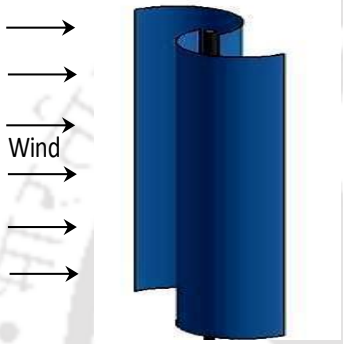

Chapter Outline

Overview

Over the preceding years, wind energy is emerging as one of the most cost-effective forms of clean, renewable energy with very significant increases in global annual installed capacity. Although wind energy conversion systems involving horizontal axis wind turbines (HAWTs) are dominating the large scale and offshore wind market with their relatively higher efficiency, it is still equally important to develop small-scale systems with vertical axis wind turbines (VAWTs) those can effectively be exploited to provide easy and safe installation in confined spaces for autonomous power generation. In this context, the Savonius-style wind turbines (SSWTs), a class of small VAWTs, can be a viable option for off grid energy conversion in certain cases of confined space and low wind speed region, where the counterpart of these turbines cannot work efficiently. This chapter gives an overview of the present situation of the wind energy, and the motivation behind the present study. This chapter also includes the objective of the present investigation and a detailed roadmap to attain the intended objective. Finally, the chapter briefly describes the layout of the thesis.

1.1 Preface

With the rapid increase of technological and industrial growth, global economy and human life style, the energy requirements have been amplified significantly. In contrast, the high depletion rate of conventional energy sources and its price hike enforces the demand of an alternative source of energy. Further, the recent impacts of global-warming and climate change caused by the carbon derivatives and the nuclear plant calamities are a major concern for the global environment. To encounter this problem, the first strategy is to reduce the energy consumption by applying energy savings programs focused on energy demand reduction and energy efficiency in industrial and social applications. A second strategy consists of using a safe, reliable and economical source of renewable energy, not only for large-scale energy production, but also for stand-alone systems.

From a modest beginning in 1970s, considerable progress has been achieved in several renewable technologies that include wind power, solar photovoltaic and geothermal energy, as well as production of biogas, bio-ethanol and bio-diesel from biomass feed stock. However, the overall contribution of non-hydro renewable energy technologies is still very limited as compared to their potential. In a recent report of REN21 (Renewable Energy Policy Network for the 21st Century), non-hydro renewable share at the end of 2013 is only 5.7% of the global installed capacity, whereas the hydro power share is 16.4%. The share of non-hydro renewable sources include wind, solar PV, bio-power, geothermal-CSP-ocean as 2.9%, 1.8%, 0.7% and 0.4%, respectively (REN21, 2014). Thus, an urgent need of improvement is being sensed in the existing designs and technologies of non-hydro renewable energy conversion devices.

It is being observed that among the non-hydro renewable sources, wind energy can be a feasible alternative to reduce the dependency on conventional energy sources. It is environment friendly and abundant in nature. Thus, in recent years, the annual installed capacity of wind energy has been increased significantly on global, national, and regional levels. An assessment on the global wind energy reports of Global Wind Energy Council (GWEC, 2012–2014) shows that the global annual installed capacity of wind energy has been increased to 318.11 GW in 2013 as compared to 283.19 GW (2012) and 238.05 GW (2011), a growth of 12.33% and 33.63%, respectively. As per the latest report (April, 2014), China leads the wind energy market with an installed capacity of 91.41 GW followed by USA (61.09 GW), Germany (34.25 GW), Spain (22.96 GW) and India (20.15 GW).

A wind energy conversion unit mainly consists of (a) a wind turbine, (b) a mechanical power transmission device i.e. gear box, (c) an electric generator, and (d) an electricity storage and transmission device (Figure 1.1).

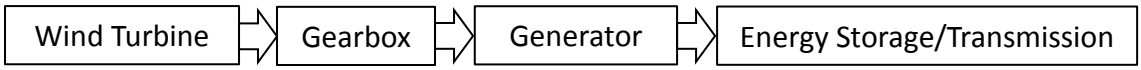

Figure 1.1: A basic wind energy conversion system (WECS)

As is known, the wind turbines can broadly be categorized into two configurations viz., horizontal-axis wind turbine (HAWT) and vertical-axis wind turbine (VAWT). In many instances, the HAWTs are found its position to supply power directly to the grid. On the contrary, in some cases, wind power is generated more locally, at or near the site of power usage. In these conditions, the wind is typically generated by smaller VAWTs that are in single-unit or in clusters of units with an addition of energy storage system. However, the selection of the turbine for such cases largely depends upon the economic viability of installation, availability of space, operating range of wind speed and integration of the system to connecting grid.

With an intension of designing a wind turbine for instances of confined space, low-cost, low wind speed, easily operated and maintained wind energy conversion system, the Savonius-style vertical axis wind turbines are among the best possible solutions. However, it is worth mentioning that the power conversion capability of these turbines is inferior to other wind energy convertors, and thus, this style of turbines is more suitable for specific purposes. In this regard, the present investigation attempts to improve the power conversion capability of these turbines by modifying its geometric parameters.

1.2 Savonius-style wind turbine

The most basic type of vertical-axis wind turbine (VAWT) is the Savonius-style wind turbine (SSWT). This class of wind turbine was introduced by a Finish engineer named Savonius in the 1920s and was named after its inventor (Savonius, 1929). This is basically a modification of the Flettner's rotor used in ships (large cylinders mounted on the vertical axis). With a Flettner's rotor, the wind pressure difference created across the cylinder by means of the "Magnus effect" (forces generated on curved objects that move through a fluid) was mainly responsible to propel the ships.

The Savonius-style turbine is a simple device, designed by cutting a cylinder into halves, along its central axis and relocating the semi-cylindrical surfaces sideways. The outlook of this turbine is analogous to an 'S' when viewed from the top. These turbines are designed to be driven by the wind drag forces on the turbine blades, and in this regard, they differ in appearances from their more common counterparts that are lift-driven VAWTs. The schematic diagrams of 'S'-shaped and helical-shaped Savonius-style turbines are shown in Figure 1.2 along with the most important dimensions depicted in Figure 1.3.

Conventional S-shape Helical-shape

Figure 1.2: Two-bladed "S"-shaped and helical-shaped Savonius-style vertical-axis wind turbines.

The power-conversion capability of these turbines is inferior to that of other wind energy convertors. A typical conventional Savonius-style turbine possesses a power conversion efficiency of 12%–20%, as compared to the efficiency of 30%–40% of vertical-axis Darrieus-style wind turbines. Horizontal-axis wind turbines, on the other hand, give efficiency in the range of 40%–50%. Thus, Savonius-style turbines are not competitive with other styles of wind turbines in terms of their aerodynamic performance, and should only be considered as application-specific devices for the conversion of wind energy, and small-scale technological alternatives to other wind turbines. Nevertheless, it is worth mentioning that with a modified design of Savonius-style turbines, the peak power conversion efficiency can reach up to 30% (Shepherd and Zhang, 2011; Abraham *et al.* 2012; Akwa *et al.* 2012).

These turbines have a very low cut-in speed and can operate in winds as low as 3 m/s (6.7 mph). They can operate in a wide range of wind speeds and produce lesser vibrational loads on the supporting structure due to their lower rotational speed. Design simplicity, low cost, and easy assembly are the advantages of these turbines. These devices are insensitive to the wind flow directions, and thus, are very useful for the specific locations of variable wind

directions. Their vertical rotational axis allows them to be positioned in multiple numbers in a confined space or atop buildings (Abraham *et al.* 2012; Akwa *et al.* 2012).

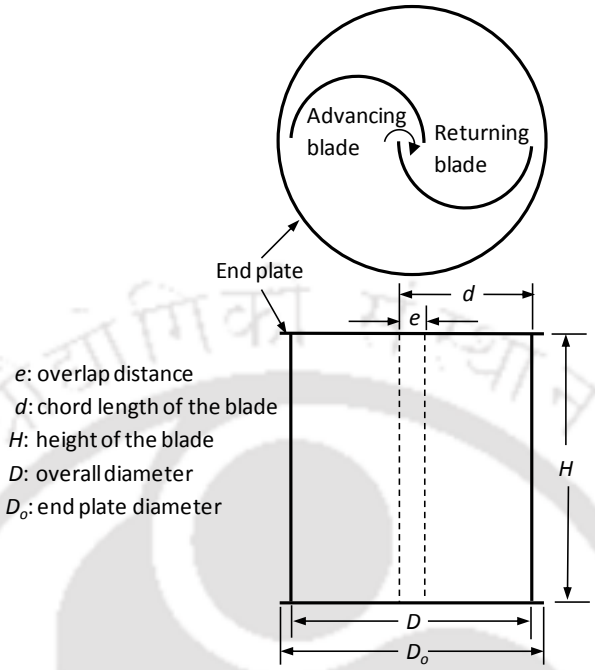

Figure 1.3: Dimensions of a Savonius-style vertical-axis wind turbine.

This class of turbine is a very useful device for water pumping in agricultural purposes, particularly, in rural areas where the water level is within a distance of 5 m (16.4 ft) below the ground. The installation and maintenance costs are very low and it can be installed on rooftops for local electricity production. It is also useful in buildings for ventilation and air-conditioning purposes. A Flettner ventilator, which is often seen on the roofs of vans and buses and is used as a cooling device is another practical application of the Savonius-style VAWTs. Other applications are in decentralized small-scale electricity generation for remote areas. A robust wind turbine system equipped with battery storage capacity can be a viable option for intermittent electricity generation. This stored electricity can be used for running electronic equipment, lighting or charging mobiles. Nowadays, another promising application of these turbines can be observed on cellular communication towers. In a modern communication tower, the usual power requirement is around 1–3 kW for cell-phone electronics associated with it, which is collected either from the grid connections or from a generator system. With the rapid advancement of cellular technology, communication towers with antennas are being built in urban as well as rural areas. In some rural areas where grid connectivity is not available, these small-scale turbines can be a viable option to generate the

required power. Moreover, they will generate more power at high altitudes due to higher wind speeds and lesser obstructions. This application gives an additional benefit of reduction in the requirement of the separate base and tower (Abraham *et al.* 2011; Shepherd and Zhang, 2011; Abraham *et al.* 2012; Akwa *et al.* 2012; Plourde *et al.* 2012). Currently, another application of these turbines is observed in association with the Darrieus-style VAWTs due to better starting ability of the Savonius-style wind turbines. A photograph showing a typical combined Savonius–Darrieus-style turbine is presented in Figure 1.4.

Figure 1.4: Historic Gold Mine Savonius–Darrieus combined VAWT in Taiwan (November, 2009). Source: Courtesy of Fred Hsu, reproduced under GNU Free Documentation License 1.2.

1.3 Present objective and roadmap

It is perceived that the SSWTs can be a viable option for off grid energy conversion in certain cases of confined space and low wind speed region, where the counterpart of these turbines cannot work efficiently. However, the existing design is yet a matter of research to make it more useful in particular situations. In view of this, *the objective of the present investigation is set to develop a novel Savonius-style wind turbine with the intention of improving its performance in terms of power coefficient, torque coefficient, and starting characteristics.*

The following roadmap (Figure 1.5) shows how the objective has been established and how the improvement of the turbine has been brought about through numerical simulation and wind tunnel experiments.

Road Map

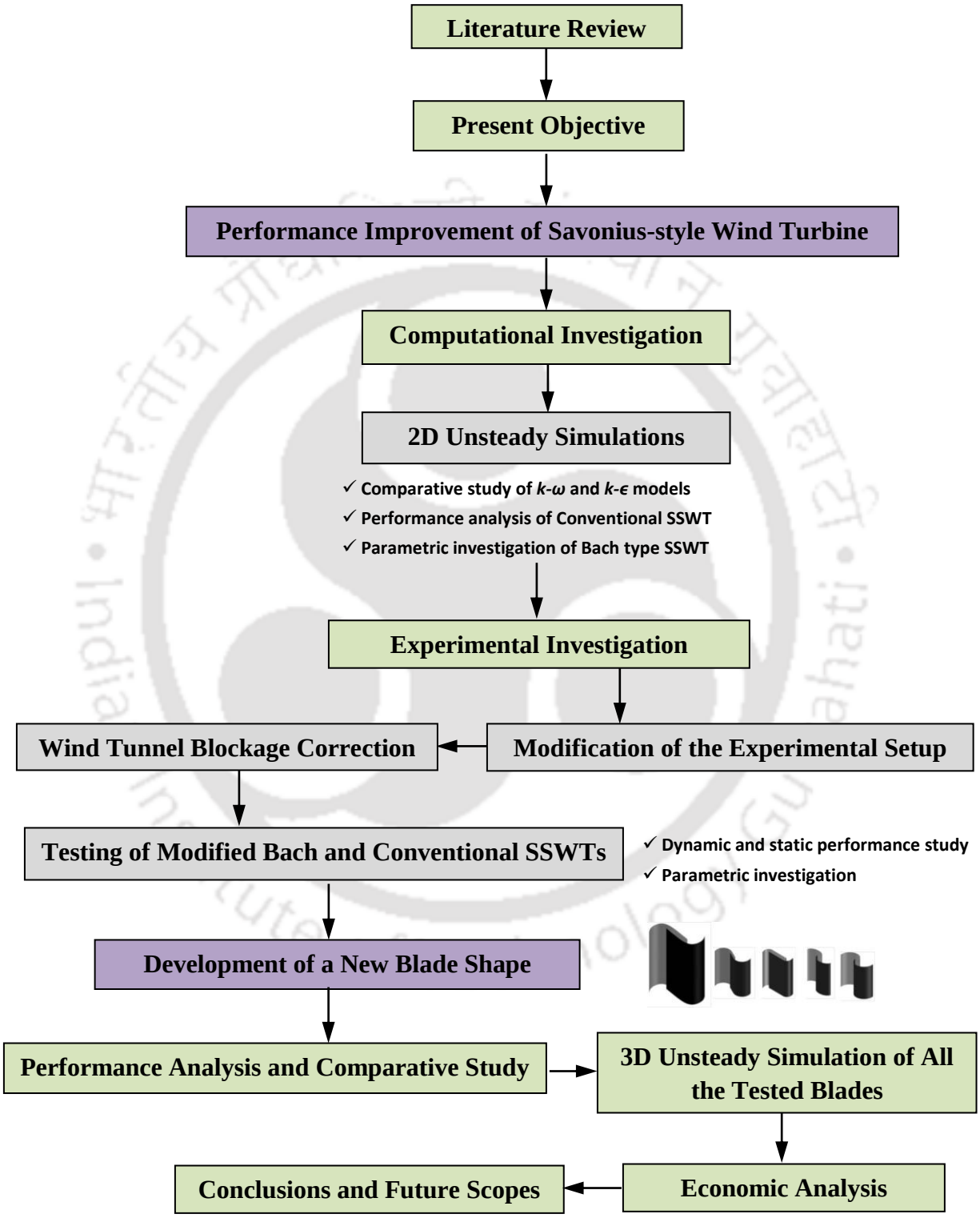

Figure 1.5: Roadmap of the present investigation

1.4 Organization of the thesis

The thesis has been organized in ten chapters, the details of which are summarized below:

Chapter – 1 introduces the motivation behind the present study followed by the objective and the roadmap.

Chapter – 2 gives the basic theory followed by a detailed review of literature on Savonius-style wind turbines addressing both the experimental and computational work.

Chapter – 3 is devoted to the 2D unsteady simulations of conventional and Bach type SSWTs. The influences of overlap distance, blade arc angle, and tip speed ratio are studied and an improved design of Bach type turbine is reported.

Chapter – 4 gives a complete description of the experimental facility and the instruments used in the present investigation.

Chapter – 5 outlines the new correlations developed for the wind tunnel blockage correction with an open type test section.

Chapter – 6 focuses on the wind tunnel experiments of conventional and modified Bach type SSWT by varying its design parameters.

Chapter – 7 presents the development of a new blade shape and its performance analysis in comparison with other existing blade shapes such as modified Bach, Benesh, semi-elliptical and semi-circular types. The effects of wind speed on the dynamic and static characteristics are also discussed

Chapter – 8 describes the 3D unsteady simulation of the newly developed SSWT in comparison with other tested models. Further, the flow behavior around these turbines is also reported.

Chapter – 9 gives an estimation on the overall efficiency and payback period of the wind energy conversion system (WECS) using the newly developed blade design.

Chapter – 10 concludes the entire research work and highlights the application potential along with the scope for future studies.

CHAPTER –2

Theory and Literature Review

Chapter Outline

Overview

Since its inception, a host of researchers have carried out experimental and numerical investigations to analyze and improve the design and performance of SSWTs. However, most of these studies revolved around conventional semi-circular blades. A few investigators have carried out the performance analysis with helical and twisted blades. Although noticeable performance gains were achieved, the designs reported seemed to have been more complex and expensive. Improvement in the performance coefficients and static torque characteristics were also reported with the use of deflectors, guide vanes, or curtains placed upstream to the turbine blades. In this aspect, some studies with modified blade shapes were also attempted. Further, in order to predict the performance characteristics and flow behavior around the SSWTs, computational studies using different turbulence models have been reported. This chapter gives a thorough discussion on various experimental and computational work reported in open literature.

2.1 Basic concept

Savonius-style wind turbines (SSWTs) mainly rotate due to exertion of wind drag force between the convex and concave parts of the turbine blades when they rotate around a vertical shaft. However, lift also contributes to the power generation at various rotational angular positions.

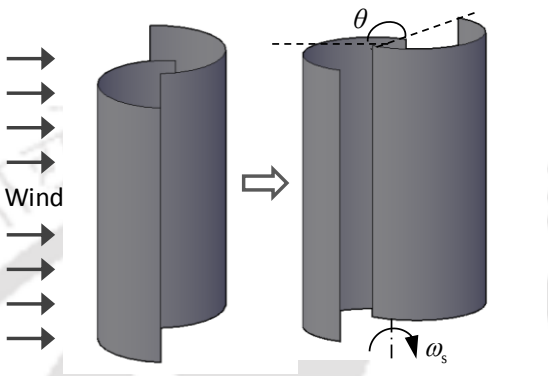

Figure 2.1: A typical Savonius-style wind turbine

The performance of these turbines is more often articulated in terms of the power coefficient (C_P), torque coefficient (C_T), and static torque coefficient (C_{TS}), which are expressed by the following equations:

$$C_T = \frac{T}{\frac{1}{2}\rho A V^2 R} \tag{2.1}$$

$$C_P = \frac{P_{turbine}}{P_{available}} = \frac{T\omega_s}{\frac{1}{2}\rho A V^3} = \frac{T}{\frac{1}{2}\rho A V^2 R}\frac{R\omega_s}{V} = C_T \times \mathrm{TSR} \tag{2.2}$$

$$C_{TS} = \frac{T_S}{\frac{1}{2}\rho A V^2 R} \tag{2.3}$$

where, ρ is the density of air [kg/m^3], V is the free stream wind speed [m/s], A is the swept area of the turbine [m^2], TSR is the tip speed ratio, R is the radius of rotation of the turbine [m], ω_s is the rotational speed of the turbine [rad/s], $P_{turbine}$ is the power produced by the

turbine [W], $P_{available}$ is the power available in the wind [W], T and T_S are the dynamic and static torques on the turbine [Nm], respectively.

The graphical representation as shown in Figure 2.2 is widely used to compare the performance of SSWTs with those of other existing wind turbines (Akwa *et al.*, 2012). This figure shows a lower average power coefficient for conventional SSWTs as compared to other turbines. This is mainly due to the negative torque produced on the returning blade of the SSWTs. A performance comparison obtained from wind tunnel tests in terms of maximum power coefficient (C_{Pmax}) for conventional SSWTs is demonstrated in Table 2.1. It is observed that the conventional SSWT without any overlap distance (e) possesses a C_{Pmax} of 0.12–0.20, which are obtained in the range of TSR = 0.7–0.9. With blade overlap, the highest attainable C_P was found to be 0.24 as reported by Sandia laboratory, USA (Blackwell *et al.*, 1977; Benesh, 1996).

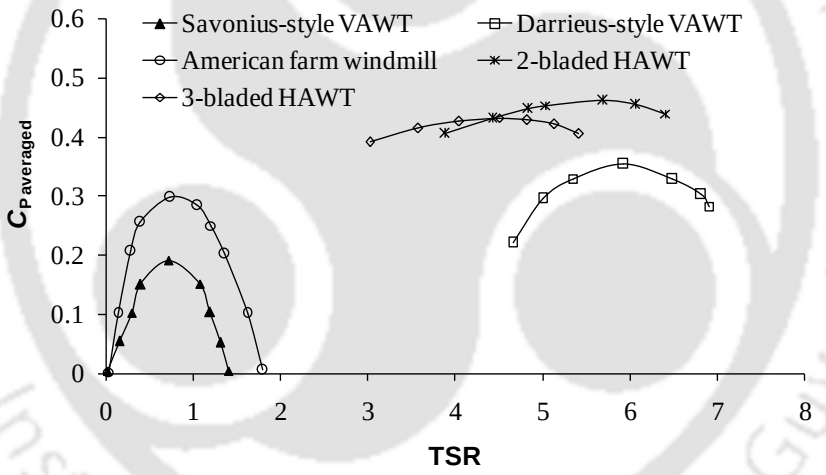

Figure 2.2: Power coefficient of conventional SSWT as compared to other turbines (Akwa *et al.*, 2012)

The starting ability is of great importance for SSWTs, which is specified by the turbine static torque performance. However, the static torque of the conventional Savonius turbines has two major drawbacks; one of which is its large static torque variation at various rotor angular positions and the second one is its negative torque value in the 2nd and 4th quarter of the rotor rotational cycle). Figure 2.3 shows the static torque characteristics at different angular positions. For conventional SSWTs, a better static torque characteristics is observed in the range of θ = 30°–60°, whereas, negative torques characteristics are apparent in the range of θ = 100°–150° (Fujisawa and Gotoh, 1994; Kamoji *et al.*, 2009a; Kianifar and Anbarsooz, 2011).

Table 2.1: Maximum power coefficient (C_{Pmax}) of conventional Savonius-style wind turbines

Investigators	$H \times D$ (m × m)	Test section size (m × m)	TSR	C_{Pmax}
Baird and Pender (1980)	0.076 × 0.06	0.305 × 0.305	0.78	0.19
Bergeles and Athanassiadis (1982)	0.70 × 1.40	3.5 × 2.5	0.70	0.13
Sivasegaram and Sivapalan (1983)	0.12 × 0.15	0.46 × 0.46	0.75	0.20
Bowden and McAleese (1984)	0.164 × 0.162	0.76 (circular)	0.72	0.15
Ogawa and Yoshida (1986)	0.175 × 0.3	0.8 × 0.6	0.86	0.17
Fujisawa and Gotoh (1992)	0.32 × 0.32	0.5 × 0.5	0.90	0.17
Huda *et al*. (1992)	0.185 × 0.32	0.5 (circular)	0.71	0.17
Hayashi *et al*. (2005)	0.23 × 0.33	1.5 × 1.5	0.75	0.18
Kamoji *et al*. (2008)	0.208 × 0.208	0.4 × 0.4	0.78	0.16
Dobrev and Massouh (2011)	0.20 × 0.22	1.35 × 1.65	0.80	0.18

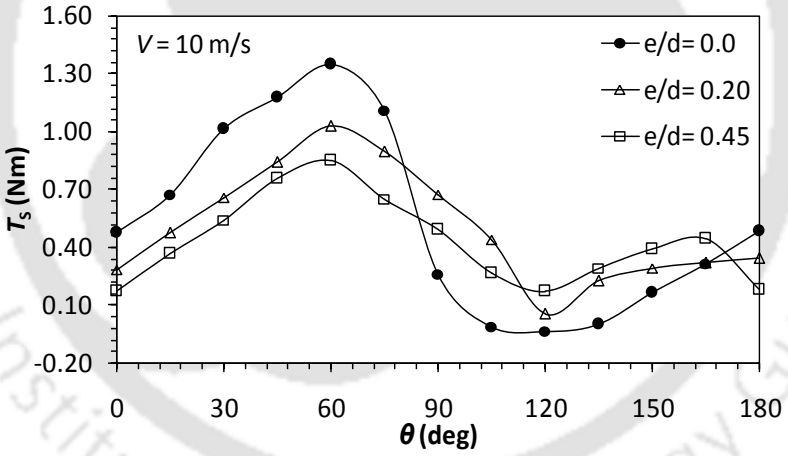

Figure 2.3: Static torque characteristics of conventional SSWTs (Kianifar and Anbarsooz, 2011)

The main aerodynamic forces acting on the SSWT are the drag and lift forces as shown in Figure 2.4. The drag force (F_D) is usually defined as the force parallel to the direction of the incoming air flow. It is due to both (i) the viscous frictional forces at the blade surface and (ii) the unequal pressure on the blade surfaces facing toward and away from the incoming flow. For a simplified rotating SSWT, the drag force is a function of the relative wind speed at the turbine blade surface. The relative wind speed is defined as the difference between the wind speed (V) and the turbine rotational speed (u). The drag coefficient (C_D) is expressed as

$$C_D = \frac{F_D}{\frac{1}{2}\rho A(V-u)^2} \tag{2.4}$$

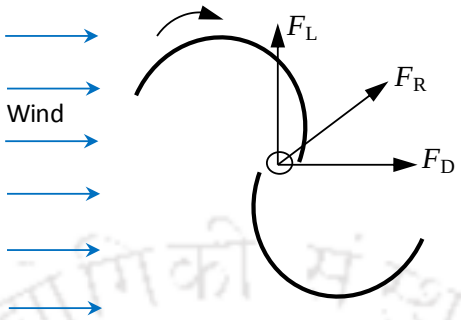

Figure 2.4: Aerodynamic forces acting on the SSWTs

The lift force (F_L) is defined as the force perpendicular to the direction of incoming air flow and is a consequence of the unequal pressure distribution between the upper and lower blade surfaces. The lift coefficient (C_L) is given by

$$C_L = \frac{F_L}{\frac{1}{2}\rho A(V-u)^2} \tag{2.5}$$

A very few investigations on the drag and lift behavior of SSWT have been reported (Chauvin and Benghrib, 1989; Islam *et al.*, 1995; Kamal and Islam, 2008). Although the drag force is the main driving force, the SSWT is not a pure drag device. It has been reported that at some rotational positions, the turbine behaves like a slender body and a small lift force contributes to the net power (Modi and Fernando, 1989; Modi and Fernando, 1993).

2.2 Design parameters of SSWTs

In order to design an efficient Savonius-style wind turbine, the most important design parameters are scaling factor, solidity factor of the turbine, turbine height-to-diameter ratio, overlap distance, and separation gap between the blades, turbine end plates, and blade profile. In this section, a detailed description is given, focusing on the current status of this turbine.

2.2.1 Scaling factor

One of the major parameters that affect the performance and design optimization of a Savonius-style turbine is the scaling of large turbines into the small models. In practice, the

tested results of small models often suffer from inaccuracy. That is mainly due to the presence of electrical and mechanical losses related to energy conversion from shaft to generator in the large models, and also due to the blade geometry to mass relationships. To maintain the similarity of performance parameters (C_P and C_T), the flow conditions must be the same. Using the theory of similarity, this can be achieved by (i) maintaining the same TSR; (ii) maintaining the blade profile, number of blades used, and the materials used; and (iii) making proportional adjustments to all dimensions like chord length, blade radius, aspect ratio, overlap ratio, and so forth (Gasch and Twele, 2012).

2.2.2 Solidity factor

The solidity factor (S_f) is an important criterion for designing a wind turbine and is defined as,

$$S_f = \frac{\text{Total area of the turbine blades}}{\text{Swept area normal to the direction of wind flow}} \tag{2.6}$$

In an efficiently designed Savonius-style wind turbine, a comparatively larger area of the turbine blades is intercepted by a small area of wind, while the area is compared with the case of lift-driven turbines. It therefore has a high-solidity factor, which is not desirable for a higher-rotational system. This style of turbines with high solidity factor usually suffers from a high degree of aerodynamic interference between the blades, which results in low values of TSR and power coefficient C_P. Consequently, this type of turbine usually operates at low operating speeds but has high-starting torque and in this regard, it differs from its counterparts that are lift driven. A better understanding can be drawn from the examples demonstrated in Figures 2.5 and 2.6. The former depicts the solidity of Savonius-style turbine and the latter shows the solidity of its counterpart Darrieus-style turbine, keeping the swept area constant.

2.2.3 Aspect ratio

The turbine aspect ratio is derived as a non-dimensional parameter through dividing the height of the turbine (H) by its diameter (D). It is a decisive parameter for satisfactory performance of Savonius-style turbines considering the effect of solidity factor because of its impact on the performance coefficient (C_P). It is often expressed as:

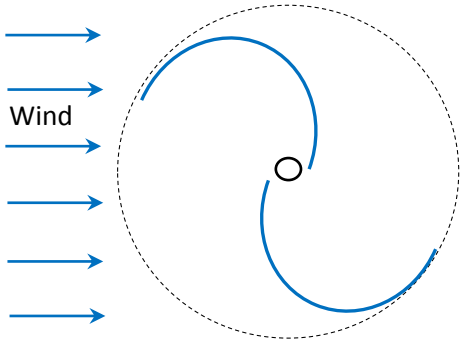

Figure 2.5: Solidity of Savonius-style turbines

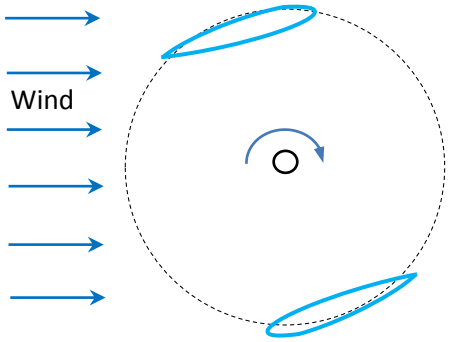

Figure 2.6: Solidity of Darrieus-style turbines

$$\mathrm{AR} = \frac{H}{D} \tag{2.7}$$

The dimensions of this style of turbine are demonstrated in Figure 1.3 and a clear picture of different aspect ratios can be seen from Figure 2.7. A low aspect ratio (<1.5) is often preferred for these turbines to give structural stability. A small diameter always causes sharp turns in the direction of airflow that accelerate the turbine rotational speed. In contrast, with an increase of diameter, the torque generated by the turbine blades increases at the cost of decreased rotational speed. As depicted in Table 2.1, the value of AR varies from 0.6–1.3.

2.2.4 Overlap ratio

The overlap ratio of the Savonius-style turbines plays a vital role in optimizing the performance of these turbines. This ratio is obtained by dividing the overlap distance between the turbine blades (e), by the blade chord length (d) and is given by,

$$\delta = \frac{e}{d} \tag{2.8}$$

An effective design of a conventional Savonius-style turbine with overlapping blades proved to have better starting characteristics compared to that of a non-overlapping system (Figure 2.7). This improvement is mainly triggered by the overlapping flow between the turbine blades. This flow reduces the negative torque produced by the returning blade of the turbine by inserting an opposite effect on the concave side of the returning blade. Hence, the average power of the turbine gets increased. It is obvious that as the overlap ratio increases beyond an optimum value, the effective pressure on the concave side of the advancing blade reduces. Thus, a small overlap ratio of δ = 0.15–0.25 is always preferable in order to have a better

performance of these turbines (Mojola, 1985; Ushiyama and Nagai, 1988; Biswas *et al*., 2007; Kianifar and Anbarsooz, 2011; Akwa *et al*., 2012).

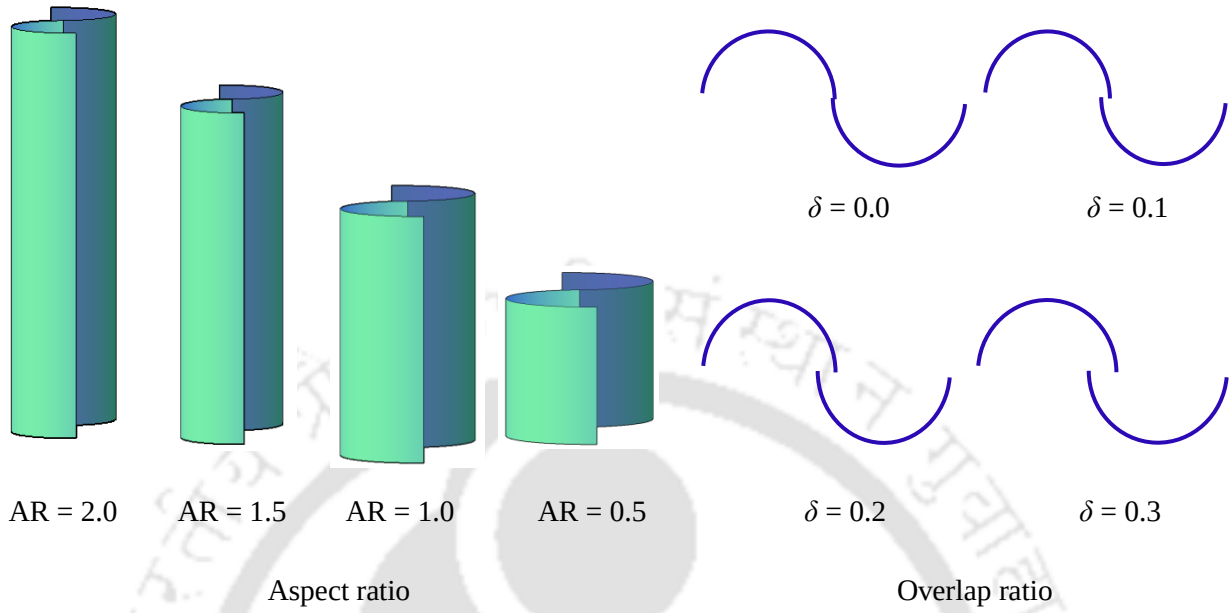

Figure 2.7: Examples of Savonius-style wind turbines with different aspect ratios and overlap ratios (Akwa *et al*., 2012)

2.2.5 Separation gap

The separation gap (*s*) is responsible for the airflow through the space between the blades (Figure 2.8). With the addition of a separation gap, wind cannot focus on the concave portion of the returning blade, and as a result, the advantage of restoring pressure drag on the returning blade through the overlapping flow and dragging flow is much reduced, which in turn reduces the average power of the turbine. Most of the investigations showed a better performance with no separation gap than the design comprising a separation gap (Akwa *et al*., 2012).

2.2.6 End plates

The application of end plates in the turbine design seemed to have enhanced the performance. It is a simple device with a negligible thickness, and is installed as a cap on the top and bottom of the turbine blades, as shown in Figure 2.9. The addition of end plates on a Savonius-style turbine increases the maximum average power coefficient, and also helps in better operation at higher TSRs. It is mainly due to the fact that the end plates inhibit the air

outflow from the concave side of the blades, keeping the pressure difference between concave and convex sides of the blades at satisfactory levels over the height of the turbine. The diameter of the end plates is recommended to be 1.1 times the turbine diameter to give a better performance (Shepherd and Zhang, 2011; Plourde *et al.* 2011; Abraham *et al.* 2012; Akwa *et al.* 2012; Plourde *et al.* 2012).

(a) With seperation gap (b) Without any seperation gap

Figure 2.8: Savonius-style wind turbines with and without separation gap

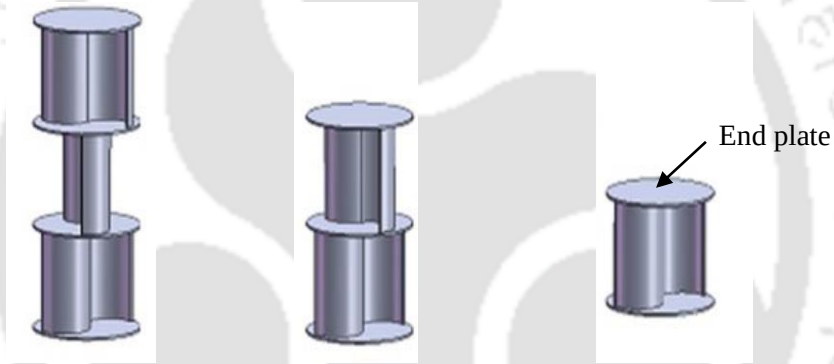

Three-stage Two-stage Single-stage

Figure 2.9: Use of end plates and multi-staging (Akwa *et al*., 2012)

2.2.7 Multi-staging

As discussed in the earlier sections, a high starting torque and slow operating wind speed are a major advantage of Savonius-style turbines. However, at some angular positions (θ = 110°–170°), it is observed that changes in the wind direction cause a low starting torque such that the turbine cannot start on its own. To overcome this drawback, the use of multi-staging has shown a significant improvement over the single-stage Savonius-style turbines. A two-stage design of this style is accomplished by setting the upper and lower blade pairs at 90° to each other, and it is 120° to each other in the case of a three-stage design. Figure 2.9 shows the arrangement for different staged systems. The use of multi-staging reduces the high

fluctuation of torque without significant performance loss of the turbine, operating with cycles lagged relative to one another (Hayashi *et al*., 2005; Saha *et al*., 2008).

2.2.8 Number of blades

The number of blades for Savonius-style wind turbines is an effective parameter depending on the operating conditions. Two-bladed turbines of this style have shown a better performance over their three-bladed counterparts. However, three-bladed turbines have a higher starting torque as compared to two-bladed turbines. This is mainly due to the reduction in angular positions of the advancing blade, resulting in a "cascade effect" in which each blade affects the performance of the following blade. As a consequence, a lesser amount of energy released by the moving air is converted into mechanical energy by higher-bladed systems. The power coefficient of a two-bladed turbine is about 1.5 times higher than that of the three-bladed turbine (Blackwell *et al*., 1977). A better performance is observed with the two-bladed system. However, as discussed earlier, the starting capability can be enhanced for a two-bladed turbine by adapting a multi-staging system.

2.2.9 Blade profiles

The benefit on the use of a simple blade profile for Savonius-style wind turbines gives the flexibility in variable blade profile optimization. The first Savonius-style turbine of "S"-shape was patented by Savonius in 1929 (Savonius, 1929). Thereafter, he modified the design to increase the efficiency of the turbine 1930 (Savonius, 1930). These designs were further modified by Bach (1931), Benesh (1988, 1996) and Mohamed *et al*. (2011). These modified designs are reported to be more efficient then the semi-circular blade profile. The various blade profiles used for SSWTs are shown in Figure 2.10.

Apart from these "S" type or "hook" type profiles, the other type of profile that is found in some applications is the twisted blades. As reported in open literatures, the twisted bladed turbines have marginally improved the efficiency and starting characteristics of these turbines (Saha *et al.,* 2008; Grinspan *et al*., 2004; Saha and Rajkumar, 2006). A modification of twisted blades is the helical turbines, can be assumed as a turbine of number of stages with negligible heights which are stacked one upon another in such a fashion that it smoothly tends to yield a twist of 180° (Kamoji *et al.,* 2009b). The effect of helical designs reduces the large fluctuations in the torque characteristic of a single-stage Savonius-style turbine;

however, behavior is close to adding stages in the conventional turbines. However, the performance of these helical-shaped turbines does not differ significantly from that of modified "S" or "hook" type turbines (Plourde *et al*., 2011).

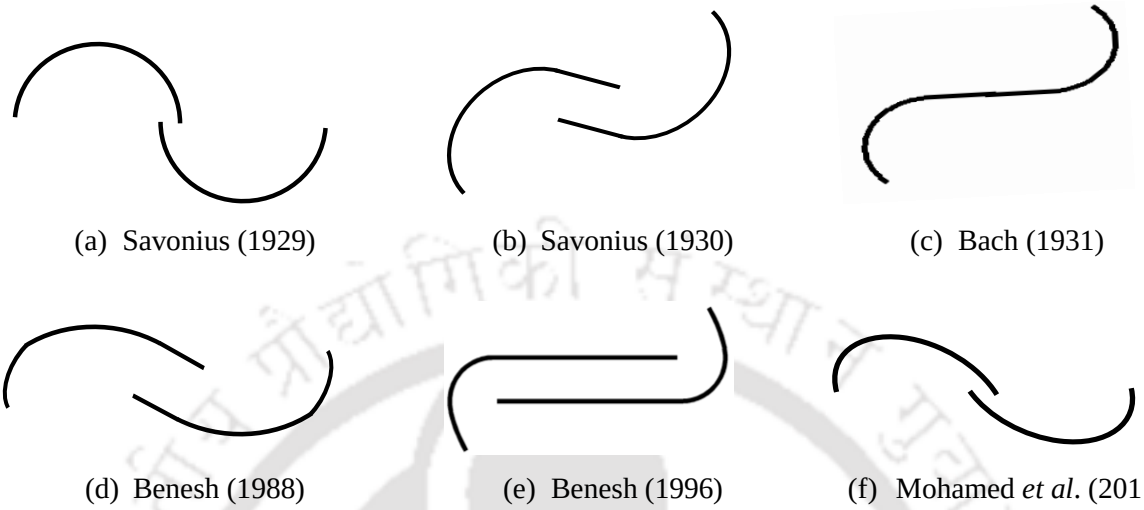

(a) Savonius (1929) (b) Savonius (1930) (c) Bach (1931)

(d) Benesh (1988) (e) Benesh (1996) (f) Mohamed *et al*. (2011)

Figure 2.10: Various blade profiles used for SSWTs

2.3 Power augmentation techniques

As reported in open literature, the performance of a Savonius rotor can be much improved by installing various power augmenters such as curtains, wind shields, convergent nozzle, deflector plate etc. in front of the turbine blades (Figure 2.11). It is to be noted that the wind pressure exerted to the returning blade of this turbine generates a high negative torque, and this declines its total power. Using various augmentation techniques, the net power output and starting characteristics of SSWTs can be improved in two ways viz., (i) reduction of wind resistance on the returning blade, and (ii) local acceleration of airflow incident on the advancing blade.

It has been observed that with the installation of curtains, a C_{Pmax} of 0.38 is obtained for two-SSWT, a performance gain of 140.6% was achieved over without curtians (Altan and Atilgan, 2010). These are placed in front of the turbine as shown in Figure 2.11, and are used to reduce the negative torque caused by the returning blade, thus enhance the static torque as well as dynamic characteristics of the turbine. With the help of flat plate wind shield, Alexander and Holownia (1978) have reported an optimum power coefficient of 0.243 for SSWTs. Mohamed *et al*. (2010) have also done a similar type of study with obstacle wind shields, where a highest power coefficient is found to be 0.258. The deflectors which are very similar to wind shields are reported to be a power augmenter by several researchers. Huda *et*

al. (1992) and Ogawa and Yoshida (1986) have studied the use of flat deflectors and observed the C_{Pmax} to be 0.21. V-shaped deflector also increases the C_P by 19% as compared to conventional SSWTs (Shaughnessy and Probert, 1992) as shown in Table 2.2.

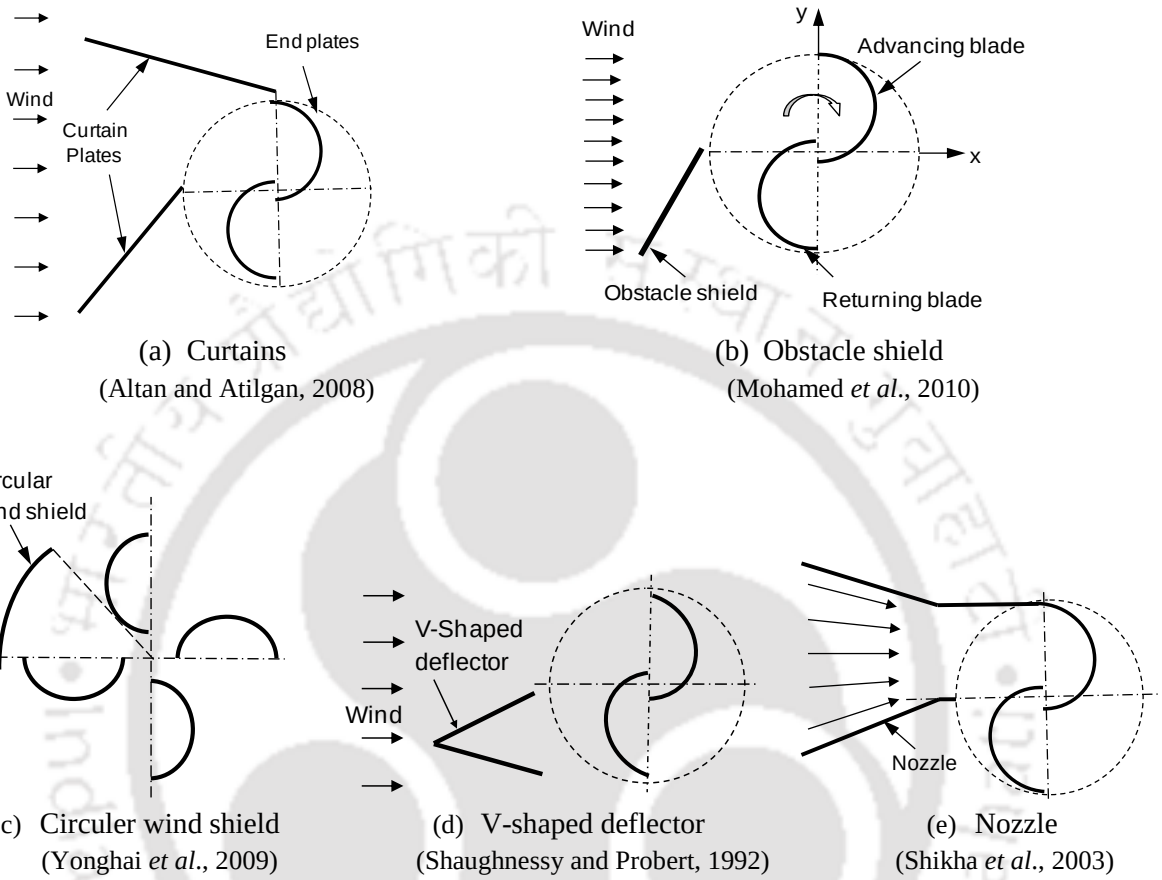

(a) Curtains (Altan and Atilgan, 2008)

(b) Obstacle shield (Mohamed *et al*., 2010)

(c) Circuler wind shield (Yonghai *et al*., 2009)

(d) V-shaped deflector (Shaughnessy and Probert, 1992)

(e) Nozzle (Shikha *et al*., 2003)

Figure 2.11: Power augmentors in front of the SSWT blades

Table 2.2: Power augmentation techniques used for Savonius-style wind turbines

Investigators	Augmenter used	% increase of C_{Pmax}
Morcos *et al.* (1981)	Flat plate shield	54.5%
Ogawa *et al*. (1989)	Deflector plate	27.0%
Shaughnessy and Probert (1992)	V-shaped deflector	19.7%
Altan *et al.* (2008)	Curtains	140.6%
Mohamed *et al*. (2010)	Flat plate shield	27.3%
Mahamed and Thevenin (2010)	Obstacle shielding	49.6%
Golecha *et al.* (2011)	Deflector plate	50.0%

To avoid the effect of negative torque, some investigations have been carried out using nozzles and ducts (Sabzevari, 1978; Sivasegaram, 1979; Shikha *et al*., 2003; Irabu and Roy, 2007). Sabzevari (1978) has tested several ducts, concentrators and diffusers on a split SSWT and reported an increase of C_P by 1.25 times. Sivasegaram (1979) also tested several straight walled ducted concentrator configurations in the wind tunnel and obtained an optimum geometry. Results have shown an increase in the power by about 1.5 times through moderate concentrators. Subsequent studies using convergent nozzles have reported an enhancement of power at low wind speeds (Shikha *et al*., 2003).

2.4 Computational investigations

The flow around a SSWT is time dependent and complex in nature; separation and vortex formation are common phenomena. Thus, the complex unsteady flow characteristic of the SSWTs is often impossible to investigate through classical aerodynamic tools such as blade element theory. The classical momentum theory fails to analyze the performance of such a turbine accounting the effect of various parameters (Modi and Fernando, 1989).

The stream-tube model, based on the blade element theory, is found effective for the analysis of a Darrieus-style turbine at low TSRs (Islam *et al*., 2008). However, it is argued to be ineffective in predicting the performance of a Savonius-style turbine (Paraschivoiu, 2002; Biadgo *et al*., 2013). It is mainly due to the larger turbine area of Savonius-style turbine to the flow swept area. Moreover, the staggered curved blades restrict the stream-tube model to form the entire flow field as an isolated cross-sectional flow pattern and also to calculate the forces on the curved surfaces.

For SSWTs, the initial analytical studies considering the vortex shedding have not assumed the effect of flow separation, and as a result, unrealistic performance predictions were observed; however, these formed the basis of many later theoretical studies (Wilson *et al*., 1976; Van Dusen and Kirchhoff, 1978). To deal with the problems of flow separation and vortex formation around these turbines, available literatures show a qualitative potential of the discrete vortex method considering the effect of separation, where the flow is assumed to be a blend of a finite number of discrete vortices (Ogawa, 1984; Modi and Fernando, 1989; Kotb and Aldoss, 1991). The velocities and pressure distributions on both sides of the turbine blades are obtained with an assumption of uniformly distributed vortices over the length of the element. The torque and power generated can be obtained from the velocity and pressure distribution.

Consequently, various computational fluid dynamics (CFD) methods such as finite volume method, finite difference method and finite element method have been implemented for discretizing the flow governing equations around the SSWT. Due to complex computational geometry, finite difference method is overruled by the other two methods. A few studies have been made using finite element method (Saha *et al*., 2005; Yaakob *et al*., 2010). However, the recent developments of three-dimensional finite volume–based commercial codes (e.g., ANSYS Fluent, CFX, Star CCM+) have shown a remarkable potential for predicting the flow behavior and performance of Savonius-style wind turbines. The computational methodology, more explicitly the selections of turbulence model, grid size, and boundary layer formed on the turbine blades are regarded as the most important criteria.

Among the various turbulence models, the Spalart-Allmaras (SA) model is a simple one-equation turbulence model, where the near wall gradients of the transported variable are much smaller than the turbulent kinetic energy equation based (k-ϵ) models. This might made this model less sensitive in the near walls treatment around the Savonius rotor. However, a 3D CFD simulation using SA model was carried out to compare the performance of vertical-axis spiral rotor with two end plates and one middle plate with a conventional Savonius rotor. Results of the simulation depicted that torque performance of the spiral rotor was more favorable during its whole rotation cycle (Can *et al*., 2010).

The standard k-ϵ model (Launder and Spalding, 1974) is the basic k-ϵ turbulence model and more suitable when flow is fully turbulent and has given better results than SA model for turbine analysis (Pope *et al*., 2010). Two-dimensional steady computational studies were subsequently carried out for Savonius rotor and for combined Savonius-Darrieus rotor. However, due to high unsteadiness and two-dimensional assumption, the computational results have not guaranteed the accuracy of the standard k-ϵ model (Debnath *et al.*, 2008; Debnath *et al.*, 2009). Using the standard k-ϵ turbulence model, a 3D study was made on a helical Savonius rotor and the results obtained (Zhao *et al*., 2009) had shown a general agreement with the experimental data (Kamoji *et al*., 2009). Renormalization of the k-ϵ model gives an additional term in the ϵ-equation and significantly improved the accuracy for swirl flows, which is well known as RNG k-ϵ turbulence model. The prediction ability of the RNG model is also observed in the studies of Yonghai *et al*. (2009) and Emmanuel and Jun (2011). In another study using RNG k-ϵ turbulence model, it is observed that 2D simulation has over predicted the rotor performance, whereas 3D simulation has shown more accurate predictions (Howell *et al*., 2010). The realizable k-ϵ model gives a new formulation for turbulent

viscosity and dissipation rate and is comparatively newer from the other *k-ϵ* turbulence models. As seen from the reported investigations, both the realizable and RNG *k-ϵ* models have found to be significantly improved models over the standard *k-ϵ* and SA models.

The shear stress transport (SST) *k-ω* turbulence model is a two-equation eddy viscosity model combining the advantages of both *k-ϵ* formulation for free stream flow and *k-ω* formulations in the blade surfaces (Menter, 1993; Menter, 1994). Using this model, Abraham *et al.* (2011) have carried out a two-dimensional study on the SSWTs. There seems to be a general agreement between computational and experimental data as shown in Figure 2.12. Further, using three-dimensional SST *k-ω* turbulence model, a very good agreement with the experimental results is found in the work of Plourde *et al.* (2012). The prediction capability of the SST *k-ω* turbulence model for flow analysis over a Savonius-style wind turbine is also observed in the recent studies of Edwards *et al*. (2012) and Jaohindy *et al*. (2013).

Apart from CFD, various soft-computing techniques like fuzzy logic, artificial neural networks (ANN) and genetic algorithms have shown significant capability for prediction of power factor of several energy systems. Sargolzaei (2007) has predicted the power ratio with different Reynolds number and different wind speed for Savonius turbines through the ANN study. The results have shown a reasonable agreement with the experimental results for maximizing the power and efficiency of the turbine. Further research on adaptive neuro-fuzzy inference system (ANFIS) has been carried out in order to find out the effectiveness of ANFIS with comparison to fuzzy inference system (FIS) and RBF-ANN simulation. Figure 2.13 shows a comparative study of these approaches, which is depicting the advantages of ANFIS over other methods (Sargolzaei and Kianifar, 2010).

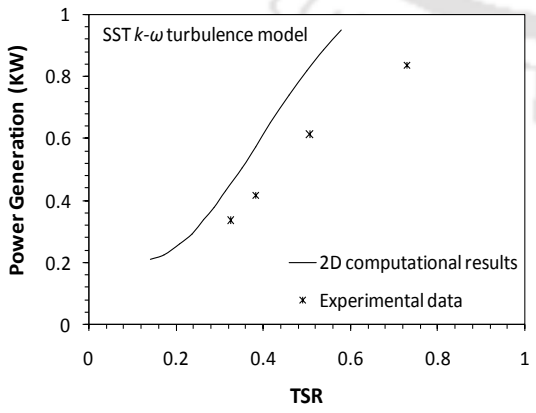

Figure 2.12: Simulation results with SST $k-\omega$ turbulence model (Abraham *et al.*, 2011)

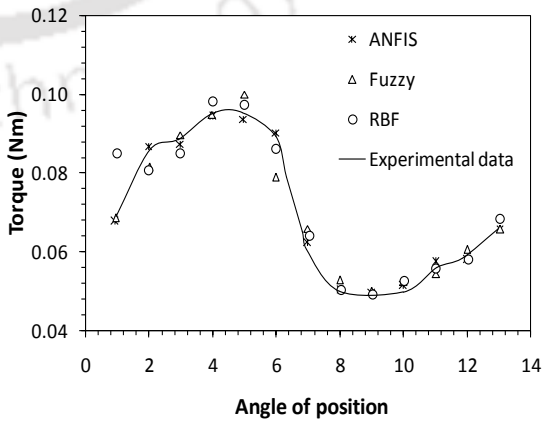

Figure 2.13: Comparative study of different soft computing techniques (Sargolzaei and Kianifar, 2010)

2.5 Summary

Arguing the options for small, low-cost, easily operated, and easily maintained wind energy conversion systems for rural and urban uses, the Savonius-style wind turbines can be a viable option. It can be said that out of all the renewable machines, the Savonius-style turbine is the simplest and of lowest cost but it has comparatively low efficiency and a low power output.

This class of turbines has a high solidity factor compared to other well-established counterparts of lift-type convertors, and thus, is not suitable for large-scale power generation. However, a further modification in the design of SSWTs will make it a good contender for small-scale applications where the advantages of confined space of installation, low wind speed, low cost and simple construction, decentralized power generation, and the direction-independent operation of turbines are the prime concerns. The computational methodology used set a platform for further analysis using various turbulence models to predict the flow behaviour around these SSWTs. Thus, the objective of the present investigation is set to develop a novel Savonius-style wind turbine with the intention of improving its performance in terms of power and torque coefficients, starting characteristics, and also to analyze the flow behaviour around this turbine. This is accomplished by the following steps:

(a) Performance and flow analysis of conventional Savonius-style wind turbine at rotating conditions through unsteady simulations.
(b) Unsteady simulations for the Bach type blade profile by varying its blade arc angle and blade overlap distance so as to obtain a better Bach type design.
(c) Development of new correlations for the wind tunnel blockage correction.
(d) Wind tunnel experiments of the turbine models obtained from the simulation studies.
(e) Evolving a new blade shape from the experiments of above models by varying their blade arc length, blade profile, and overlap.
(f) Wind tunnel tests of the newly developed SSWT followed by its comparative analysis with other existing designs.
(g) 3D unsteady simulation of the newly developed SSWT to analyze its performance and flow behavior.
(h) Estimating of overall efficiency and payback period of a wind energy conversion system (WECS) using the newly developed SSWT.

CHAPTER –3

2D Unsteady Simulations

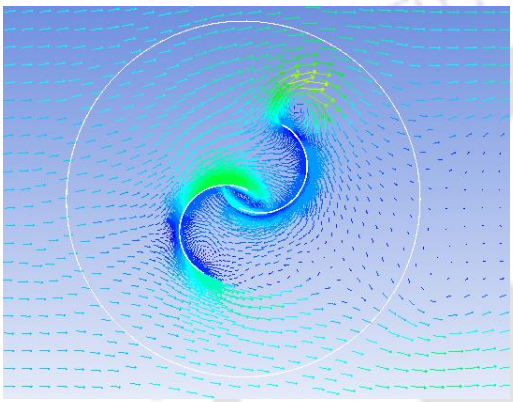

Chapter Outline

Overview

This chapter reports the 2D unsteady simulations carried out on the conventional and Bach type SSWTs. Initially, various turbulence models are tested to predict the performance of a conventional SSWT and using the most suitable model, the performance and flow properties are analyzed at rotating conditions. The various flow patterns are discussed. The performance indices such as torque coefficient (C_T) and power coefficient (C_P) are calculated. The effect of blade overlap ratio on the conventional design is analyzed in the range of δ = 0.00–0.30. A better performance is identified at δ = 0.20. Further, a series of unsteady simulations are carried out on Bach type SSWTs by varying the overlap ratio in the range of δ = 0.00–0.50 and blade arc angle, ϕ = 90–165°. The simulation studies show an improved Bach type design at δ = 0.40 and ϕ = 135°. Simulations are also carried out at static conditions to the analyze drag and lift coefficients for the best designs of conventional and Bach type SSWTs. Results indicate a significant improvement in the lift characteristics of Bach type SSWT over that of conventional semi-circular SSWT.

3.1 Background

To study the flow characteristics and performance of SSWTs, the opportunity for computational fluid dynamics is being highlighted in some of the recent investigations (D'Alessandro *et al*., 2010; Abraham *et al*., 2012; Plourde *et al*., 2012; McTavish *et al*., 2012; Jaohindy *et al*., 2013; Kacprzak *et al*., 2013). The selection of computational methodology plays a vital rule to predict the performance of these turbines (Akwa *et al*., 2012). To discretize the flow governing equations over the SSWTs, various CFD methods such as finite volume method, finite difference method and finite element method have been implemented till now and a general agreement of using finite volume method is found more suitable due to the complex geometries of SSWTs.

As found in the open literature, a host of authors have reported computational investigations on (SSWT) with unsteady as well as steady flow assumptions. In an earlier numerical work by Fujisawa *et al*. (1995), a comparative study was made with the experimental data where the pressure contours and flow visualization were studied with a steady state flow assumption. The impacts of steady two-dimensional studies are also found in some of the recent numerical investigations (Altan and Atilgan, 2008; Gupta *et al*., 2009; Debnath *et al*., 2009). As the flow around these turbines is highly unsteady and turbulent in nature, the unsteady simulations would give necessarily more accurate results, and these are observed in the recent numerical investigations (Afungchui *et al*., 2010; Abraham *et al*., 2011; Abraham *et al*., 2012; Zhou *et al*., 2013). In the aspect of prediction capability, the three-dimensional computational studies always give improved performance over two-dimensional studies; however, they involve very high computational cost as compared to later (Abraham *et al*., 2012). Since, the flow pattern is almost symmetric throughout the height of the turbine, for larger aspect ratios (AR $\geq$1) the two-dimensional studies can adequately capture the significant features of the fluid flow with lesser computational cost (Abraham *et al*., 2011).

In reality, it is possible to optimize the performance of the turbine by changing the electrical loads. As the load changes the rotational rate of the turbine also changes. Thus, optimization can be performed at various loads so that a dynamic electrical system can adjust as the wind speed altered in the reality. The performance can be studied with respect to various TSRs. However, in the computational study, it is not possible to incorporate directly electrical loads; rather it is possible to give a certain rotational rate to the turbine to form a dynamic system.

Initially, a static 2D simulation study was carried out on conventional semi-circular SSWTs at different angular positions. The effect of overlap ratio (δ) on the static performance of SSWTs were tested for δ = 0.00, 0.10, 0.15, 0.20, 0.25 and 0.30 at wind speeds in the range of 5–11 m/s. For conventional SSWT without any overlap, a large variation of the static torques was observed in the complete rotational cycle of the turbine (θ = 0° to 360°). High negative torque values on the returning blade of the turbine were found to be the major drawback for this turbine. However, with the increase in the blade overlap distance, large variations and the effect of negative torque was slightly reduced. A better performance characteristics was identified for δ = 0.20. Higher values of static torque coefficients were observed at angular positions of θ = 30° to 70° and 210° to 250°; whereas, lower static torque coefficients were obtained at θ = 105° to 150° and 285° to 330°.

In the present work, 2D unsteady simulations are carried out to study the performance and flow characteristics of conventional SSWT at rotating conditions. The influence of overlap ratio (δ) is studied at various TSR. Further, a series of unsteady simulations are performed on Bach type SSWTs by varying its overlap ratio and blade arc angle. Finally, an improved design of the SSWT is identified.

3.2 Computational methodology

The flow around the SSWTs is assumed to be unsteady and turbulent, operating at a free stream wind speed of 6.2 m/s. The dynamic simulations are carried out by assigning a certain rotational rate (ω_s in rad/s) to the rotating zone (Figure 3.1) to predict the performance of the turbine in terms of torque coefficient (C_T) and power coefficient (C_P) with respect to TSR. Hence, an artificial dynamic condition is formed as in the real case of dynamic electrical loading. The overall diameter (D) and thickness of SSWT models are taken as 209 mm and 0.63 mm, respectively. Initially, 2D simulations are carried out on a conventional SSWT without any blade overlap, and the trend of C_P variation is compared with the experimental trends of Blackwell *et al*. (1977).

The turbulent flow over the Savonius-style wind turbine is resolved applying the finite volume method into the computational domain and solving the unsteady RANS equations. The governing mass conservation and momentum equations are represented in Eqs. 3.1 and

3.2. In mass conservation equation, $\bar{u}_i$ indicates the mean flow velocity and u_i' indicates the fluctuating velocity due to turbulence, and x indicates the direction of flow. In momentum equation, t is the time, $\bar{p}$ is the mean pressure, μ and ρ represent the dynamic viscosity and density of air, respectively.

$$\frac{\partial}{\partial x_i}\left(\bar{u}_i + u_i'\right) = 0 \tag{3.1}$$

$$\frac{\partial \bar{u}_i}{\partial t} + \bar{u}_j \frac{\partial \bar{u}_i}{\partial x_j} = -\frac{1}{\rho}\frac{\partial \bar{p}}{\partial x_i} + \frac{\mu}{\rho}\frac{\partial^2 \bar{u}_i}{\partial x_j \partial x_j} - \frac{\partial}{\partial x_j}\overline{u_i' u_j'} \tag{3.2}$$

By applying the RANS equations, the fluctuating and mean terms of velocity and pressure increases the number of unknown terms as compared to number of equations. Thus, turbulence models are introduced to solve the unknown terms of RANS equations (Appendix: A).

In the present study, various turbulence models such as standard k-ε turbulence model, realizable k-ε turbulence model, k-ω turbulence model, and shear stress transport (SST) k-ω turbulence model are used and the most suitable model is selected for the further analysis. The details of the computational methodology are discussed in the subsequent sections.

3.2.1 Description of the computational domain

The dimensions of the computational domain as shown in Figure 3.1 are given in multiples of the turbine diameter. The size of the computational domain is selected in such a way that the results are not affected by the boundaries of computational domain. The computational domain includes a circular region with rotating mesh bounded turbine. This circular region (interface) has a dimension of 2D. The turbine models are placed at a distance 3D from the upper and lower sides of the domain. At the inlet of the domain, an inlet velocity of 7 m/s is given, whereas, at the outlet of the domain, the pressure is considered equivalent to atmospheric pressure. The sides of the computational are assumed as symmetrical planes.

3.2.2 Details of the domain discretization

The computational domain is spatially discretized by quad cells to solve the equations using finite volume method. It consists of 2 parts: the first part is fixed mesh region and the other is

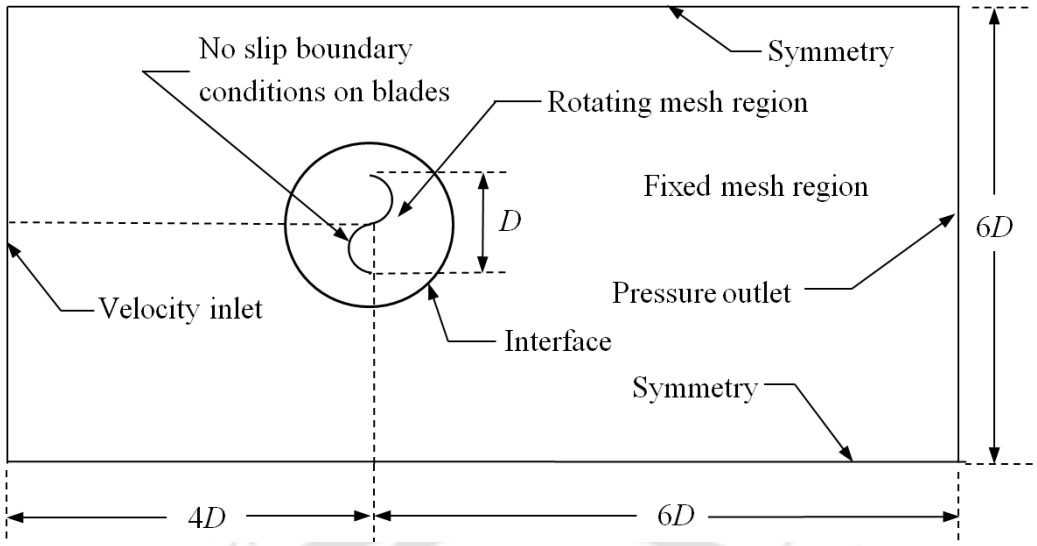

Figure 3.1: Schematic diagram of the computational domain

rotating mesh region as shown in Figure 3.1. The rotating mesh is bounded by the interface of both the parts. The mesh generation in the computational domain is shown in Figure 3.2. The finite volume discretization transforms the differential equations into a set of algebraic equations, which is solved by iterative methods. Thus, the solution is heavily dependent on the number of discretized volumes. For grid convergence, time (Δt) and space (Δx) have been varied and CFL ($=V.\Delta t/\Delta x$) close to 1 is ensured with Δt = 0.001 and Δx = 0.0001. Grid independent test has been carried out (Figure 3.3) and a total of 358542 quad cells have been taken after satisfactory grid refinement.

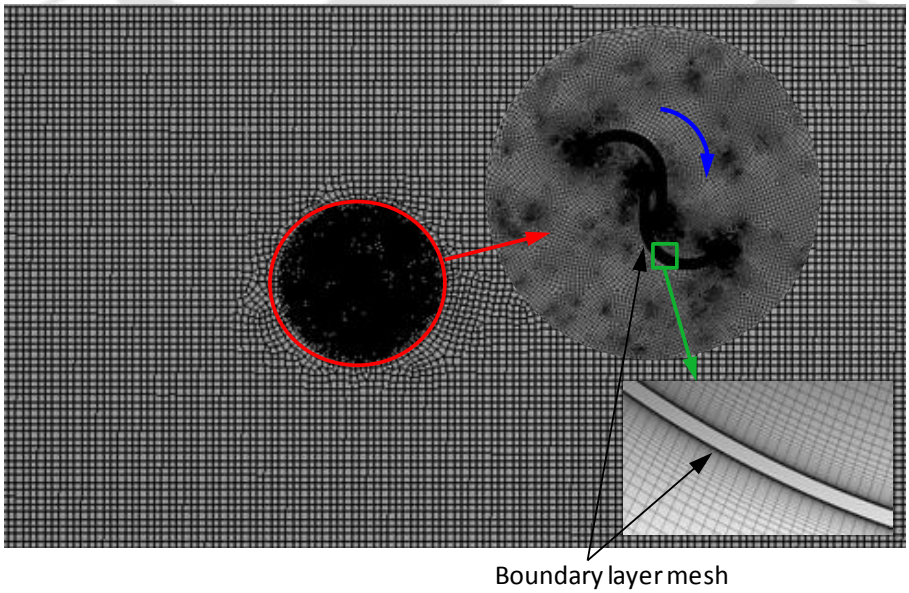

Figure 3.2: Generated mesh in the computational domain

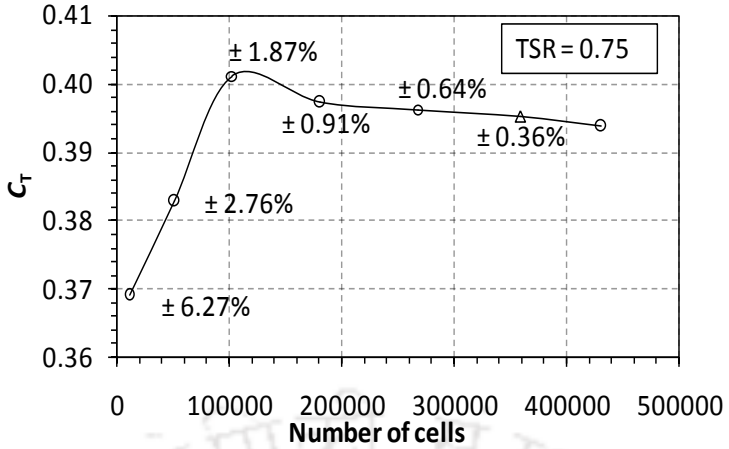

Figure 3.3: Grid independence test

Fine boundary layers are adjusted near the blade surfaces with a first layer thickness of 0.00004 m and the increment ratio of 1.12. Figure 3.4 shows the y+ variations at different time intervals corresponding to half rotation of the turbine. An average y+ value of less than one is ensured throughout the simulations in order to capture the flow properties near the blade surfaces.

3.2.3 Details of the solver

A pressure based transient FVM solver, ANSYS Fluent is used to discretize the equations. The spatial discretization of the conservative equations is treated with 2^{nd} order upwind scheme and the temporal terms of the conservative equations are discretized using 2^{nd} order fully implicit temporal scheme. Good solution stability is ensured through the pressure-velocity coupling with the SIMPLE method (Semi Implicit Linked Equations). For the solution iteration, the time step size and the number of iterations per time step are taken as 0.001 and 20, respectively.

3.2.4 Calculation of performance coefficients

As the simulation is carried out with the unsteady flow assumptions, the performance coefficients are averaged to capture a more accurate time averaged value. The simulations are run for 10 rotational cycle of the turbine. Figure 3.5 shows the variations of torque coefficients at different time intervals. It is observed that after the initial period, it follows almost a cyclic path, and hence, averaged to give a more accurate value.

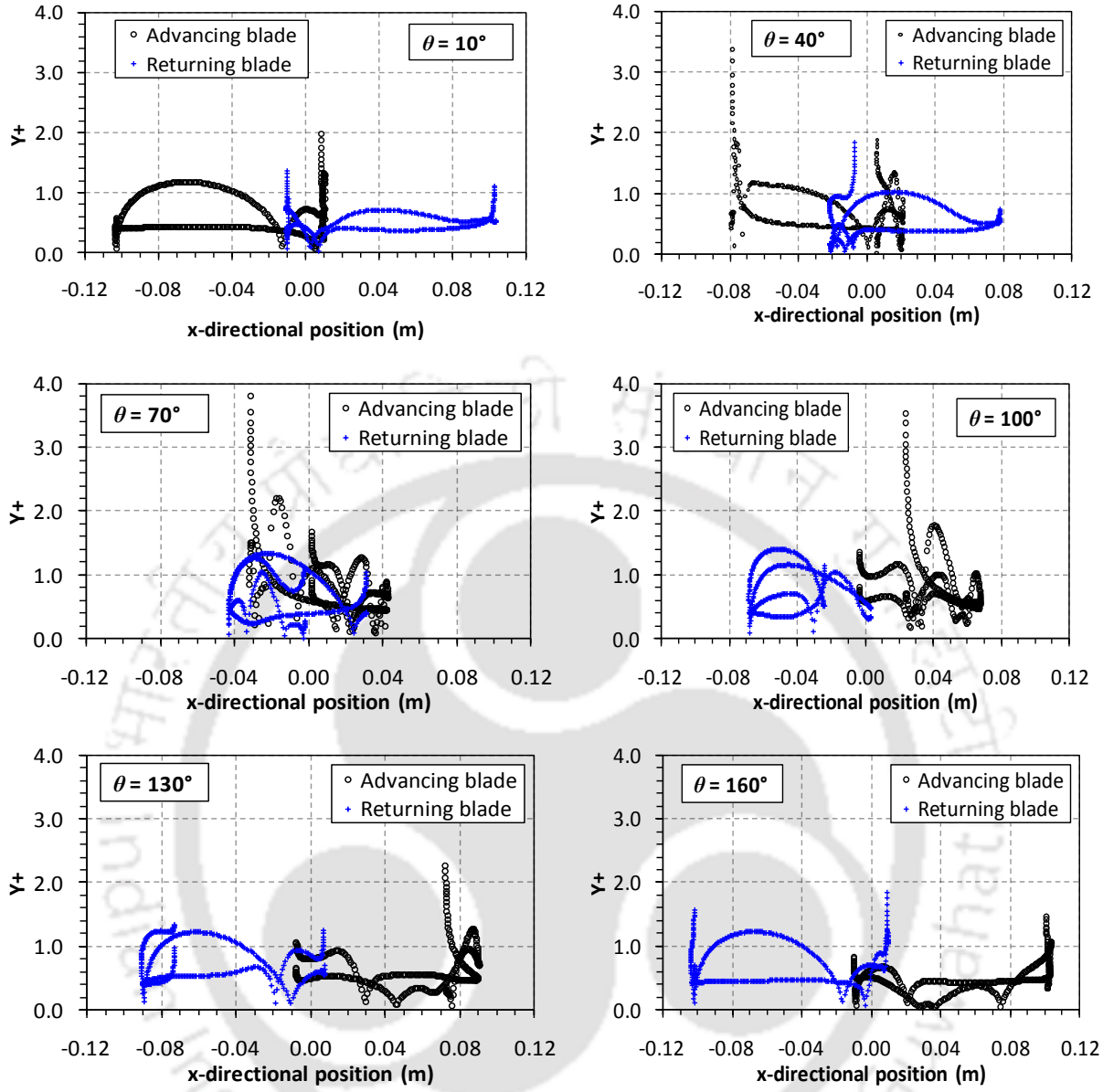

Figure 3.4: Y+ on the turbine blades at different turbine positions

3.2.5 Selection of turbulence model

As the flow field around a SSWT is turbulent in nature, the selection of turbulence models plays a vital role to acquire the desired solution. However, each of the turbulence models has their own merits and demerits. In this research, standard *k*-*ε* turbulence model, realizable *k*-*ε* turbulence model, *k*-*ω* turbulence model, and SST *k*-*ω* turbulence model (Appendix: A) are used to predict the performance of conventional SSWT without any overlap (Figure 3.6). The velocity inlet is given as 7 m/s. The trend of averaged C_P is compared with the experimental trend of Blackwell *et al*. (1977). The SST *k*-*ω* turbulence model is found to be suitable for

further analysis of the turbine as compared to other turbulence models. It is due to fact that the SST *k-ω* turbulence model is a blended model of *k-ω* and *k-ε* turbulence models, comprising the benefits of near wall and free stream capabilities, respectively. The prediction capability of the SST *k-ω* turbulence model is also observed in other recent numerical investigations (Abraham *et al*., 2011; Plourde *et al*., 2012; Abraham *et al*., 2012; Kacprzak *et al*., 2013). With the present computational methodology, the simulation data show an almost similar trend to those of experiments. However, it is observed that due to two-dimensional flow assumption, the numerical results marginally over predicted the experimental data.

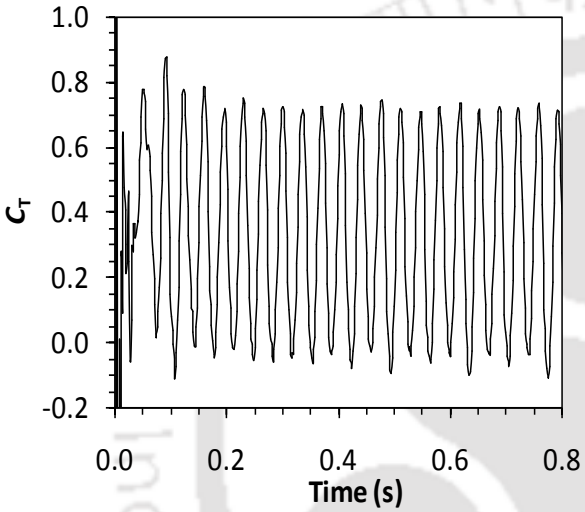

Figure 3.5: Variation of C_T at different time intervals

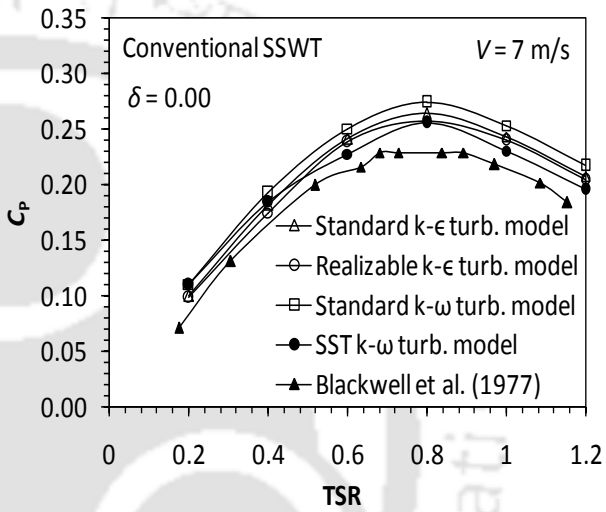

Figure 3.6: Validation and comparative study of various turbulence models

3.3 Analysis on the conventional SSWT

With the SST *k-ω* turbulence model, at V = 6.2 m/s, 2D unsteady simulations are carried out on the conventional SSWT without any blade overlap. The torque coefficient (C_T) and power coefficient (C_P) obtained are shown in Figures 3.7 and 3.8. The variation of C_T shows the effect of rotational speed on the torque generation by the turbine. It indicates a gradual decrease in the generated torque increases the rotational speed of the turbine. This phenomenon is analogous to the electrical loading on the turbine, where with the gradual application of electrical load, the turbine torque increases, which in turn, reduces the rotational speed of the turbine. In this process, for conventional SSWT without any overlap, a highest C_P of 0.25 is obtained at TSR = 0.80.

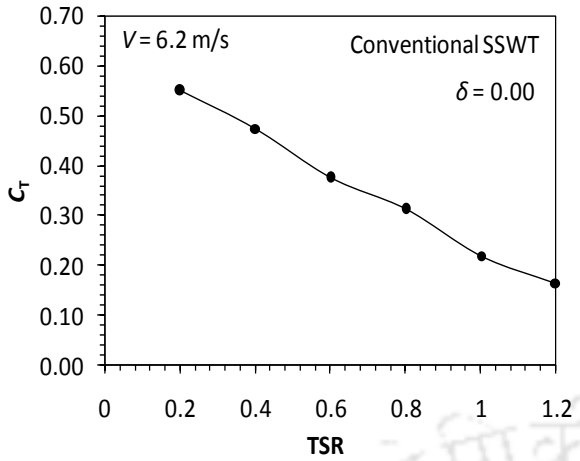

Figure 3.7: Variation of C_T for conventional SSWT without any overlap

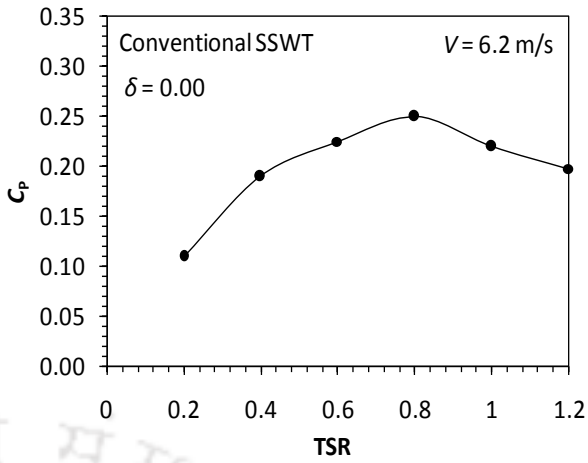

Figure 3.8: Variation of C_P for conventional SSWT without any overlap

Figures 3.9 and 3.10 demonstrate the velocity vector and pressure contour diagrams at different time intervals for conventional SSWT without any blade overlap. During the complete cycle of SSWT, various types of flow phenomena such as free stream flow, Coanda type flow, returning flow, stagnation, separation, and vortices formation are observed around the turbine blades (Figure 3.9).

The free stream wind flow proceeds to various flow patterns once it acts on the Savonius-style wind turbines as shown in Figure 3.9. Coanda-type flow, primarily accountable for producing lift forces on the turbine blades, is observed at angular positions in the range of θ = 0–60° over the advancing blade and θ = 150–170° over the returning blade. Thus, a contribution of lift forces is expected in these regions of Coanda type flow, and hence, the SSWTs cannot be regarded as a pure drag type device. At θ = 90–150°, the Coanda effect is found negligible. Flow separation takes place near the tip of the advancing blade which causes the vortices to form at the downstream of the turbine blades.

At θ = 30–100°, high pressure is observed in the advancing blade (Figure 3.10). In contrast, at θ = 70–160°, the high pressure on the returning blade causes the negative torque generation in the turbine, which adversely affects the power generation capability of the turbine. The negative impact of this pressure is restored to some extent by the returning flow behind the advancing blade which impacts the concave side of the returning blade. The effect of this pressure can be observed in the velocity vector diagrams also, where stagnation zones are visible at θ = 90–160° (Figure 3.9). The flow stagnation, flow separation and formation of vortices are found responsible to reduce the average power of the conventional SSWT.

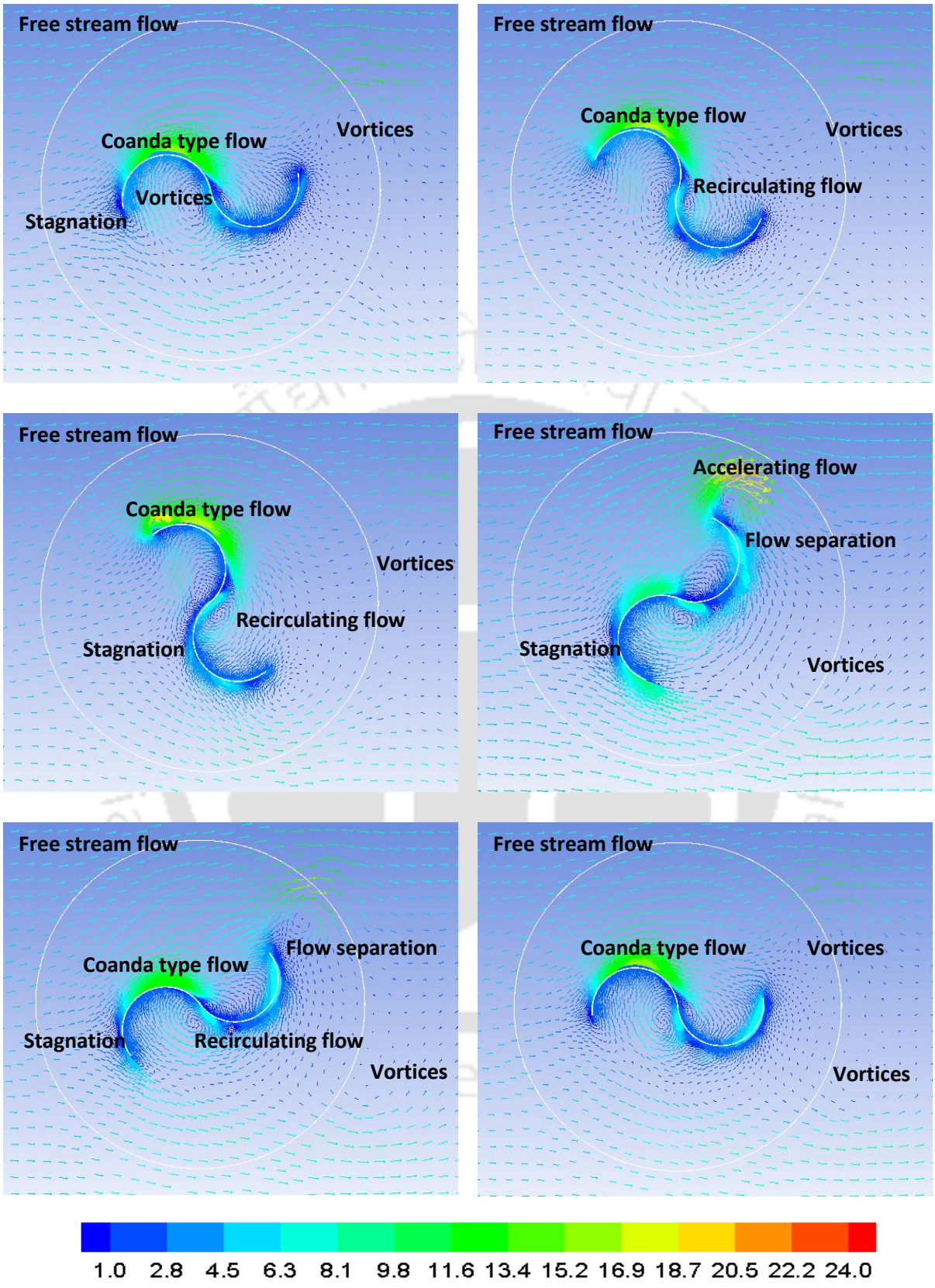

Figure 3.9: Velocity vectors (m/s) around a conventional SSWT without any blade overlap at different time steps under rotating conditions

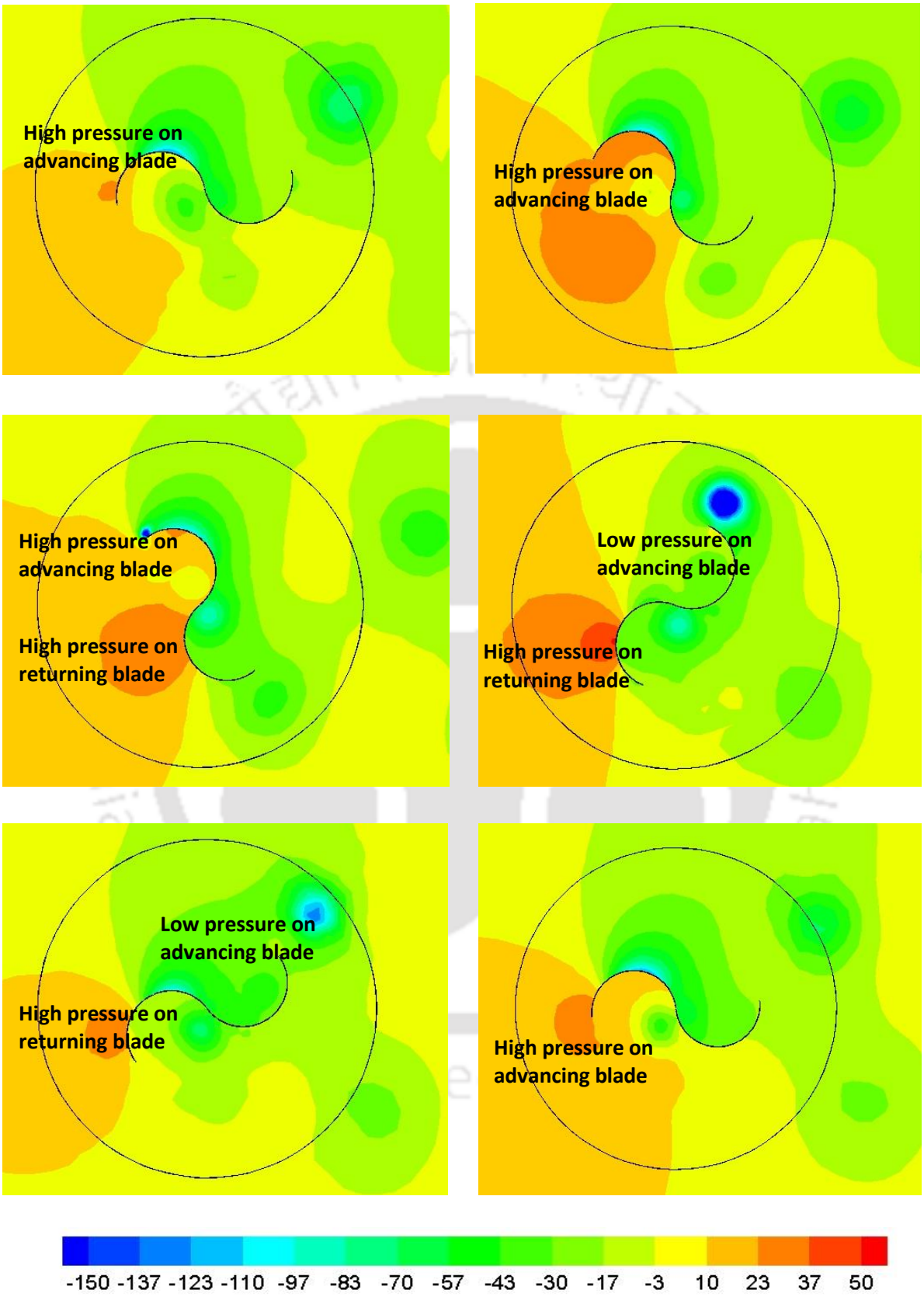

Figure 3.10: Pressure contours (Pascal) around a conventional SSWT without any blade overlap at different time steps under rotating conditions

The effect of overlap ratio (δ) on the performance of conventional semi-circular blades is carried out for δ = 0.00–0.30. The schematic diagrams of various δ are shown in Figure 3.11. The inlet air velocity of V = 6.2 m/s is kept similar to that of the blades without overlap.

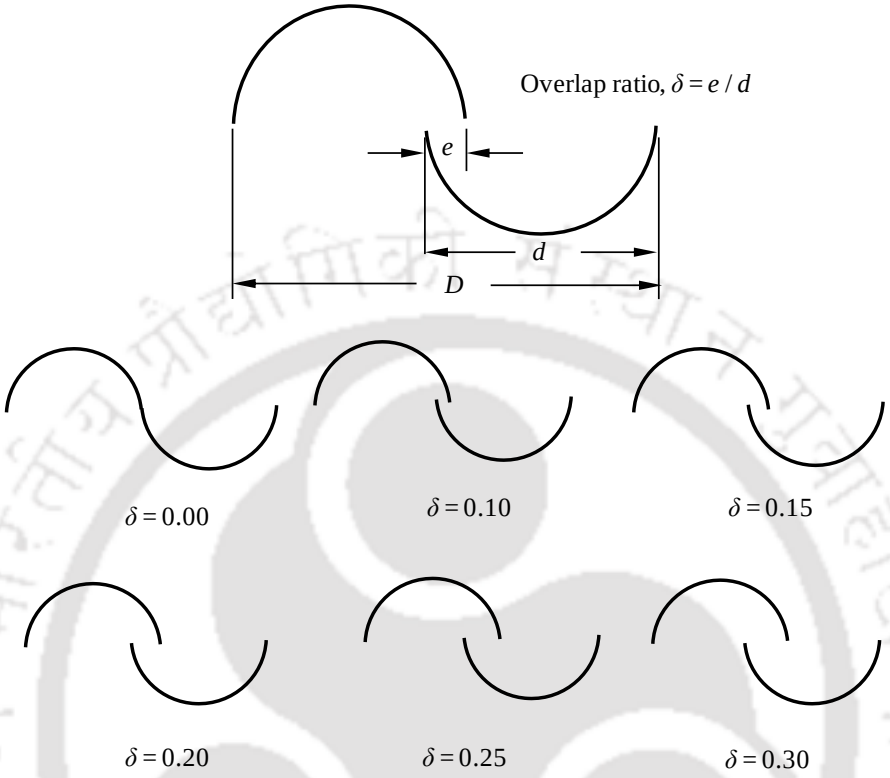

Figure 3.11: Conventional SSWT with various δ

Figures 3.12 and 3.13 show the variations of C_T and C_P for various blade overlap ratios with respect to TSR. It is observed that with the increase of overlap, the C_T and C_P of SSWT have improved up to δ = 0.20, beyond which the performance deteriorated. For conventional SSWT, the highest C_P is found to be 0.29 with δ = 0.20 at TSR = 0.80. Table 3.1 shows the simulation results obtained for various overlap ratios.

Table 3.1: Simulation results of C_T and C_P for conventional SSWT with variable δ

TSR	δ = 0.00		δ = 0.10		δ = 0.15		δ = 0.20		δ = 0.25		δ = 0.30	
	C_T	C_P	C_T	C_P	C_T	C_P	C_T	C_P	C_T	C_P	C_T	C_P
0.20	0.55	0.11	0.58	0.12	0.60	0.12	0.61	0.12	0.58	0.12	0.56	0.11
0.40	0.48	0.19	0.50	0.20	0.52	0.21	0.55	0.22	0.52	0.21	0.49	0.20
0.60	0.38	0.23	0.41	0.25	0.42	0.25	0.45	0.27	0.43	0.26	0.41	0.25
0.80	0.31	0.25	0.34	0.27	0.35	0.28	0.37	0.29	0.36	0.29	0.34	0.27
1.00	0.22	0.22	0.25	0.25	0.26	0.26	0.27	0.27	0.26	0.26	0.26	0.26
1.20	0.17	0.19	0.19	0.23	0.19	0.23	0.20	0.24	0.20	0.23	0.19	0.23

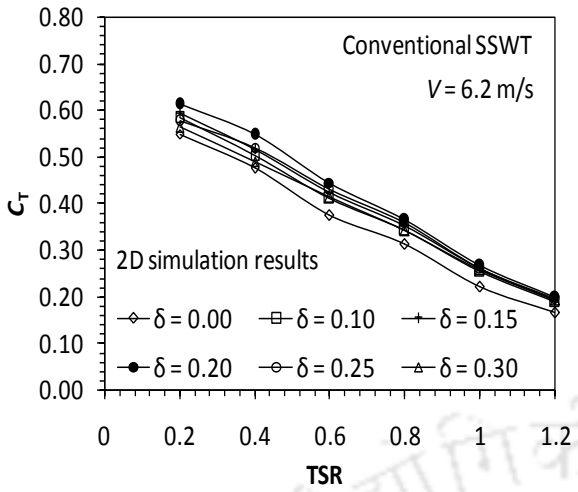

Figure 3.12: Effect of δ on the C_T characteristics of conventional SSWT

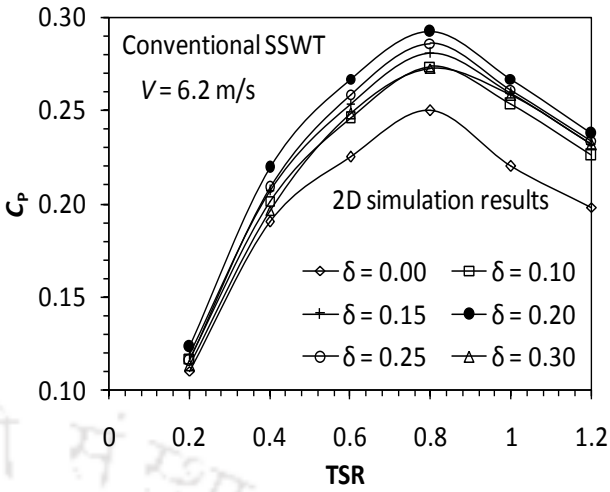

Figure 3.13: Effect of δ on the C_P characteristics of conventional SSWT

Figures 3.14 and 3.15 show the velocity vectors and pressure contours for various overlap ratios in the range of δ = 0.00–0.30. With the implementation of overlap in the conventional design, the flow accelerates near the tip of returning blade and also in the passage of the overlap (Figure 3.14). This enables an additional force to the concave side of the returning blade as well to the advancing blade of the turbine.

In contrast, with the increase of overlap ratio, the pressure contour diagrams show an increase in pressure on the returning blade (Figure 3.15). Thus, an optimum overlap ratio exists at δ = 0.20 where the benefits of flow acceleration retained with the increased pressure on the returning blade. Moreover, for δ > 0.20, a lesser effective pressure is observed on the concave side of the advancing blade due to reduction in the flow incident area. With higher overlap distances, the chances of recirculation in the overlap region reduce the resultant torque on the turbine. Thus, a superior performance is observed at δ = 0.20 over other tested overlap ratios.

Figures 3.16 and 3.17 show the velocity vectors and pressure contours at different time intervals for δ = 0.20. Similar to δ = 0.00 (Figure 3.9), various flow phenomena such as Coanda type flow, recirculating flow, flow separation and stagnation etc. are observed in case of δ = 0.20. However, one exception is the accelerating flow near the tip of the returning blade, which proceeds as an overlapping flow through the blade overlap region and also as the flow incident on the advancing blade (Figure 3.16). Due to this overlapping flow, the pressure on the concave side of the returning blade is found to improve over δ = 0.00 (Figure 3.17).

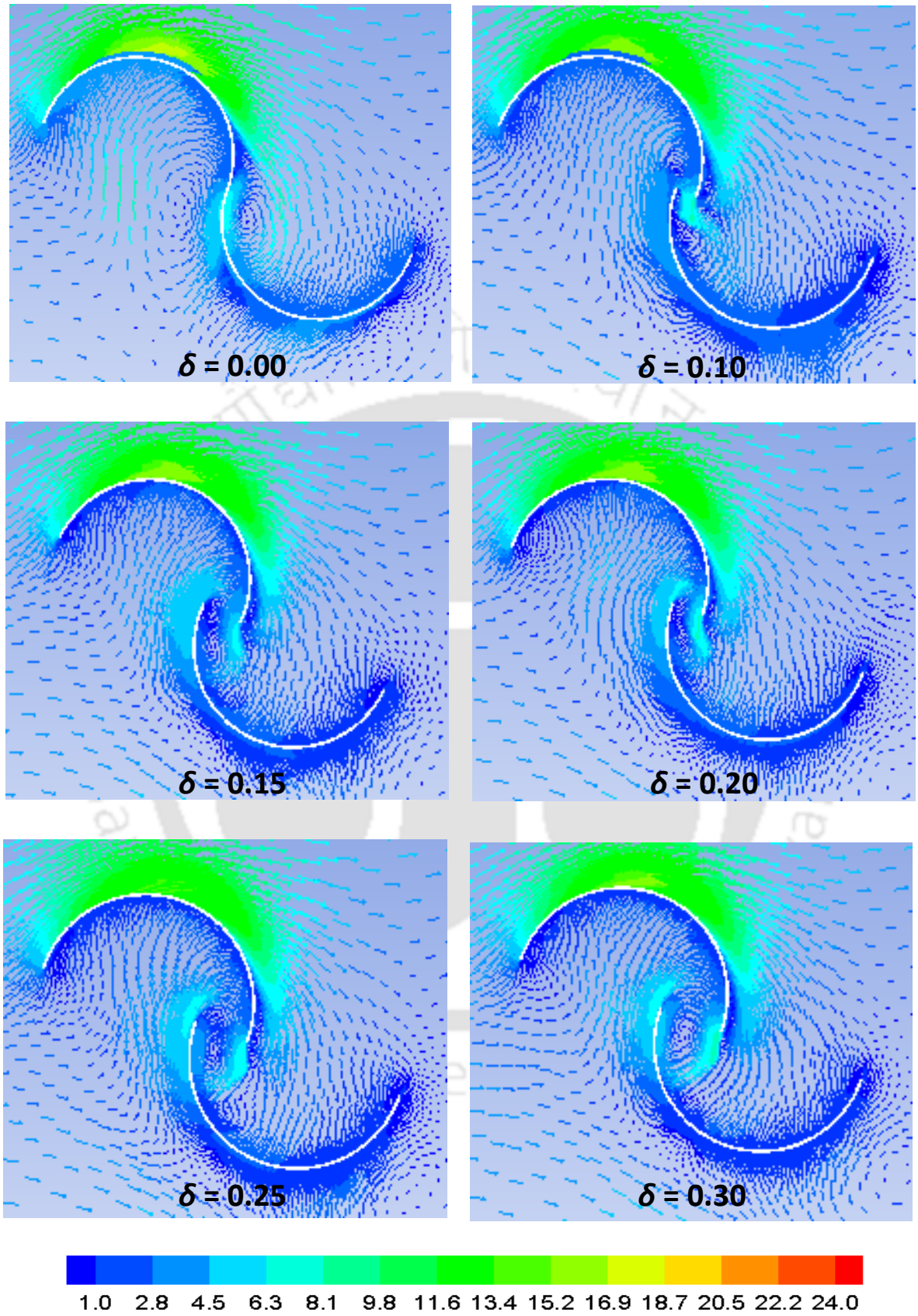

Figure 3.14: Velocity vectors (m/s) around a conventional SSWT with variable δ

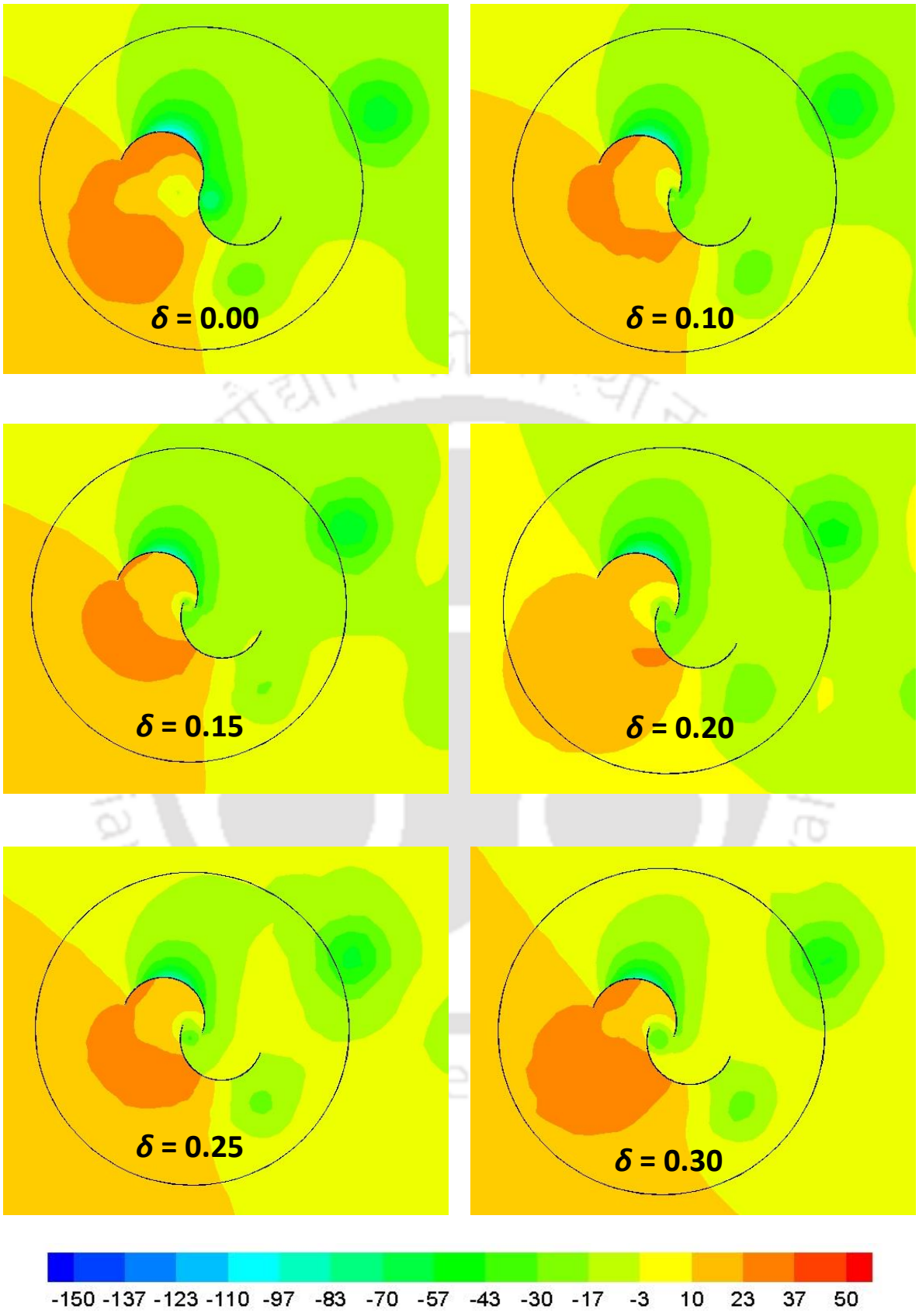

Figure 3.15: Pressure contours (Pascal) around a conventional SSWT with variable δ

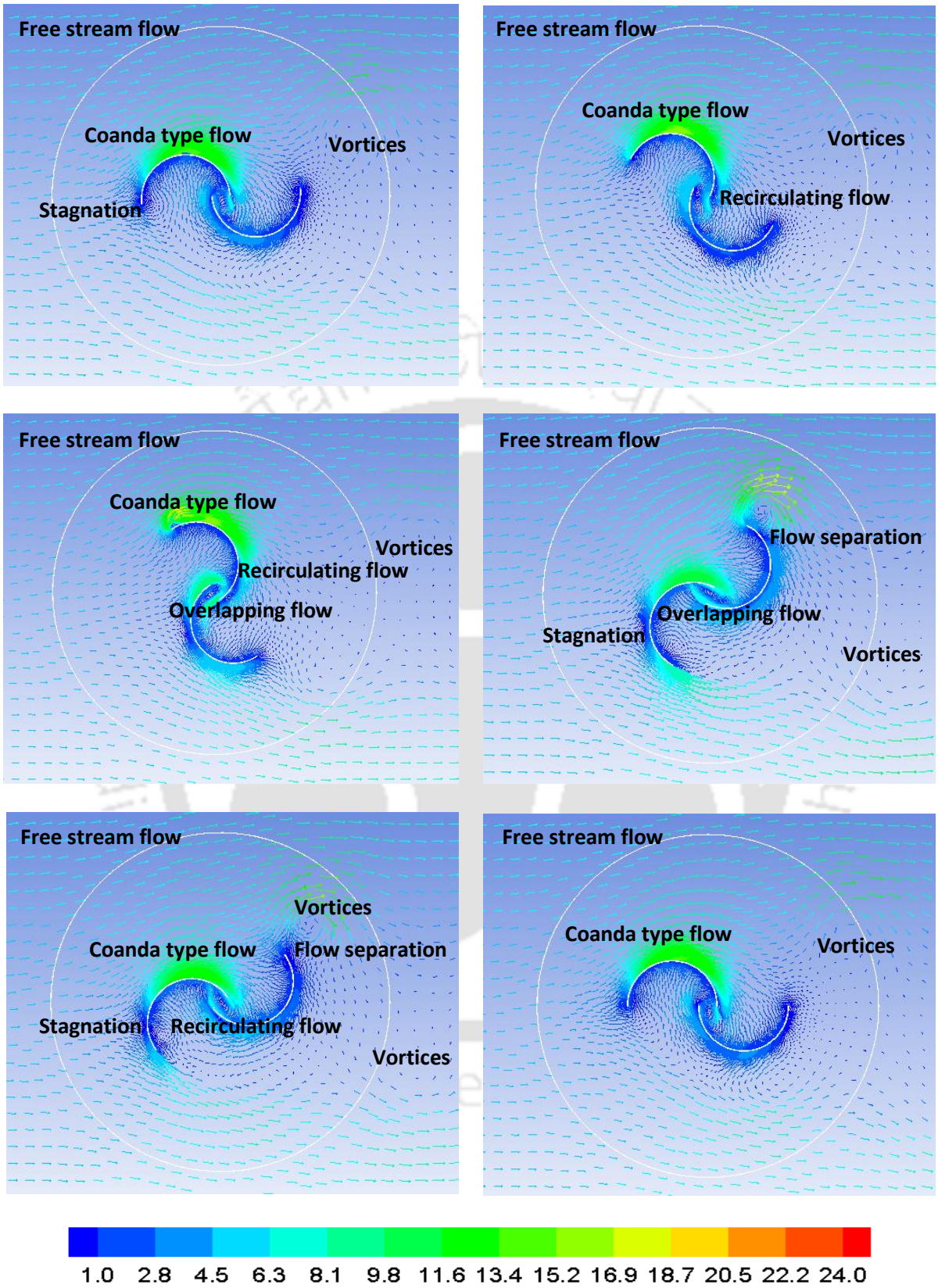

Figure 3.16: Velocity vectors (m/s) around a conventional SSWT with δ = 0.20 at different time steps under rotating conditions

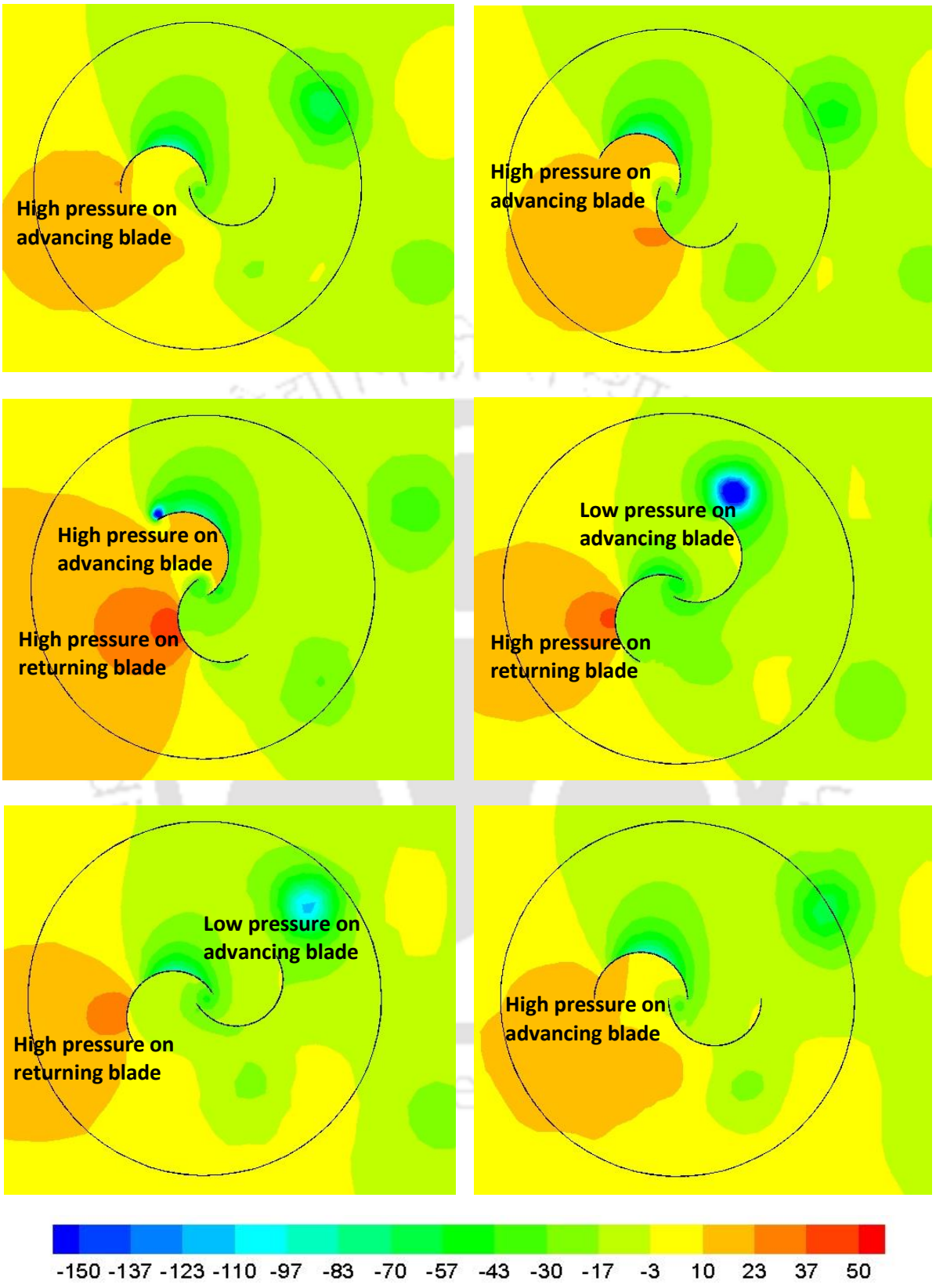

Figure 3.17: Pressure contours (Pascal) around a conventional SSWT with δ = 0.20 at different time steps under rotating conditions

3.4 Analysis on the Bach type SSWT

Apart from the conventional semi-circular design, Bach type blade profiles also find their existence because of their comparatively higher performance indices (Bach, 1931). In the present study, a series of unsteady simulations are carried out on the Bach type SSWT by varying the overlap ratio ($\delta = e / d$) from 0.00–0.50 and by varying the blade arc angle (ϕ) in the range of 90–165°. A typical Bach type blade profile is shown in Figure 3.18, whereas, various blade arc angles are shown in Figure 3.19.

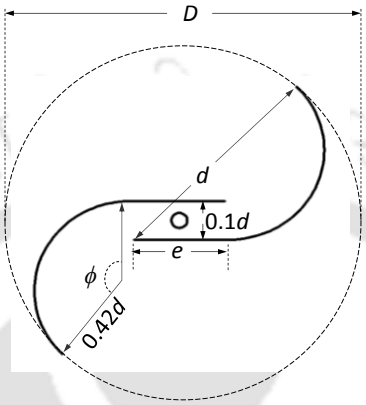

Figure 3.18: Schematic diagram of a Bach type blade profile

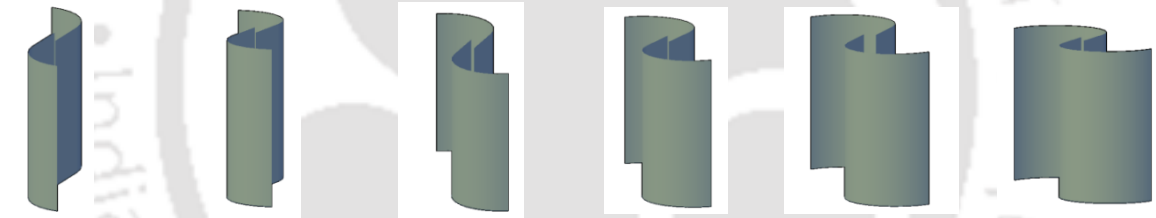

Figure 3.19: Bach type SSWT with variable blade arc angles

Figures 3.20 and 3.21 show the effect of overlap ratios on the performance characterics of Bach type SSWT with a blade arc angle, ϕ = 120°. It has been observed that the performance of Bach type turbines increases with the increase of blade overlap distances. However, the benefits of overlapping flow is observed only up to δ = 0.40, beyond which the performance again deteriorates. It is mainly due to the shortening the flow incident on the advancing blade. Table 3.2 shows the obtained simulation results for various overlap ratios at ϕ = 120°. For ϕ = 120°, a highest C_P of 0.32 is obtained at δ = 0.40, whereas without any overlap, the peak value obtained as 0.28. Thus, at constant δ = 0.40, further analysis have been carried out for various blade arc angles in the range ϕ = 90–165°.

Figures 3.22 and 3.23 show a comparative analysis of various blade arc angles (ϕ), where performance gains are observed with the increase of blade arc angle from ϕ = 90°–135°,

beyond which again decreases. All the simulations have confirmed peak performances at TSR = 0.8. Table 3.3 show the simulation results for the tested blade arc angles. For Bach type SSWT, The highest C_P is found to be 0.34 at ϕ = 135° and δ = 0.40. Thus, with a modified Bach type design, a performance gain of 17.2% can be achieved over conventional semi-circular design.

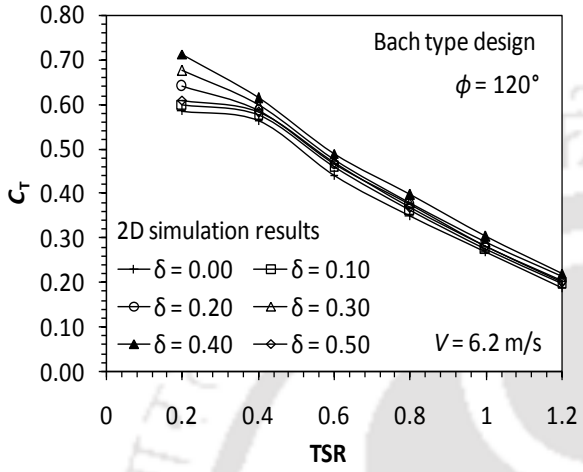

Figure 3.20: Variation of C_T for Bach type SSWT at variable δ with ϕ = 120°

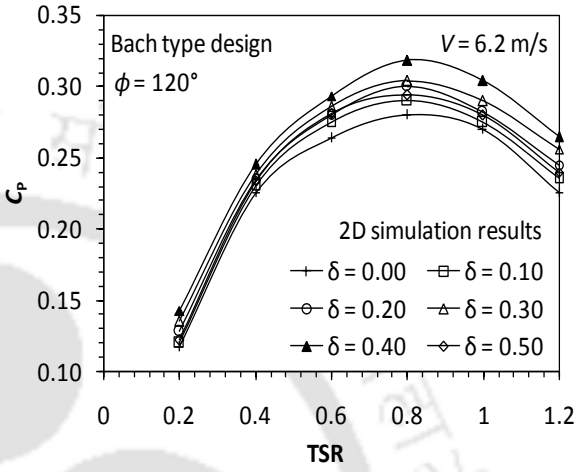

Figure 3.21: Variation of C_P for Bach type SSWT at variable δ with ϕ = 120°

Table 3.2: Simulation results of C_T and C_P for Bach type SSWT with variable δ at ϕ = 120°

TSR	δ = 0.00		δ = 0.10		δ = 0.20		δ = 0.30		δ = 0.40		δ = 0.50	
	C_T	C_P	C_T	C_P	C_T	C_P	C_T	C_P	C_T	C_P	C_T	C_P
0.20	0.59	0.12	0.60	0.12	0.64	0.13	0.67	0.14	0.71	0.14	0.61	0.12
0.40	0.56	0.23	0.58	0.23	0.59	0.23	0.60	0.24	0.61	0.25	0.58	0.23
0.60	0.44	0.26	0.46	0.28	0.47	0.28	0.48	0.29	0.49	0.29	0.47	0.28
0.80	0.35	0.28	0.36	0.29	0.38	0.30	0.38	0.30	0.40	0.32	0.37	0.29
1.00	0.27	0.27	0.28	0.28	0.28	0.28	0.29	0.29	0.30	0.31	0.28	0.28
1.20	0.19	0.23	0.20	0.24	0.20	0.25	0.21	0.26	0.22	0.27	0.20	0.24

The conventional SSWT always suffers from low performance indices because of its high negative torque developed on the returning blades. In the Bach type designs, these negative effects are much overcame due to backflow through the overlapping region and also for the accelerating flow over the convex side of the returning blade (Figures 3.24). It is realized that at ϕ = 90°, the blade arc becomes much shorter and straighter, thereby reducing the effective pressure on the advancing blade as compared higher blade arc angles (Figures 3.25). Again, with the increase of blade arc angle the effective pressure on the convex side of the returning

blade increases. Thus, a better net pressure on the both the advancing and returning blade is observed in an intermediate value of ϕ = 135° (Figures 3.25).

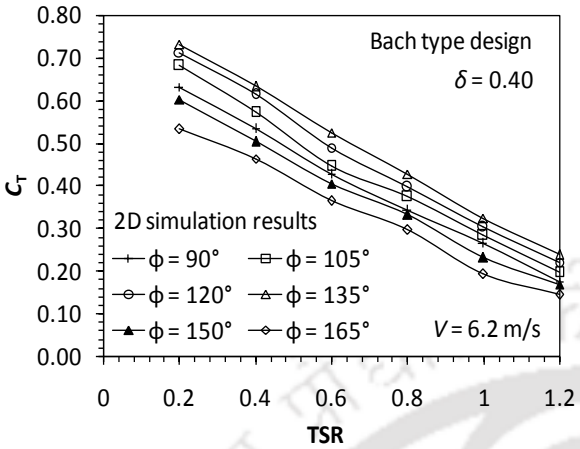

Figure 3.22: Variation of C_T for Bach type SSWT with variable blade arc angle at δ = 0.40

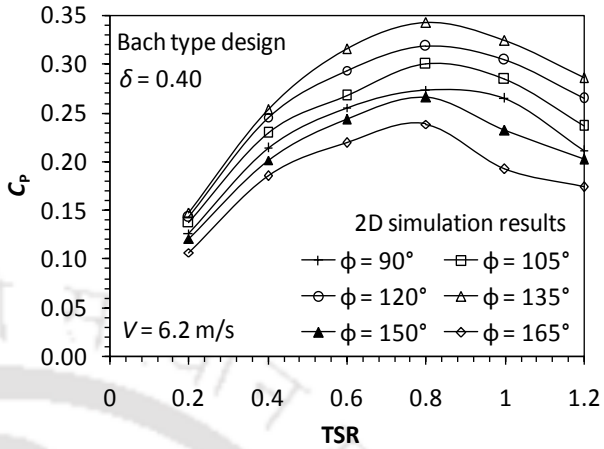

Figure 3.23: Variation of C_P for Bach type SSWT with variable blade arc angle at δ = 0.40

Table 3.3: Simulation results of C_T and C_P for Bach type SSWT with variable ϕ at δ = 0.40

TSR	ϕ = 90°		ϕ = 105°		ϕ = 120°		ϕ = 135°		ϕ = 150°		ϕ = 165°	
	C_T	C_P	C_T	C_P	C_T	C_P	C_T	C_P	C_T	C_P	C_T	C_P
0.20	0.63	0.13	0.68	0.14	0.71	0.14	0.73	0.15	0.60	0.12	0.53	0.11
0.40	0.53	0.21	0.57	0.23	0.61	0.25	0.63	0.25	0.50	0.20	0.46	0.19
0.60	0.43	0.26	0.45	0.27	0.49	0.29	0.53	0.32	0.41	0.24	0.37	0.22
0.80	0.34	0.27	0.38	0.30	0.40	0.32	0.43	0.34	0.33	0.27	0.30	0.24
1.00	0.27	0.27	0.29	0.29	0.30	0.31	0.33	0.33	0.23	0.23	0.19	0.19
1.20	0.18	0.21	0.20	0.24	0.22	0.27	0.24	0.29	0.17	0.20	0.15	0.17

Figures 3.26 and 3.27 show the velocity vectors and pressure contours at different time intervals for the modified Bach type design (ϕ = 135° and δ = 0.40). Apart from the overlapping effect, the effect of Coanda type flow during the complete rotational cycle is also much improved in the Bach type design (Figure 3.26). This improvement will definitely increase the lift contribution to the net power output of the turbine. On the other hand, the pressure contour diagrams (Figure 3.27) indicate a higher pressure on the trailing edge of the returning blade (beyond the axis of rotation) and also at the concave portion of the returning blade. This improved pressure zones certainly offer a positive effect on the net power output of the turbine. Thus, the overall performance coefficients are found to be much higher than the conventional semi-circular SSWT.

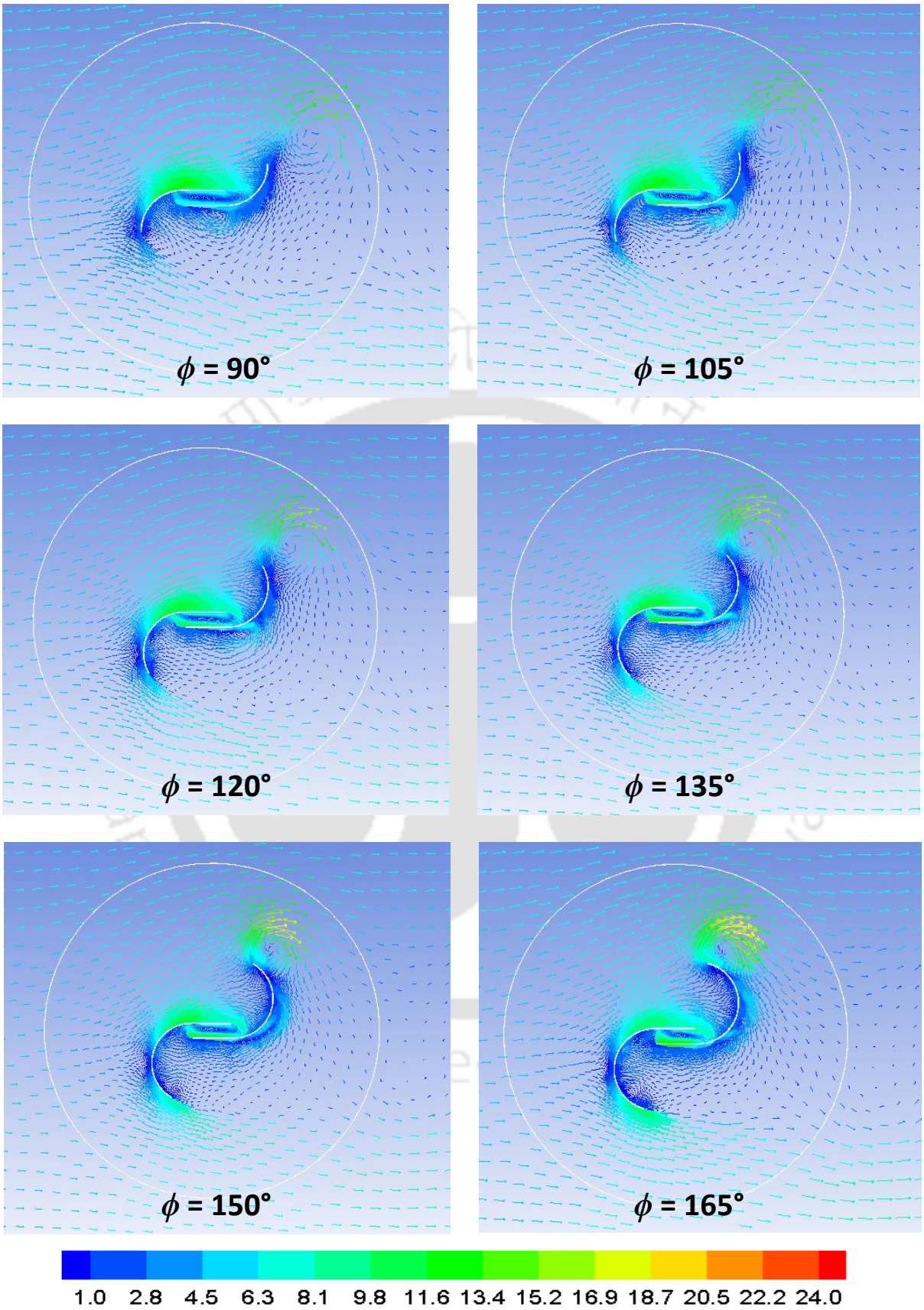

Figure 3.24: Velocity vectors (m/s) around a Bach type SSWT with variable ϕ

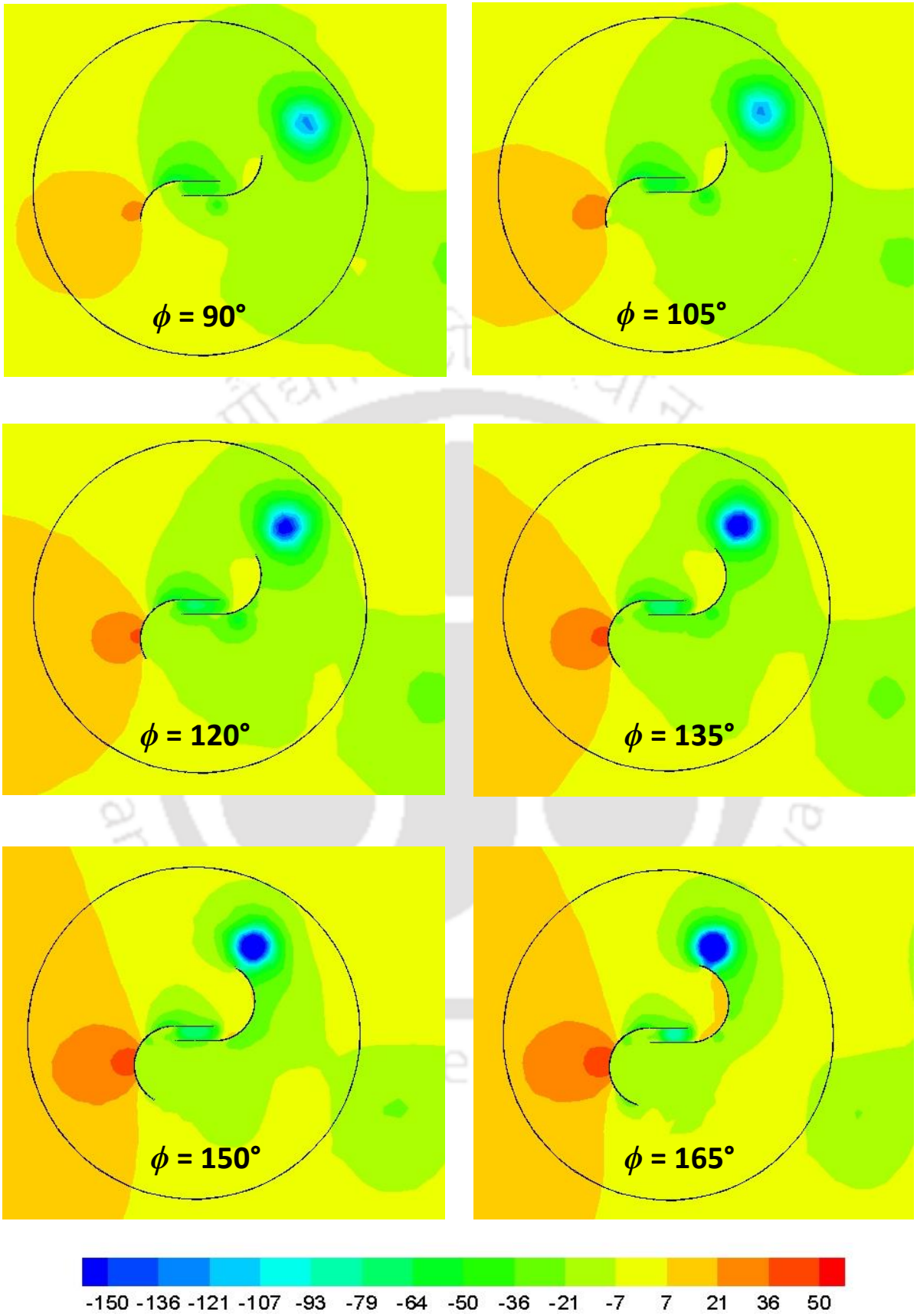

Figure 3.25: Pressure contours (Pascal) around a Bach type SSWT with variable ϕ

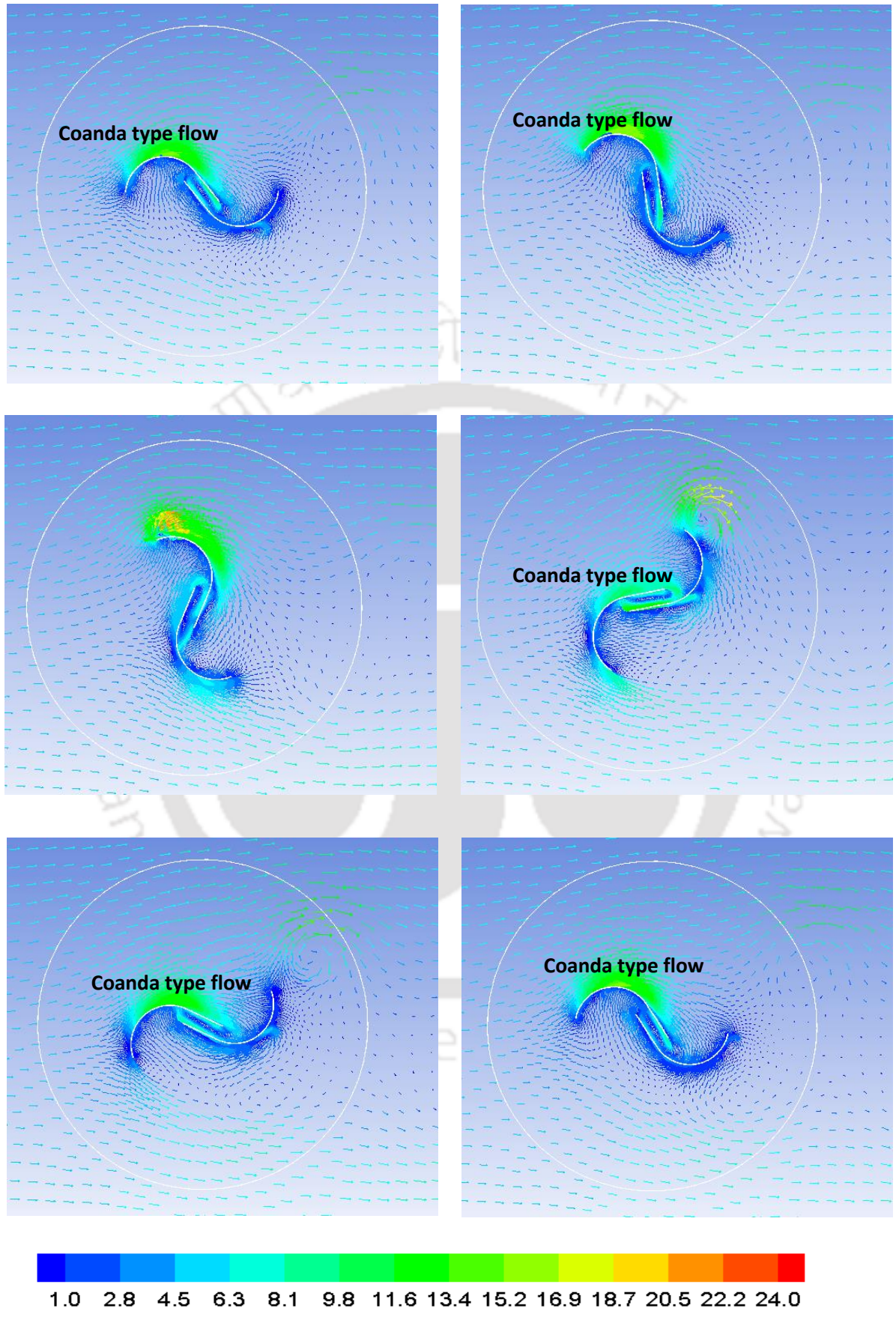

Figure 3.26: Velocity vectors (m/s) around a Bach type SSWT with ϕ= 135° and δ = 0.40

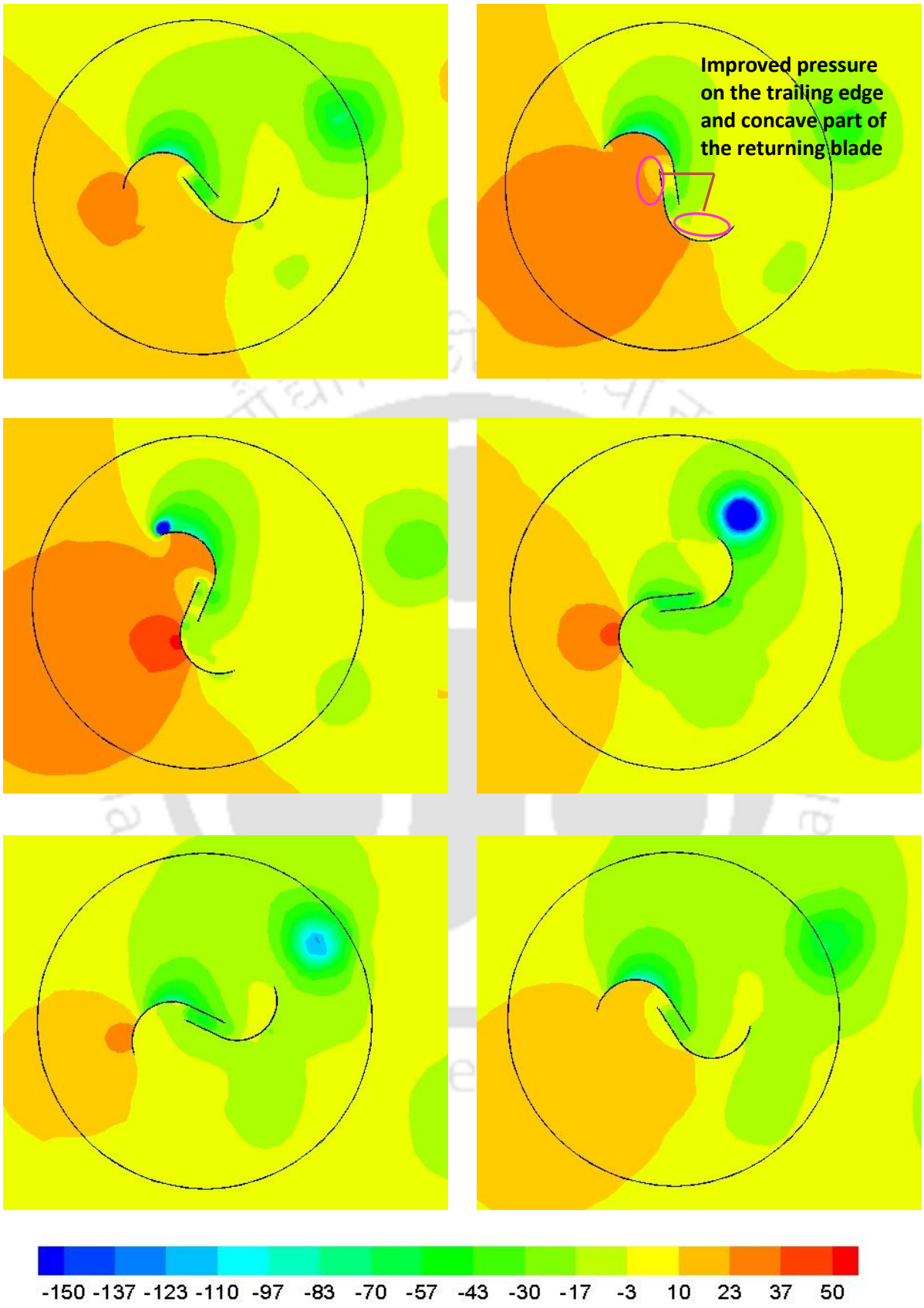

Figure 3.27: Pressure contours (Pascal) around a Bach type SSWT with ϕ= 135° and δ = 0.40

To extend the analysis, static simulations are carried out in order to study the effects of drag and lift coefficients for the modified Bach type SSWT (δ = 0.40, ϕ = 135°) in comparison with conventional semi-circular type SSWT (δ = 0.20) in the complete rotational cycle. The turbine models are fixed at a certain angular positions (θ = 0–360°). In this study, no rotational speeds are assigned to the turbine. For each of the angular positions, the drag and lift coefficients are calculated by averaging the values over different time intervals as shown in Figures 3.28 and 3.29.

Figure 3.28 shows that the drag coefficient (C_D) increases gradually as the turbines rotate from 0° to 90° and attains peak values of 1.17 and 1.04 for modified Bach and conventional SSWTs, respectively. Again, from 90° to 180°, the values decreased gradually. These variations repeat in the next half rotational cycle of the turbines. Comparatively high values of C_D is obtained for modified Bach type design at angular positions of 30° < θ < 150° and 210° < θ < 330°. At θ = 30° and 210°, the effect of C_D is almost similar. However, at θ = 0° and 180°, C_D for modified Bach-type design is less than that of conventional turbine. The major improvement in the modified design is depicted in the analysis of lift coefficient, C_L (Figure 3.29). In all the rotational angles, the values of C_L are found superior for the modified Bach type SSWT. It is observed that at rotational angles of θ = 90° to 150°, the turbines experience very low, more precisely negative values of C_L. However, it is understood that although the drag is the dominating force, the lift is also contributing to the turbine power output. A highest value of C_L = 0.58 is achieved for the modified Bach type design at θ = 30°.

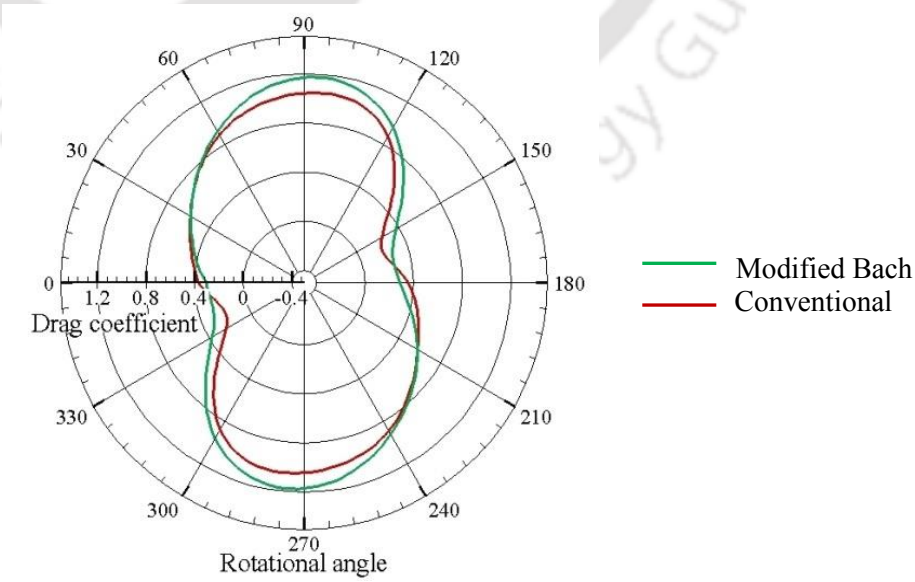

Figure 3.28: Variation of drag coefficients for modified Bach type (ϕ= 135° and δ = 0.40) and conventional SSWT (δ = 0.20)

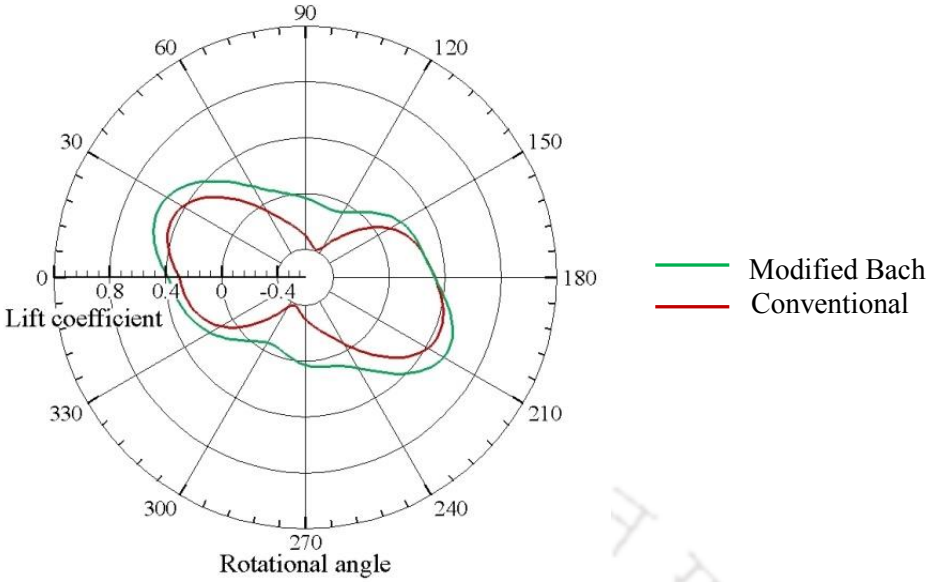

Figure 3.29: Variation of lift coefficients for modified Bach type (ϕ= 135° and δ = 0.40) and conventional SSWT (δ = 0.20)

3.5 Summary

A series of 2D unsteady simulations are carried out to develop an improved blade shape of the Savonius-style wind turbine (SSWT). In this connection, initially, the conventional semi-circular design of SSWT is analyzed which indicates a low performance characteristics due to high pressure drag acting on the returning blade. During the complete cycle of SSWT, various types of flow phenomena such as free stream flow, Coanda type flow, returning flow, stagnation, separation, and vortices formation are observed. The effect of overlap ratio (δ) on the conventional design is studied for δ = 0.00–0.30. It is observed that with the inclusion overlapping flow in the overlap region and accelerating flow near the tip of the returning blade, the pressure effect on the returning blade is marginally compensated. For conventional SSWT, a highest C_P of 0.29 is found at δ = 0.20.

Further, simulations carried out on Bach type designs for various overlap ratios (δ = 0.00–0.50) and blade arc angles (ϕ = 90°–165°). From this study, an improved configuration of Bach type SSWT is identified at ϕ = 135° and δ = 0.40, showing a highest C_P of 0.34. It is observed that the effect of Coanda type flow is more prominent in the modified Bach type SSWT (ϕ = 135° and δ = 0.40) that increases the lift contribution to the net power output of the turbine. This improvement in the lift characteristics over semi-circular SSWT is further observed through the static simulation study. The outcome of these unsteady simulations set the platform for further investigations on SSWTs through wind tunnel experiments.

CHAPTER –4

Experimental Setup

Chapter Outline

Overview

Looking at the outcome of computational study, the experimental investigation is planned and executed. In this chapter, a detailed description is presented on the experimental facility and the instruments used in the present investigation. The existing setup of low speed wind tunnel is repaired, modified and a new test section has been designed to test the performance of Savonius-style wind turbines. The area averaged wind speeds are measured corresponding to various input voltages to the fan-motor assembly. Analogous to the demand of the situations, 3 types of power measurement devices are opted to measure the performance of these turbines; however, the results obtained were found very poor due to large electrical losses in the generator. A mechanical dynamometer is designed and the results obtained with all the measuring devices are validated with the available experimental data obtained under identical conditions. The mechanical measurement shows a reasonable agreement. However, the validation indicates the need of wind tunnel blockage correction in the present experimental setup.

4.1 Experimental facility

An essential tool to study the experimental aerodynamics is the wind tunnel, where a number of aerodynamic designs are tested either inside (closed type test section) or at the exit of wind tunnels (open type test section). This practice continues to evolve and remains to be a keystone in the development for a wide range of wind turbines, vehicles and other aerodynamic devices. In this aspect, to study the performance of Savonius-style wind turbines (SSWTs) under various loading conditions, a low speed wind tunnel was designed, developed and fabricated in 2002 at IIT Guwahati (Grinspan, 2002). As reported in literatures, this wind tunnel has been extensively used for testing of conventional and twisted bladed SSWTs, multi-staging etc. (Grinspan *et al*., 2004; Rajkumar, 2004; Mobinuddin, 2005; Thotla, 2006; Saha and Raj Kumar, 2006; Saha *et al.*, 2008). However, the wind tunnel blockage correction is neglected in all the studies considering a lower blockage correction factor. In the present investigation, this experimental facility has been repaired and modified according to need of present investigation. The schematic diagram of the present experimental set up is shown in Figure 4.1. This experimental facility mainly consists of: (i) a fan section followed by an inlet section, (ii) diffuser section, (iii) settling chamber that contains the coarse screen, a honeycomb structure and a fine screen to make the wind flow streamlined, (iv) a nozzle section to accelerate the flow, and (v) an open test section which includes the turbine model and the necessary instrumentation.

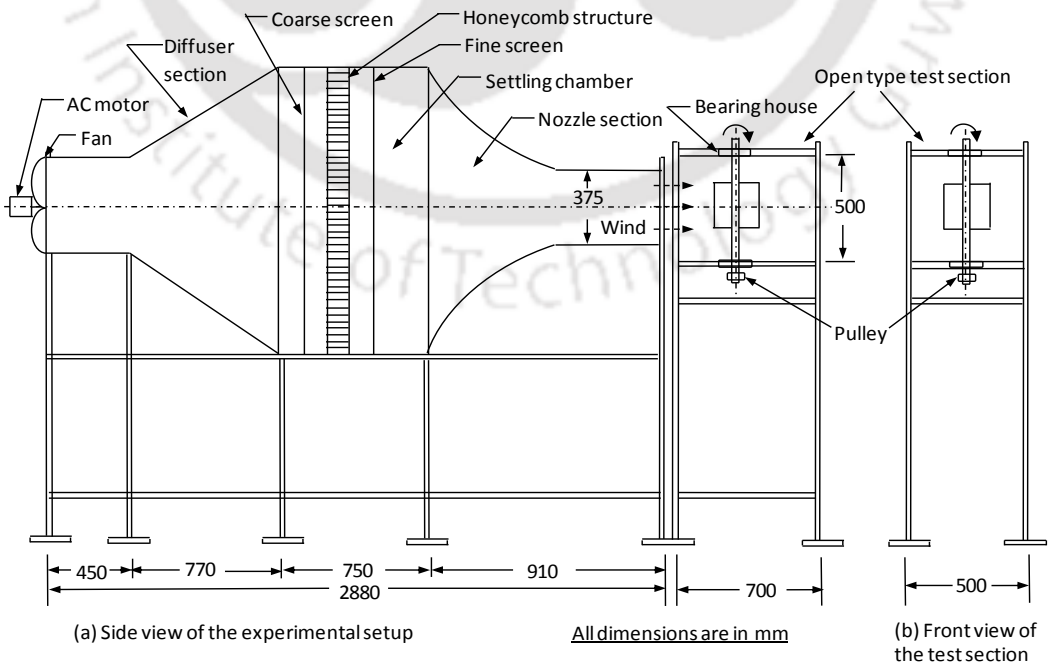

Figure 4.1: Schematic diagram of the wind tunnel

A new open test section facility has been designed, developed and fabricated. As shown in Figure 4.1, the test section is placed at the exit of the nozzle section, having the dimensions of 500 mm width, 500 mm height and 700 mm length, forming a frontal test section area of 500 × 500 mm^2. Figure 4.2 shows dimensions of the new test section and its different parts. The test section is made of mild steel angles of 50 mm × 50 mm × 4 mm, whereas tunnel sides were fabricated from galvanized iron sheets of thickness 1.6 mm.

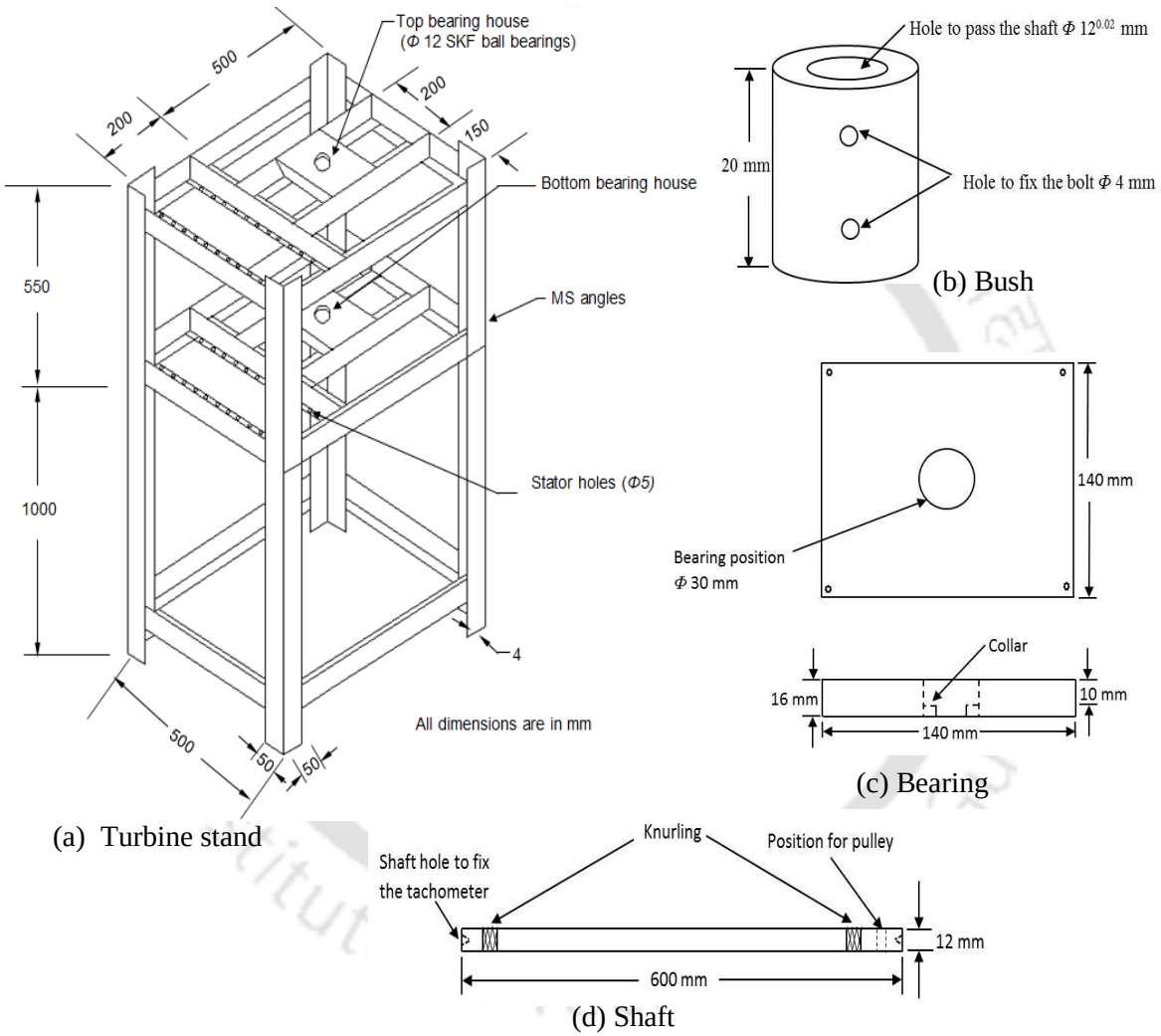

Figure 4.2: Dimensions of the test section and its different parts

The turbine blades are fabricated from galvanized iron sheets of thickness 0.63 mm (Figure 4.3). In the wind tunnel, the wind speed can be obtained in the range of 0–10 m/s by varying the input voltage to a fan-motor assembly. The rating of the motor connected to the fan is 0.5 HP. The wind speed is recorded with help of a hot wire anemometer having an operating range of 0–20 m/s and an accuracy of ± 2% (Model: Testo 490), whereas the rotational speed

of the turbine is measured with the help of a digital tachometer having an accuracy of ± 1% and operating range of 0–50000 rpm (Model: System HTM 590).

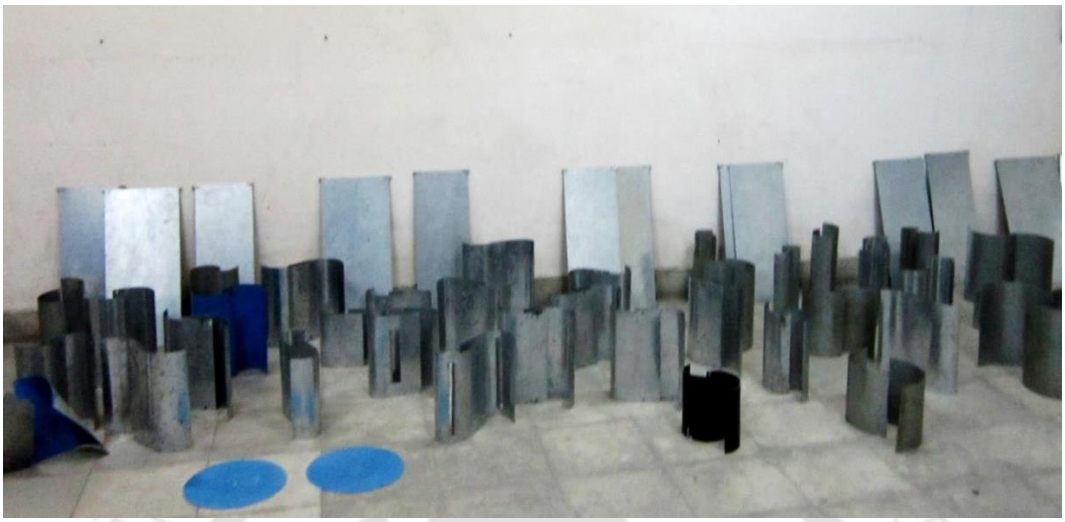

Figure 4.3: Fabricated blades of Savonius-style wind turbines

4.2 Wind speed measurement

The wind speeds corresponding to different input voltages are measured at different locations at the exit section of wind tunnel, and the free-stream wind speed (V) is calculated as an area averaged wind speed using the following equations:

$$\rho AV = \rho A_1 V_1 + \rho A_2 V_2 + ... + \rho A_n V_n \tag{4.1}$$

$$V = \frac{\rho A_1 V_1 + \rho A_2 V_2 + ... + \rho A_n V_n}{\rho A} \tag{4.2}$$

The input voltage is varied from 160–230 volts by means of voltage regulator. Figure 4.4 shows the contour of measured wind speeds at 190 volts. It is observed that at a region of 250 mm × 250 mm, the wind speed is found almost constant. However, at the corners of the exit section (at a distance near to 375 mm), a marginal increase in the wind speed is observed. It is mainly due to the corner effects of nozzle section. As shown in Figure 4.4, at 190 volts, the average wind speed is found to be 6.2 m/s. Similarly, for all other input voltages the wind speeds are recorded at different locations and the area averaged wind speeds are calculated (Table 4.1). The peak wind speed is obtained to be 9.8 m/s at an input voltage of 230 volts, whereas, V = 3.8 m/s is measured at an input voltage of 160 volts.

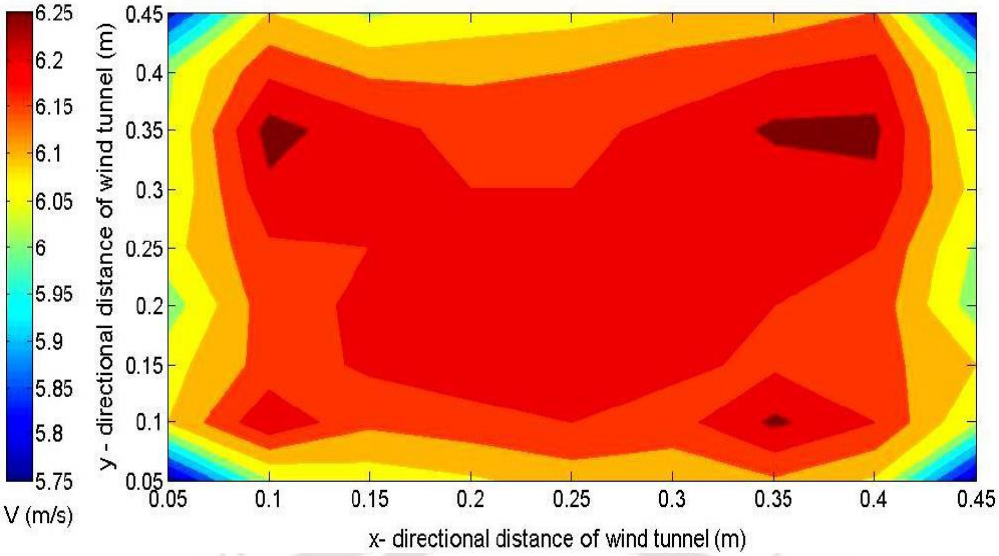

Figure 4.4: Contour of wind speeds at a input voltage of 190 volts

Table 4.1: Area averaged wind speed measurement at different input voltages

Input Voltage to Fan (volts)	Area Averaged Wind Speed (V)
160	3.8
170	4.5
180	5.3
190	6.2
200	7.0
210	7.8
220	8.9
230	9.8

4.3 Power and torque measurement

Initially, analogous to the demand of the situations, 3 types of power measurement devices are opted to measure the performance of these turbines. First of all, a self-made AC generator was used with 1-phase 2-coil windings and 4 permanent magnets (PM), and the results obtained were found very poor due to large electrical losses in the generator. Secondly, a 1-phase AC generator with 4-coil windings and 4 permanent magnets was fabricated. Thereafter, a 30W/15V 3-phase AC generator is installed by means of a gear arrangement.

Loads are connected in series and in parallel connections in order to measure the power output, which is calculated from the electrical voltage and current by the following equation:

$$\text{Power} = \text{Voltage} \times \text{Current} \tag{4.3}$$

With these 3 electrical means of power generation, tests are carried out at different wind speeds in the range of V = 3.8–9.8 m/s. Two earlier 1-phase alternators ran well in the whole range of wind speeds, however, they suffer from large electrical losses. Hence, the power coefficients (C_P) are found to be very poor (Figures 4.5 to 4.10). For 1-phase–2coil and 1-phase–4coil PM alternators, the highest voltage and the current generated are 12.9 volts and 0.56 amps, and 13.8 volts and 0.67 amps at V = 9.8 m/s, respectively (Figures 4.5 to 4.6). At this wind speed, the voltage-current relation indicates a maximum C_P of 0.10 and 0.12 using 1-phase–2coil and 1-phase–4coil PM alternators, respectively (Figure 4.7). In contrast, at V = 7.8 m/s, a C_{Pmax} of 0.11 and 0.13 are obtained using 1-phase–2coil and 1-phase–4coil PM alternators, respectively (Figure 4.10).

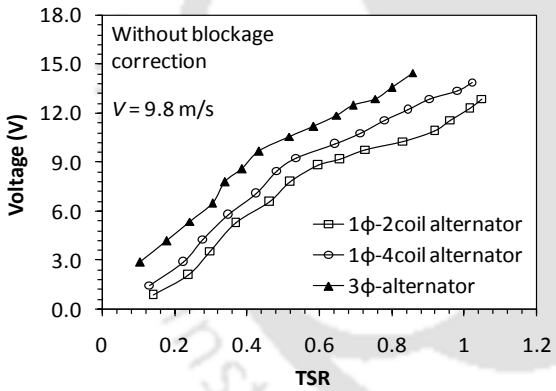

Figure 4.5: Voltage generation at V = 9.8 m/s

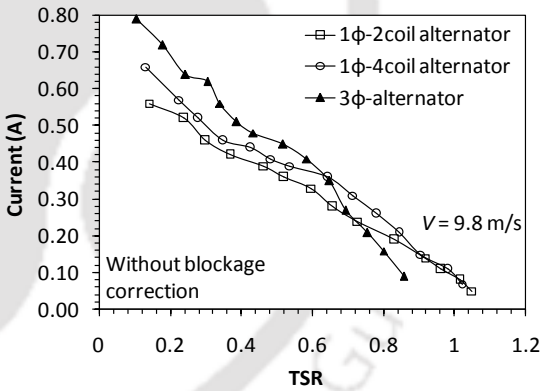

Figure 4.6: Current generation at V = 9.8 m/s

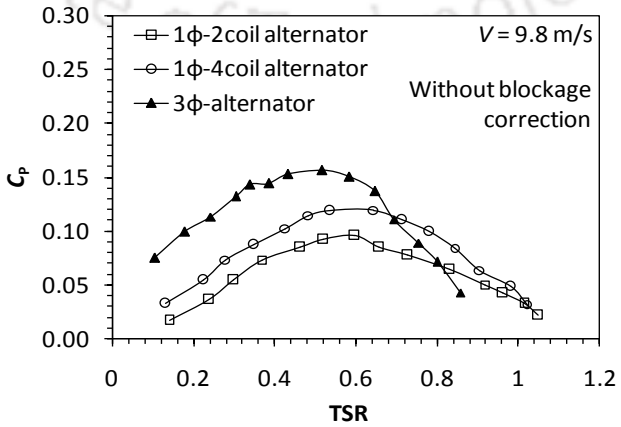

Figure 4.7: Variation of C_P at V = 9.8 m/s using different alternators

The 3-phase alternator although suffers from electrical losses gives a reasonable increase in the C_P at higher wind speeds. It is worth mentioning that the 3-phase alternator has not performed well at low wind speeds (below 5 m/s) due to frictional losses within the alternator. Thus, the noticeable results at higher wind speeds are presented in Figures 4.5 to 4.10. It has been observed that with the 3-phase alternator, the highest voltage and current obtained are 14.5 volts and 0.8 amps at 9.8 m/s, respectively (Figures 4.5 to 4.6). As shown in Figure 4.7, at 9.8 m/s, the maximum C_P is found to be 0.15, whereas at V = 7.8 m/s, the maximum C_P obtained as 0.16 (Figure 4.10).

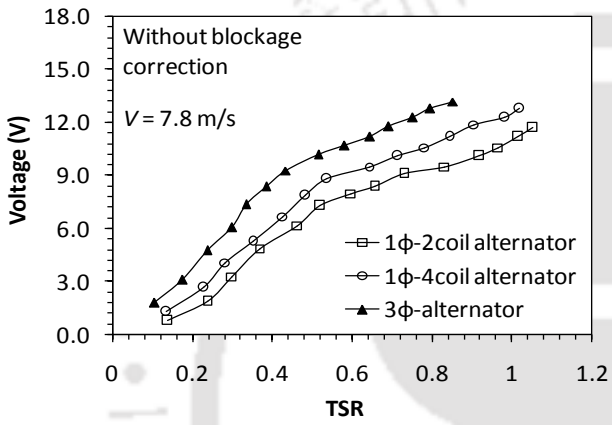

Figure 4.8: Voltage generation at V = 7.8 m/s

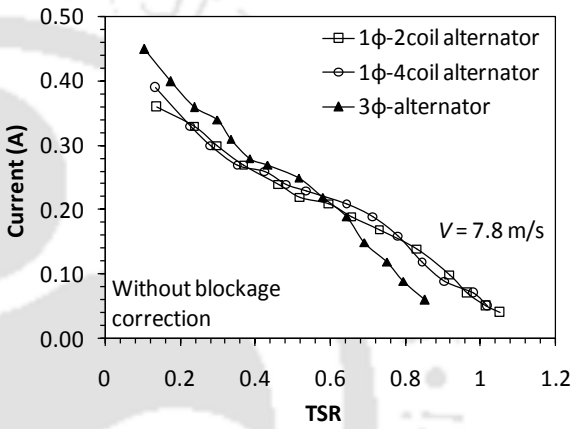

Figure 4.9: Current generation at V = 7.8 m/s

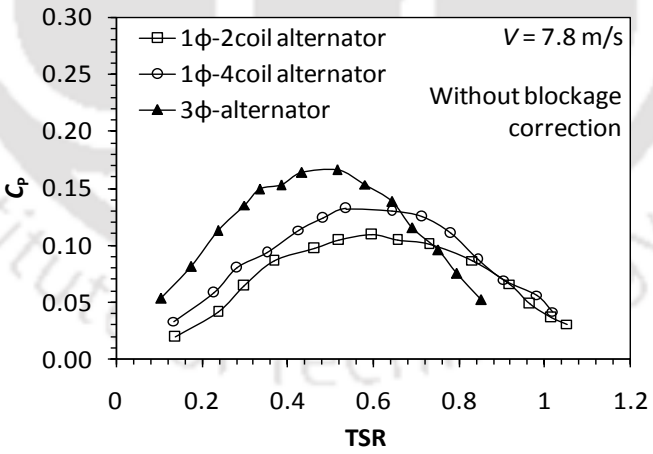

Figure 4.10: Variation of C_P at V = 7.8 m/s using different alternators

Thus, in brief, the 3-phase AC generator is found to be more efficient over other 2 electrical measurement devices. However, the C_P obtained is still found poor as compared to the results reported in the literature (Irabu and Roy, 2007). The experimental validation at V = 6.0 m/s is shown in Figure 4.11. It is to be noted that the selection of the reference data (Irabu and Roy,

2007) is dependent on following major factors: (i) the reference data should be of wind tunnel blockage free, and (ii) small SSWT models should be tested in the wind speed range of 0–10 m/s so as to have a direct comparison. The lower values of C_P from the electrical means are mainly due to large losses occurred in the power conversion and gear transmission devices. Thus, a brake dynamometer is designed with two spring balances, which is connected to the turbine shaft by means of set of reaction pulleys and a rope to measure the torque of the turbine. The results obtained are compared with the reference data for conventional SSWT (δ = 0.20) as shown in Figure 4.11. It is noted that end plates (D_o = 1.1D) are used for all the test cases. At V = 6.0 m/s, the maximum C_P obtained with the mechanical measurement device is 0.25; whereas Irabu and Roy (2010) reported a maximum C_P of 0.23. This comparative study emphasizes a better adaptability to the present system of spring balance dynamometer. The spring balance dynamometer arrangement is shown in Figure 4.12.

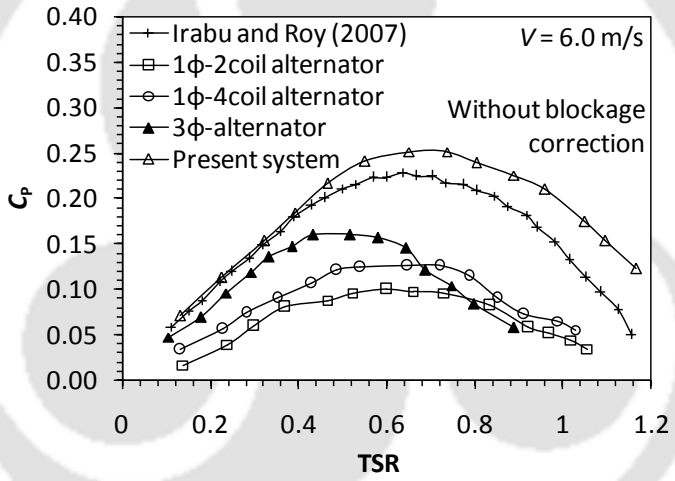

Figure 4.11: Experimental validation using various power and torque measuring devices

The turbine models are tested under various mechanical loads applied through the pulley attached to shaft. The pulley designs attached to the dynamometer are shown in Figures 4.13 to 4.14. The dynamometer specification varies depending on the need: spring balances in the range of 0–5 N, 0–10 N and 0–20 N are used to measure the mechanical loads. Here, the mechanical loads are applied gradually on the turbine shaft with the help of spring balances and load control mechanism. As the load is increased on the turbine, the rotational speed of the turbine reduces as is observed in case of electrical loading. This system has given the flexibility to analyze the turbine performance with respect to various TSR. The load (F) multiplied by the radius of the rotating pulley attached to shaft (r_p) gives the torque applied (T) to the turbine models.

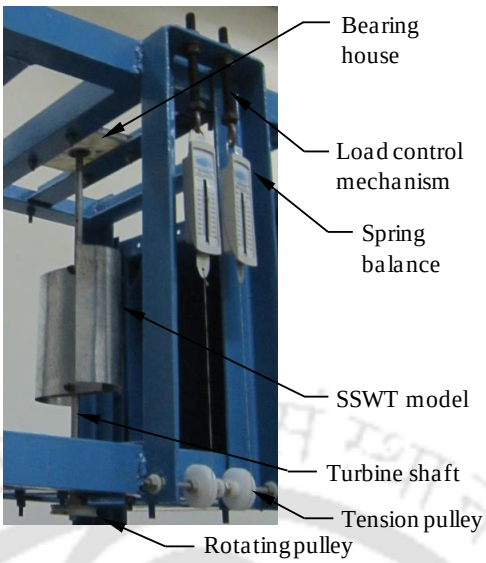

Figure 4.12: Spring balance Dynamometer

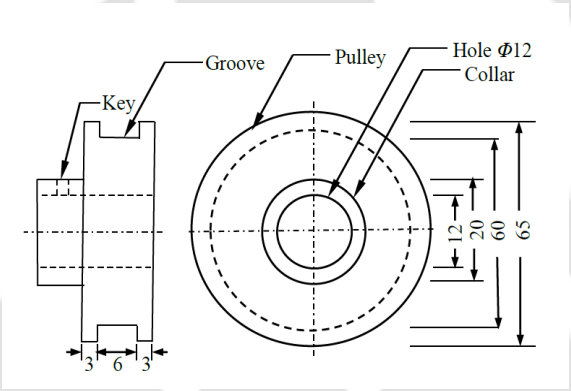

Figure 4.13: Design of rotating pulley

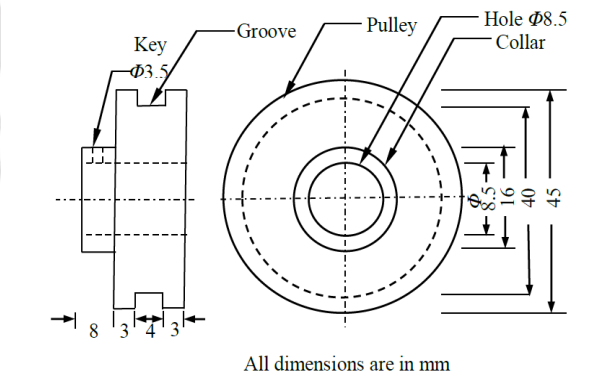

Figure 4.14: Design of tension pulley

The experimental uncertainties are calculated by using the sequential perturbation technique, which are found to be ± 2%, ± 4.6%, and ± 4.9% for torque, torque coefficient and power coefficient, respectively (Kline and McClintock, 1953; Moffat, 1982; Rajkumar, 2004; Thotla, 2006). A photograph showing the experimental setup is presented in Figure 4.15.

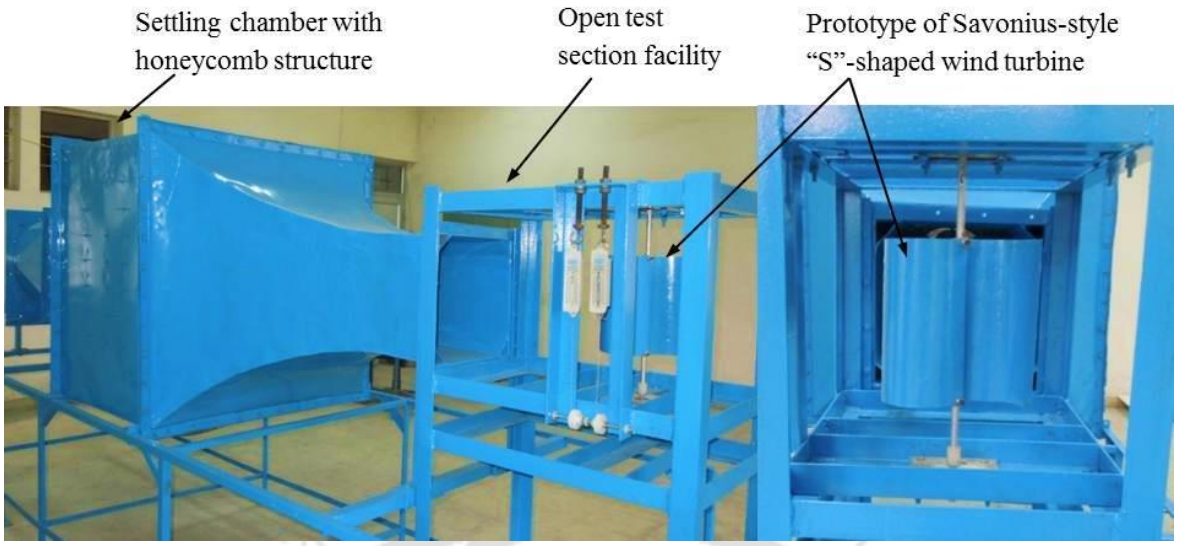

Figure 4.15: Photograph of the experimental setup

4.4 Error analysis

During the experimental procedure, it is obvious that the data taken fluctuate from reading to reading. Thus, several data are taken for a particular mechanical load (F) and rotational rate of the turbine (N).

It is observed that for each experimental case, the measured data are deviated by a certain percentage. Accordingly, for repeatability context, the mean value of all the measured data is taken for each experimental case. The percentage standard deviations from the mean value are calculated by the following equation:

$$\sigma = \sqrt{\frac{1}{J}\sum_{i=1}^{J}(x_i - m)^2} \times 100\,\% \qquad (4.4)$$

where, σ is the percentage standard deviation, J is the number of data taken, m is the mean value and x is the measured value. Figures 4.16 to 4.21 show the percentage deviations for C_T and C_P at different wind speeds. It is observed that the percentage deviations are within ± 6.9 % for lower wind speeds, whereas it decreases with an increase in wind speed. At V = 6.2 m/s, the percentage deviations are found to be within ± 4.5 %. A further increase in the wind speed to V = 8.9 m/s, the percentage deviations are observed to be within ± 3.9 %. In all the later reported results, the mean values of all the measured data have been used for the analysis of SSWTs.

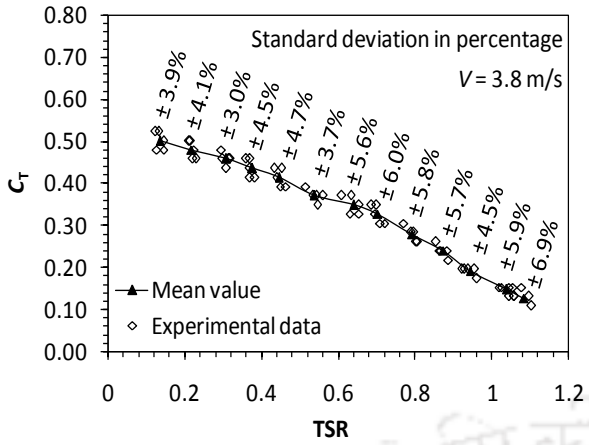

Figure 4.16: Standard deviations of C_T at V = 3.8 m/s

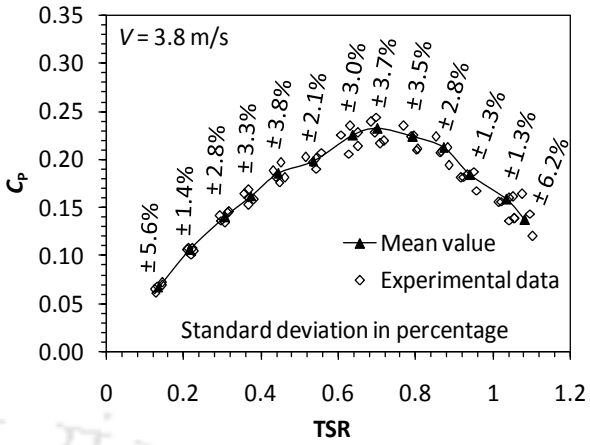

Figure 4.17: Standard deviations of C_P at V = 3.8 m/s

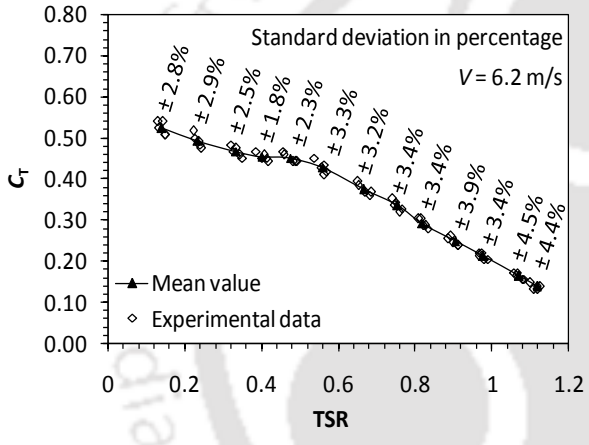

Figure 4.18: Standard deviations of C_T at V = 6.2 m/s

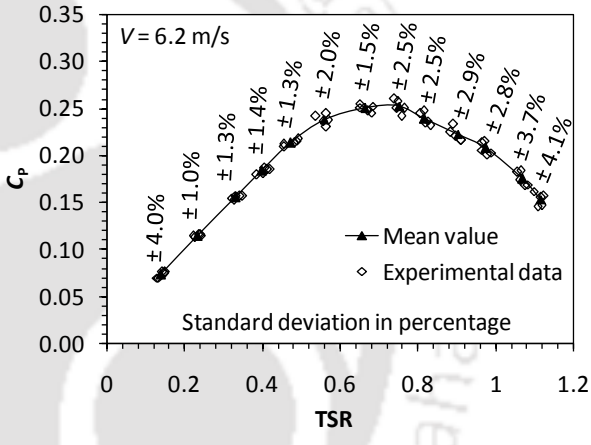

Figure 4.19: Standard deviations of C_P at V = 6.2 m/s

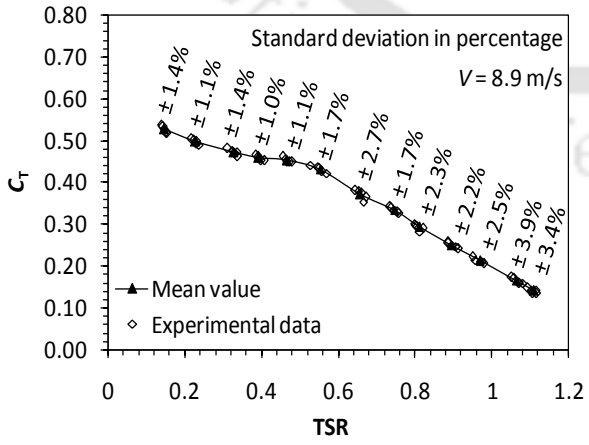

Figure 4.20: Standard deviations of C_T at V = 8.9 m/s

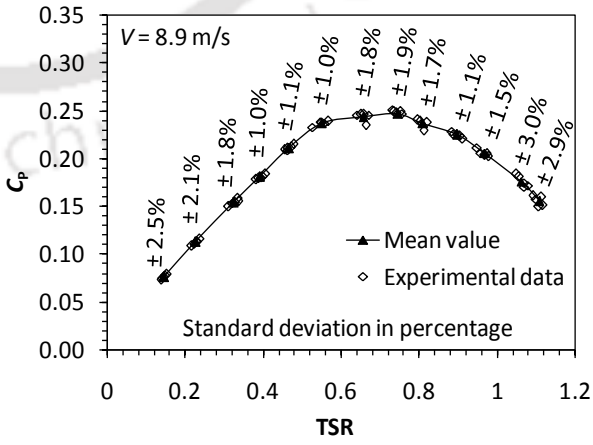

Figure 4.21: Standard deviations of C_P at V = 8.9 m/s

4.5 Summary

A detailed description is presented on the experimental facility and the instruments used in the present investigation. An open type test section facility has been fabricated and installed at the exit section of the wind tunnel. The wind speed is varied by means of a voltage regular and is recorded at different locations at the wind tunnel exit section. The area averaged wind speeds are calculated. Initially, 3 types of power measurement devices are opted to measure the performance of Savonius-style wind turbines. Experiments are carried out at different wind speeds in the range of V = 3.8–9.8 m/s under the application of various loads. At V = 7.8 m/s, the maximum C_P is found to be 0.11, 0.13 and 0.16 for 1-phase–2coil, 1-phase–4coil and 3-phase PM alternators, respectively. The experimental results obtained are validated with the established data at similar experimental conditions and are found to be very poor due to large electrical losses in the generator. Thus, a spring balance dynamometer is fabricated. The percentage standard deviations of all the measured data are calculated and the mean value is used to present the results for all the experimental case. The validation study shows a better compliance with the mechanical measurement device as compared to other measurement means. However, the results deviated from the established data that indicates the need of wind tunnel blockage correction in the existing experimental setup.

CHAPTER –5

Wind Tunnel Blockage Correction

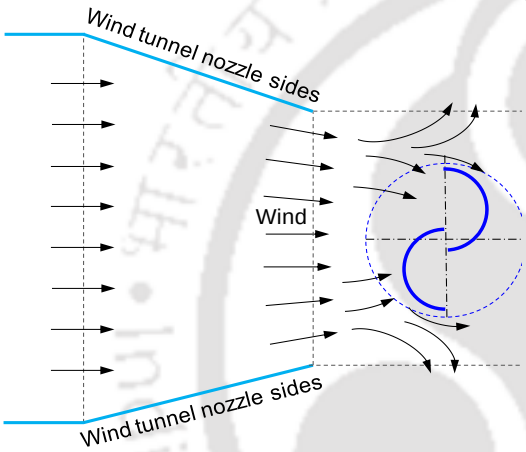

Chapter Outline

Overview

This chapter reports the new correlations developed for the wind tunnel blockage corrections in the open type test section. As the available correlations for the closed type test sections may not be appropriate for the open test section under dynamic loading conditions, new correlations are adapted for the blockage correction factors with free stream wind speed, turbine rotational speed and variable load applied to the turbine to quantify the energy conversion coefficients more precisely. These are obtained for a blockage ratio of 21.16% through a comparison of present experimental data with those of established experimental data under dynamic loading conditions. Further, the accuracy of the adapted correlations is substantiated into the experiments with smaller blockage ratios of 16% and 12.25%. The relationships of the tip speed ratios and blockage ratios with the blockage correction factor are also discussed.

5.1 Wind tunnel blockage

Over the decades, wind tunnels have been extensively used to analyze and estimate the performance of Savonius-style wind turbines (SSWTs) with or without considering the wind tunnel blockage effect. As a result, all the available literature cannot be claimed to be quantitatively accurate. The results often suffer from the effects of solid blockage, wake blockage, nozzle blockage and so on (Barlow *et al*., 1999; Chen and Liou, 2011).

The blockage correction largely depends upon the type of test section used in the wind tunnel, i.e. closed type or open type. The open type test sections are often regarded as a blockage tolerant test section because of its ability to allow the flow to expand around the turbine as opposed to the restricted flow within the closed type test section (Ross and Altman, 2011). This benefit allows the open type test section to have a lower blockage correction as compared to its counterpart.

The blockage ratio, BR (area of the model to the area of the test section) is another deciding factor in correcting the results of wind tunnel experiments. Since long, the standard practice is to operate a low speed wind tunnel within BR = 10 (Pope and Harper, 1966). An example of this standard can be seen in the investigations of Schreck *et al*. (2007), where a BR of 9.3% was used. Another example is found in the experiments of Irabu and Roy (2007), where small SSWTs were tested in a low speed wind tunnel with a BR of 8%. A further confirmation of no blockage correction for a BR less than 10% is observed in the findings of Chen and Liou (2011) for closed type test sections. In contrary, wind tunnel blockage correction can be seen in the investigations of Biswas *et al*. (2007), where three-bladed SSWTs are tested in a closed type wind tunnel with BR = 17.8%. A detailed study for the closed type test section is found in the investigations of Ross and Altman (2011) accounting the static pressure measurement, wake interactions and wake propagations around SSWTs. Modi and Fernando (1989) have reported the effect of blockage correction for SSWTs inside a closed type test section with a BR of 19.67%. They have varied the wall confinement from 2–20% and observed an increase in performance of the turbine by 70%. This signified the effect of blockage correction in the wind tunnel experiments without which it leads to an unrealistic design of turbine.

For BR > 10, the investigations reported in open literature are mostly based on the blockage correction in closed type test section. The analysis of blockage problems in open type test

sections is in fact difficult and can be based on the correlations between the variables responsible for the performance calculation. Based on the test section and model dimensions, Theodorsen (1996) has developed correlations for open type test sections for static airfoil. However, it seems hardly feasible for the analysis of SSWTs in dynamic calculations. As suggested by Abraham *et al*. (2012), an approach to obtain the correction factor could be a comparison between computational and wind tunnel results. However, it essentially depends on the computational accuracy. Another methodology can be opted for determining the blockage correction is to compare the results with similar type of experiments in open air or with similar type of wind tunnel experiments (Plourde *et al*., 2011; Abraham *et al*., 2011).

5.2 Need of blockage correction

In the present study, the open type test section is placed at the exit of the nozzle section (Figure 4.1). The dimensions of the tested turbine model are of $H = D_o$ = 230 mm (Figure 1.3), creating a blockage ratio of 21.16% that caters the need of blockage correction of the measured parameters. As shown in Figures 5.1 and 5.2, a large variation is observed from the referred data (Irabu and Roy, 2007). It is mainly due to the blockage present in the existing setup. The percentage deviations of the present experimental data are shown in Table 5.1. It is observed that these percent deviations are lesser at low TSRs. However, at TSR > 0.5, the percentage deviations are significantly increasing. Thus, it implies that the assumption of a single value for the blockage correction factor will not necessarily give the corrected data of measured parameters; rather the factor may vary with TSR.

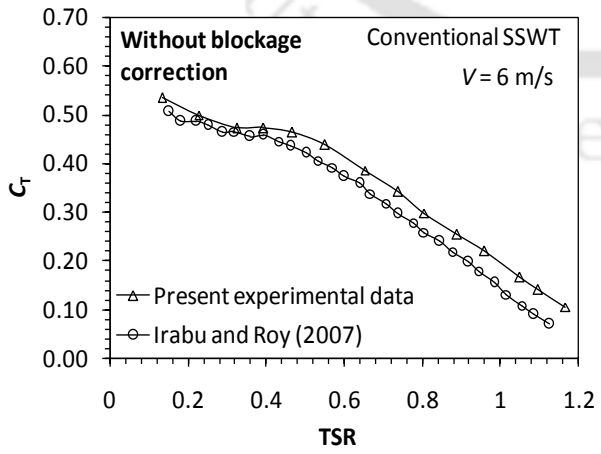

Figure 5.1: Variation of C_T without blockage correction

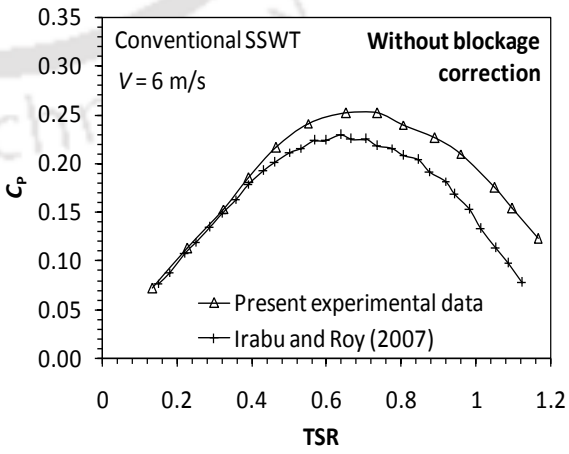

Figure 5.2: Variation of C_P without blockage correction

The overlap ratio between the turbine blades (δ) is selected as 0.20. The end plates are used at top and bottom of the turbine blades, having dimensions D_o = 1.1D. The results of the investigation are compared with the experimental data of Irabu and Roy (2007). It is to be noted that the selection of the reference data for blockage correction should be of wind tunnel blockage free. In reference (Irabu and Roy, 2007), BR was of 8%, and thus, it can be assumed to be blockage free so that the percentage deviations can be estimated in the open type test sections if higher blockage ratios are used. Also small SSWT models were tested in the wind speed range of 0–10 m/s.

The present investigation is aimed at determining the blockage correction factor (f), and its correlation with the variables responsible for the calculation of the performance parameters of Savonius-style wind turbines. The correlations adapted are further applied to analyze the blockage correction factors for blockage ratios of BR = 16% and 12.25%.

Table 5.1: Percentage deviations of the experimental data from Irabu and Roy (2007)

Irabu and Roy (2007)			Present Experimental Data ± Percentage Deviation		
TSR	C_P	C_T	TSR	C_P	C_T
0.1334	0.0679	0.5092	0.1334	0.0712 ± 4.9%	0.5339 ± 4.9%
0.2267	0.1106	0.4880	0.2266	0.1130 ± 2.2%	0.4989 ± 2.2%
0.3240	0.1516	0.4679	0.3240	0.1559 ± 2.8%	0.4814 ± 2.9%
0.3912	0.1793	0.4583	0.3917	0.1851 ± 3.2%	0.4726 ± 3.1%
0.4652	0.2021	0.4345	0.4658	0.2161 ± 6.9%	0.4639 ± 6.8%
0.5509	0.2186	0.3969	0.5505	0.2409 ± 10.2%	0.4376 ± 10.3%
0.6522	0.2245	0.3442	0.6522	0.2511 ± 11.8%	0.3851 ± 11.9%
0.7370	0.2170	0.2945	0.7368	0.2515 ± 15.9%	0.3413 ± 15.9%
0.8043	0.2074	0.2579	0.8046	0.2394 ± 15.4%	0.2976 ± 15.4%
0.8892	0.1915	0.2154	0.8893	0.2257 ± 17.9%	0.2538 ± 17.8%
0.9594	0.1628	0.1697	0.9592	0.2099 ± 28.9%	0.2188 ± 28.9%
1.0501	0.1202	0.1145	1.0502	0.1746 ± 45.3%	0.1663 ± 45.2%
1.0960	0.0931	0.0849	1.0968	0.1536 ± 65.0%	0.1400 ± 64.1%
1.1654	0.0441	0.0379	1.1667	0.1225 ± 177.8%	0.1050 ± 177.0%

5.3 Methodology of blockage correction

Based on the correlations, very few studies are found on wind tunnel blockage corrections (Maskell, 1963; Blackwell *et al.*, 1977; Hackett *et al.*, 1979; Barlow *et al.*, 1999). As suggested by Blackwell *et al.* (1977), modifications of free stream wind speed (V) and dynamic pressure (q) are given by Equations 5.1 and 5.2, where '*' represents the corrected values.

$$V^* = V(1+f) \tag{5.1}$$

$$q^* = q(1+f)^2 \tag{5.2}$$

According to Pope and Harper (1966), the blockage correction factor (*f*) for an unusual shape under closed type test section can be defined by Equation 5.3, where *f* is correlated with the dependable parameters by Equations 5.3 to 5.6.

$$f = \frac{1}{4}\left(\frac{\text{Model frontal area}}{\text{Test section area}}\right) \tag{5.3}$$

$$V^* = V(1+f) \tag{5.4}$$

$$q^* = q(1+2f) \tag{5.5}$$

$$Re^* = Re(1+f) \tag{5.6}$$

However, the above corrections can only be useful for testing SSWTs in closed type sections, which otherwise is not applicable to describe the blockage corrections in open type test sections under dynamic loading. Thus, in the present analysis of studying the blockage effects in an open type test section, the basic performance equations can be expressed as:

$$C_P^* = \frac{P_{turbine}^*}{P_{available}^*} \tag{5.7}$$

$$P_{available}^* = \frac{1}{2}\rho A V^{*3} \tag{5.8}$$

$$P_{turbine}^* = \frac{2\pi N^*(F^* \times r_p)}{60} \tag{5.9}$$

$$C_T^* = \frac{(F^* \times r_p)}{\frac{1}{2}\rho A V^{*2} R} \tag{5.10}$$

$$\mathrm{TSR}^{*} = \frac{2\pi N^{*}}{60}\frac{R}{V^{*}} \tag{5.11}$$

From the above equations, the measurable parameters that can affect the present experimental results due to nozzle blockage and solid blockage are:

$$f = f(V, N, F) \tag{5.12}$$

As shown in Figure 5.3, a concentrated flow is assumed to take place at the wind tunnel exit section, where the wind speed is expected to accelerate. In contrast, an expandable flow is likely to take place at the downstream of the test section due to open test section facility. The area averaged wind speed is measured just upstream of the turbine. It is expected that in the vicinity of the turbine, the wind speed gets affected by the flow expansion occurring in the open section and also due to obstructions created by the solid turbine blades. Since, it is an open type test section, it is sure that the wind speed will reduce near the turbine blades (was confirmed through the experimental measurements). However, the factor by which this wind speed should be corrected is unknown. The value of factor is selected in such a way that the corrected wind speed will give a value less than or equal to the measured wind speed. Barlow *et al.* (1999) suggests that the blockage correction factor (*f*) in an open type test section should be of opposite sign and is smaller than that of closed type. In this context, one new variable '*n*' is inserted into Equation 5.13. The opposite sign is used and '*n*' is assumed to vary from 1 to 5 so that the required fraction of *f* can be determined.

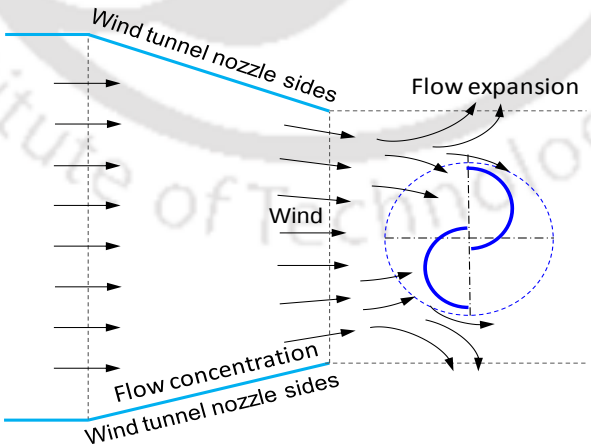

Figure 5.3: Concentrated and expandable flow in the experimental setup

$$V^{*} = V\left(1 - \frac{n}{5} f\right) \quad [n = 1, 2, 3, 4, 5] \tag{5.13}$$

The mechanical load applied to the turbine gets increased due to flow acceleration caused by the solid blockage present in the experimental setup. Thus, it should be taken into account by a factor of reduction. The same observation can be found in case of rotational speed measurement of the turbine. Thus, to correct the measured data of mechanical load (F) and rotational speed of the turbine (N), these parameters are correlated as follows:

$$F^* = F(1-f) \tag{5.14}$$

$$N^* = N(1-f) \tag{5.15}$$

All the measurement parameters are correlated by a single blockage correction factor f. Experimental results are corrected for f = 1–10% by an increment of 1% to obtain a suitable blockage correction factor for BR = 21.16% at various TSR. Further, these correlations are validated for smaller turbine models and the suitable value of f is obtained for BR = 16% and 12.25%.

5.4 Results and discussion

Wind tunnel experiments are carried out in open type test section for Savonius-style wind turbines with a blockage ratio of 21.16%. In order to study the effectiveness of the blockage correction in the present experimental setup, the above correlations of correction factor (f) with the free stream wind speed (V), turbine rotational speed (N) and applied load (F) for each case have been applied to the wind tunnel test data. As presented in Figures 5.1 and 5.2, without any blockage correction, the experimental results show C_{Pmax} and C_{Tmax} of 0.251 and 0.534, respectively at δ = 0.20, while the target values of C_{Pmax} and C_{Tmax} from the established data (Irabu and Roy, 2007) are 0.228 and 0.544, respectively. The blockage correction factor, f is varied from 1–10% by an increment of 1% and for all the cases (f = 1–10%) the 'n' value is varied from 1 to 5. The tip speed ratio, power coefficient and torque coefficient have been evaluated for each value of n and f to fully integrate the correlations into the established data. However, in each 1% variation of f, small deviations are observed and all the curves follow the similar trends for C_P and C_T with respect to TSR. Thus, variations of f = 1–9% by an increment of 2% are presented in Figures 5.4 through 5.13. Further, the effect of blockage correction factor is analyzed for various tip speed ratios.

Figures 5.4 and 5.5 provide a comparative study for n = 1–5, showing the effect of blockage correction factor, f = 1%. The desired values of C_P and C_T are obtained with n = 1, where C_{Pmax} and C_{Tmin} are found to be 0.248 and 0.531, respectively. Figures 5.6 to 5.13 show similar plots for f = 3–9%. In all the plots, clear trends can be observed with the corrected data of C_P and C_T approaching towards the established data. It has been observed that the blockage correction factor depends significantly on the value of corrected TSRs. For BR = 21.16%, the desired value of f is found to be in the range of 4–10%.

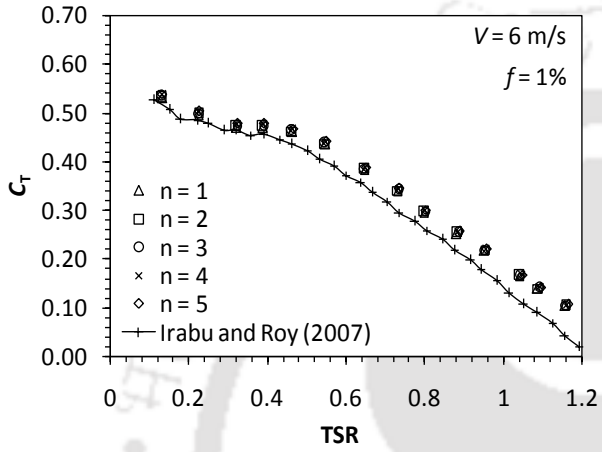

Figure 5.4: Variation of C_T with f = 1%

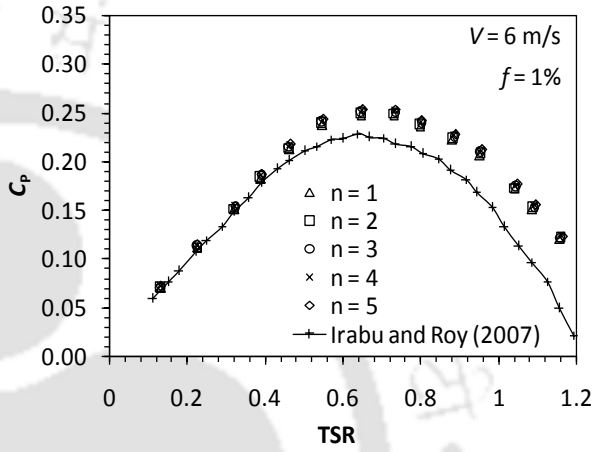

Figure 5.5: Variation of C_P with f = 1%

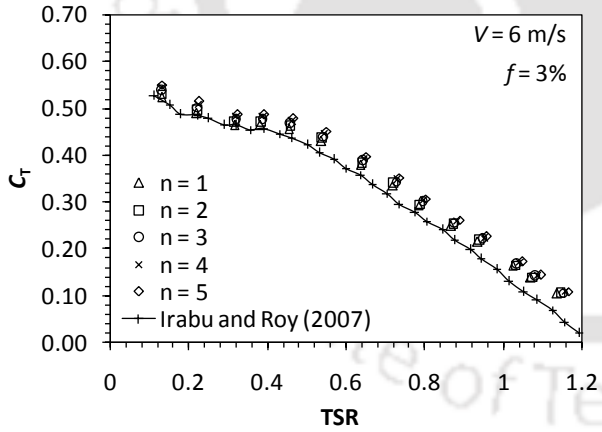

Figure 5.6: Variation of C_T with f = 3%

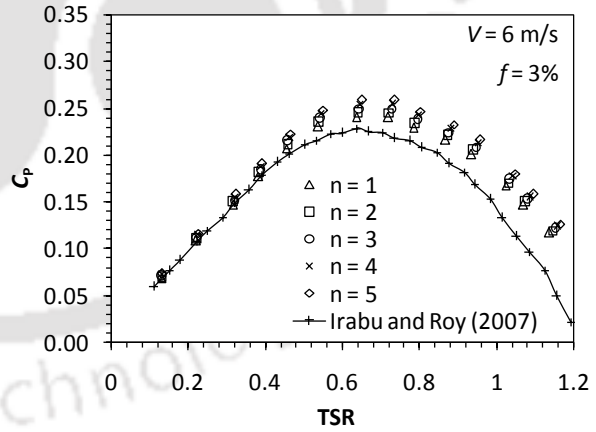

Figure 5.7: Variation of C_P with f = 3%

The percentage deviations of the blockage corrected data with respect to reference data (Irabu and Roy, 2007) are shown in Table 2. At a low TSR of 0.22, with f = 4% and n = 1, the percentage deviations of C_P and C_T are found to be ± 1.3% and ± 0.7%, respectively. In contrast, at a high TSR of 1.07, n = 1 and f = 10% are found to be more suitable that gives percentage deviations of ± 0.4% in C_P and C_T calculations.

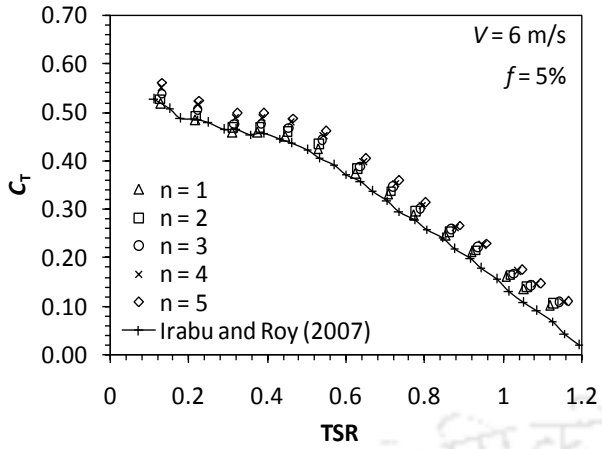

Figure 5.8: Variation of C_T with f = 5%

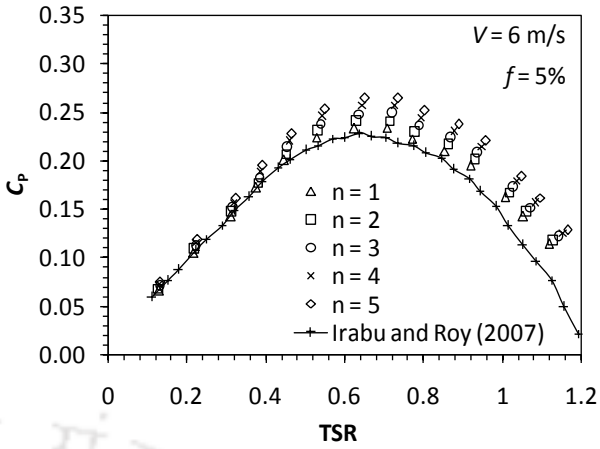

Figure 5.9: Variation of C_P with f = 5%

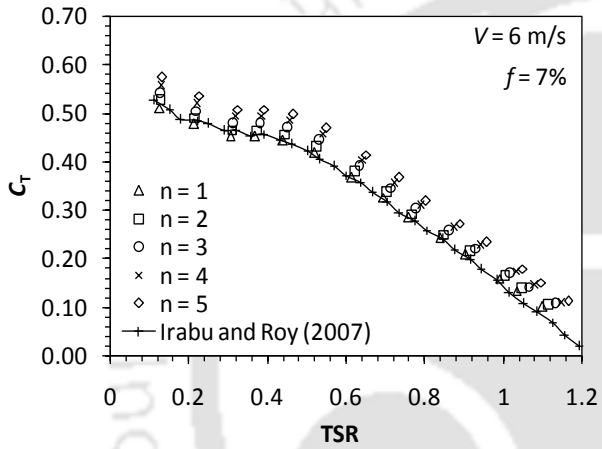

Figure 5.10: Variation of C_T with f = 7%

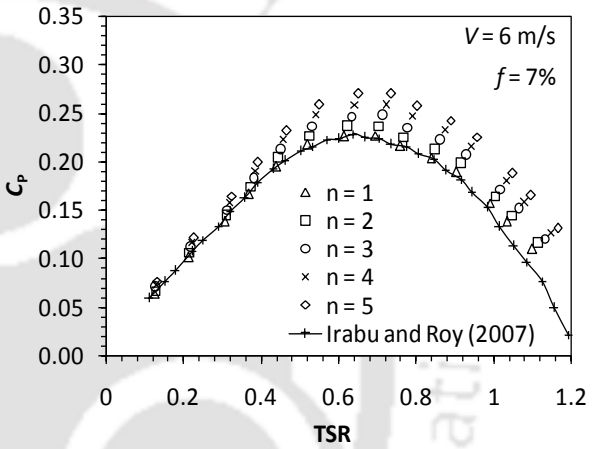

Figure 5.11: Variation of C_P with f = 7%

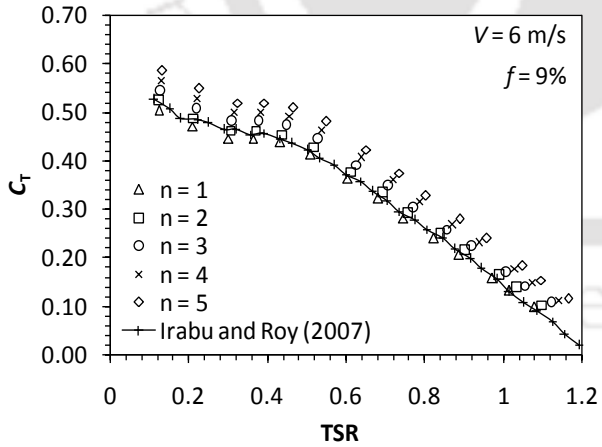

Figure 5.12: Variation of C_T with f = 9%

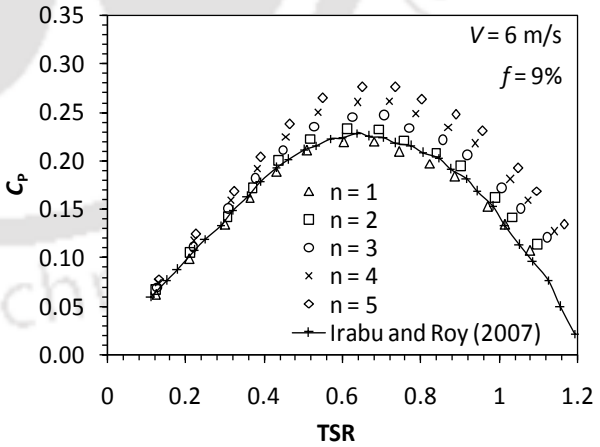

Figure 5.13: Variation of C_P with f = 9%

For n = 3 and f = 4%, at low TSR of 0.22, the percentage deviations of C_P and C_T are obtained as ± 5.8% and ± 4.9%, respectively. Whereas, for n = 3, very large deviations are observed at high TSRs. Likewise, with the further increase of n, the percentage deviations increased substantially.

Table 5.2: Effect of correlations for BR = 21.16%

n	Irabu and Roy [38]			Present Experimental Data				Corrected Data (BR = 21.16%) ± Percentage Deviation from Reference Data		
	TSR	C_P	C_T	TSR	C_P	C_T	f	**TSR***	C_P^*	C_T^*
1	0.2179	0.1053	0.4832	0.2266	0.1130	0.4989	4%	0.2193	0.1067 ± 1.3%	0.4867 ± 0.7%
	0.5333	0.2149	0.4029	0.5505	0.2409	0.4377		0.5328	0.2274 ± 5.8%	0.4269 ± 6.0%
	0.7789	0.2128	0.2732	0.8046	0.2394	0.2976		0.7786	0.2260 ± 6.2%	0.2903 ± 6.3%
	1.1253	0.0739	0.0657	1.1667	0.1225	0.1050		1.1290	0.1157 ± 56.6%	0.1025 ± 56.0%
	0.2160	0.1048	0.4851	0.2266	0.1130	0.4989	6%	0.2156	0.1036 ± 1.1%	0.4804 ± 1.0%
	0.5226	0.2128	0.4071	0.5505	0.2409	0.4377		0.5238	0.2147 ± 0.9%	0.4099 ± 0.7%
	0.7662	0.2168	0.2830	0.8046	0.2394	0.2976		0.7655	0.2194 ± 1.2%	0.2866 ± 1.3%
	1.1097	0.0851	0.0767	1.1667	0.1225	0.1050		1.1100	0.1123 ± 32.0%	0.1011 ± 31.8%
	0.2121	0.1032	0.4865	0.2266	0.1130	0.4989	8%	0.2118	0.1004 ± 2.7%	0.4740 ± 2.6%
	0.5139	0.2117	0.4120	0.5505	0.2409	0.4377		0.5147	0.2040 ± 3.6%	0.3963 ± 3.8%
	0.7526	0.2184	0.2902	0.8046	0.2394	0.2976		0.7523	0.2127 ± 2.6%	0.2827 ± 2.6%
	1.0921	0.0947	0.0867	1.1667	0.1225	0.1050		1.0908	0.1089 ± 15.0%	0.0998 ± 15.1%
	0.2082	0.1016	0.4880	0.2266	0.1130	0.4989	10%	0.2081	0.0973 ± 4.2%	0.4675 ± 4.2%
	0.5061	0.2116	0.4181	0.5505	0.2409	0.4377		0.5056	0.2013 ± 4.9%	0.3981 ± 4.8%
	0.7399	0.2188	0.2957	0.8046	0.2394	0.2976		0.7389	0.2061 ± 5.8%	0.2789 ± 5.7%
	1.0716	0.1059	0.0988	1.1667	0.1225	0.1050		1.0714	0.1055 ± 0.4%	0.0984 ± 0.4%
3	0.2209	0.1059	0.4792	0.2266	0.1130	0.4989	4%	0.2228	0.1120 ± 5.8%	0.5028 ± 4.9%
	0.5421	0.2154	0.3974	0.5505	0.2409	0.4377		0.5415	0.2388 ± 10.7%	0.4410 ± 11.0%
	0.7916	0.2112	0.2668	0.8046	0.2394	0.2976		0.7914	0.2373 ± 12.4%	0.2999 ± 12.4%
	1.1468	0.0601	0.0524	1.1667	0.1225	0.1050		1.1475	0.1214 ± 102.0%	0.1058 ± 101.9%
	0.2209	0.1059	0.4792	0.2266	0.1130	0.4989	6%	0.2209	0.1115 ± 5.3%	0.5046 ± 5.3%
	0.5363	0.2154	0.4017	0.5505	0.2409	0.4377		0.5368	0.2376 ± 10.3%	0.4426 ± 10.2%
	0.7848	0.2122	0.2704	0.8046	0.2394	0.2976		0.7846	0.2362 ± 11.3%	0.3010 ± 11.3%
	1.1370	0.0665	0.0585	1.1667	0.1225	0.1050		1.1376	0.1209 ± 81.8%	0.1062 ± 81.5%
	0.2179	0.1053	0.4832	0.2266	0.1130	0.4989	8%	0.2189	0.1109 ± 5.3%	0.5064 ± 4.8%
	0.5314	0.2138	0.4024	0.5505	0.2409	0.4377		0.5320	0.2363 ± 10.5%	0.4442 ± 10.4%
	0.7779	0.2133	0.2742	0.8046	0.2394	0.2976		0.7776	0.2349 ± 10.1%	0.3021 ± 10.2%
	1.1253	0.0739	0.0657	1.1667	0.1225	0.1050		1.1275	0.1202 ± 62.7%	0.1066 ± 62.2%
	0.2160	0.1048	0.4851	0.2266	0.1130	0.4989	10%	0.2169	0.1102 ± 5.2%	0.5081 ± 4.7%
	0.5265	0.2133	0.4051	0.5505	0.2409	0.4377		0.5271	0.2349 ± 10.1%	0.4457 ± 10.0%
	0.7701	0.2138	0.2776	0.8046	0.2394	0.2976		0.7701	0.2335 ± 9.2%	0.3031 ± 9.2%
	1.1175	0.0793	0.0709	1.1667	0.1225	0.1050		1.1170	0.1195 ± 50.7%	0.1070 ± 50.9%
5	0.2267	0.1106	0.4880	0.2266	0.1130	0.4989	4%	0.2266	0.1177 ± 6.4%	0.5197 ± 6.5%
	0.5509	0.2186	0.3969	0.5505	0.2409	0.4377		0.5505	0.2509 ± 14.8%	0.4558 ± 14.8%
	0.8043	0.2074	0.2579	0.8046	0.2394	0.2976		0.8046	0.2494 ± 20.3%	0.3100 ± 20.2%
	1.1654	0.0441	0.0379	1.1667	0.1225	0.1050		1.1667	0.1276 ± 189.3%	0.1094 ± 188.7%
	0.2267	0.1106	0.4880	0.2266	0.1130	0.4989	6%	0.2266	0.1202 ± 8.7%	0.5307 ± 8.8%
	0.5509	0.2186	0.3969	0.5505	0.2409	0.4377		0.5505	0.2563 ± 17.2%	0.4655 ± 17.3%
	0.8043	0.2074	0.2579	0.8046	0.2394	0.2976		0.8046	0.2547 ± 22.8%	0.3166 ± 22.8%
	1.1654	0.0441	0.0379	1.1667	0.1225	0.1050		1.1667	0.1304 ± 195.7%	0.1117 ± 194.7%
	0.2267	0.1106	0.4880	0.2266	0.1130	0.4989	8%	0.2266	0.1229 ± 11.1%	0.5422 ± 11.1%
	0.5509	0.2186	0.3969	0.5505	0.2409	0.4377		0.5505	0.2619 ± 19.8%	0.4757 ± 19.9%
	0.8043	0.2074	0.2579	0.8046	0.2394	0.2976		0.8046	0.2602 ± 25.4%	0.3234 ± 25.4%
	1.1654	0.0441	0.0379	1.1667	0.1225	0.1050		1.1667	0.1332 ± 202.0%	0.1142 ± 201.3%
	0.2267	0.1106	0.4880	0.2266	0.1130	0.4989	10%	0.2266	0.1256 ± 13.6%	0.5543 ± 13.6%
	0.5509	0.2186	0.3969	0.5505	0.2409	0.4377		0.5505	0.2677 ± 22.5%	0.4862 ± 22.5%
	0.8043	0.2074	0.2579	0.8046	0.2394	0.2976		0.8046	0.2660 ± 28.3%	0.3306 ± 28.2%
	1.1654	0.0441	0.0379	1.1667	0.1225	0.1050		1.1667	0.1361 ± 208.6%	0.1167 ± 207.9%

The assumption of n = 1 gives the most effective corrected results those are well matched with the established data (Irabu and Roy, 2007). Thus, the velocity correction can be rewritten as:

$$V^* = V(1-\frac{1}{5}f) \tag{5.16}$$

To verify the accuracy of the applied correlations in this analysis for 230 × 230 mm^2 turbine model (BR = 21.16%), these correlations are further tested for comparatively smaller models such as 200 × 200 mm^2 turbine model and 175 × 175 mm^2 turbine model for blockage ratios, BR = 16% and 12.25%, respectively. The free stream wind speed for the experimental analysis is kept identical to that of V = 6 m/s. Without any blockage correction, for BR = 16%, the C_{Pmax} and C_{Tmax} obtained from wind tunnel experiments are 0.247 and 0.525, respectively; whereas, for BR = 12.25%, these values are found to be 0.242 and 0.516, respectively. For both the later mentioned models, the blockage correction factor, f is varied from 1–10%. The results followed almost similar trends in all the cases. Conversely, the magnitude of f is varied under variable loading conditions.

For 200 × 200 model, the effectiveness of these correlations are presented in Figures 5.14 and 5.15 with f = 3%, 5% and 7% to precisely display the corrected data of C_P and C_T with respect to TSR. Figures 5.16 and 5.17 demonstrate the corrected data for 175 × 175 model with f = 2%, 4% and 6%. A more distinct analysis of the blockage corrections is apparent in Table 5.3, which shows the blockage corrections of f = 1–7% by an increment of 2% for BR = 16% and 12.25%.

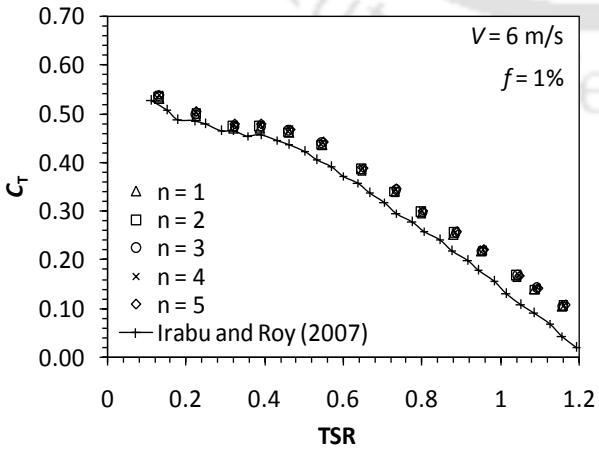

Figure 5.14: Variation of C_T for 200 × 200 model

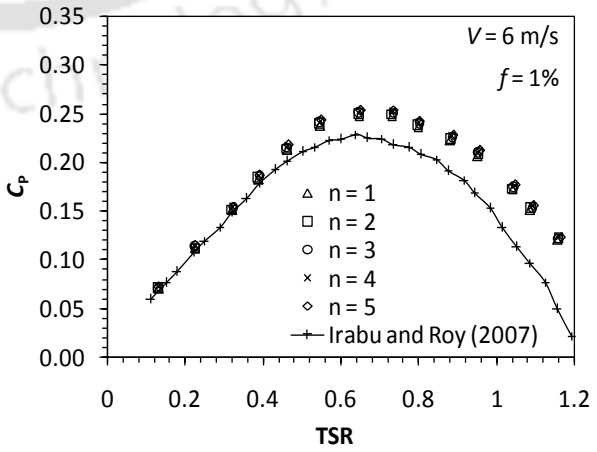

Figure 5.15: Variation of C_P for 200 × 200 model

For BR = 16%, using f = 3% at a low TSR of 0.32, the percentage deviations of C_P and C_T are obtained as ± 0.3% and ± 0.6%, respectively. On the other hand, for BR = 12.25%, using f = 1% at TSR = 0.33, the percentage deviations of C_P and C_T are found to be ± 0.8% and ± 0.9%, respectively. Similarly, for all other cases the percentage deviations are estimated. However, it is observed that the desired value of f varies with respect to TSR and BR.

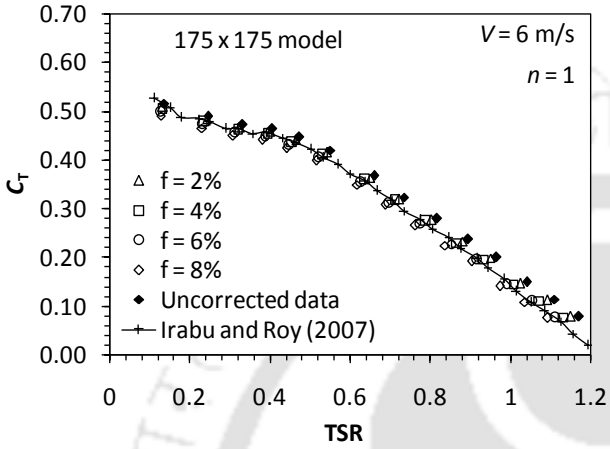

Figure 5.16: Variation of C_T for 175 × 175 model

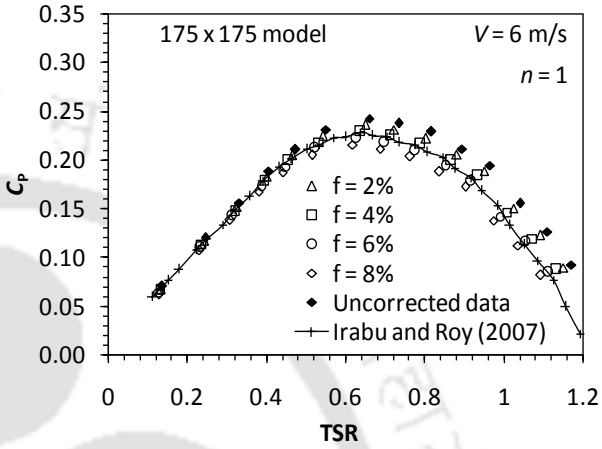

Figure 5.17: Variation of C_P for 175 × 175 model

The relationships of tip speed ratio (TSR) and blockage ratio (BR) with the blockage correction factor (f) are presented in Figure 5.18. For a blockage ratio of 21.16%, at lower tip speed ratios (TSR < 0.5), $f \leq 6\%$ correction well approached the established data, whereas for TSR = 0.5–0.9, f = 7% and for TSR > 0.9, a comparatively higher blockage correction ($f \geq$ 8%) are found to be useful. For BR = 16%, a less than f = 5% correction gives the expected results for tip speed ratios less than 5. However, for TSR = 0.5–0.9, f = 5–6% and for TSR > 0.9, f = 7% corrections are observed in the dependable parameters. A further decrease in the blockage ratio (BR = 12.26%) has shown quite encouraging results. For TSR < 1.0, $f \leq 5\%$ correction in the wind speed, rpm and load well matched the established data. More precisely, for tip speed ratios less than 0.5, the correction factor is found to be $f \leq 3\%$. However, TSR > 1.0, f = 6% provides the expected data.

5.5 Summary

This chapter makes an attempt to consider the blockage correction factor (f) in wind tunnel experiments of a small-scale wind energy conversion system involving Savonius-style wind turbines (SSWTs) under an open test section.

Table 5.3: Accuracy testing of correlations for BR = 16% and 12.25%

BR	Irabu and Roy (2007)			Present Experimental Data				Corrected Data (n = 1) ± Percentage Deviation from Reference Data		
	TSR	C_P	C_T	TSR	C_P	C_T	f	**TSR***	C_P^*	C_T^*
16%	0.1362	0.0681	0.4999	0.1376	0.0723	0.5251		0.1365	0.0713 ± 4.7%	0.5220 ± 4.4%
	0.3260	0.1510	0.4651	0.3282	0.1551	0.4726		0.3256	0.1530 ± 1.3%	0.4698 ± 1.4%
	0.6541	0.2239	0.3423	0.6585	0.2478	0.3763	1%	0.6532	0.2444 ± 9.2%	0.3741 ± 9.3%
	0.9545	0.1649	0.1728	0.9634	0.2024	0.2101		0.9557	0.1995 ± 21.0%	0.2088 ± 20.8%
	1.1566	0.0500	0.0432	1.1667	0.1021	0.0875		1.1573	0.1008 ± 101.6%	0.0870 ± 101.4%
	0.1334	0.0679	0.5092	0.1376	0.0723	0.5251		0.1343	0.0692 ± 1.9%	0.5155 ± 1.2%
	0.3208	0.1490	0.4643	0.3282	0.1551	0.4726		0.3203	0.1486 ± 0.3%	0.4640 ± 0.6%
	0.6425	0.2234	0.3477	0.6585	0.2478	0.3763	3%	0.6426	0.2374 ± 6.3%	0.3695 ± 6.3%
	0.9408	0.1713	0.1821	0.9634	0.2024	0.2101		0.9401	0.1939 ± 13.2%	0.2062 ± 13.2%
	1.1370	0.0665	0.0585	1.1667	0.1021	0.0875		1.1385	0.0978 ± 47.1%	0.0859 ± 46.8%
	0.1323	0.0660	0.4985	0.1376	0.0723	0.5251		0.1321	0.0672 ± 1.8%	0.5090 ± 2.1%
	0.3123	0.1479	0.4734	0.3282	0.1551	0.4726		0.3149	0.1443 ± 2.4%	0.4581 ± 3.2%
	0.6317	0.2274	0.3600	0.6585	0.2478	0.3763	5%	0.6319	0.2305 ± 1.4%	0.3648 ± 1.3%
	0.9233	0.1787	0.1936	0.9634	0.2024	0.2101		0.9245	0.1882 ± 5.3%	0.2036 ± 5.2%
	1.1185	0.0852	0.0762	1.1667	0.1021	0.0875		1.1195	0.0950 ± 11.5%	0.0848 ± 11.3%
	0.1288	0.0637	0.4948	0.1376	0.0723	0.5251		0.1298	0.0652 ± 2.4%	0.5023 ± 1.5%
	0.3094	0.1457	0.4710	0.3282	0.1551	0.4726		0.3096	0.1399 ± 4.0%	0.4521 ± 4.0%
	0.6220	0.2278	0.3662	0.6585	0.2478	0.3763	7%	0.6211	0.2236 ± 1.8%	0.3600 ± 1.7%
	0.9086	0.1846	0.2031	0.9634	0.2024	0.2101		0.9087	0.1826 ± 1.1%	0.2009 ± 1.1%
	1.1001	0.0893	0.0811	1.1667	0.1021	0.0875		1.1004	0.0921 ± 3.1%	0.0837 ± 3.2%
12.25%	0.1348	0.0684	0.5074	0.1355	0.0699	0.5164		0.1344	0.0690 ± 0.9%	0.5133 ± 1.1%
	0.3279	0.1527	0.4655	0.3303	0.1561	0.4726		0.3277	0.1539 ± 0.8%	0.4698 ± 0.9%
	0.6561	0.2245	0.3421	0.6606	0.2428	0.3676	1%	0.6553	0.2394 ± 6.6%	0.3654 ± 6.8%
	0.9574	0.1638	0.1711	0.9655	0.1944	0.2013		0.9578	0.1916 ± 17.0%	0.2001 ± 16.9%
	1.1624	0.0473	0.0407	1.1709	0.0922	0.0788		1.1615	0.0909 ± 92.8%	0.0783 ± 92.4%
	0.1323	0.0660	0.4985	0.1355	0.0699	0.5164		0.1322	0.0670 ± 1.5%	0.5069 ± 1.7%
	0.3230	0.1511	0.4676	0.3303	0.1561	0.4726	3%	0.3223	0.1496 ± 1.0%	0.4640 ± 0.8%
	0.6447	0.2290	0.3551	0.6606	0.2428	0.3676		0.6447	0.2326 ± 1.6%	0.3609 ± 1.6%
	0.9428	0.1691	0.1794	0.9655	0.1944	0.2013		0.9422	0.1862 ± 10.1%	0.1976 ± 10.1%
	1.1419	0.0628	0.0550	1.1709	0.0922	0.0788		1.1426	0.0884 ± 40.8%	0.0773 ± 40.5%
	0.1288	0.0637	0.4948	0.1355	0.0699	0.5164		0.1300	0.0651 ± 2.2%	0.5005 ± 1.2%
	0.3172	0.1479	0.4662	0.3303	0.1561	0.4726		0.3170	0.1452 ± 1.8%	0.4581 ± 1.7%
	0.6347	0.2234	0.3520	0.6606	0.2428	0.3676	5%	0.6339	0.2259 ± 1.1%	0.3563 ± 1.2%
	0.9272	0.1771	0.1910	0.9655	0.1944	0.2013		0.9265	0.1808 ± 2.1%	0.1951 ± 2.1%
	1.1234	0.0826	0.0735	1.1709	0.0922	0.0788		1.1236	0.0858 ± 3.9%	0.0763 ± 3.8%
	0.1288	0.0637	0.4948	0.1355	0.0699	0.5164		0.1278	0.0621 ± 2.5%	0.4859 ± 1.8%
	0.3123	0.1479	0.4734	0.3303	0.1561	0.4726		0.3116	0.1409 ± 4.7%	0.4521 ± 4.5%
	0.6220	0.2278	0.3662	0.6606	0.2428	0.3676	7%	0.6231	0.2191 ± 3.8%	0.3516 ± 4.0%
	0.9115	0.1840	0.2019	0.9655	0.1944	0.2013		0.9106	0.1754 ± 4.7%	0.1926 ± 4.6%
	1.1029	0.0883	0.0801	1.1709	0.0922	0.0788		1.1044	0.0832 ± 5.8%	0.0753 ± 6.0%

Over the decades, the existing low speed wind tunnel has been extensively used to analyze and estimate the performance of SSWTs without considering the wind tunnel blockage effect. As a result, the reported data in the literature cannot be claimed to be quantitatively accurate. However, in order to incorporate this effect in an open test section type wind tunnel, necessary correlations are to be developed, and accordingly, the estimated data need to be

corrected. On the other hand, the correlations reported for closed type test sections may not be appropriate for the open test section under dynamic loading conditions.

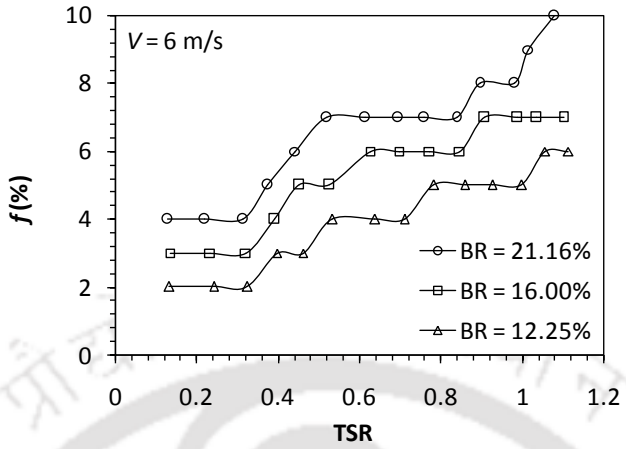

Figure 5.18: Relationship of blockage correction factor with TSR and BR

The effectiveness of the correlations adapted for this type of wind tunnel with an open test section under different tip speed ratios (TSRs) and blockage ratios (BRs) is presented. Consequently, this study shows that the dimensions of the wind tunnel test section and turbine models are not sufficient enough to describe the magnitude of the blockage correction under various loading conditions. Rather, it is significantly influenced by the change in TSR and BR. It is evident that the blockage effects are very much sensitive, and increase (f = 1–10%) with the increase of TSR and BR, and hence, this should be taken into account. With the increase of rotational speed of the turbine (increase of TSR), the intensity of flow expansion also increases. In contrast, with the increase BR, the blockage caused by the turbine blades increases significantly. Thus, at higher TSR and BR, the measured data require a higher magnitude of blockage correction.

For BR = 21.16%, the desired value of f lies in the range of 4–10%. At low TSR (<0.5), $f \leq$ 6% correction is required, whereas for TSR = 0.5–0.9, f = 7% and for TSR > 0.9, a comparatively higher blockage correction (f = 8–10%) are found to be useful. For BR = 16%, f in the range of 3–7% has to be taken into account with respect to TSR. However, as the BR further approached to a lower value (BR = 12.25%), at low TSR (<0.5), the correction required is only 2–3% and at higher TSR (>0.5), f = 4–6% is found to be incorporated.

CHAPTER –6

Experiments on Conventional and Modified Bach Type SSWTs

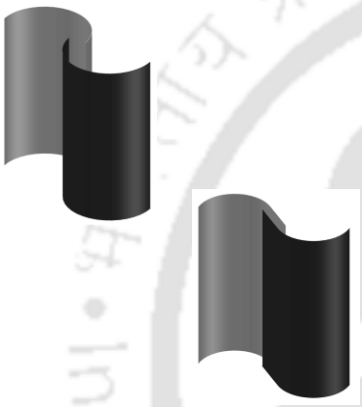

Chapter Outline

Overview

This chapter details the experimental investigation carried out on the conventional and modified Bach type SSWTs that are achieved from the computational studies. As aspect ratio (height to diameter of the turbine) is one of the very important parameters for designing a suitable small-scale wind turbine, a number of turbine models with different aspect ratios are tested in the low speed wind tunnel. Performance indices such as power and torque coefficients are calculated corresponding to variable tip speed ratio. Upon arriving at a suitable aspect ratio, experiments are further conducted to substantiate the effect of overlap ratio on the performance of the conventional SSWT. Further, experimental data of the modified Bach type SSWT are compared to the classical Bach and semi-circular type SSWTs. The results depicted a similar trend of performance improvement for modified SSWT as perceived in the simulation studies.

6.1 Experiments on conventional SSWT

Through unsteady simulations, the effect of overlap ratio (δ) on the performance of SSWT is discussed in Chapter-3. Looking at the outcome of study, initially experiments are planned with conventional SSWT models. As already discussed in Chapter-2, the turbine aspect ratio, AR (H/D) plays an important role in achieving a satisfactory turbine performance. However, the available literature does not give a clear-cut indication on the selection of a suitable AR. In view of this, experiments are executed to find the effect of AR on the performance of SSWTs.

6.1.1 Effect of aspect ratio

The conventional SSWT models in the range of AR = 0.7–1.2 are studied. This is accomplished by altering the overall diameter of the turbine and keeping the height constant at 230 mm. The effect of end plates ($D_o = 1.1D$) is also considered. The performance indices such as torque and power coefficients are calculated corresponding to variable rotational rate and mechanical load applied to the turbine. Tests are carried out at different wind speeds ranging between V = 3.8–9.8 m/s. Figures 6.1 through 6.8 show the effect of AR on the performance indices of SSWT at 4.5 m/s, 6.2 m/s, 7.8 m/s and 9.8 m/s, respectively. It is observed that low aspect ratios (AR< 1.0) are giving better performance at low TSR. However, to be precise, AR = 0.70 stands better only upto TSR < 0.30, AR = 0.80 to 0.90 for 0.3 > TSR < 0.50 and AR = 0.90 to 1.0 give a better power characteristics at TSR = 0.50 to 0.60. In contrast, with the increase of TSR beyond 0.6, AR = 1.1–1.2 give better performance characteristics. It is mainly due to fact that with the increase of both AR and TSR, the turbine power to weight ratio increases and the effect of inertia on the turbine rotational rate reduces.

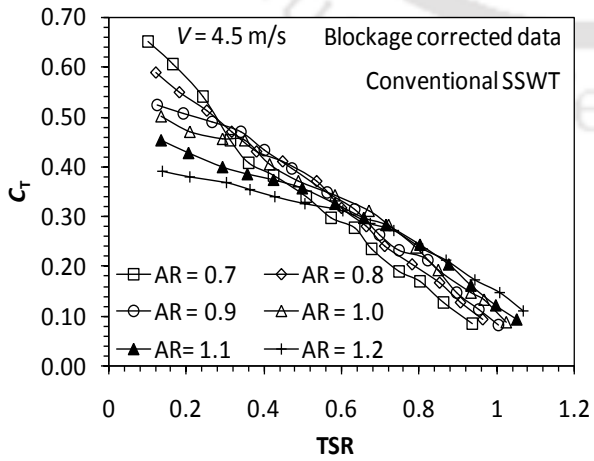

Figure 6.1: Variation of C_T for variable AR at V = 4.5 m/s

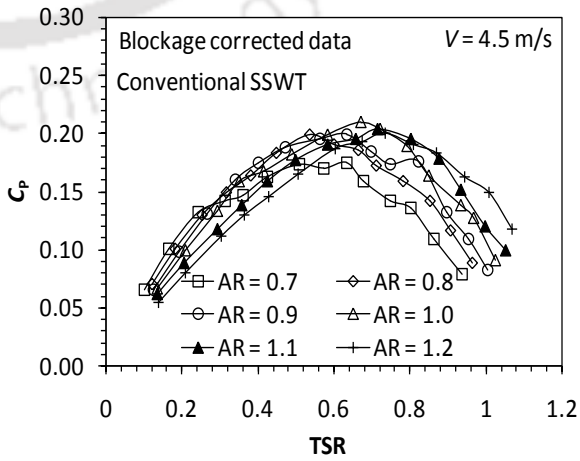

Figure 6.2: Variation of C_P for variable AR at V = 4.5 m/s

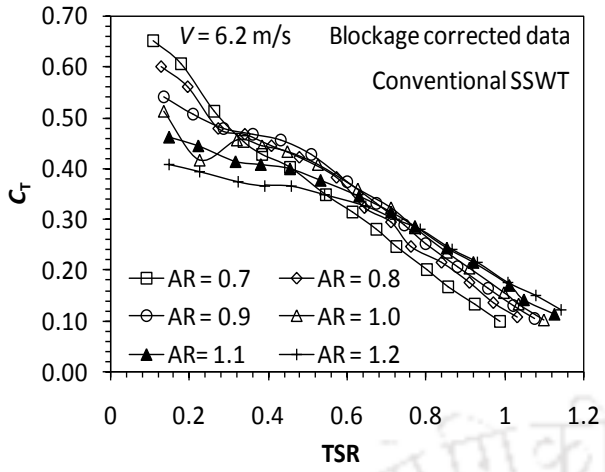

Figure 6.3: Variation of C_T for variable AR at V = 6.2 m/s

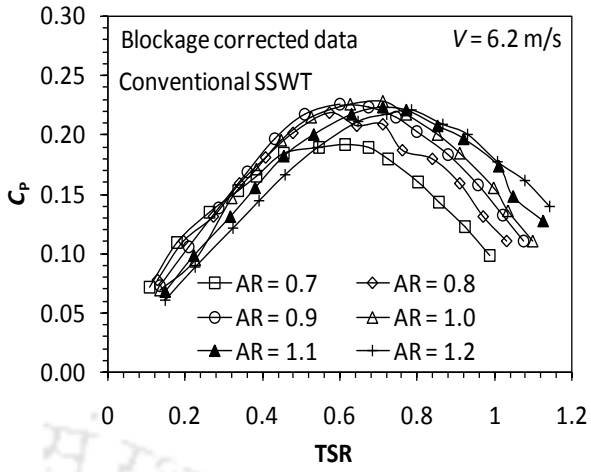

Figure 6.4: Variation of C_P for variable AR at V = 6.2 m/s

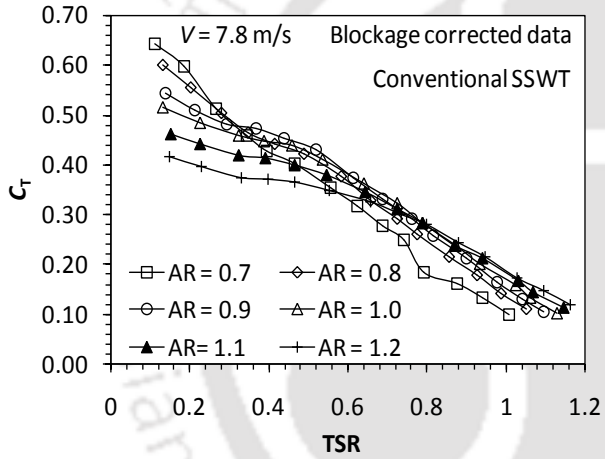

Figure 6.5: Variation of C_T for variable AR at V = 7.8 m/s

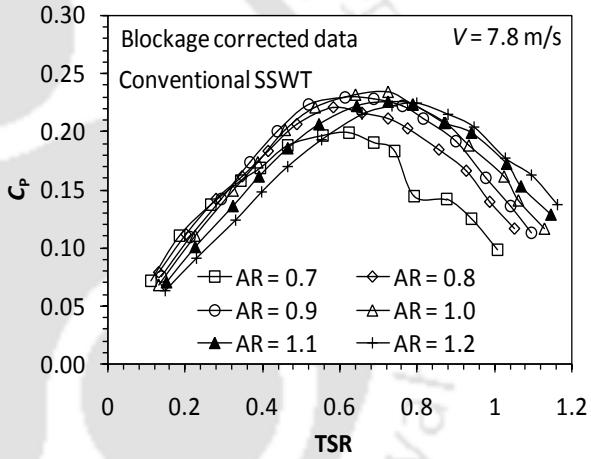

Figure 6.6: Variation of C_P for variable AR at V = 7.8 m/s

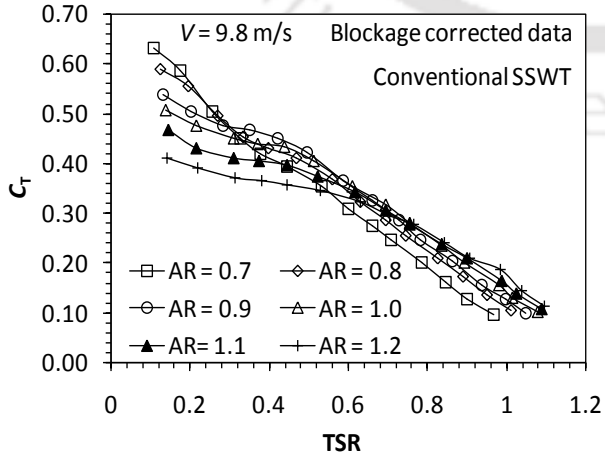

Figure 6.7: Variation of C_T for variable AR at V = 9.8 m/s

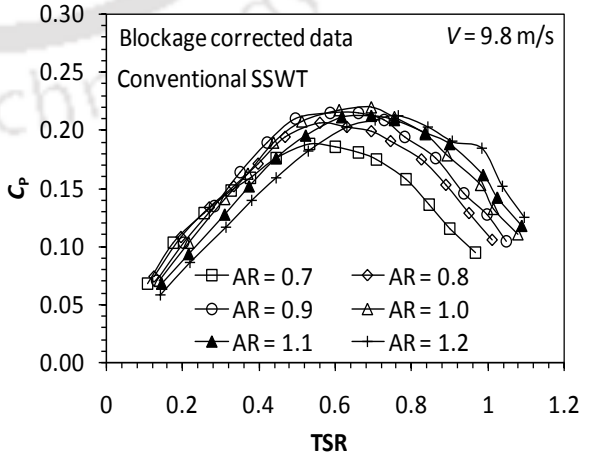

Figure 6.8: Variation of C_P for variable AR at V = 9.8 m/s

6.1.2 Effect of overlap ratio

The SSWT model with an overlap ratio (δ = 0.20) is fabricated for carrying out wind tunnel tests. This overlap ratio is selected from the simulation studies, details of which are reported in Chapter-3. The turbine aspect ratio of AR = H/D = 1.1 is chosen on the basis of the above experimental studies (Section 6.1.1). The overlapped blades are tested and compared with non-overlapped blades at different wind speeds. The torque and power characteristics curves obtained are shown in Figures 6.9 to 6.16.

At V= 4.5 m/s, a better torque characteristics is observed with overlapped blades (Figure 6.9), which in turn while plotted as power characteristics, gives C_{Pmax} of 0.21 at TSR = 0.67 (Figure 6.10). In contrast, for non-overlapped SSWT, the C_{Pmax} is found to be 0.16 at TSR = 0.59. Thus, a performance gain of 31.25% is achieved with overlapped SSWT (δ = 0.20). This power improvement is mainly due to acceleration of flow through the overlap region that inserts pressure drag on the concave side of the returning blade and thus, enhances the net torque characteristics in the rotational direction of the turbine.

Similarly, for other wind speeds, the semi-circular SSWTs are tested for overlapped and non-overlapped conditions. For overlapped SSWT, at V= 6.2 m/s, 7.8 m/s and 9.8 m/s, the C_{Pmax} is found to be 0.23 (TSR = 0.71), 0.23 (TSR = 0.73), and 0.22 (TSR = 0.69), respectively, whereas, for non-overlapped SSWT, the obtained C_{Pmax} is 0.16 (TSR = 0.62), 0.17 (TSR = 0.64), and 0.16 (TSR = 0.61), respectively. This analysis indicates that the value of maximum C_P for conventional SSWT can reach up to 0.23 with a suitable AR = 1.1 and δ = 0.20.

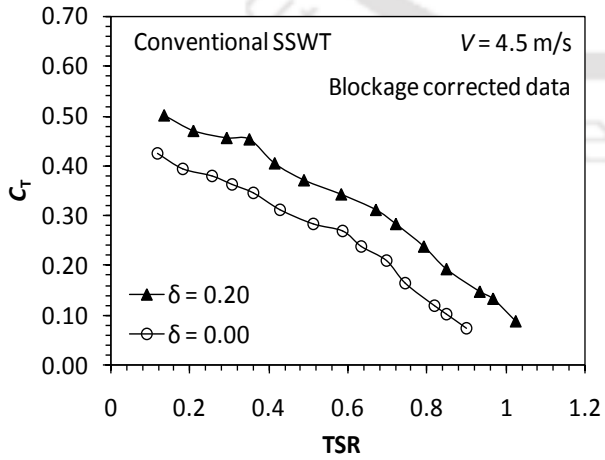

Figure 6.9: Variation of C_T for conventional SSWT with and without overlap at V = 4.5 m/s

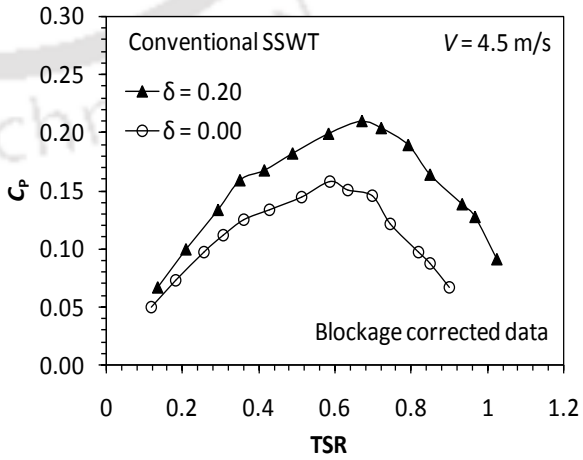

Figure 6.10: Variation of C_P for conventional SSWT with and without overlap at V = 4.5 m/s

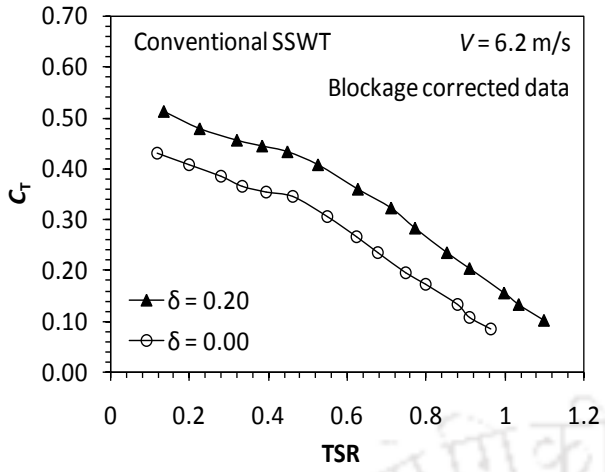

Figure 6.11: Variation of C_T for conventional SSWT with and without overlap at V = 6.2 m/s

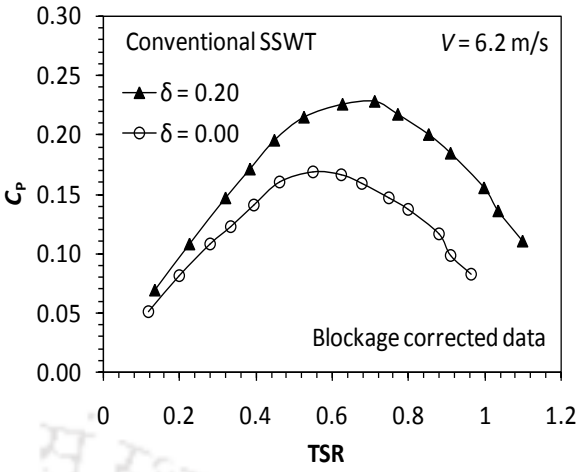

Figure 6.12: Variation of C_P for conventional SSWT with and without overlap at V = 6.2 m/s

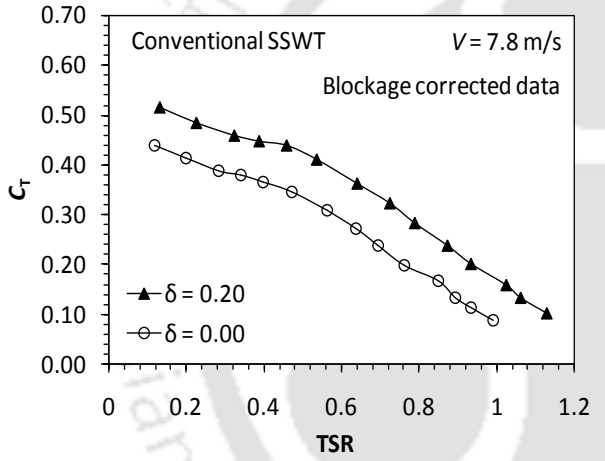

Figure 6.13: Variation of C_T for conventional SSWT with and without overlap at V = 7.8 m/s

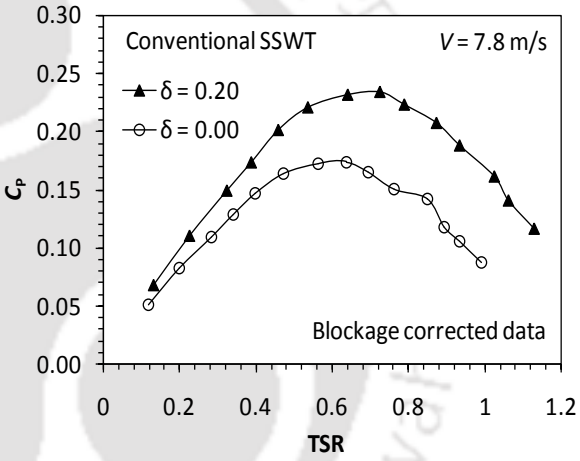

Figure 6.14: Variation of C_P for conventional SSWT with and without overlap at V = 7.8 m/s

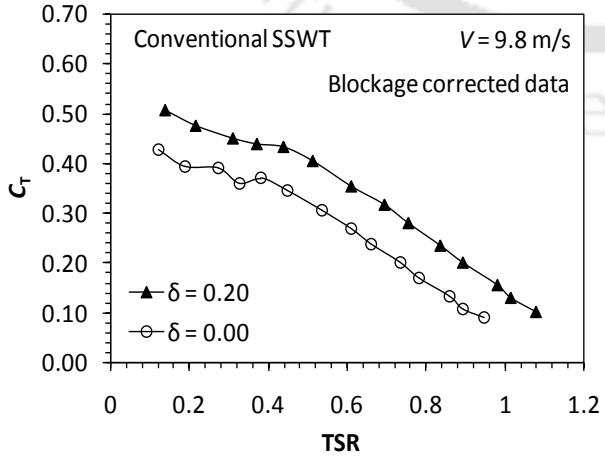

Figure 6.15: Variation of C_T for conventional SSWT with and without overlap at V = 9.8 m/s

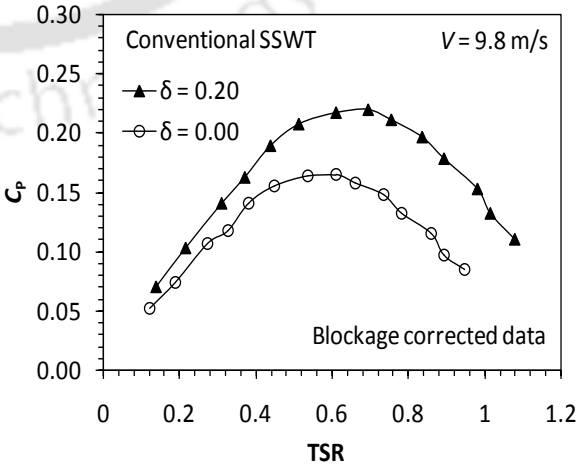

Figure 6.16: Variation of C_P for conventional SSWT with and without overlap at V = 9.8 m/s

6.2 Experiments on modified Bach type SSWT

As discussed in Chapter-3, the best Bach type design is obtained with ϕ = 135° and δ = 0.40, where ϕ is the blade arc angle and δ is the blade overlap ratio. This design has been named as modified Bach type SSWT. This Bach type model is fabricated and tested in the low speed wind tunnel. Experiments are carried out at different wind speeds under the effect of dynamic loading as discussed in Chapter-4. The turbine height to diameter ratio (AR) is selected as H/D = 1.1, where $H = D_o$ = 230 mm. As per standard practice, the end plate diameter is taken as D_o = 1.1D. The results obtained from these experiments are compared with that of conventional SSWT (δ = 0.20) and are shown in Figures 6.17 to 6.24.

At, V = 4.5 m/s, the modified Bach SSWT (ϕ = 135° and δ = 0.40) has shown a better torque and power characteristics as compared to conventional semi-circular blades (Figures 6.17 and 6.18). At this wind speed, for modified Bach type SSWT has shown a maximum C_P of 0.27 (TSR = 0.72), whereas conventional SSWT (δ = 0.20) has shown a maximum C_P of 0.21 (TSR = 0.67).

Similarly, the modified Bach type model at other wind speeds gives a better torque and power characteristics as compared to conventional SSWT (Figures 6.19 to 6.24). At V= 6.2 m/s, 7.8 m/s and 9.8 m/s, the C_{Pmax} for modified SSWT is found to be 0.29 (TSR = 0.78), 0.30 (TSR = 0.80), and 0.28 (TSR = 0.77), respectively, which indicates a performance gain of 31.82%, 30.43% and 27.27% over conventional SSWT, respectively.

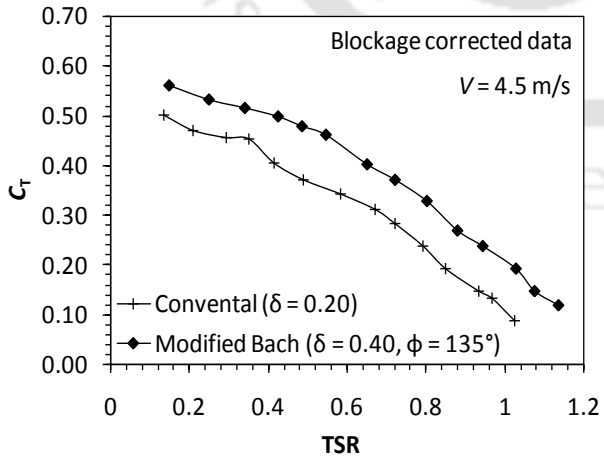

Figure 6.17: Variation of C_T for modified Bach type SSWT at V = 4.5 m/s

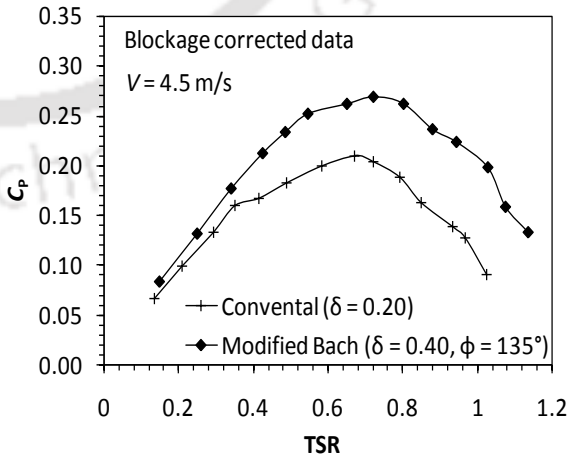

Figure 6.18: Variation of C_P for modified Bach type SSWT at V = 4.5 m/s

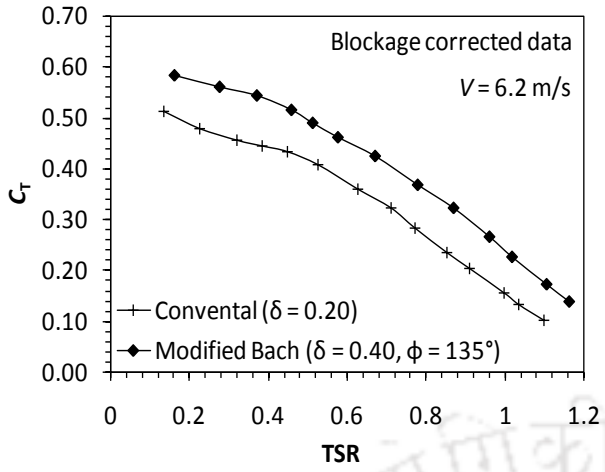

Figure 6.19: Variation of C_T for modified Bach type SSWT at V = 6.2 m/s

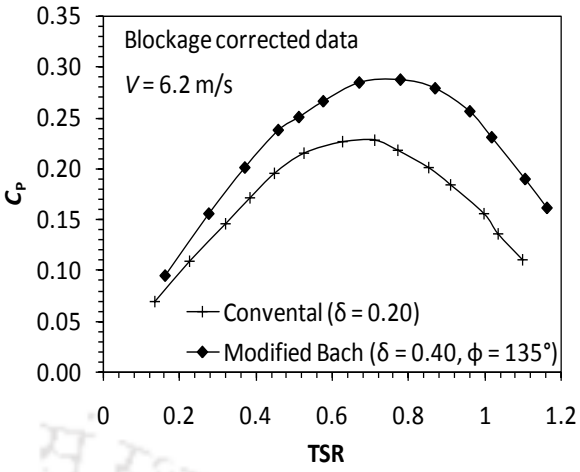

Figure 6.20: Variation of C_P for modified Bach type SSWT at V = 6.2 m/s

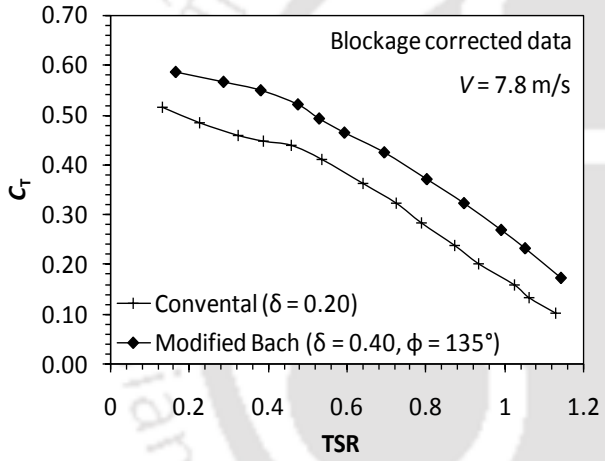

Figure 6.21: Variation of C_T for modified Bach type SSWT at V = 7.8 m/s

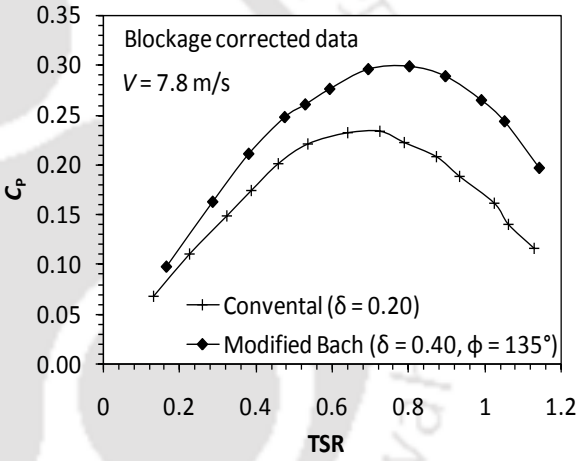

Figure 6.22: Variation of C_P for modified Bach type SSWT at V = 7.8 m/s

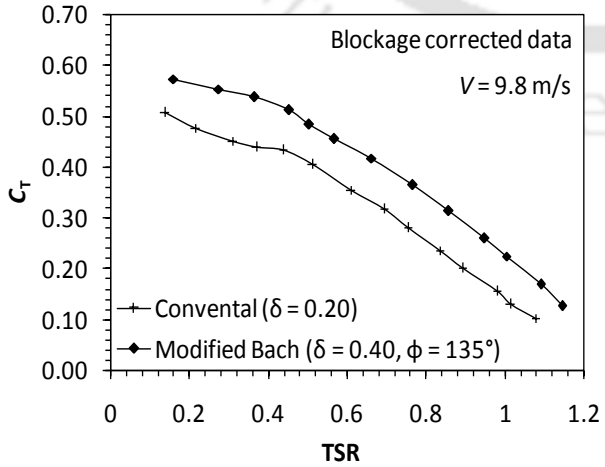

Figure 6.23: Variation of C_T for modified Bach type SSWT at V = 9.8 m/s

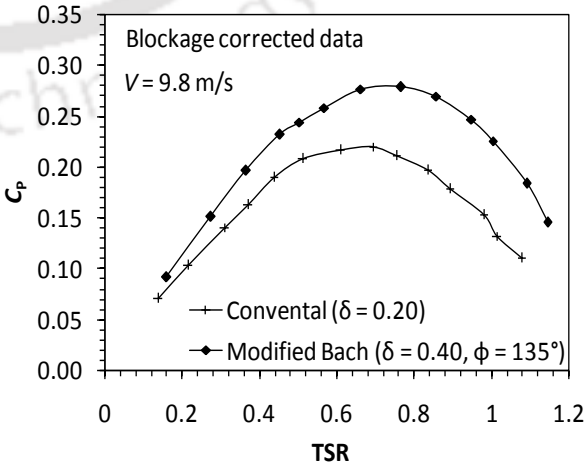

Figure 6.24: Variation of C_P for modified Bach type SSWT at V = 9.8 m/s

A comparative study was carried out for modified and classical Bach type SSWTs at V = 6.2 m/s (Figures 6.25 and 6.26). A numerical study on classical Bach type turbine is reported recently (Kacprzak *et al*., 2013). In the present investigation, the classical Bach type has shown a C_{Pmax} of 0.26 at TSR = 0.73. The modified Bach type, on the other hand, has shown a C_{Pmax} of 0.30 at TSR = 0.81. Thus, a performance gain of 15.4% is obtained with the modified Bach type over the former one. This is basically due to the flow acceleration through the overlap passage, which enabled an additional force to the concave side of the returning blade.

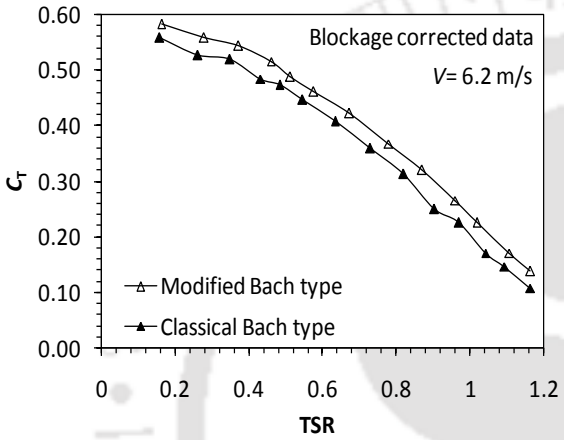

Figure 6.25: Variation of C_T for classical and modified Bach type SSWTs

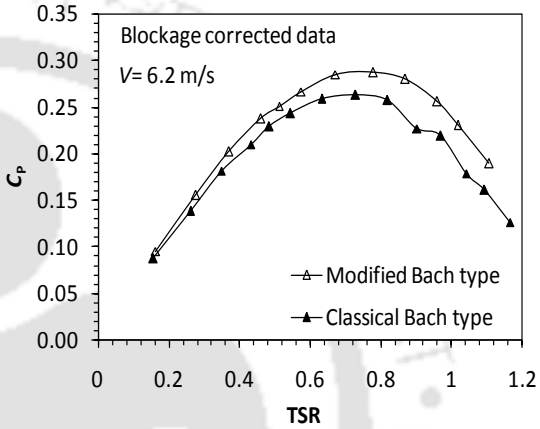

Figure 6.26: Variation of C_P for classical and modified Bach type SSWTs

6.3 Summary

The aspect ratio, which is an important design parameter for SSWTs, is assessed by testing various turbine models in the wind tunnel. At low rotational rate, the inertia effects are more prominent. Thus, at low tip speed ratios (TSR <0.6), low aspect ratios (AR = 0.7–1.0) have shown a better torque and power characteristics. However, with the increase of turbine rotational rate, i.e. with the increase in TSR beyond 0.6, the inertia effects reduces, and the higher aspect ratios (AR = 1.1–1.2) give better performance characteristics. Observing the performance trends at different wind speeds, AR =1.1 is selected for the further analysis of SSWTs. The conventional SSWT (δ = 0.20) and modified Bach type SSWT (ϕ = 135° and δ = 0.40) obtained from the 2D simulation study (Chapter-3) are tested. It is observed that with overlapped blades, conventional SSWT shows a C_{Pmax} of 0.23 at TSR = 0.73. In contrast, the modified Bach type SSWT depicts a C_{Pmax} of 0.30 at TSR = 0.81, indicating a performance gain of 30.4% and 15.4% over conventional and classical Bach type SSWT, respectively.

CHAPTER –7

Development and Analysis of the Newly Developed SSWT

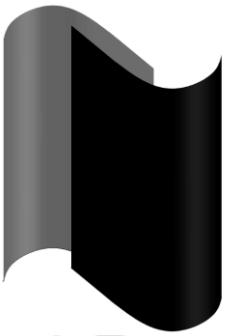

Chapter Outline

Overview

This chapter presents the development of a new blade shape for Savonius-style wind turbines. This novel shape of the turbine blade is evolved from a series of experiments with different types of blades in the recent past. The performance and starting characteristics of this newly developed turbine blade are reported. The results obtained are compared with other standard blades such as semi-circular, semi-elliptic, Benesh and Bach types. All the reported experimental data are inclusive of wind tunnel blockage corrections. Further, the effects of wind speed on the dynamic and static characteristics are also discussed. With the newly developed SSWT, noticeable improvements in the performance and starting characteristics are observed over other tested models. Further, the performance of the newly developed SSWT is analyzed under the effects of flow orientation with the help of deflectors placed upstream to the turbine.

7.1 Development of new blade profile

During the last 40 years, a host of researchers have carried out investigations on SSWTs. However, most of the studies revolved around conventional semi-circular blades. A few investigators carried out the performance analysis with helical and twisted blades. Although noticeable performance gains were achieved, however, the designs reported seemed to have been more complex and expensive (Grinspan *et al*., 2004; Saha and Rajkumar, 2006; Kamoji *et al*., 2009a; Damak *et al*., 2013). Since one of the major benefits of SSWT is its design simplicity, and low cost, a design modification having more complexity should probably not be encouraging. In this aspect, some studies with modified blade shapes were attempted reporting encouraging results. This has brought a renewed interest among the researchers to pursue further and detailed assessment of the blade design (Modi *et al*., 1984; Modi and Fernando, 1989; Kamoji *et al*., 2009b). Thus, in order to boost the applicability of these turbines, a novel but simple SSWT is developed and tested in a low speed wind tunnel.

Figure 7.1 shows the newly developed blade profile that consists of several individual arcs, where the dimensions are given with respect to chord length (*d*) of the blade. This novel blade profile was generated from a series of experimental studies on Bach and Benesh type turbines by altering the geometric arcs, overlap distances and dimensions of blade profiles. The impression of the new blade shape was measured and pattern has been prepared. Based on this blade geometry, a pattern was fabricated which was then used for manufacturing the turbine blades.

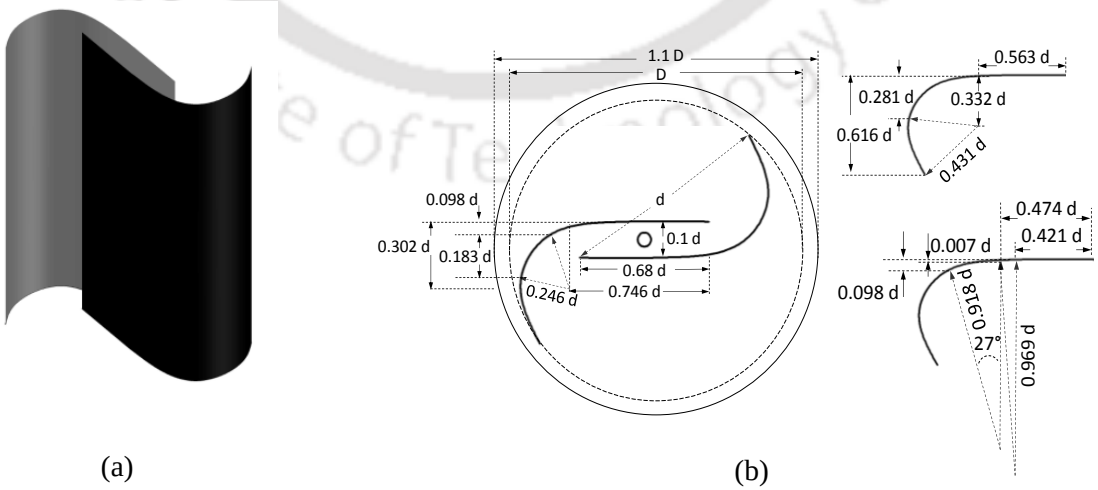

Figure 7.1: (a) 3D view, and (b) dimensions of the newly developed SSWT

In order to have a direct comparison under an identical platform, an experimental analysis has been carried out with the newly developed SSWT in comparison with other standard blades such as semi-circular, semi-elliptic, Benesh and Bach types SSWT at different wind speeds (Figure 7.2).

Figure 7.2: Various Savonius-style wind turbines tested in the present study

7.2 Description of blade profiles

Figure 7.3 shows the dimensions of various blade profiles tested in this experimental study. As seen from Figures 7.3(a) and 7.3(b), the overlap distance between the semi-circular and semi-elliptic blade profiles are kept as 20% of the blade chord length. The Benesh type blade profile (Figure 7.3c) claimed to be one of the most efficient SSWT blade profiles (Benesh, 1996) is also tested. Figure 7.3(d) shows modified Bach type blade profile (ϕ = 135° and δ = 0.40) as discussed in the previous chapters. The dimensions of the newly developed blade profile are demonstrated in Figure 7.1.

In the present work, the end plates are used at the top and at the bottom of turbine models. For all the test cases, the height of the turbine (H) to end plate diameter (D_o = 1.1 D) ratio is maintained at 1 keeping $H = D_o$ = 230 mm. All the blades are fabricated from galvanized iron sheets of thickness 0.63 mm.

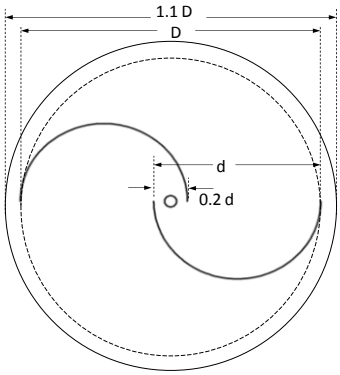

(a) Conventional semi-circular

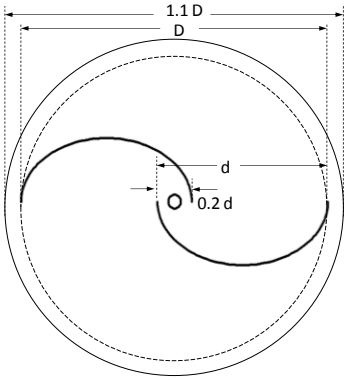

(b) Semi-elliptic

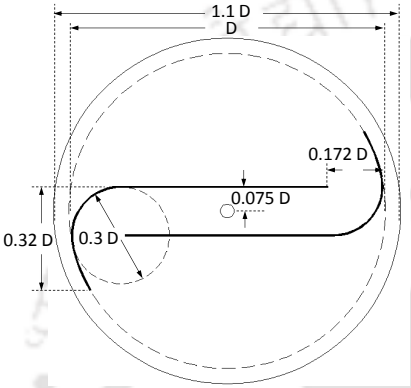

(c) Benesh type

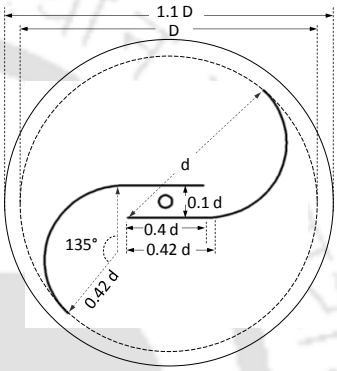

(d) Modified Bach type

Figure 7.3: Dimensions of various blade profiles

7.3 Analysis of performance characteristics

The torque and power characteristics of the newly developed SSWT are shown in Figures 7.4 and 7.5. It is observed that at 6.2 m/s, the C_{Pmax} is found to be 0.30 at TSR = 0.81. As discussed in chapter-6, at this wind speed, for modified Bach and conventional SSWTs, the C_{Pmax} are 0.29 (TSR = 0.78), and 0.23 (TSR = 0.71), respectively.

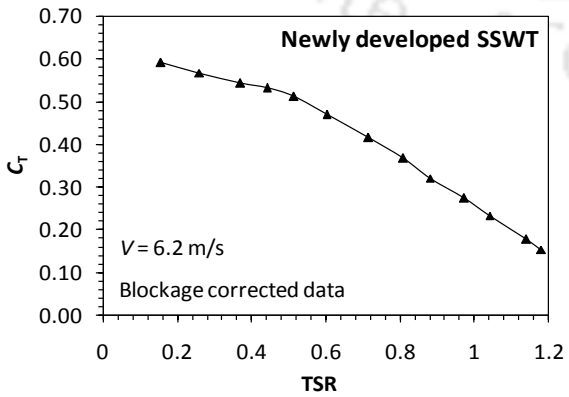

Figure 7.4: Variation of C_T for the newly developed SSWT at V = 6.2 m/s

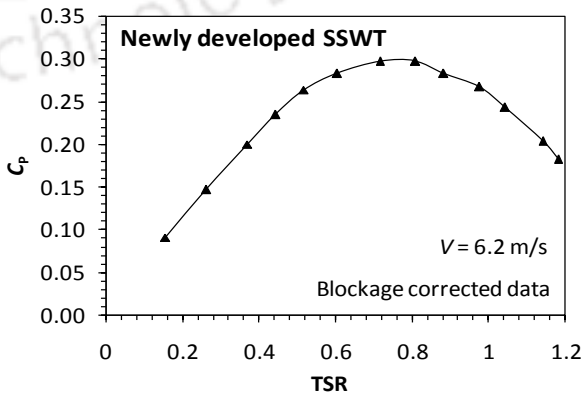

Figure 7.5: Variation of C_P for the newly developed SSWT at V = 6.2 m/s

Figures 7.6 and 7.7 show the torque and power coefficients of newly developed SSWT at V = 3.8 m/s. These performance indices are also presented for other tested turbines. It may be observed that the torque coefficient values decrease with the increase of TSR. This is mainly caused by the gradual loads applied to the turbine shaft, which in turn, reduces the rotational speed of the turbine. On the other hand, the power coefficient increases with an increase of TSR up to a certain maximum value, beyond which it decreases with further increase in TSR. The newly developed blade gives a C_{Pmax} of 0.27 at TSR = 0.77. At this low wind speed (V = 3.8 m/s), the modified Bach type has shown a nearly similar performance to the newly developed SSWT; whereas, the conventional semicircular blade has displayed the lowest power and torque coefficients. The performance gains of the newly developed SSWT over conventional, semi-elliptic and Benesh type turbines are found to be 28.6%, 17.4% and 3.8%, respectively.

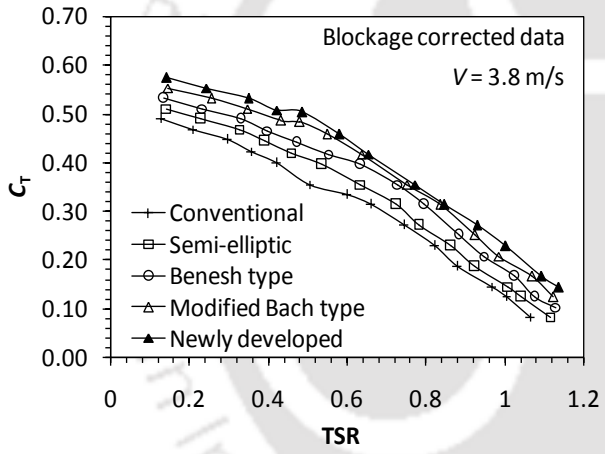

Figure 7.6: Variation of C_T at V = 3.8 m/s

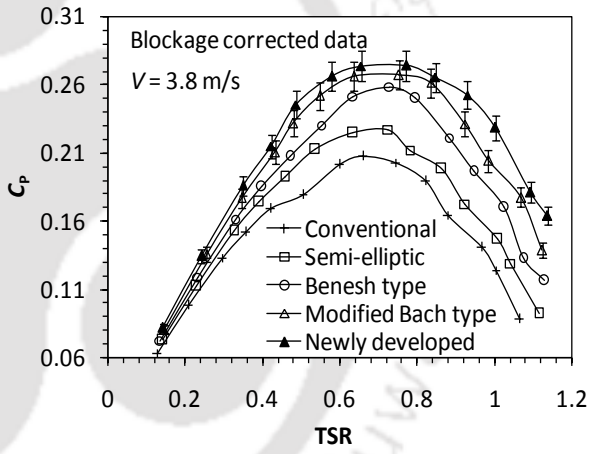

Figure 7.7: Variation of C_P at V = 3.8 m/s

Similarly, Figures 7.8 to 7.21 demonstrate the variations of torque and power coefficients at V = 4.5 m/s, 5.3 m/s, 6.2 m/s, 7.0 m/s, 7.8 m/s, 8.9 m/s, and 9.8 m/s, respectively. In all the cases, the newly developed two-bladed turbine shows an improvement in the power and torque coefficients as compared to other tested turbines.

With blockage correction, a C_{Pmax} of 0.31 is obtained for the newly developed turbine at V = 7.8 m/s and TSR = 0.82. In contrary, the C_{Pmax} for modified Bach type, Benesh type, semi-elliptic and conventional blade profiles are found to be 0.30, 0.29, 0.26 and 0.23, respectively at V = 7.8 m/s.

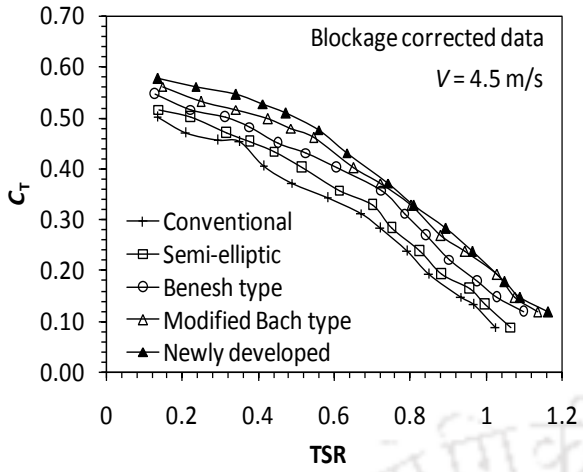

Figure 7.8: Variation of C_T at V = 4.5 m/s

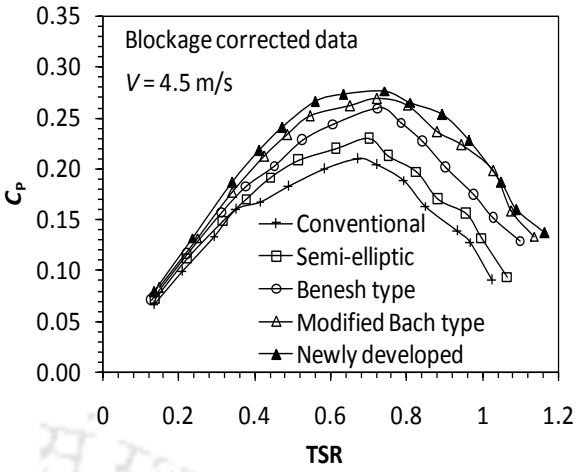

Figure 7.9: Variation of C_P at V = 4.5 m/s

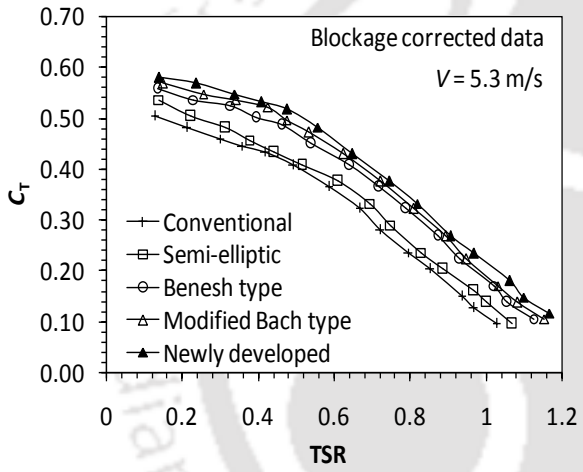

Figure 7.10: Variation of C_T at V = 5.3 m/s

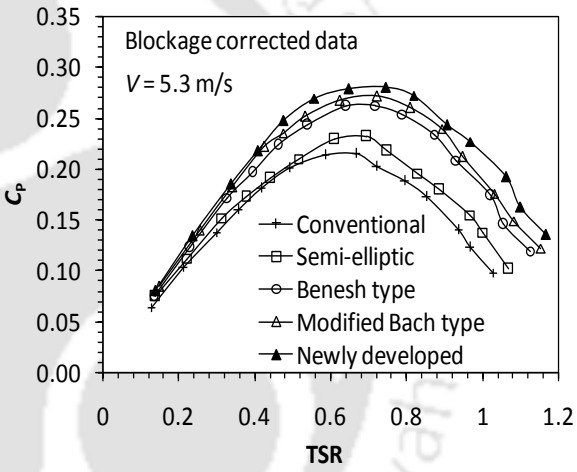

Figure 7.11: Variation of C_P at V = 5.3 m/s

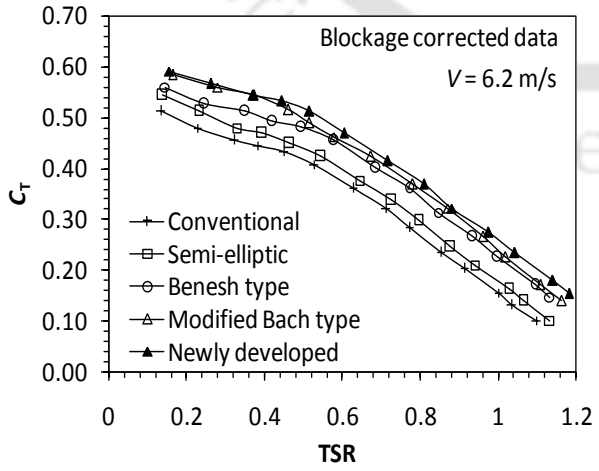

Figure 7.12: Variation of C_T at V = 6.2 m/s

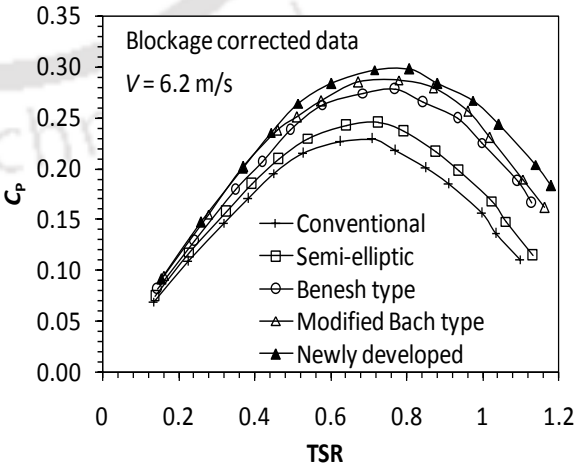

Figure 7.13: Variation of C_P at V = 6.2 m/s

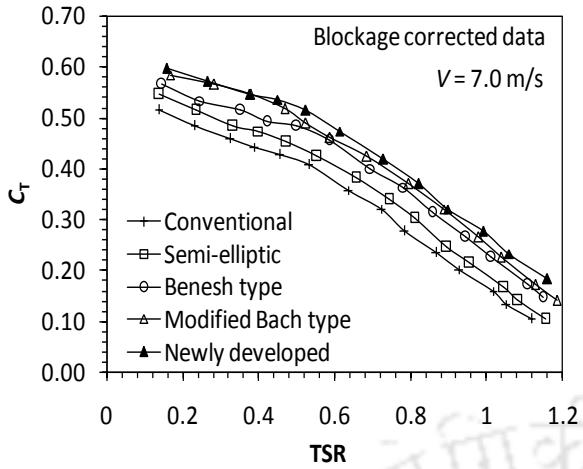

Figure 7.14: Variation of C_T at V = 7.0 m/s

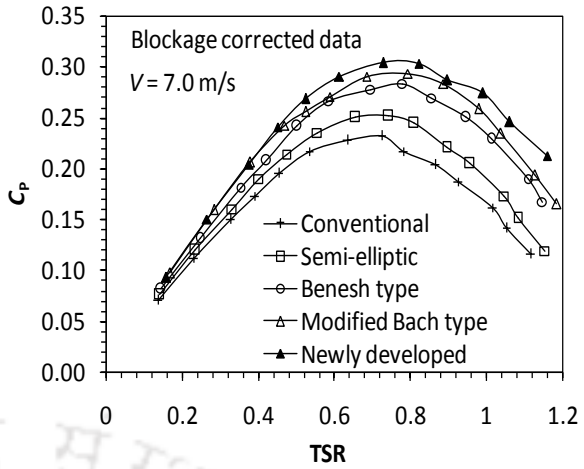

Figure 7.15: Variation of C_P at V = 7.0 m/s

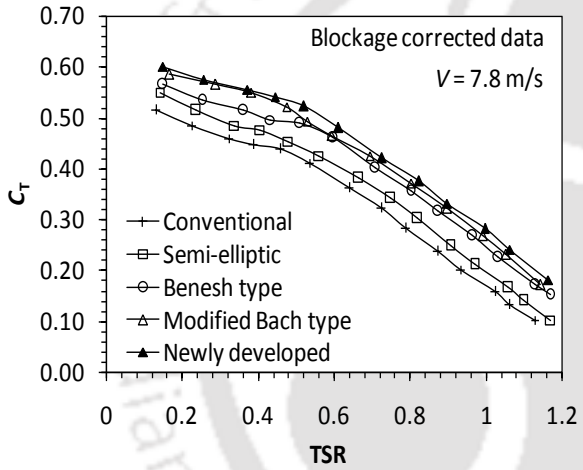

Figure 7.16: Variation of C_T at V = 7.8 m/s

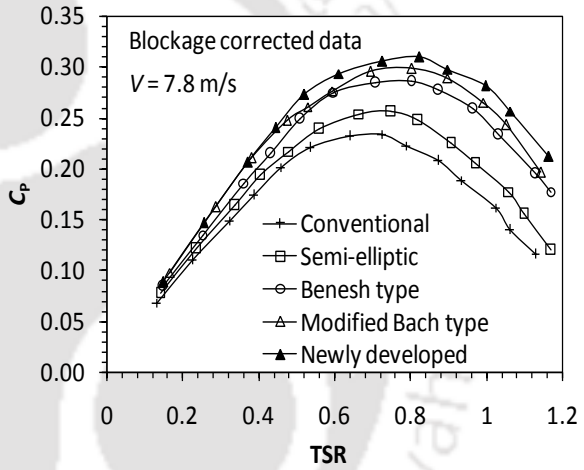

Figure 7.17: Variation of C_P at V = 7.8 m/s

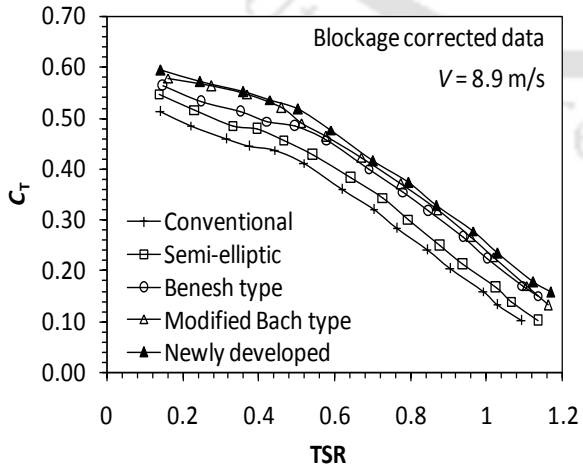

Figure 7.18: Variation of C_T at V = 8.9 m/s

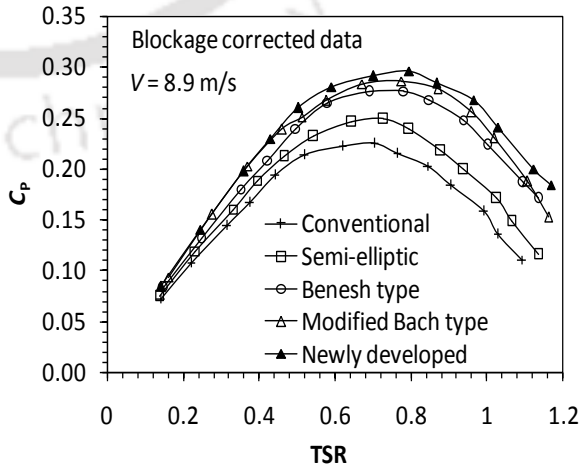

Figure 7.19: Variation of C_P at V = 8.9 m/s

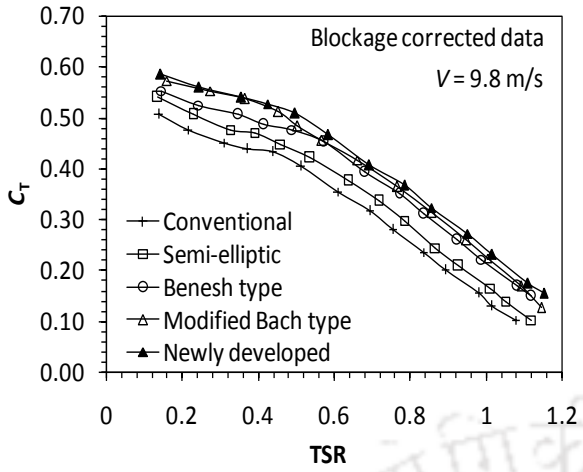

Figure 7.20: Variation of C_T at V = 9.8 m/s

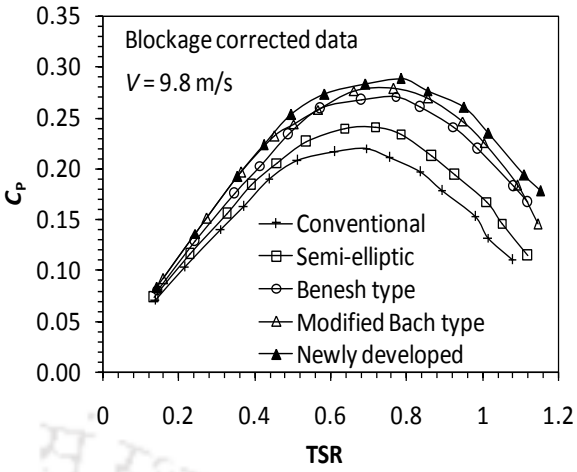

Figure 7.21: Variation of C_P at V = 9.8 m/s

Table 7.1 shows the values of maximum power coefficients corresponding to various TSRs at V = 3.8 m/s to 9.8 m/s. It is observed that for the new developed blade profile, the maximum power coefficients are obtained in the range of TSR = 0.74–0.83. Whereas, for modified Bach, Benesh, semi-elliptic and conventional type turbines, the C_{Pmax} values are found at TSR= 0.66–0.73, 0.69–0.75, 0.71–0.81 and 0.72–0.81, respectively. Thus, in each case, there is a shift in the range of optimum TSR. Figure 7.22 indicates the effect of wind speed on dynamic performances of the newly developed blade profile. It is seen that with the increase of wind speed up to V = 7.8 m/s, the C_{Pmax} increases, beyond which it again decreases.

Table 7.1: Maximum power coefficients corresponding to tip speed ratios (blockage corrected data)

Blade profile	V = 3.8 m/s		V = 5.3 m/s		V = 6.2 m/s		V = 7.8 m/s		V = 9.8 m/s	
	C_{Pmax}	TSR	C_{Pmax}	TSR	C_{Pmax}	TSR	C_{Pmax}	TSR	C_{Pmax}	TSR
New SSWT	0.27	0.77	0.28	0.75	0.30	0.81	**0.31**	**0.82**	0.29	0.79
Modified Bach	0.27	0.75	0.27	0.72	0.29	0.78	0.30	0.80	0.28	0.77
Benesh	0.26	0.73	0.26	0.72	0.28	0.77	0.29	0.80	0.27	0.77
Semi-elliptic	0.23	0.73	0.23	0.70	0.25	0.73	0.26	0.75	0.24	0.72
Conventional	0.21	0.66	0.22	0.67	0.23	0.71	0.23	0.73	0.22	0.69

However, without any blockage correction, the calculated experimental data representing the maximum values of torque and power coefficients are shown in Figures 7.23 and 7.24. For the newly developed, modified Bach, Benesh, semi-elliptic, and conventional bladed turbines, the C_{Pmax} values are found to be 0.34, 0.33, 0.32, 0.28 and 0.26, respectively.

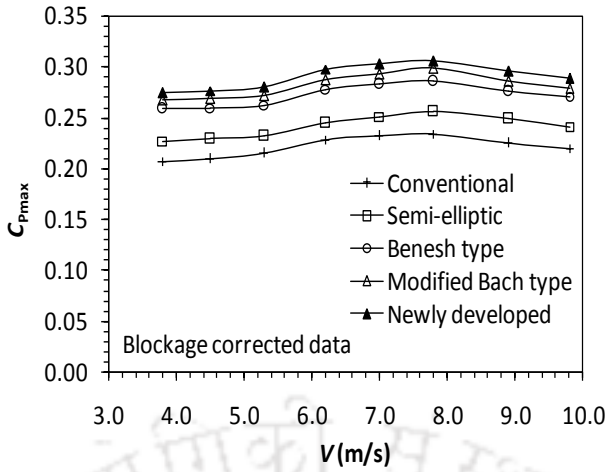

Figure 7.22: Effect of wind speed on the performance of SSWTs

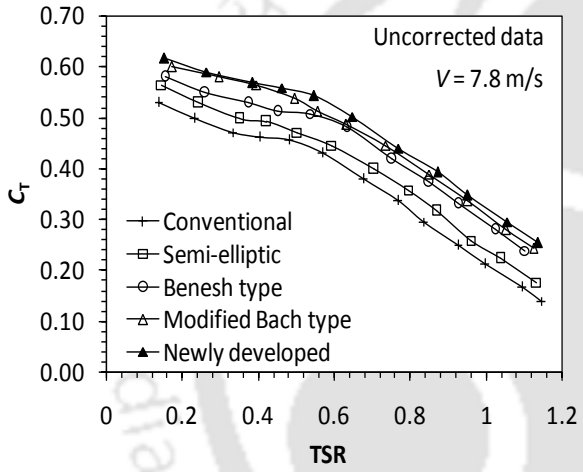

Figure 7.23: Variation of C_T without blockage correction at V = 7.8 m/s

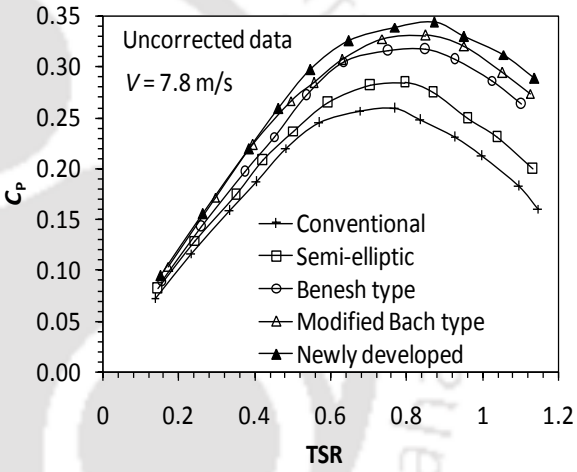

Figure 7.24: Variation of C_P without blockage correction at V = 7.8 m/s

7.4 Analysis of starting characteristics

The starting characteristic of SSWTs is often described through the analysis of static torque coefficients. Figures 7.25 to 7.32 demonstrate the static torque coefficients for various tested blade profiles at V = 3.8 m/s to 9.8 m/s. At V = 3.8 m/s, the conventional semi-circular blades show a very low static torque coefficients in the range of θ = 110°–170° and 290°–350° (Figure 7.25). During the experimental process, in this range, the conventional SSWT does not start by itself. More precisely, in the range of θ = 140°–170° and 320°–350°, the negative pressure on the returning blade caused the negative static torque coefficients. With the further increase of wind speed, similar starting problems are observed for conventional SSWT; however, the values of static torque coefficients are slightly increased (Figures 7.26

to 7.32). The peak starting performance is seen at angular positions of θ = 30°–60° and 210°–240° and at V = 9.8 m/s, the C_{TSmax} is obtained as 0.39 (Figure 7.32).

At V = 3.8 m/s, the semi-elliptic type shows poor starting performances in the range of θ = 120°–170° and 300°–350°, while the negative static torque coefficients are seen at θ = 150°–170° and 330°–350° (Figure 7.25). However, with the increase of wind speed, the starting performance got improved and the negative range got reduced to θ = 150°–160° and 330°–340° at V = 6.2 m/s (Figure 7.30). This has been further amended at V = 9.8 m/s, where the negative static torque coefficients were found only at θ = 160° and 360°. With the semi-elliptical blade, the highest static torque coefficient of C_{TSmax} = 0.41 is obtained at V = 9.8 m/s (Figure 7.32).

The Benesh type turbine has shown an improvement in terms of starting characteristics over semi-circular and semi-elliptical type turbines. The Benesh type, unlike the above two turbines, has completely overcome the negative values of C_{TS}. However, lower positive values are observed in the range of θ = 140°–170° and 320°–350°. At these angular positions, the positive values of C_{TS} obtained are insufficient for self-starting at lower wind speeds.

The modified Bach type has displayed improved C_{TS} over the Benesh type. At low wind speeds, the modified Bach type shows its self-starting incapability in the range of θ = 150°–170° and 330°–350°. Like previous models, this turbine also indicates high C_{TS} in the range of θ = 30°–60° and 210°–240°. For the Benesh and the modified Bach types, the C_{TSmax} values are found to be 0.46 and 0.49 at V = 9.8 m/s, respectively (Figure 7.32).

Among all the test cases, the newly developed SSWT is found to be most effective considering the self-starting criterion (Figures 7.25 to 7.32). With this turbine, the problems of self-starting can be substantially reduced, however, at low wind speed, this problem predominates in the range of θ = 160°–170° and 340°–350°. With the increase of wind speed, the starting problem at these angular positions gets significantly reduced. At V = 9.8 m/s, the maximum and minimum static torque coefficients are found to be 0.51 and 0.08, respectively (Figure 7.32).

A clear observation of maximum and minimum static torque coefficients for various turbine models is depicted in Table 7.2. It is noted that unlike the dynamic characteristics (Figure 7.22), the static characteristics increases with an increase of wind speed.

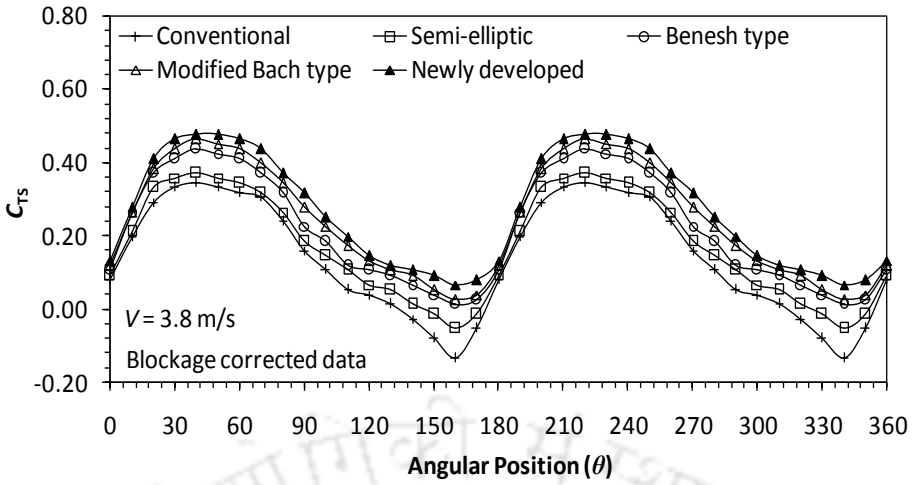

Figure 7.25: Variation of C_{TS} at V = 3.8 m/s

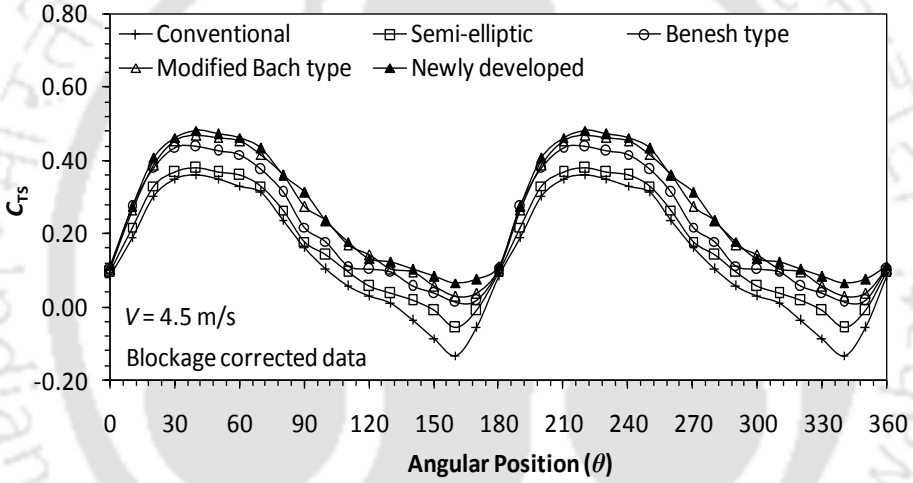

Figure 7.26: Variation of C_{TS} at V = 4.5 m/s

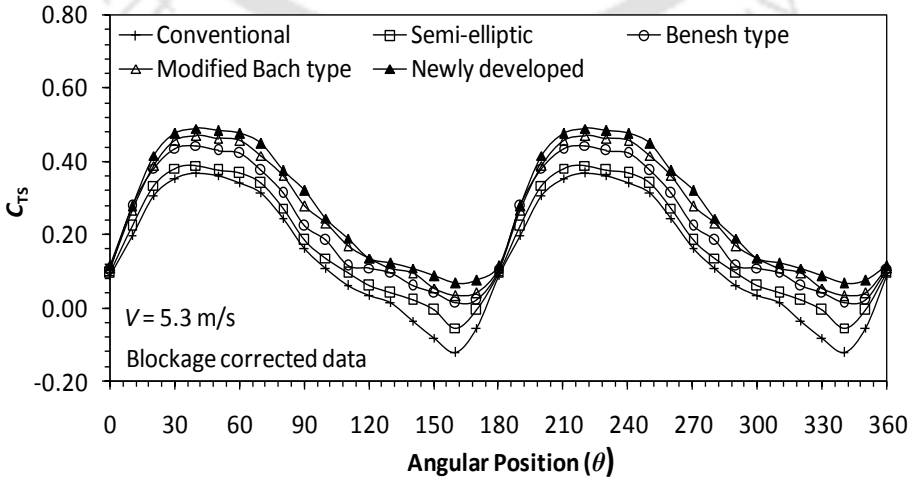

Figure 7.27: Variation of C_{TS} at V = 5.3 m/s

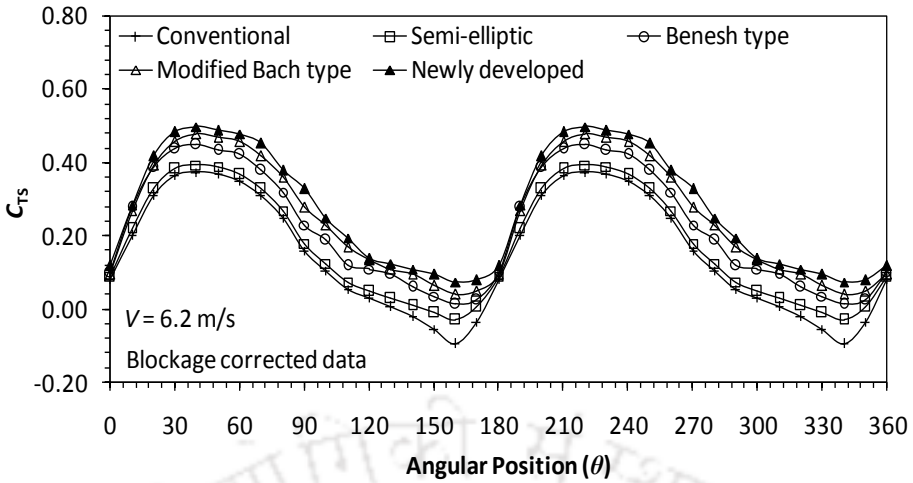

Figure 7.28: Variation of C_{TS} at V = 6.2 m/s

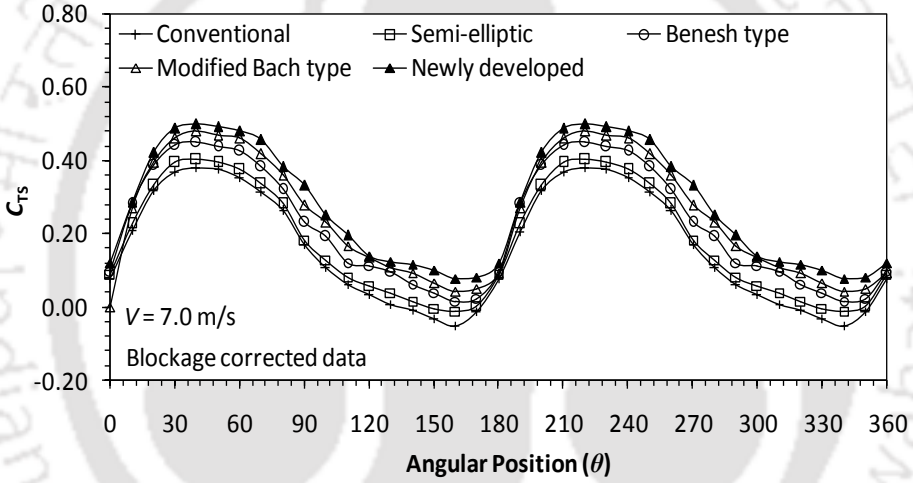

Figure 7.29: Variation of C_{TS} at V = 7.0 m/s

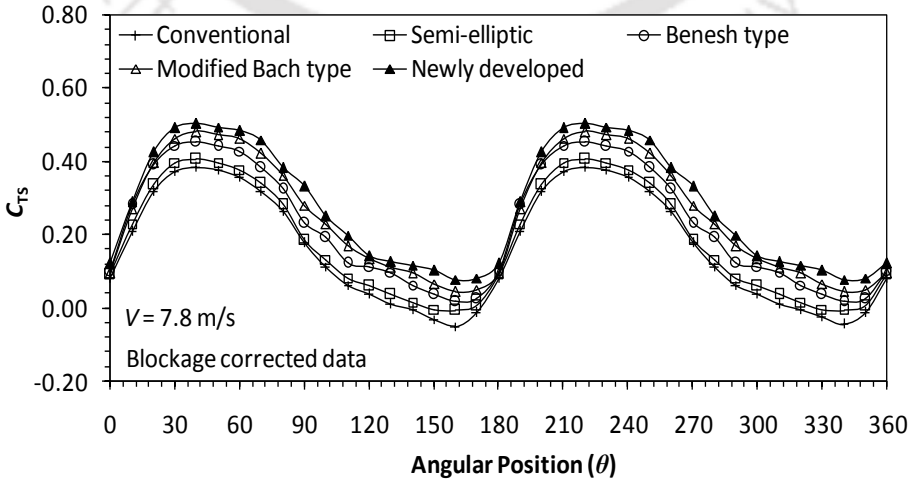

Figure 7.30: Variation of C_{TS} at V = 7.8 m/s

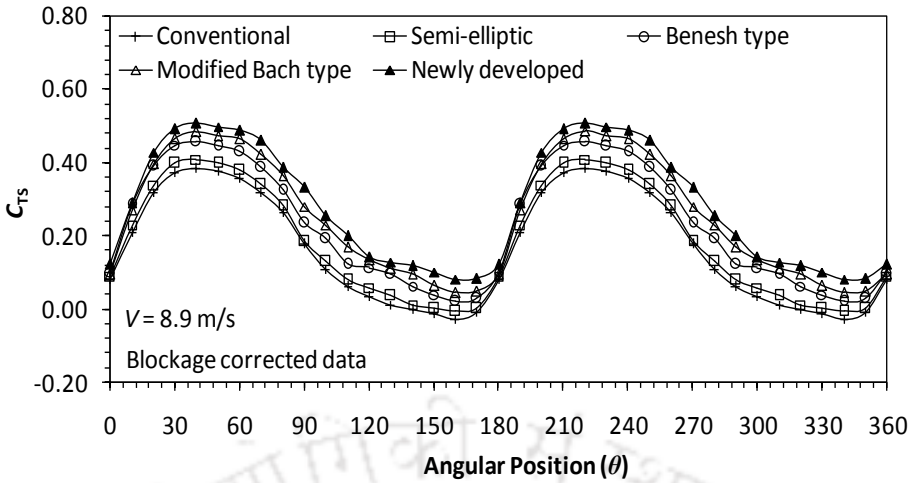

Figure 7.31: Variation of C_{TS} at V = 8.9 m/s

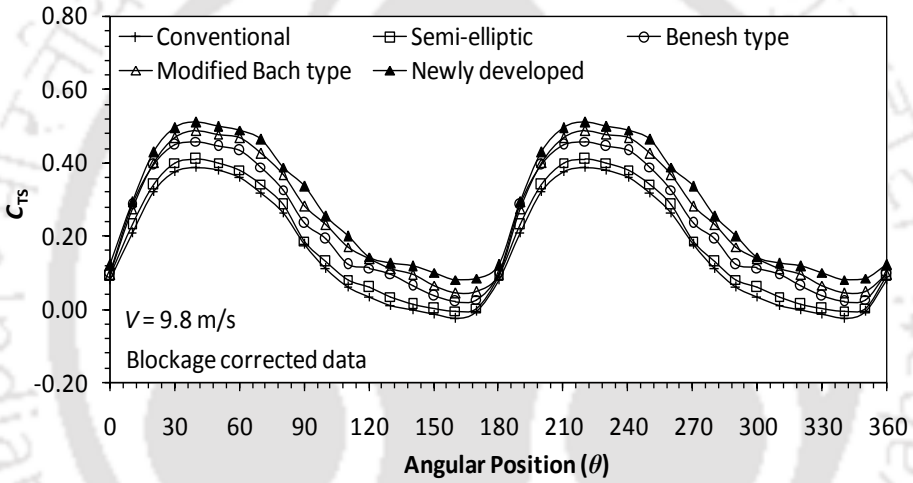

Figure 7.32: Variation of C_{TS} at V = 9.8 m/s

Table 7.2: Maximum and minimum coefficients of static torque at various wind speeds

Blade profile	V = 3.8 m/s		V = 5.3 m/s		V = 6.2 m/s		V = 7.8 m/s		V = 9.8 m/s	
	C_{TSmax}	C_{TSmin}	C_{TSmax}	C_{TSmin}	C_{TSmax}	C_{TSmin}	C_{TSmax}	C_{TSmin}	C_{TSmax}	C_{TSmin}
New SSWT	0.48	0.07	0.49	0.07	0.50	0.08	0.50	0.08	0.51	0.08
Modified Bach	0.46	0.03	0.47	0.03	0.48	0.04	0.48	0.04	0.49	0.05
Benesh	0.44	0.01	0.44	0.01	0.45	0.02	0.45	0.02	0.46	0.02
Semi-elliptic	0.37	-0.06	0.39	-0.06	0.39	-0.03	0.41	-0.01	0.41	-0.01
Conventional	0.35	-0.13	0.37	-0.12	0.37	-0.10	0.38	-0.05	0.39	-0.02

7.5 Effect of oriented flows

An attempt has been made to improve the efficiency of the SSWTs concentrated and oriented flows through installation of deflectors at different positions ahead of the turbine. For all the

experiments, the wind speed in the tunnel is kept constant at 6.2 m/s. The installation of deflectors in front of these turbines can augment the power in two ways viz., (i) the local acceleration of air flow incident on the advancing blade of the turbine, and (ii) the reduction in the negative torque created by the returning blade of the turbine.

7.5.1 Orientation of the deflectors

The concentrated flows are formed by varying the orientations of the deflectors ahead of the turbine blades. The flat type deflectors are selected based on the work reported in literature (Ushiyama and Nagai, 1988; Huda *et al*., 1992; Altan *et al*., 2008). These are made out of GI sheets of 1.2 mm thickness and a height of 450 mm and are placed either in front of the returning blade or in front of the both of the blades as shown in Figure 7.33.

The influence of deflector orientation is highly significant in order to reduce the negative torque produced by the returning blade. As indicated, the length of the deflectors was kept dissimilar to vary α and β, while the horizontal distances along the wind direction from section-1 to section-2 is kept constant at 250 mm. In the test section, the angles fabricated for deflector fitting at sections 1 and 2 are drilled at suitable locations so as to have proper orientations such as α, β, (R/X_r), and (R/X_a). The angles, α and β, are formed by the deflectors along the wind direction, while X_r and X_a are the horizontal distances of the deflectors from center of the shaft to the perpendicular direction of flow for the returning and advancing blades, respectively. However, in the present analysis, the deflector placed in front of the returning blade is tested for cases of α = 20° and 40° with dimensionless factors of (R/X_r) = 0.83 and 2.34 respectively. On the other hand, the deflector placed in front of advancing blade is tested for β = 0°, 10°, 20° and 30° with dimensionless factors of (R/X_a) = 0.55, 0.66, 0.83 and 1.17, respectively.

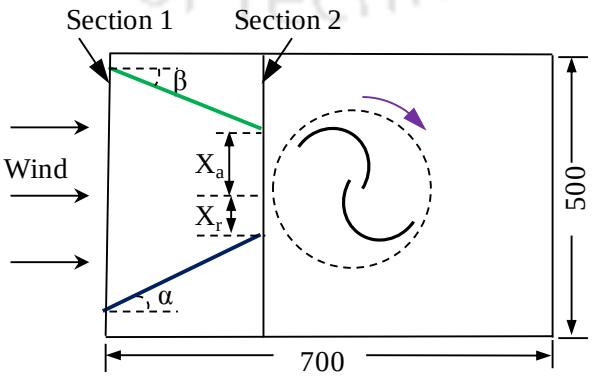

Figure 7.33: Deflectors positioned upstream to the turbine blades (all the dimensions are in mm)

Initially, to properly orient the deflectors, tests are conducted on conventional SSWTs (with δ = 0.20). In this perspective, the deflectors were placed in front of returning blade of overlapped turbine at α = 20° and 40°. The power and torque coefficients are calculated. The swept area is not considered the same for both the calculation. Without the deflector, the swept area is considered as the frontal area of the turbine. However, with deflector, the swept area is considered as (X_a + X_r) × height of the turbine. The obtained results are shown in Figures 7.34 and 7.35. With deflector placed at α = 40°, a significant improvement in the torque and power characteristics are observed. At α = 40°, the C_{Pmax} is found to be 0.30 at TSR = 0.82, while at α = 20°, the C_{Pmax} is obtained as 0.29 at TSR = 0.80. As discussed in previous chapters, without any deflector the conventional SSWT (with δ = 0.20) has shown a C_{Pmax} of 0.23 at TSR = 0.71. Thus, with deflectors placed ahead of the returning blade (α = 40°), a performance gain of 30.4% is achieved over without deflector SSWT.

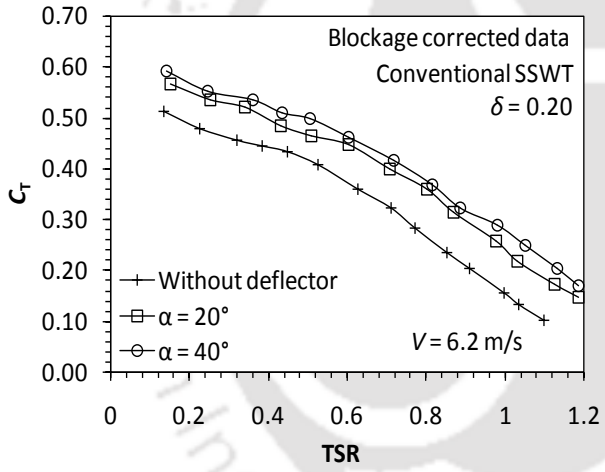

Figure 7.34: Variation of C_T with deflector in front of returning blade

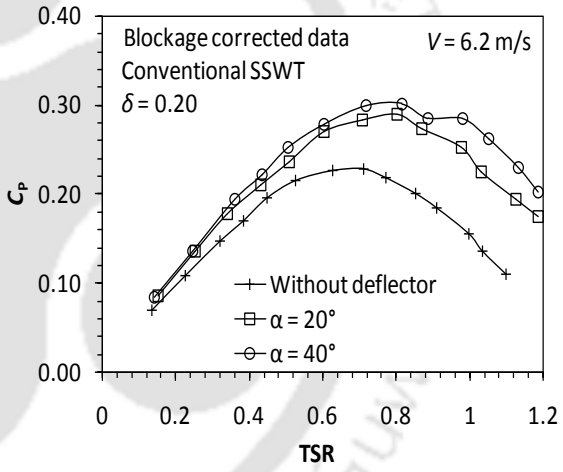

Figure 7.35: Variation of C_P with deflector in front of returning blade

Further, in order to accelerate the air flow incident on the advancing blade, the deflectors are placed in front of the advancing blade at angular positions of β = 0°, 10°, 20° and 30° with dimensionless factors of (R/X_a) = 0.55, 0.66, 0.83 and 1.17, respectively. The performance analysis in terms of C_T and C_P are shown in Figures 7.36 and 7.37. It is observed that at β = 0° and α = 40°, the C_{Pmax} is found to be 0.31 at TSR = 0.82. Similarly, for β = 20° and α = 40°, β = 30° and α = 40°, the C_{Pmax} is obtained as 0.29 at TSR = 0.80 and 0.22 at TSR = 0.70, respectively. A higher performance is noticed at α = 40°, and β = 10° with C_{Pmax} = 0.33 at TSR = 0.87, confirming a performance gain of 10% over deflector positioned in front of the

returning blade (α = 40°). It is mainly due to fact that at certain position of deflector, the air incident on the advancing blade is maximum, beyond which it adversely affects the incident flow. Thus, it is observed that under properly oriented flows (deflectors placed ahead of both the blades), an overall performance gain of 43.5% can be achieved over without deflector condition.

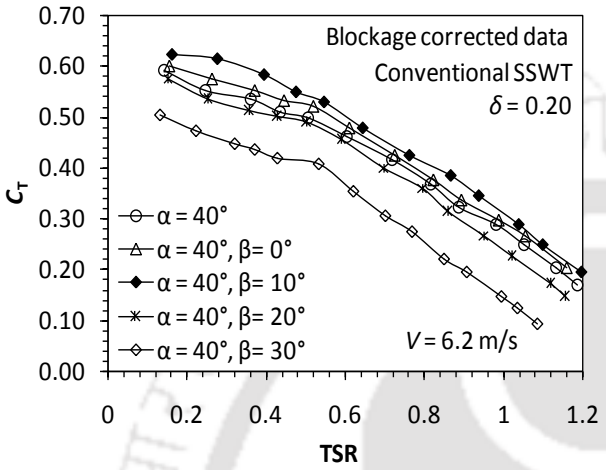

Figure 7.36: Variation of C_T with deflector in front of both the blades

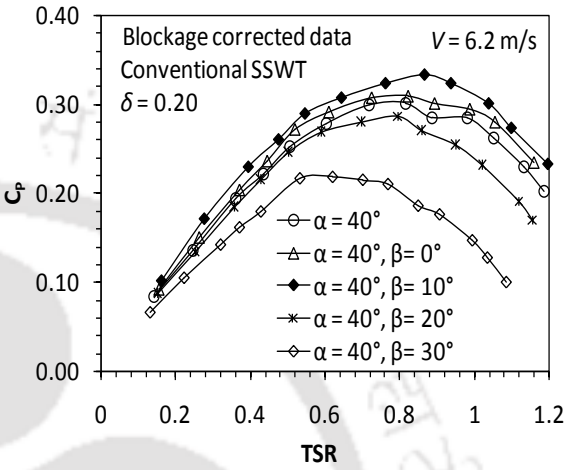

Figure 7.37: Variation of C_P with deflector in front of both the blades

7.5.2 Newly developed SSWT under orientated flows

Based on the suitable location of deflectors, an analysis has been carried out on the newly developed SSWT under the influence of oriented flows (Figure 7.38). The results obtained are compared with the modified Bach (Figure 7.39) and conventional semi-circular type SSWTs. All the tests are conducted at a wind speed of V = 6.2 m/s.

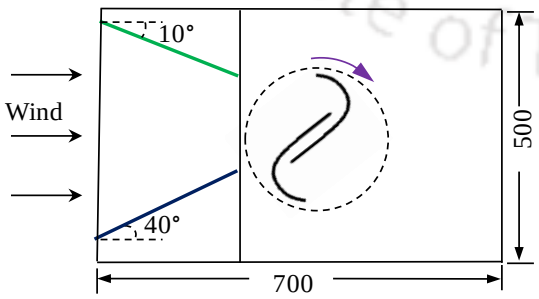

Figure 7.38: Newly developed SSWT under oriented flows (all the dimensions are in mm)

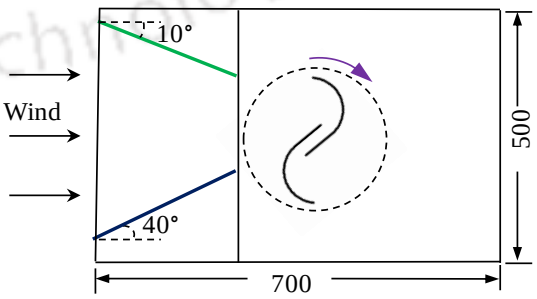

Figure 7.39: Modified Bach type SSWT under oriented flows (all the dimensions are in mm)

The torque and power coefficients calculated with and without deflectors are plotted in Figures 7.40 and 7.41. For the newly developed SSWT under the effect of oriented flows, the C_{Pmax} is found to be 0.41 at TSR = 0.95. In contrast, without deflectors, the C_{Pmax} is obtained as 0.31 at TSR = 0.82. Thus, for newly developed SSWT under the oriented and concentrated flows, a performance gain of 32.25% is achieved over free stream flow condition.

Similarly, for modified Bach type SSWT under the oriented and concentrated flows, the C_{Pmax} is found to be 0.39 at TSR = 0.90, a performance gain of 30% is attained over free stream flow condition. Figures 7.40 and 7.41 show a comparative study among the different SSWTs under the influence of concentrated and oriented flows.

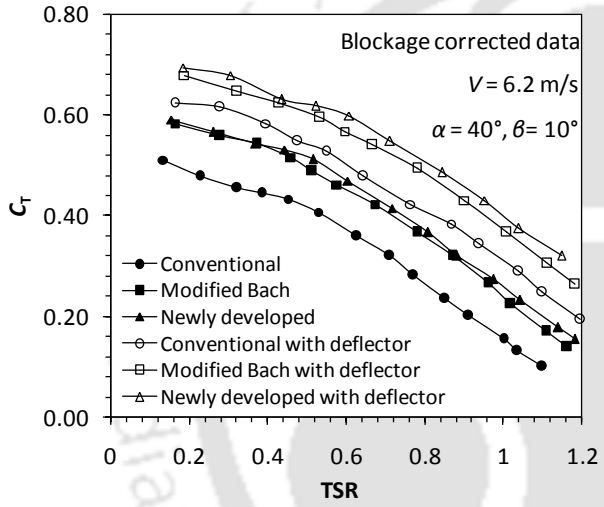

Figure 7.40: Variation of C_T for newly developed, modified Bach and conventional SSWTs under concentrated and oriented flows

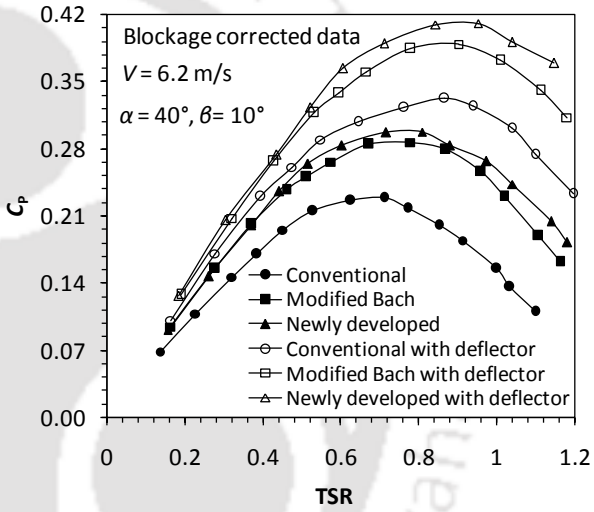

Figure 7.41: Variation of C_P for newly developed, modified Bach and conventional SSWTs under concentrated and oriented flows

7.6 Summary

A novel blade shape has been developed. The performance of the newly developed SSWT is reported and the results are compared and discussed with modified Bach, Benesh, semi-elliptical and conventional semi-circular bladed SSWTs. The main observations are summarized as follows:

(a) With the newly developed SSWT, a noticeable improvement in the maximum power coefficient (C_{Pmax}) is observed over other tested models. Performance gains of 3.3%, 6.9%, 19.2% and 34.8% are achieved over modified Bach, Benesh, semi-elliptical, and conventional SSWTs, respectively.

(b) The newly developed SSWT not only can increase the magnitude of the static torque coefficient, but also overcome the effects of negative torque due to change in the blade arc geometry. In terms of self-starting prospect, the results indicate that the C_{TSmax} of the newly developed blade profile is higher by 31.6%, 22.0% and 11.1% than the conventional, semi-elliptical and Benesh blade profiles, respectively. However, a marginal improvement of 4.2% is recorded over modified Bach type blade profile.

(c) With the increase of wind speed, the dynamic performance index i.e. the power coefficient increases up to a certain limit of V = 7.8 m/s, beyond which it again decreases. In contrary, with the increase of wind speed, the starting performance index i.e. the static torque coefficient increases irrespective of the magnitude of wind speed.

(d) For each of the tested blade profiles, the C_{Pmax} values are experienced at an optimum range of TSR such as 0.75–0.82, 0.72–0.80, 0.72–0.80, 0.70–0.75 and 0.66–0.73 for the newly developed, modified Bach, Benesh, semi-elliptical and conventional blades, respectively.

(e) For the newly developed SSWT, the maximum power coefficient recorded is 0.34 without any blockage correction; however, 0.31 is calculated with wind tunnel blockage correction.

(f) The newly developed SSWT while tested under properly oriented flows (α = 40°, and β = 10°), gives a maximum C_P of 0.41 at TSR = 0.95. In contrast, modified Bach type and conventional semi-circular type SSWT have shown a maximum C_P of 0.39 at TSR = 0.90 and 0.33 at TSR = 0.87, respectively.

This power improvement sets a platform to study the flow physics around the newly developed SSWT. Thus, 3D unsteady simulations are planned and executed on this turbine, which is discussed in the next chapter.

CHAPTER –8

3D Unsteady Simulations

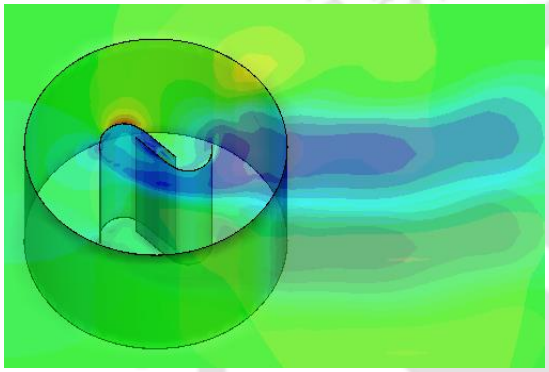

Chapter Outline

Overview

This chapter analyzes the 3D unsteady simulations carried out on the newly developed SSWT in comparison with conventional, modified Bach type and Benesh type SSWTs at V = 6.2 m/s. To accurately predict the flow behavior, the SST k-ω turbulence model is used in FVM based CFD software ANSYS-Fluent. The time dependent torque coefficients are obtained through averaging over different time intervals. The turbine performances are analyzed in respect of averaged torque and power coefficients. For each case, the obtained results are compared to the experimental data. The results showed a better prediction capability of 3D simulations as compared to the 2D simulations. Further, flow analysis around these turbines is carried out in terms velocity magnitude contours and pressure contours. The effects of Coanda type flow on the turbine performances are discussed. The computation analysis shows the justification for performance enhancement with the newly developed SSWT.

8.1 Computational methodology

To study the flow behaviour of the newly developed turbine, 3D unsteady simulations are carried out and compared with the results of modified Bach, Benesh, and semi-circular type SSWTs. The turbine models are considered to have D = 209 mm and H = 230 mm and thickness of 0.63 mm. The computational domain has dimensions of 10*D* × 6*D* × 1*D*. It is segmented into two parts separating outer fluid zone (fixed mesh) and the inner fluid zone (rotating mesh). Figure 8.1 displays the computational domain around the turbine model.

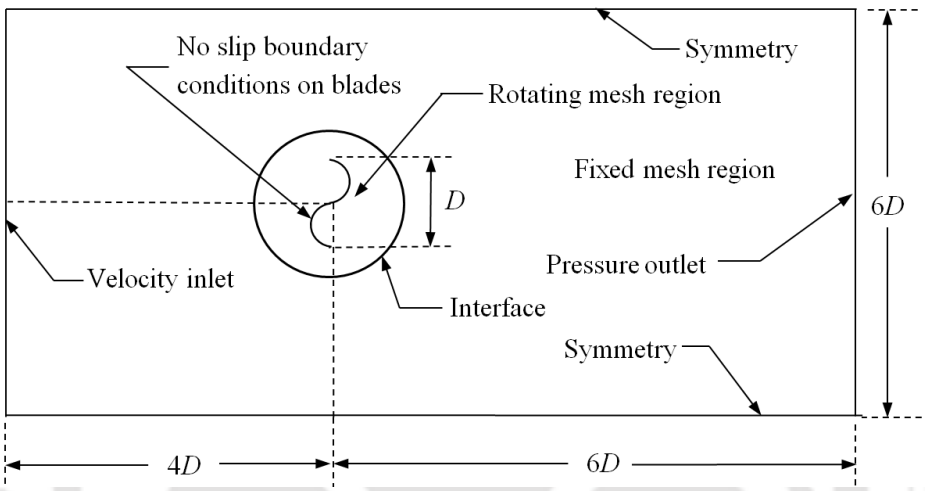

Figure 8.1: Schematic diagram of the computational domain

Figures 8.2 shows the computational models, whereas, Figure 8.3 demonstrates mesh generation around turbine blades. Initially, grid independence test was carried out and after satisfactory refinement, 1146594 nodes were taken for the unsteady simulations.

As shown in Figure 8.3, near the blades, fine meshing has been used in order to adequately capture the flow properties. To accurately predict the flow behavior, the SST *k-ω* turbulence model is used (Abraham *et al*., 2011; Edwards *et al*., 2012; Jaohindy *et al*., 2013). A pressure based transient FVM solver, ANSYS Fluent 14.5 is used to discretize the equations. The spatial discretization of the conservative equations is treated with 2nd order upwind scheme and the temporal terms of the conservative equations are discretized using 2nd order fully implicit temporal scheme. Good solution stability is ensured through the pressure-velocity coupling with the SIMPLE method (Semi Implicit Linked Equations). The time step size and the number of iterations per time step are taken as 0.001 and 20, respectively. The dynamic study is carried out by assigning a certain rotational rate to the rotating zone to predict the

performance of the turbine in terms of torque coefficient (C_T) and power coefficient (C_P) at different TSR = 0.2–1.2. The value of C_T is averaged over different time intervals.

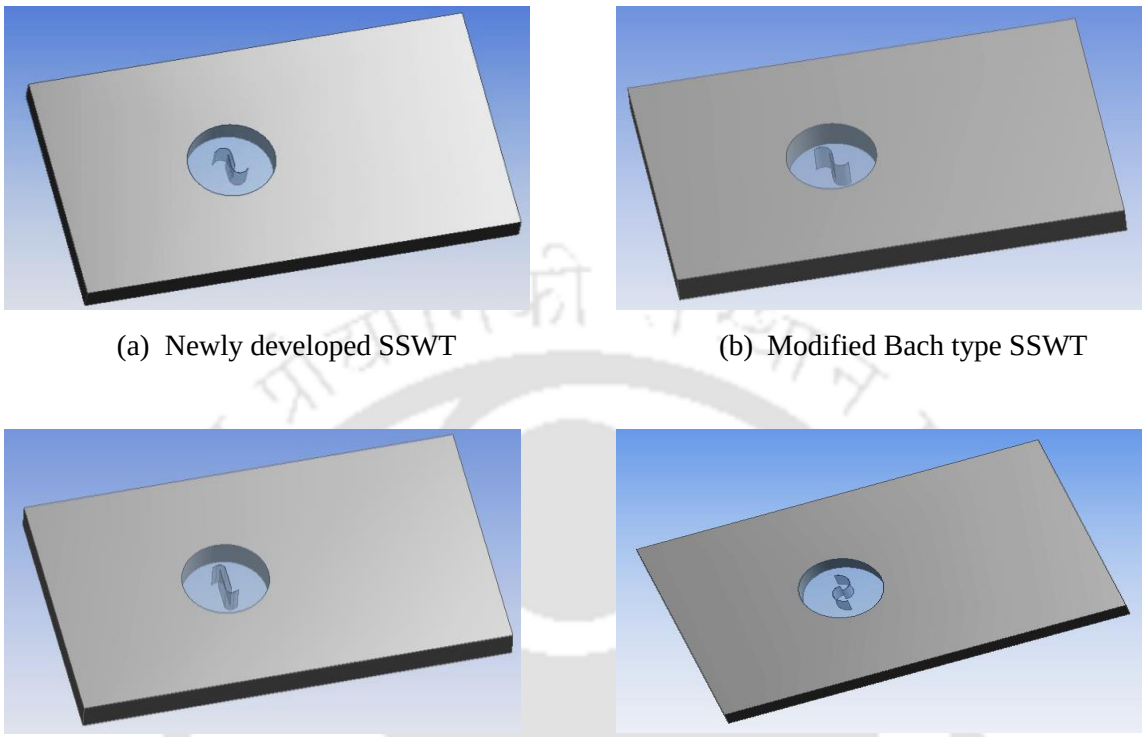

(a) Newly developed SSWT (b) Modified Bach type SSWT

(c) Benesh type SSWT (d) Conventional SSWT

Figure 8.2: 3D computational models for SSWTs

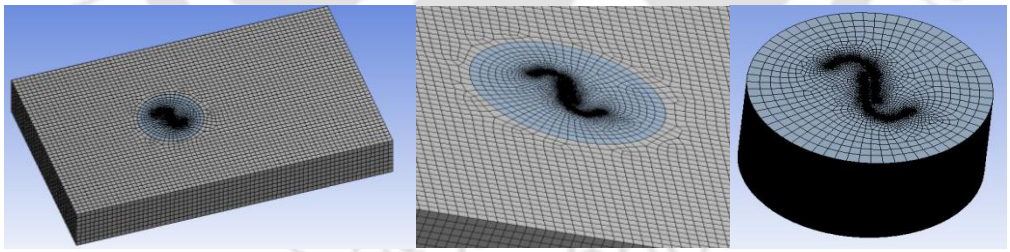

Figure 8.3: 3D grid generation for newly developed SSWT

8.2 Performance analysis

Figures 8.4 and 8.5 show the variations of C_T and C_P for the newly developed SSWT at V = 6.2 m/s, where the simulation results indicate similar trend as can be seen in experiments. From the 3D simulations, a maximum C_P of 0.27 at TSR = 0.80 is obtained for the newly developed SSWT.

Figures 8.6 and 8.7 demonstrate the variations of C_T and C_P for the modified Bach type SSWT through 3D simulations, where, the maximum C_P is found to be 0.26 at TSR = 0.80. The 3D simulation results are compared with the experimental data and with the 2D simulation results (as discussed in Chapter 3). A better prediction capability is achieved with the 3D simulations. Although, 2D simulation results followed the same trend as can be observed for experimental data, however, over predicted the magnitude due to two-dimensional flow assumptions. For Benesh type SSWT, comparisons among the experimental and computational results are shown in Figures 8.8 and 8.9, where a maximum C_P of 0.25 is achieved at TSR = 0.80. For conventional SSWT, Figures 8.10 and 8.11 show the 3D and 2D simulation results in comparison with the experimental data. The 3D simulations show the maximum C_P to be 0.19 at TSR = 0.60. It is to be noted that a similar over prediction behavior has been found for two-dimensional simulations as can be seen in case of modified Bach type SSWT.

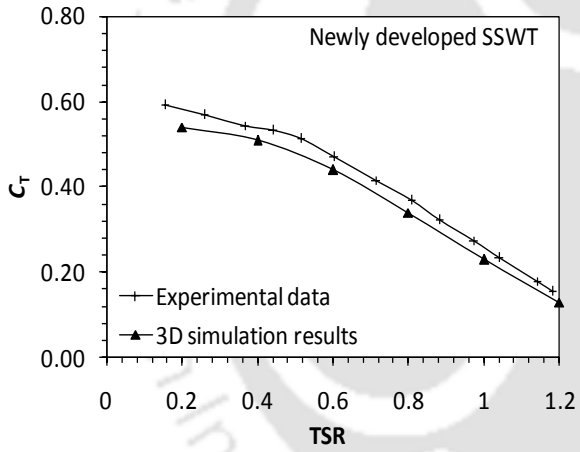

Figure 8.4: Variation of C_T for newly developed SSWT

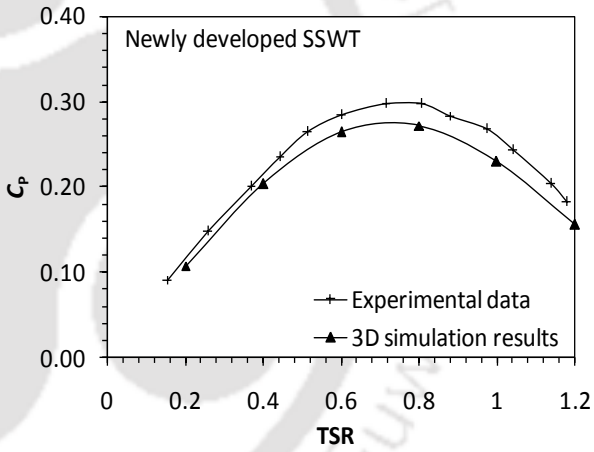

Figure 8.5: Variation of C_P for newly developed SSWT

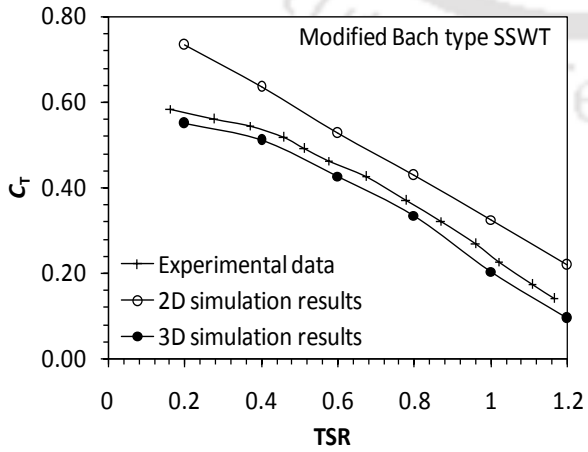

Figure 8.6: Variation of C_T for modified Bach type SSWT

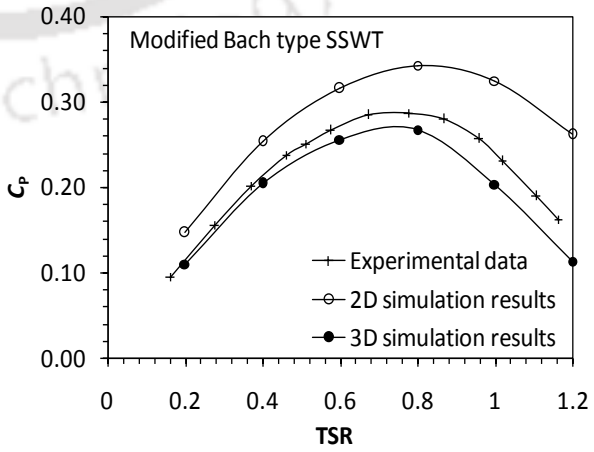

Figure 8.7: Variation of C_P for modified Bach type SSWT

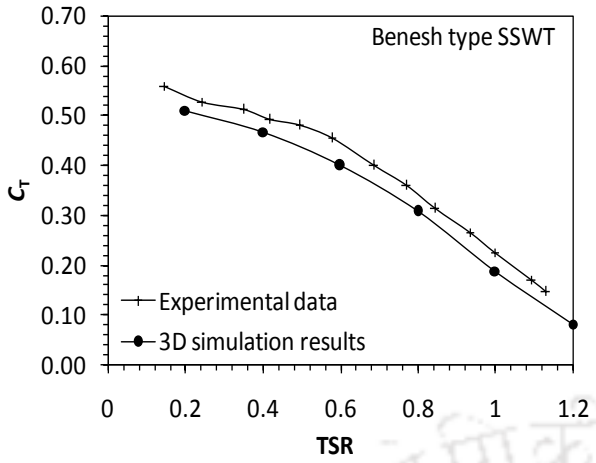

Figure 8.8: Variation of C_T for Benesh type SSWT

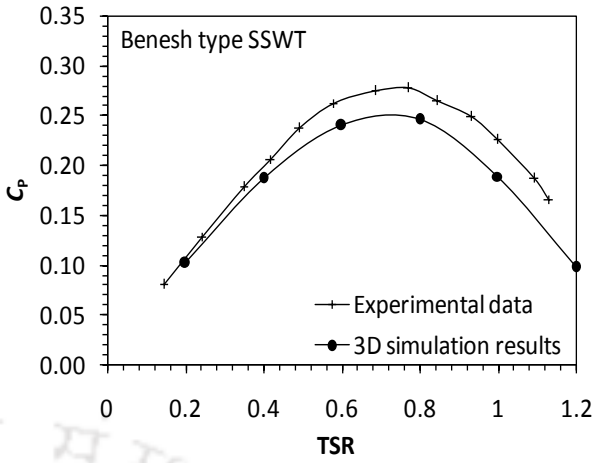

Figure 8.9: Variation of C_P for Benesh type SSWT

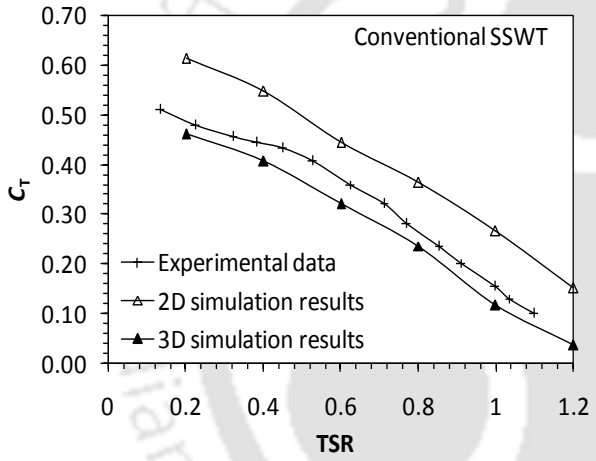

Figure 8.10: Variation of C_T for conventional SSWT

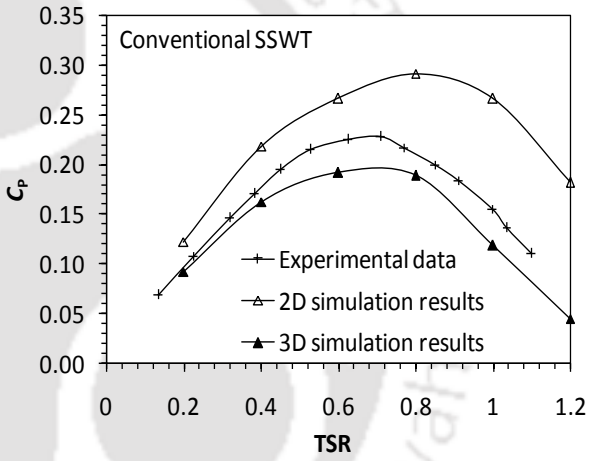

Figure 8.11: Variation of C_P for conventional SSWT

Table 8.1 shows the maximum values of C_P for newly developed, modified Bach type, Benesh type and conventional SSWT from 3D simulation and experimental study. A comparison of all the blade profile at similar TSRs is shown in Figures 8.12 and 8.13.

Table 8.1: Maximum C_P obtained from 3D simulation and experimental study at V = 6.2 m/s

Blade profile	3D simulation data		Experimental data	
	C_{Pmax}	TSR	C_{Pmax}	TSR
Newly developed SSWT	0.27	0.80	0.30	0.81
Modified Bach type SSWT	0.26	0.80	0.29	0.78
Benesh type SSWT	0.25	0.80	0.28	0.77
Conventional SSWT	0.19	0.60	0.23	0.71

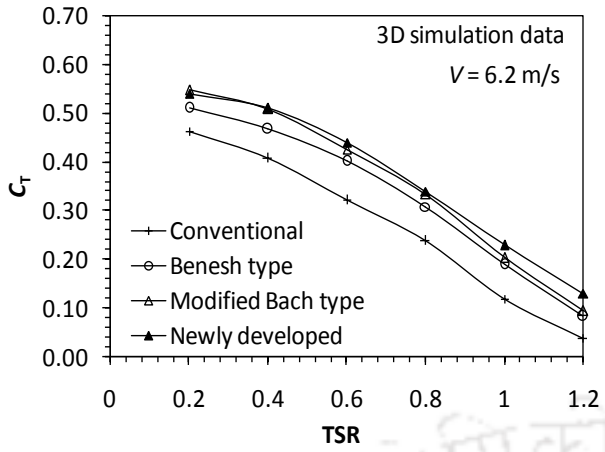

Figure 8.12: Variation of C_T for different SSWTs at similar TSRs

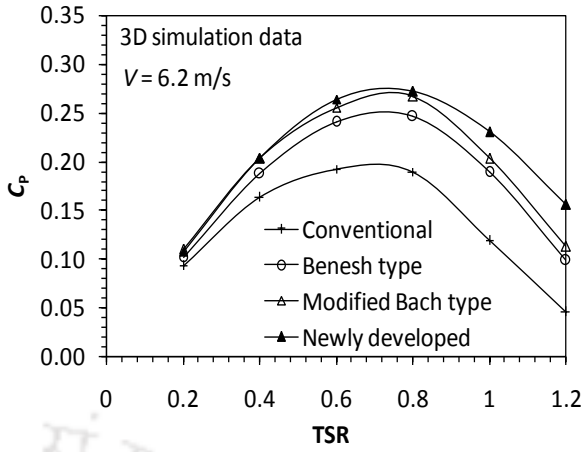

Figure 8.13: Variation of C_P for different SSWTs at similar TSRs

8.3 Flow analysis

From the performance analysis through experiments and 3D simulations, it has been observed that the newly developed SSWT gives a better torque and power characteristics over other tested SSWTs. In this section, an attempt is made to analyze the flow around these turbines to have a proper justification on the performance improvement of the newly developed SSWT.

As discussed in Chapter-3, the flow characteristic around the Sanious-style wind turbines is a combination of several flow types. The position of flow separation over the turbine blades is a very important phenomenon for SSWTs, which is responsible for the Coanda type flow (attached flow) and is also accountable for the strength of wake formation at the downstream of the turbine. The Coanda effect contributes to the lift force generation on the turbine blades, which in turn increases the power generation by the turbines. For airfoil blades in horizontal wind turbines, Coanda effect is more prominent, due to which lift based turbines are more efficient. For conventional SSWTs, the Coanda effect is very limited to small angular positions (0°–45°). Thus, conventional SSWTs are mainly regarded as a drag type device and the maximum C_P is found to be lower as compared to other wind turbines. However, through modification in the blade design, the Coanda effect can be increased, which will increase the power output of the turbine.

Figure 8.14 shows the velocity magnitude contours for the (a) newly developed, (b) modified Bach, (c) Benesh, and (d) conventional SSWTs. The low velocity region at the downstream of the newly developed SSWT is much lesser. This indicates a better velocity field in the rotational conditions and also a prominent Coanda-effect on the turbine blades that accounts

for the late separation. Thus, an obvious increase in the lift force contribution is expected for the newly developed turbine, which necessarily increase the power output of the turbine. A similar effect is observed for the modified Bach type SSWTs. The contribution of the lift force for modified Bach design as compared to conventional design is already discussed in Chapter-3.

In contrast, for the Benesh type and conventional SSWTs, a long low velocity region downstream to the turbine blades is observed. This indicates an early flow separation and a reduced influence of Coanda type flow. Thus, a less lift force contribution is expected for the Benesh type and conventional SSWTs.

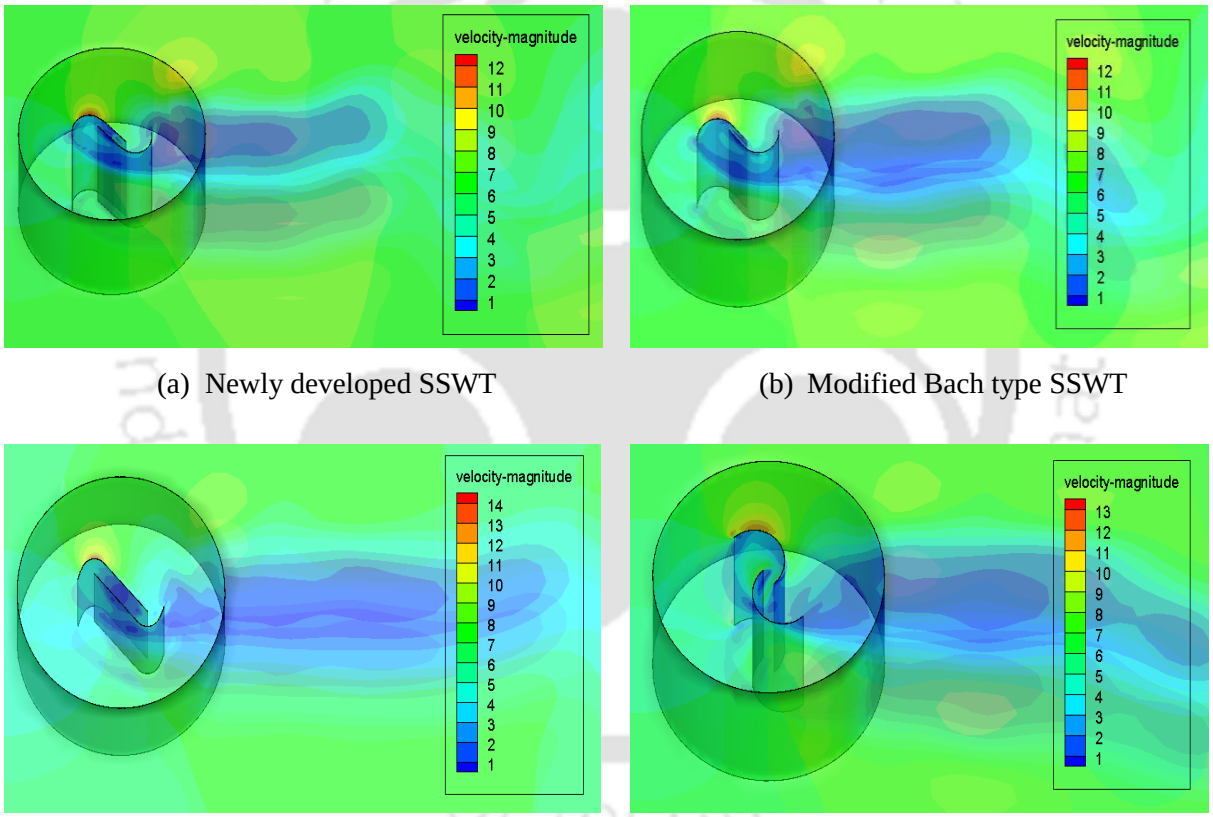

(a) Newly developed SSWT (b) Modified Bach type SSWT

(c) Benesh type SSWT (d) Conventional SSWT

Figure 8.14: Velocity magnitude contour plots on the SSWTs at TSR = 0.8

The pressure distributions around the (a) newly developed, (b) modified Bach, (c) Benesh, and (d) conventional SSWTs are shown in Figure 8.15. It is observed that for conventional and Benesh type SSWTs, the adverse effect on the returning blade is prominent. However, for the newly developed and modified Bach type SSWTs, this adverse effect is much lesser.

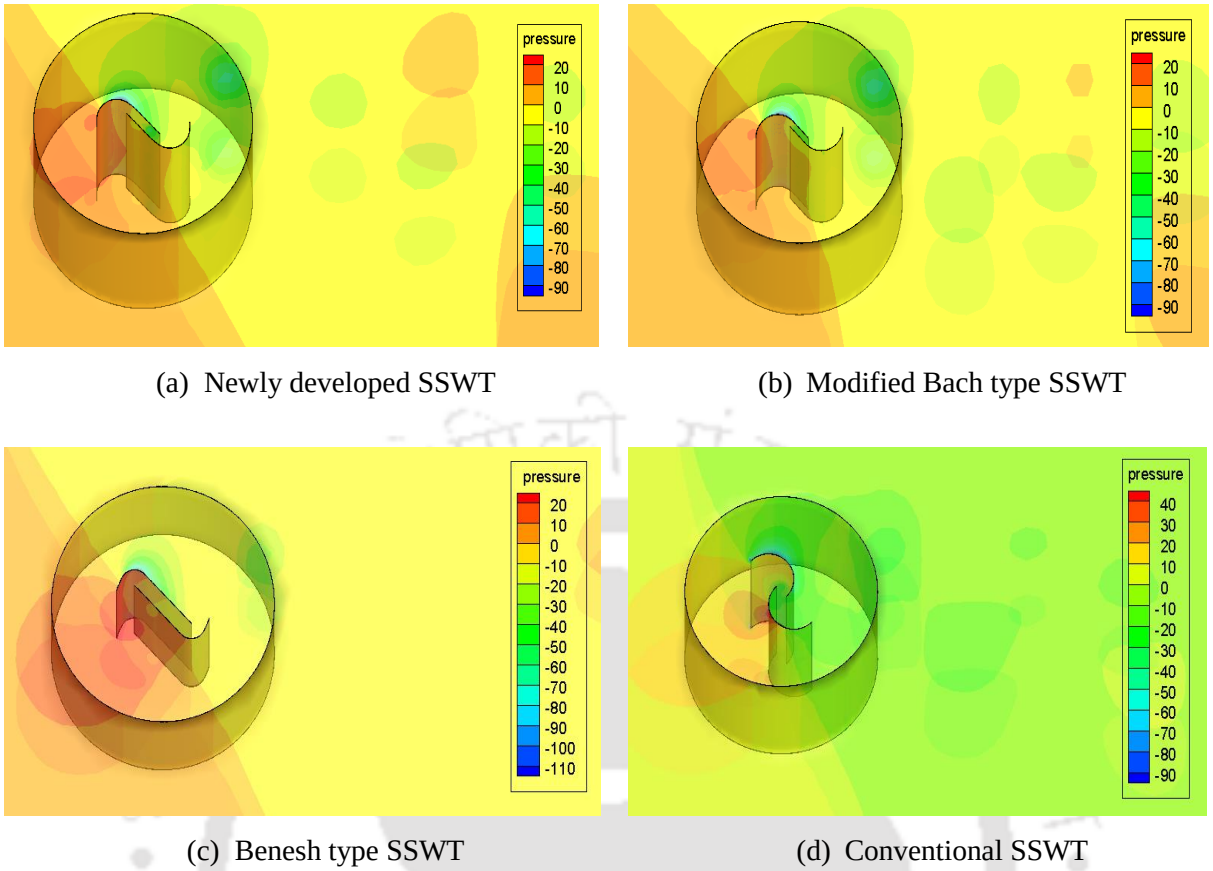

(a) Newly developed SSWT (b) Modified Bach type SSWT

(c) Benesh type SSWT (d) Conventional SSWT

Figure 8.15: Pressure contour plots on the SSWTs at TSR = 0.8

8.4 Summary

The 3D simulation study has been carried out on the newly developed, modified Bach, Benesh, and conventional type SSWTs at V = 6.2 m/s. The results showed a better prediction capability (trend line within ± 10%) with the 3D simulations as compared to the 2D simulation results. Although 2D simulation results followed the same trend of experimental data, however, over predicted the magnitude due to two-dimensional flow assumptions. The 3D simulation results show the C_{Pmax} to be 0.27, 0.26, 0.25 and 0.19 for the newly developed, modified Bach, Benesh and semi-circular type SSWTs, respectively. An improved velocity region at the downstream of the blades is obtained for newly developed and modified Bach SSWTs. The Coanda effect, and hence, the increased contribution of the lift force on the newly developed and modified Bach type SSWTs is expected to increase the power output of the turbine. The adverse effect of pressure on the returning blade is prominent on the semicircular and Benesh type of SSWTs. However, it is much lesser in case of newly developed and modified Bach type SSWTs.

CHAPTER –9

Economic Analysis

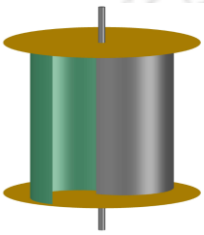

Chapter Outline

Overview

The Savonius-style wind turbines can be a viable option for small-scale electricity generation in the range of 0.5–3.0 kWh. However, to use this turbine in reality, it is essential to estimate the cost of the electricity generation and payback period of the complete wind energy conversion unit. In this context, this chapter presents the economic analysis for the wind energy conversion system (WECS) using the newly developed SSWT. The overall efficiency and the power output of a WECS are estimated taking into account the losses experienced in the turbine, generator and energy storage-transmission systems. The results obtained are compared with the other tested designs of SSWT such as semi-circular, semi-elliptic, Benesh and Bach types. Further, the payback periods of the WECS with each of the tested turbines are calculated and analyzed based on the overall efficiency and total cost of the WECS.

9.1 Wind energy conversion system

The Savonius-style wind turbines (SSWTs) can be useful for local electricity generation in certain cases of confined space and low wind speed region with an energy storage device. However, the cost of the electricity generation and payback period for such a turbine depends upon the overall efficiency of a wind energy conversion system (WECS). A complete WECS includes a wind turbine, a support structure, an electrical generator, an energy storage device and the transmission auxiliaries. Figure 9.1 shows the schematic diagram of a WECS. The capacity of WECS with a SSWT lies in the range 0.5–3.0 kWh depending on the dimensions of the turbine.

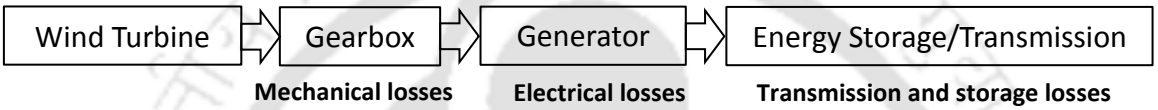

Figure 9.1: Wind energy conversion system with losses

9.2 Overall efficiency of a WECS

A wind energy conversion system always experiences power losses in the turbine section and in the gear arrangements, which are treated as mechanical losses in the system (Figure 9.1). Next the electrical generator for converting mechanical turbine shaft energy into electrical energy that always suffers from multiple internal losses such as copper, eddy-current, hysteresis and mechanical losses. Thus, the efficiency of an electrical generator always lies in the range of 80–90%. Another consideration is that the use of this electrical energy would be much easier if the energy is directly useful at the time of generation, but in reality the energy demand fluctuates with respect to time. This scenario caters the need of a suitable energy storage device. The use of lead acid batteries is a feasible solution but these generally only have efficiencies of around 70–80%. Thus, to estimate the power output of a WECS, these losses have to be taken into account. Considering these losses, the overall efficiency (η_O) and the power output of a WECS are calculated by the following equation:

$$\eta_O = \eta_T \times \eta_G \times \eta_{TS} \tag{9.1}$$

$$\text{Power output of WECS} = \text{Power available in the wind} \times \text{overall efficiency} \tag{9.2}$$

$$= \frac{1}{2}\rho A V^3 \times \eta_O \quad (9.3)$$

where, η_T, η_G, and η_{TS} are the efficiencies corresponding to wind turbine, electrical generator, and transmission and storage systems, respectively.

Now, considering C_{Pmax} of SSWTs to be the turbine efficiency (η_T), η_G = 80% (a more commonly found efficiency), and η_{TS} = 70% (considering a maximum loss), the overall efficiency of the WECS with the newly developed blade is estimated to be 17.4%. Whereas, the overall efficiencies of the WECS with modified Bach, Benesh, semi-elliptic and semi-circular turbines are estimated to be 16.8%, 16.2%, 14.6%, and 12.9%, respectively. Using these values of η_O in Equation 9.1, the power outputs of the WECS with the newly developed, modified Bach, Benesh, semi-elliptic and semi-circular turbines ($H = D_O$ = 1 m) are estimated to be 46.0 W, 44.4 W, 42.8 W, 38.6 W and 34.1 W, respectively.

9.3 Payback period of a WECS

Assuming the turbine capital cost and maintenance cost to be Rs. 25000.00 and Rs. 6000 (Al-Bahadly, 2009), the payback period for a WECS involving the newly developed SSWT can be calculated by the following equation:

$$\text{Pay back period} = \frac{\text{Total cost}}{\text{Power cost per kWh} \times \text{Power output in kWh/day}} \quad (9.4)$$

$$= \frac{(25000 + 6000)}{(1.10 \times 5)} = 5637 \text{ days} = 15.4 \text{ years}$$

Table 9.1 shows the details of the assessment on the payback periods for all the tested SSWTs using Equations 9.1–9.4 (Al-Bahadly, 2009). The installation and maintenance cost is assumed to be constant for all the turbines. It has been observed that the payback period for a conventional SSWT is 20.7 years, which is much higher than the newly developed blade design. However, the payback periods for modified Bach, Benesh, and semi-elliptic type are calculated as 15.9, 16.5 and 18.3 years, respectively.

Table 9.1: Overall efficiency and payback period for all the tested SSWTs ($H = D_O = 1$ m, $V = 7.8$ m/s)

Parameters	Newly developed	Modified Bach	Benesh	Semi-elliptic	Semi-circular
Turbine efficiency, η_T	31%	30%	29%	26%	23%
Generator efficiency, η_G	80%	80%	80%	80%	80%
Transmission-Storage efficiency, η_{TS}	70%	70%	70%	70%	70%
Overall efficiency of WECS, η_O	17.4%	16.8%	16.2%	14.6%	12.9%
Available power in the wind	264.2 W	264.2 W	264.2 W	264.2 W	264.2 W
Power output	46.0 W	44.4 W	42.8 W	38.6 W	34.1 W
Power output in kWh per day	1.10 kWh	1.07 kWh	1.03 kWh	0.93 kWh	0.82 kWh
Power cost per kWh (Rs)	5.00	5.00	5.00	5.00	5.00
Turbine Capital cost (Rs)	25,000.00	25,000.00	25,000.00	25,000.00	25,000.00
Maintenance cost (Rs)	6,000.00	6,000.00	6,000.00	6,000.00	6,000.00
Payback period	15.4 years	15.9 years	16.5 years	18.3 years	20.7 years

9.4 Summary

The overall efficiency and the payback periods for a wind energy conversion system (WECS) are estimated for all the tested SSWTs considering the mechanical, electrical and storage-transmission losses. The overall efficiencies of a WECS with the newly developed, modified Bach, Benesh, semi-elliptical, and conventional SSWTs are calculated as 17.4%, 16.8%, 16.2%, 14.6% and 12.9%, respectively. Whereas, the payback periods for the newly developed, modified Bach, Benesh, semi-elliptical, and conventional SSWTs are found to be 15.4, 15.9, 16.5, 18.3 and 20.7 years, respectively. Thus, with the newly developed design, a 34.4% improvement can be achieved in the payback period over the conventional semi-circular design.

CHAPTER –10

Conclusions and Future Scopes

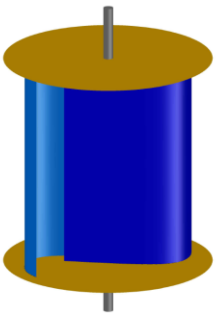

Chapter Outline

Overview

The present study attempts to improve the performance of Savonius-style wind turbine (SSWT) in terms of power and torque coefficients, starting characteristics, and also to analyze the flow behaviour around the turbine blades. In this context, a series of 2D unsteady simulations and wind tunnel experiments are conducted on various designs of SSWT. Existing experimental setup has been modified, and new correlations are developed for wind tunnel blockage corrections. A novel blade shape has been evolved through a series of experiments with different types of blades, and the results obtained are compared to those of the existing designs. Further, 3D unsteady simulations are executed to study the flow behavior around these turbines. An economic assessment is carried out for a wind energy conversion system (WECS) with the newly developed SSWT along with the other tested blades. In this chapter, the important issues and the outcome of the present investigation are discussed followed by the application potentials of SSWTs and future scopes of research.

10.1 Contribution of the present work

The Savonius-style wind turbines (SSWTs), a class of vertical axis wind turbine can be a viable option for small-scale, low-cost off-grid energy conversion in certain cases of confined space and low wind speed region, where the other wind turbines cannot work efficiently. However, the existing design of SSWTs is yet a matter of research to make it more useful in such situations. In this context, the present study attempts to improve the performance of SSWT by evolving a new blade shape through a series of unsteady simulations and wind tunnel experiments.

Initially, 2D unsteady simulations are carried out on the conventional semi-circular design to study its performance and flow characteristics by varying the blade overlap distances. This analysis is followed by a series of 2D unsteady simulations on Bach type blade profiles by varying its blade arc angle and blade overlap distance and an improved Bach design is identified. Looking at the outcome of the above mentioned simulation studies, experiments are conducted on conventional and modified Bach type SSWTs. New correlations are developed to incorporate the wind tunnel blockage effects.

A new blade shape has been evolved through a series of experiments by varying the blade arc length, blade profile, and overlap distance of the above models. Wind tunnel tests are conducted on the newly developed SSWT followed by its comparative analysis with other existing designs. Further, to analyze the flow characteristics, 3D unsteady simulations are carried out on the newly developed SSWT in comparison with the other tested designs. Finally, an economic analysis is reported estimating the overall efficiency and payback period of a wind energy conversion system (WECS) using the newly developed SSWT. A flowchart of the present investigation is demonstrated in Figure 10.1.

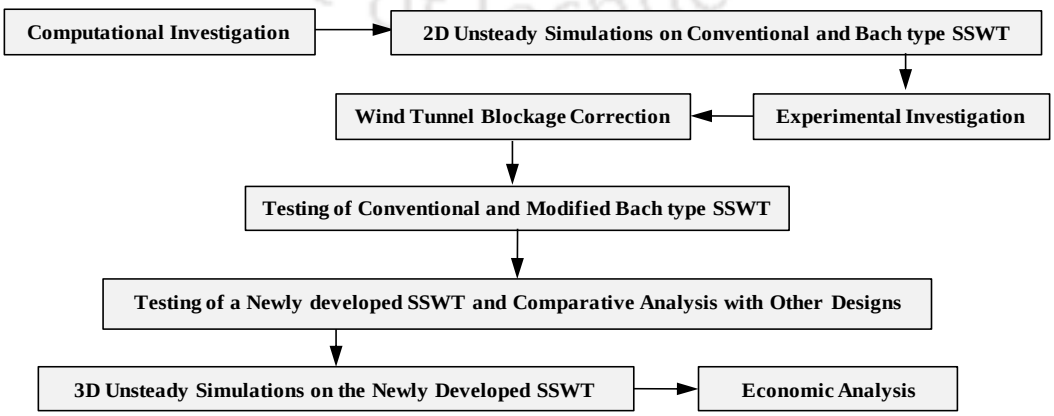

Figure 10.1 : Flowchart of the present investigation

The key findings of the present investigation are summarized in the subsequent sections.

10.1.1 2D unsteady simulations on conventional SSWT

A series of 2D unsteady simulations are carried out to analyze the performance and flow characteristics of a conventional semi-circular SSWT. The influence of overlap ratio (δ) on the performance and flow characteristics of SSWT is studied for δ = 0.00–0.30. The results are summarized in the following key points:

- The conventional semi-circular design of SSWT without any blade overlap possesses a low performance characteristic due to high pressure drag acting on the returning blade.
- During the complete cycle of SSWT, various types of flow phenomena such as free stream flow, Coanda type flow, returning flow, stagnation, separation, and vortices formation are observed.
- A highest C_P of 0.25 is observed without any blade overlap.
- With blade overlap (δ = 0.10–0.30), the presence of overlapping flow in the overlap region and accelerating flow near the tip of the returning blade marginally compensated the pressure effect on the returning blade. Thus, the performance coefficients are found to be improved.
- A highest C_P of 0.29 is obtained at δ = 0.20, indicating a performance improvement of 16% over δ = 0.00.

10.1.2 2D unsteady simulations on Bach type SSWT

Apart from the conventional semi-circular design, a series of unsteady simulations are carried out on the Bach type SSWT by varying the overlap ratio ($\delta = e/d$) from 0.00–0.50 and by varying the blade arc angle (ϕ) in the range of 90–165°.

- The performance of Bach type turbines increases with the increase of blade overlap. However, the benefits of overlapping flow is observed only up to δ = 0.40, beyond which the performance again deteriorates. This is because, beyond δ = 0.40, the incident flow gets a lesser exposed area of the advancing blade.
- Keeping ϕ to be constant at 120°, analysis on the overlap ratio (δ) indicates a highest C_P of 0.32 at δ = 0.40, whereas without any overlap, the peak C_P shows a value of 0.28.

- Apart from the overlapping effect, the effect of Coanda type flow during the complete rotational cycle is much improved with the Bach type design.

- At δ = 0.40, the smaller blade arc angles suffers from a reduced effective pressure on the advancing blade as compared to higher blade arc angles. Again, with the increase of blade arc angle the effective pressure on the convex side of the returning blade increases. Thus, an improved net pressure on both the advancing and returning blade is observed in an intermediate value of ϕ = 135°.

- The effect of Coanda type flow is more predominant in the modified Bach type SSWT (ϕ = 135° and δ = 0.40) that contributes to the lift resulting an increase in the net power output of the turbine. This improvement in the lift characteristics over semi-circular SSWT is further observed through the static simulation study.

10.1.3 Wind tunnel blockage correction

In the present study, new correlations are developed to incorporate the wind tunnel blockage corrections in the experimental results. It is observed that the dimensions of the wind tunnel test section and turbine models are not sufficient enough to describe the magnitude of the blockage correction under various loading conditions. Rather, it is significantly influenced by the change in TSR and BR. The salient points are briefly discussed below.

- To correct the experimental data, the selection of the blockage correction factor is very much sensitive. The value of *f* is found to increase (*f* = 1–10%) with the increase of TSR and BR.

- For BR = 21.16%, the desired value of *f* lies in the range of 4–10%. At low TSR (<0.5), *f* ≤ 6% correction is required, whereas for TSR = 0.5–0.9, *f* = 7% and for TSR > 0.9, a comparatively higher blockage correction (*f* = 8–10%) are found to be useful.

- For BR = 16%, blockage corrections in the range of *f* = 3–7% has to be taken into account with respect to TSR.

- However, as the BR further approached to a lower value (BR = 12.25%), at low TSR (<0.5), the correction required is only 2–3% and at higher TSR (>0.5), *f* = 4–6% is found to be incorporated.

10.1.4 Experiments on conventional and Bach type SSWTs

Wind tunnel experiments are conducted on the conventional and modified Bach type SSWTs that are achieved from the computational studies. The results obtained are summarized below.

- Thus, at low tip speed ratios (TSR <0.6), low aspect ratios (AR = 0.7–1.0) have shown a better torque and power characteristics. However, with the increase of turbine rotational rate, i.e. with the increase in TSR beyond 0.6, the inertia effects reduces, and the higher aspect ratios (AR = 1.1–1.2) give better performance characteristics. Observing the performance trends at different wind speeds, AR =1.1 is selected for the further analysis of SSWTs.

- The conventional SSWT shows a C_{Pmax} of 0.17 at TSR = 0.64 and 0.23 at TSR = 0.73 with δ = 0.00 and δ = 0.20, respectively.

- The modified Bach type SSWT (ϕ = 135° and δ = 0.40) depicted a C_{Pmax} of 0.30 at TSR = 0.81, indicating a performance gain of 30.4% and 15.4% over conventional and classical Bach type SSWT, respectively.

10.1.5 Experiments on the newly developed SSWT

The performance of the newly developed SSWT is summarized below in comparison with modified Bach, Benesh, semi-elliptical and conventional semi-circular bladed SSWTs.

- For the newly developed SSWT, the maximum power coefficient recorded is 0.34 without any blockage correction; however, 0.31 is calculated with wind tunnel blockage correction.

- With the newly developed SSWT, a noticeable improvement in the maximum power coefficient (C_{Pmax}) is observed over other tested models. With blockage corrections, the performance gains of 3.3%, 6.9%, 19.2% and 34.8% are achieved over modified Bach, Benesh, semi-elliptical, and conventional SSWTs, respectively.

- The newly developed SSWT not only can increase the magnitude of the static torque coefficient, but also overcome the effects of negative torque due to change in the blade arc geometry. In terms of self-starting prospect, the results indicate that the C_{TSmax} of the

newly developed blade profile is higher by 31.6%, 22.0% and 11.1% than the conventional, semi-elliptical and Benesh blade profiles, respectively. However, a marginal improvement of 4.2% is recorded over modified Bach type blade profile.

- For the newly developed SSWT, the C_{Pmax} is found in the range of TSR = 0.75–0.82, whereas, for modified Bach, Benesh, semi-elliptical and conventional SSWTs, the peak value is attained in the range of TSR = 0.72–0.80, 0.72–0.80, 0.70–0.75 and 0.66–0.73, respectively.

- The newly developed SSWT while tested under properly oriented flows (α = 40°, and β = 10°), gives a maximum C_P of 0.41 at TSR = 0.95. In contrast, modified Bach type and conventional semi-circular type SSWT have shown a maximum C_P of 0.39 at TSR = 0.90 and 0.33 at TSR = 0.87, respectively.

- For all the test cases, with the increase of wind speed, the dynamic performance index i.e. the power coefficient increases up to a certain limit of V = 7.8 m/s, beyond which it again decreases. In contrary, with the increase of wind speed, the starting performance index i.e. the static torque coefficient increases irrespective of the magnitude of wind speed.

10.1.6 3D unsteady simulations on the newly developed SSWT

The 3D unsteady simulations are carried out on the newly developed SSWT and the results obtained are compared to those of modified Bach, Benesh, and conventional type SSWTs.

- An improved velocity region at the downstream of the blades is obtained for newly developed and modified Bach SSWTs. The Coanda effect, and hence, the increased contribution of the lift force on the newly developed and modified Bach type SSWTs is expected to increase the power output of the turbine.

- The adverse effect of pressure on the returning blade is prominent on the semicircular and Benesh type of SSWTs. However, it is much lesser in case of newly developed and modified Bach type SSWTs.

- From this simulation study, the C_{Pmax} is found to be 0.27, 0.26, 0.25 and 0.19 for the newly developed, modified Bach, Benesh and semi-circular type SSWTs, respectively.

10.1.7 Economic assessment of a wind energy conversion system

The overall efficiency and the payback periods for a wind energy conversion system (WECS) are estimated for the newly developed, modified Bach, Benesh, semi-elliptical and conventional SSWTs considering the mechanical, electrical and storage-transmission losses.

- The overall efficiencies of a WECS with the newly developed, modified Bach, Benesh, semi-elliptical, and conventional SSWTs are calculated as 17.4%, 16.8%, 16.2%, 14.6% and 12.9%, respectively.
- The payback periods for the newly developed, modified Bach, Benesh, semi-elliptical, and conventional SSWTs are found to be 15.4, 15.9, 16.5, 18.3 and 20.7 years,, respectively.
- Thus, with the newly developed design, a 34.4% improvement can be achieved in the payback period over the conventional semi-circular design.

10.2 Application potential

The Savonius-style wind turbine is simple in design, so it can easily be fabricated and maintained at a low cost. The cut-in speed for this turbine is also very low. These devices are insensitive to the wind flow directions, and thus, are very useful for the specific locations of variable wind directions. Moreover, their vertical rotational axis allows them to be positioned in multiple numbers in a confined space These turbines equipped with an energy storage system can be a very useful at the top of the buildings or communication towers or at the hilly locations for decentralized small-scale electricity generation. Since long, pumping water in agricultural purposes is another application of these turbines.

More recently, another application of SSWTs is observed in association with the Darrieus-style VAWTs to incorporate the better starting characteristics (Savonius) as well as improved lift characteristics (Darrieus).

Further, through the installation of deflectors ahead of the turbine, the C_{Pmax} of the newly developed SSWT is found to be 0.41. This improvement enables this turbine to be effectively installed at the directional flows in exhaust systems where air is blowing at a wind speed of 3–7 m/s. An example of such a system can be seen in the tea industry.

10.3 Scopes for future work

- A recent study on the venting and capping (Plourde *et al*., 2011) reported that venting on the turbine blades can effectively reduce the pressure drag on the returning blade. Thus, a simulation study followed by wind tunnel experiments can be carried out on the venting size and location for the newly developed SSWT.

- During the wind tunnel experiments, it was observed that at a wind speed below 3 m/s, the self-starting capability is much lesser. So, a study can be executed on the newly developed SSWT with light blade materials to make it more useful at very low wind speeds.

- The used alternators in the present study suffered from large electrical and frictional losses. Therefore, an improvement in the design of an alternator and an energy storage device specially meant for the newly developed SSWT can make it more viable for practical uses.

- The lift based Darrieus-style VAWTs possess a comparatively higher efficiency due to low solidity factor and much contribution of lift forces. However, their starting ability is much inferior to that of SSWTs. Thus, this newly developed SSWT can also be a useful device for a combined Savonius-Darrieus VAWT.

- Unstructured grids were used in the present simulation study. So implementation of the structured grids can be studied further to have a more accurate analysis of the flow behaviour around the newly developed SSWT.

References

Abraham JP, **Mowry GS**, **Plourde BP**, **Sparrow EM**, and **Minkowycz WJ**, (2011), Numerical simulation of fluid flow around a vertical-axis turbine, *Journal of Renewable and Sustainable Energy*, Vol. 3, No. 033109, pp. 1–13.

Abraham JP, **Plourde BD**, **Mowry GS**, **Minkowycz WJ**, and **Sparrow EM**, (2012), Summary of Savonius wind turbine development and future applications for small-scale power generation, *Journal of Renewable and Sustainable Energy*, Vol. 4, No. 042703, pp. 1–21.

Afungchui D, **Kamoun B**, **Helali A**, and **Djemaa AB**, (2010), The unsteady pressure field and the aerodynamic performances of a Savonius rotor based on the discrete vortex method, *Renewable Energy*, Vol. 35, No. 1, pp. 307–313.

Akwa JV, **Vielmo HA**, and **Petry AP**, (2012), A review on the performance of Savonius wind turbines, *Renewable and Sustainable Energy Reviews*, Vol. 16, No. 5, pp. 3054–3064.

Al-Bahadly I, (2009), Building a wind turbine for rural home, *Energy for Sustainable Development*, Vol. 13, No. 3, pp. 159–165.

Alexander AJ, and **Holownia BP**, (1978), Wind tunnel tests on a Savonius rotor, *Journal of Wind Engineering and Industrial Aerodynamics*, Vol. 3, No. 4, pp. 343–351.

Altan BD, **Atilgan M**, and **Ozdamar A**, (2008), An experimental study on improvement of a Savonius turbine performance with curtaining, *Experimental Thermal and Fluid Sciences*, Vol. 32, No. 8, pp. 1673–1678.

Altan BD, and **Atilgan M**, (2008), An experimental and numerical study on the improvement of the performance of Savonius wind turbine, *Energy Conversion and Management*, Vol. 49, No. 12, pp. 3425–3432.

Altan BD, and **Atilgan M**, (2010), The use of a curtain design to increase the performance level of a Savonius wind rotors, Renewable Energy, Vol. 35, No. 4, pp. 821–829.

ANSYS Inc, (2009), ANSYS Fluent Theory Guide 12.0.

Bach G, (1931), Investigations concerning Savonius rotors and related turbo-machines, Translated into English by Brace Research Institute, Quebec, Canada 1964; *Forschung aufGebiete des Ingenieurwesens*, Vol. 2, No. 6, pp. 218–23.

Barlow JB, **Rae WH**, and **Pope A**, (1999), *Low speed wind tunnel testing*, Third Edition, John Wiley & Sons, New York, USA.

Baird JP, and **Pender SF**, (1980), Optimization of a vertical axis wind turbine for small scale applications. *Proceedings of the 7th Australasian Hydraulic and Fluid Mechanics Conference*, August 18–22, Brisbane, Australia.

Benesh AH, (1988), *Wind turbine system using a vertical axis Savonius-type rotor*, US Patent No. 4,784,568.

Benesh AH, (1996), *Wind turbine with Savonius-type rotor*, US Patent No. 5,494,407.

Bergeles G, and **Athanassiadis N**, (1982), On the flow field of the Savonius rotor, *Wind Engineering*, Vol. 6, No. 3, pp. 140–148.

Biadgo AM, **Simonovic A**, **Komarov D**, and **Stupar S**, (2013), Numerical and analytical investigation of vertical axis wind turbine, *FME Transactions*, Vol. 41, pp. 49–58.

Biswas A, **Gupta R**, and **Sharma KK**, (2007), Experimental investigation of overlap and blockage effects on three-bucket Savonius rotors, *Wind Engineering*, Vol. 31, No. 5, pp. 363–368.

Blackwell BF, **Sheldahl RE**, and **Feltz LV**, (1977), *Wind tunnel performance data for two- and three-bucket Savonius rotors*, Sand 76-0131 under act AT/29-11, Sandia Laboratories, USA.

Bowden GJ, and **McAleese SA**, (1984), The properties of isolated and coupled Savonius rotors, *Wind Engineering*, Vol. 8, No. 4, pp. 271–288.

Can K, **Feng Z**, and **Xuejun M**, (2010), Comparison study of a vertical-axis spiral rotor and a conventional Savonius rotor, *Proceedings of the IEEE Power and Energy Engineering Conference*, March 28–31, Chengdu, China.

Chauvin A, and **Benghrib D**, (1989), Drag and lift coefficients evolution of a Savonius rotor, *Experiments in Fluids*, Vol. 8, No. 1–2, pp. 118–120.

Chen TY, and **Liou LR**, (2011), Blockage corrections in wind tunnel tests of small horizontal-axis wind turbines, *Experimental Thermal and Fluid Science*, Vol. 35, No. 3, pp. 565–569.

D'Alessandro V, **Montelpare S**, **Ricci R**, and **Secchiaroli A**, (2010), Unsteady aerodynamics of a Savonius wind rotor: a new computational approach for the simulation of energy performance, *Energy*, Vol. 35, No. 8, pp. 3349–3363.

Damak A, **Driss Z**, and **Abid MS**, (2013), Experimental investigation of helical Savonius rotor with a twist of 180°, *Renewable Energy*, Vol. 52, pp. 136–142.

Debnath BK, **Biswas A**, and **Gupta R**, (2008), CFD Analysis of combined three-bucket Savonius and three-bladed Darrieus rotor using Fluent package, *Proceedings of International Conference on Advances in Mechanical Engineering*, December 16–17, Surat, India.

Debnath BK, **Biswas A**, and **Gupta R**, (2009), Computational fluid dynamics analysis of a combined three- bucket Savonius & three-bladed Darrieus rotor at various overlap conditions, *Journal of Renewable and Sustainable Energy*, Vol. 1, No. 033110, pp. 1–13.

Dobrev I, and **Massouh F**, (2011), CFD and PIV investigation of unsteady flow through Savonius wind turbine, *Energy Procedia*, Vol. 6, pp. 711–720.

Edwards JM, **Danao LA**, and **Howell RJ**, (2012), Novel experimental power curve determination and computational methods for the performance analysis of vertical axis wind turbines, *ASME Journal of Solar Energy Engineering*, Vol. 134, No. 3, pp. 1–11.

Emmanuel B, and **Jun W**, (2011), Numerical study of a six-bladed Savonius wind turbine, *ASME Journal of Solar Energy Engineering*, Vol. 133, No. 4, pp. 1–5.

Fujisawa N, and **Gotoh F**, (1992), Pressure measurements and flow visualization study of a Savonius turbine, *Journal of Wind Engineering and Industrial Aerodynamics*, Vol. 39, No. 1–3, pp. 51–60.

Fujisawa N, **Ishimatsu K**, and **Kage K**, (1995), A comparative study of Navier-Stokes calculations and experiments for the Savonius rotor, *ASME Journal of Solar Energy Engineering*, Vol. 117, No. 4, pp. 344–346.

Gasch R, and **Twele J**, (2012), Scaling wind turbines and rules of similarity, In *Wind Power Plants: Fundamentals, Design, Construction and Operation*, Springer Berlin Heidelberg, New York, USA, pp. 257–271.

Golecha K, **Eldho TI**, and **Prabhu SV**, (2011), Influence of the deflector plate on the performance of modified Savonius wind turbine, *Applied Energy*, Vol. 88, No. 9, pp. 3207–3217.

Grinspan AS, (2002), *Development of a low speed wind tunnel and testing of Savonius wind turbine rotor with twisted blades*, M. Tech Thesis, Department of Mechanical Engineering, IIT Guwahati, India.

Grinspan AS, **Saha UK**, and **Mahanta P**, (2004), Experimental investigation of twisted bladed Savonius wind turbine rotor, *International Energy Journal*, Vol. 5, No. 1, pp. 1–9.

GWEC, (2014), *Global wind report: Annual market update 2013*, pp. 1–80, http://www.gwec.net/wp-content/uploads/2014/04/GWEC-Global-Wind-Report_9-April-2014.pdf

GWEC, (2013), *Global wind report: Annual market update 2012*, pp. 1–72, http://www.gwec.net/wp-content/uploads/2012/06/Annual_report_2012_LowRes.pdf

GWEC, (2012), *Global wind report: Annual market update 2011*, pp. 1–68, http://gwec.net/wp-content/uploads/2012/06/Annual_report_2011_lowres.pdf

Hackett JE, **Wilsden DJ**, and **Lilley DE**, (1979), *Estimation of tunnel blockage from wall pressure signatures: a review and data correlation*, Technical Report: NASA-CR-152241, NASA, USA, pp. 1–170.

Hayashi T, **Li Y**, **Hara Y**, and **Suzuki K**, (2005), Wind tunnel tests on a three-stage out-phase Savonius rotor, *JSME International Journal Series B: Special Issue on Experimental Mechanics in Heat and Fluid Flow*, Vol. 48, No. 1, pp. 9–16.

Howell R, **Qin N**, **Edwards J**, and **Durrani N**, (2010), Wind tunnel and numerical study of a small vertical axis wind turbine, *Renewable Energy*, Vol. 35, No. 2, pp. 412–422.

Huda MD, **Selim MA**, **Islam AKMS**, and **Islam MQ**, (1992), The performance of an S-shaped Savonius rotor with a deflecting plate, *RERIC International Energy Journal*, Vol. 14, No. 1, pp. 25–32.

Irabu K, and **Roy JN**, (2007), Characteristics of wind power on Savonius rotor using a guide-box tunnel, *Experimental Thermal and Fluid Science*, Vol. 32, No. 2, pp. 580–586.

Islam AKMS, **Islam MQ**, **Razzaque MM**, and **Ashraf R**, (1995), Static torque and drag characteristics of an S-shaped Savonius rotor and prediction of dynamic characteristics, *Wind Engineering*, Vol. 19, No. 6, pp. 363–70.

Jaohindy P, **Ennamiri H**, **Garde F**, and **Bastide A**, (2013), Numerical investigation of airflow through a Savonius rotor, *Wind Energy*, Vol. 17, No. 6, pp. 853–868.

Kacprzak K, **Liskiewicz G**, and **Sobczak K**, (2013), Numerical investigation of conventional and modified Savonius wind turbines, *Renewable Energy*, Vol. 60, pp. 578–585.

Kamal FM, and **Islam MQ**, (2008), Aerodynamic characteristics of a stationary five bladed vertical axis vane wind turbine, *Journal of Mechanical Engineering*, Transaction of the Mechanical Engineering Division, The Institute of Engineers, Bangladesh, Vol. 39, No. 2, pp. 95–99.

Kamoji MA, **Kedare SB**, and **Prabhu SV**, (2008), Experiments investigations on single stage, two stage and three stage conventional Savonius rotor, *International Journal of Energy Research*, Vol. 32, No. 10, pp. 877–895.

Kamoji MA, **Kedare SB**, and **Prabhu SV**, (2009a), Experimental investigations on single stage modified Savonius rotor, *Applied Energy*, Vol. 86, No. 7–8, pp. 1061–1073.

Kamoji MA, **Kedare SB**, and **Prabhu SV**, (2009b), Performance tests on helical Savonius rotor, *Renewable Energy*, Vol. 34, No. 3, pp. 521–529.

Kianifar A, and **Anbarsooz M**, (2011), Blade curve influences on the performance of Savonius rotors: experimental and numerical, *Proc. IMechE Part A: Journal of Power and Energy*, Vol. 225, No. 3, pp. 343–350.

Kline SJ, and **McClintock FA**, (1953), Describing uncertainties in single-sample experiments, *Mechanical Engineering*, Vol. 75, pp. 3–8.

Kotb MA, and **Aldoss TK**, (1991), Flow field around a partially-blocked Savonius rotor, *Applied Energy*, Vol. 38, No. 2, pp. 117–132.

Launder BE, and **Spalding DB**, (1974), The numerical computation of turbulent flows, *Computer Methods in Applied Mechanics and Engineering*, Vol. 3, No. 2, pp. 269–289.

Maskell EC, (1963), *A theory of the blockage effects on bluff bodies and stalled wings in a closed wind tunnel*, Reports and Memoranda No. 3400, ADA955243, Ministry of Aviation, London, UK, pp. 1–26.

McTavish S, **Feszty D**, and **Sankar T**, (2012), Steady and rotating computational fluid dynamics simulations of a novel vertical axis wind turbine for small-scale power generation, *Renewable Energy*, Vol. 41, pp. 171–179.

Menter FR, (1993), Zonal two-equation k-ω turbulence models for aerodynamic flows, *Proceedings of the 24th AIAA Fluid Dynamics Conference*, July 6–9, Orlando, FL.

Menter FR, (1994), Two-equation eddy-viscosity turbulence models for engineering applications, *AIAA Journal*, Vol. 32, No. 8, pp. 1598–1605.

Mobinuddin, (2005), *Aerodynamic performance of semi-circular three bladed Savonius rotor with deflecting and end Plates*, M. Tech. Thesis, Department of Mechanical Engineering, IIT Guwahati, India.

Modi VJ, **Roth NJ**, and **Fernando MSUK**, (1984), Optimum-configuration studies and prototype design of a wind-energy-operated irrigation system, *Journal of Wind Engineering and Industrial Aerodynamics*, Vol. 16, pp. 85–96.

Modi VJ, and **Fernando MSUK**, (1989), On the performance of the Savonius wind turbine, *ASME Journal of Solar Energy Engineering*, Vol. 111, No. 1, pp. 71–81.

Modi VJ, and **Fernando MSUK**, (1993), Unsteady aerodynamics and wake of the Savonius wind turbine: a numerical study, *Journal of Wind Engineering and Industrial Aerodynamics*, Vol. 46–47, pp. 811–816.

Moffat RJ, (1988), Describing the Uncertainties in Experimental Results, *Experimental Thermal and Fluid Science*, Vol. 1, No. 1, pp. 3–17.

Mohamed MH, **Janiga G**, **Pap E**, and **Thevenin D**, (2010), Optimization of Savonius turbines using an obstacle shielding the returning blade, *Renewable Energy*, Vol. 35, No. 11, pp. 2618–2626.

Mohamed MH, and **Thevenin D**, (2010), Performance optimization of a Savonius turbine considering different shapes for frontal guiding plates, *Proceedings of ICFD 10: 2010 Tenth International conference of Fluid Dynamics*, December 16-19, Cairo, Egypt.

Mohamed MH, **Janiga G**, **Pap E**, and **Thévenin D**, (2011), Optimal blade shape of a modified Savonius turbine using an obstacle shielding the returning blade, *Energy Conversion and Management*, Vol. 52, No. 1, pp. 236–242.

Mojola OO, (1985), On the aerodynamic design of the Savonius wind mill rotor, *Journal of Wind Engineering and Industrial Aerodynamics*, Vol. 21, No. 2, pp. 223–231.

Morcos SM, **Khalafallah MG**, and **Heikel HA**, (1981), The effect of shielding on the aerodynamic performance of the Savonius wind turbines, *Proceedings of the 16th Intersociety Energy Conversion Engineering Conference*, August 9–14, Atlanta, Georgia, USA.

Ogawa T, (1984), Theoretical study on the flow about Savonius rotor, *ASME Journal of Fluids Engineering*, Vol. 106, No. 1, pp. 85–91.

Ogawa T, and **Yoshida H**, (1986), Effects of a deflecting plate and rotor end plates on performance of Savonius type wind turbine, *Bulletin of JSME*, Vol. 29, No. 253, pp. 2115–2121.

Ogawa T, **Yoshida H**, and **Yokota Y**, (1989), Development of rotational speed control systems for a Savonius-type wind turbine, *ASME Journal of Fluids Engineering*, Vol. 111, No. 1, pp. 53–58.

Paraschivoiu I, (2002), *Wind turbine design: with emphasis on Darrieus concept*, Presses inter Polytechnique, Canada.

Plourde BD, **Abraham JP**, **Mowry GS**, and **Minkowycz WJ**, (2011), An experimental investigation of a large, vertical-axis wind turbine: effects of venting and capping, *Wind Engineering*, Vol. 35, pp. 213–220.

Plourde BD, **Abraham JP**, **Mowry GS**, and **Minkowycz WJ**, (2011), Use of small-scale wind energy to power cellular communication equipment, *Sensors & Transducers*, Vol. 13, pp. 53–61.

Plourde BD, **Abraham JP**, **Mowry GS**, and **Minkowycz WJ**, (2012), Simulations of three-dimensional vertical-axis turbines for communications applications, *Wind Engineering*, Vol. 36, No. 4, pp. 443–454.

Pope A, and **Harper JJ**, (1966), *Low speed wind tunnel testing*, John Wiley & Sons, New York, USA.

Pope K, **Dincer I**, and **Naterer GF**, (2010), Energy and exergy efficiency comparison of horizontal and vertical axis wind turbines, *Renewable Energy*, Vol. 35, No. 9, pp. 2102–2013.

Rajkumar MJ, (2004), *Experimental investigation and flow simulation of Savonius rotor*, M. Tech. Thesis, Department of Mechanical Engineering, IIT Guwahati, India.

REN21, (2014), *Renewable 2014 global status report*, pp. 1–215, http://www.ren21.net/Portals/0/documents/Resources/GSR/2014/GSR2014_full%20report_low%20res.pdf

Ross I, and **Altman A**, (2011), Wind tunnel blockage corrections: review and application to Savonius vertical-axis wind turbines, *Journal of Wind Engineering and Industrial Aerodynamics*, Vol. 99, No. 5, pp. 523–538.

Saha UK, **Rajkumar MJ**, and **Maity D**, (2005), Simulation of flow around and behind a Savonius turbine, *International Energy Journal*, Vol. 6, No. 2, pp. 83–90.

Saha UK, and **Rajkumar MJ**, (2006), On the performance analysis of Savonius rotor with twisted blades, *Renewable Energy*, Vol. 31, No. 11, pp. 1776–1788.

Saha UK, **Thotla S**, and **Maity D**, (2008), Optimum design configuration of Savonius rotor through wind tunnel experiments, *Journal of Wind Engineering and Industrial Aerodynamics*, Vol. 96, No. 8–9, pp. 1359–1375.

Sabzevari A, (1978), Power augmentation in a ducted Savonius rotor, *International Symposium of Wind Energy Systems*, October 3–6, Amsterdam, Netherland.

Sargolzaei J, (2007), Prediction of the power ratio in the wind turbine Savonius turbine using artificial neural networks, *International Journal of Energy and Environment*, Vol. 2, No. 1, pp. 51–56.

Sargolzaei J, and **Kianifar A**, (2010), Neuro-fuzzy modeling tools for estimation of torque in Savonius turbine in wind turbine, *Advances in Engineering Software*, Vol. 41, No. 4, pp. 619–626.

Savonius SJ, (1929), *Rotor adapted to be driven by wind or flowing water*, US Patent No. 1,697,574.

Savonius SJ, (1930), *Wind rotor*, US Patent No. 1,766,765.

Schreck SJ, **Sorensen NN**, and **Robinson MC**, (2007), Aerodynamic structures and processes in rotationally augmented flow fields, *Wind Energy*, Vol. 10, No. 2, pp. 159–178.

Sivasegaram S, and **Sivapalan S**, (1983), Augmentation of power in slow-running vertical-axis wind rotors using multiple vanes, *Wind Engineering*, Vol. 7, No. 1, pp. 12–19.

Shaughnessy BM, and **Probert SD**, (1992), Partially-blocked Savonius rotor, *Applied Energy*, Vol. 43, No. 4, pp. 239–249.

Shepherd W, and **Zhang L**, (2011), *Electricity generation using wind power*, World Scientific Publishing Co. Pte. Ltd., Singapore.

Shih TH, **Liou WW**, **Shabbir A**, **Yang Z**, and **Zhu J** (1995), A new eddy-viscosity model for high Reynolds number turbulent flows-Model development and validation, *Computer and Fluids*. Vol. 24, No. 3, pp. 227–238.

Shikha, **Bhatti TS**, and **Kothari DP**, (2003), Wind energy conversion systems as a distributed source of generation, *ASCE Journal of Energy Engineering*, Vol. 129, No. 3, pp. 69–80.

Theodorsen T, (1996), *Interference on an airfoil of finite span in an open rectangular wind tunnel*, Report No. 461, Langley Memorial Aeronautical Laboratory, NASA, USA.

Thotla S, (2006), *Optimum design configuration of Savonius rotor through wind tunnel testing*, M. Tech. Thesis, Department of Mechanical Engineering, IIT Guwahati, India.

Ushiyama I, and **Nagai H**, (1988), Optimum design configurations and performance of Savonius rotors, *Wind Engineering*, Vol. 12, No. 1, pp. 59–75.

Van Dusen ES, and **Kirchhoff RH** (1978), A two dimensional vortex sheet model of a Savonius rotor, *Proceedings of the ASME Winter Annual Meeting*, December 10–15, San Francisco, CA, USA.

Wilcox DC, (1998), Turbulence modeling for CFD. DCW Industries, Inc, La Canada, California.

Wilson RE, **Lissaman PBS**, and **Walker SN**, (1976), *Aerodynamic performance of wind turbines*, ERDA/NSF/04014-7611, pp. 111–164.

Yaakob OB, **Tawi KB**, and **Sunanto DTS**, (2010), Computer simulation studies on the effect overlap ratio for Savonius type vertical axis marine current turbine, *International Journal of Engineering Transactions A: Basics*, Vol. 23, No. 1, pp. 79–88.

Yonghai H, **Zhengmin T**, and **Shanshan W**, (2009), A new type of VAWT and blade optimization, *Proceedings of the IEEE international conference on technology and innovation*, October 12–14, Xian, China.

Zhao Z, **Zheng Y**, **Xu X**, **Liu W**, and **Hu G**, (2009), Research on the improvement of the performance of Savonius rotor based on numerical study, *Proceedings of the IEEE International Conference of Sustainable Power Generation and Supply*, April 6–7, Nanjing, China.

Appendix–A

Turbulence Models

Turbulent flows are characterized by fluctuating velocity fields. These fluctuations mix transported quantities such as momentum, energy and species concentrations, and cause the transported quantities to fluctuate as well. Since these fluctuations can be of small scale and high frequency, they are too computationally expensive to simulate directly in practical engineering calculations. Instead, the instantaneous (exact) governing equations can be time-averaged, ensemble-averaged, or otherwise manipulated to remove the resolution of small scale, resulting in a modified set of equations that are computationally less expensive to solve. However, the modified equations contain additional unknown variables, and turbulence model are need to determine these variables in terms of known quantities (ANSYS Inc, 2009).

In the present study the following turbulence models are applied to solve the flow governing equations:

A. Standard k-ϵ model

B. Realizable k-ϵ model

C. Standard k-ω model

D. Shear-stress transport (SST) k-ω model

A. Standard k-ϵ model:

It is the simplest of two-equation turbulence model in which the solution of two separate transport equations allows the turbulent velocity and length scales to be independently determined. The standard k-ϵ model has become the workhorse of practical engineering flow calculations since it was proposed by Launder and Spalding (1974). Robustness, economy, and reasonable accuracy for a wide range of turbulent flows explain its popularity in industrial flow and heat transfer simulations. It is a semi-empirical model, and the derivation of the model equations relies on phenomenological considerations and empiricism.

The standard *k*-ϵ model (Launder and Spalding, 1974) is a semi-empirical model based on model transport equations for the turbulence kinetic energy (*k*) and its dissipation rate (ϵ). The model transport equation for *k* is derived from the exact equation, while the model transport equation for ϵ is obtained using the physical reasoning and bears little resemblance to its mathematically exact counterpart.

In the derivation of the *k*- ϵ model, the assumption is that the flow is fully turbulent, and the effects of molecular viscosity are negligible. The standard *k*- ϵ model is therefore valid only for fully turbulent flows.

Transport equations for the standard *k*-ϵ model

The turbulence kinetic energy, *k*, and its rate of dissipation, ϵ, are obtained from the following transport equations:

$$\frac{\partial}{\partial t}(\rho k)+\frac{\partial}{\partial x_i}(\rho k u_i)=\frac{\partial}{\partial x_j}\left[\left(\mu+\frac{\mu_t}{\sigma_k}\right)\frac{\partial k}{\partial x_j}\right]+G_k+G_b-\rho\varepsilon-Y_M+S_k \qquad \text{(A.1)}$$

and

$$\frac{\partial}{\partial t}(\rho \varepsilon)+\frac{\partial}{\partial x_i}(\rho \varepsilon u_i)=\frac{\partial}{\partial x_j}\left[\left(\mu+\frac{\mu_t}{\sigma_\varepsilon}\right)\frac{\partial \varepsilon}{\partial x_j}\right]+C_{1\varepsilon}\frac{\varepsilon}{k}(G_k+C_{3\varepsilon}G_b)-C_{2\varepsilon}\rho\frac{\varepsilon^2}{k}+S_\varepsilon \qquad \text{(A.2)}$$

In Eqns. A.1 and A.2, G_k represents the generation of turbulence kinetic energy due to the mean velocity gradients, G_b represents the generation of turbulence kinetic energy due to buoyancy, Y_M represents the contribution of the fluctuating dilatation in compressible turbulence to the overall dissipation rate, $C_{1\varepsilon}$, $C_{2\varepsilon}$, and $C_{3\varepsilon}$ are constants. σ_k and σ_ε are the turbulent Prandtl numbers for *k* and ϵ, respectively. S_k and S_ε are user-defined source terms.

The turbulent (or eddy) viscosity, μ_t, is computed by combining for *k* and ϵ as follows:

$$\mu_t=\rho C_\mu\frac{k^2}{\varepsilon} \qquad \text{(A.3)}$$

where, C_μ is a constant.

The model constants: $C_{1\varepsilon} = 1.44$, $C_{2\varepsilon} = 1.92$, $C_{\mu} = 0.09$, $\sigma_k = 1.0$, $\sigma_{\varepsilon} = 1.3$

$$G_k = -\rho\overline{u_i' u_j'}\frac{\partial u_j}{\partial x_i} \tag{A.4}$$

$$C_{3\varepsilon} = \tanh\left|\frac{v}{u}\right| \tag{A.5}$$

where, v is the component of the flow velocity parallel to the gravitational vector and u is the component of the flow velocity perpendicular to the gravitational vector.

$$Y_M = 2\rho\varepsilon M_t^{\,2} \tag{A.6}$$

where, M_t is the turbulent Mach number, defined as:

$$M_t = \sqrt{\frac{k}{a^2}} = \sqrt{\frac{k}{\nu RT}} \tag{A.7}$$

B. Realizable *k*-ϵ model

The realizable *k*-ϵ model (1995) differs from the standard *k* -ϵ model in the following two ways:

- The realizable *k*-ϵ model contains a new formulation for the turbulent viscosity.
- A new transport equation for the dissipation rate, ϵ, has been derived from an exact equation for the transport of the mean-square vorticity fluctuation.

The term "realizable" means that the model satisfies certain mathematical constraints on the Reynolds stresses, consistent with the physics of turbulent flows. An immediate benefit of the realizable *k*-ϵ model is that it more accurately predicts the spreading rate of both planar and round jets. It is also likely to provide superior performance for flows involving rotation, boundary layers under strong adverse pressure gradients, separation, and recirculation.

The realizable *k*-ϵ model proposed by Shish *et al*. (1995) was intended to address these deficiencies of traditional *k*-ϵ models. One limitation of this model is that it produces non-physical turbulent viscosities in situations when the computational domain contains both

rotating and stationary fluid zones. This is due to the fact that the realizable *k-ϵ* model includes the effect of mean rotation in the definition of the turbulent viscosity.

Transport equations for the realizable *k-ϵ* model

The modeled transport equations for *k* and *ϵ* in the realizable *k-ϵ* model are:

$$\frac{\partial}{\partial t}(\rho k)+\frac{\partial}{\partial x_{\backslash j}}(\rho k u_j)=\frac{\partial}{\partial x_j}\left[\left(\mu+\frac{\mu_t}{\sigma_k}\right)\frac{\partial k}{\partial x_j}\right]+G_k+G_b-\rho\varepsilon-Y_M+S_k \tag{A.8}$$

and

$$\frac{\partial}{\partial t}(\rho\varepsilon)+\frac{\partial}{\partial x_j}(\rho\varepsilon u_j)=\frac{\partial}{\partial x_j}\left[\left(\mu+\frac{\mu_t}{\sigma_\varepsilon}\right)\frac{\partial \varepsilon}{\partial x_j}\right]+\rho C_1 S\varepsilon-\rho C_2\frac{\varepsilon^2}{k+\sqrt{\nu\varepsilon}}+C_{1\varepsilon}\frac{\varepsilon}{k}C_{3\varepsilon}G_b+S_\varepsilon \tag{A.9}$$

where, $C_1=\max\left[0.43,\frac{\eta}{\eta+5}\right]$, $\eta=S\frac{k}{\varepsilon}$, $S=\sqrt{2S_{ij}S_{ij}}$

The difference between the realizable *k-ϵ* model and standard *k-ϵ* model is that C_μ is no longer constant. It is computed from

$$C_\mu=\frac{1}{A_0+A_s\frac{kU^*}{\varepsilon}} \tag{A.10}$$

$$U^*=\sqrt{S_{ij}S_{ij}+\tilde{\Omega}_{ij}\tilde{\Omega}_{ij}} \tag{A.11}$$

$$\tilde{\Omega}_{ij}=\Omega_{ij}-2\varepsilon_{ijk}\omega_k \tag{A.12}$$

$$\Omega_{ij}=\bar{\Omega}_{ij}-\varepsilon_{ijk}\omega_k \tag{A.13}$$

where, $\bar{\Omega}_{ij}$ is the mean rate of rotation tensor in a rotating frame with the angular velocity ω_k.

The model constants, $A_0=4.04$, $A_s=\sqrt{6}\cos\phi$

$$\phi = \frac{1}{3}cos^{-1}\left(\sqrt{6}\frac{S_{ij}S_{jk}S_{ki}}{\tilde{S}^3}\right),\ \tilde{S} = \sqrt{S_{ij}S_{ij}}\ ,\ S_{ij} = \frac{1}{2}\left(\frac{\partial u_j}{\partial x_i} + \frac{\partial u_i}{\partial x_j}\right)$$

C. Standard *k-ω* model

The standard *k-ω* model is based on Wilcox *k-ω* model (Wilcox, 1998), which incorporates modifications for low Reynolds number effects, compressibility, and shear flow spreading. The Wilcox model predicts free shear flow spreading rates that are in close agreement with measurements for far wakes, mixing layers, and plane, round and radial jets, is thus applicable to wall-bounded flows and free share flows.

This model is an empirical model based on transport equations for the turbulence kinetic energy (*k*) and the specific dissipation rate (*ω*), which can also be thought of as the ratio of ϵ to *k*.

Transport equations for the standard *k-ω* model

The turbulence kinetic energy, *k*, and the specific dissipation rate, *ω*, are obtained from the following transport equations:

$$\frac{\partial}{\partial t}(\rho k) + \frac{\partial}{\partial x_i}(\rho k u_i) = \frac{\partial}{\partial x_j}\left(\Gamma_k \frac{\partial k}{\partial x_j}\right) + G_k - Y_k + S_k \qquad \text{(A.14)}$$

and

$$\frac{\partial}{\partial t}(\rho \omega) + \frac{\partial}{\partial x_i}(\rho \omega u_i) = \frac{\partial}{\partial x_j}\left(\Gamma_\omega \frac{\partial \omega}{\partial x_j}\right) + G_\omega - Y_\omega + S_\omega \qquad \text{(A.15)}$$

In the above equations, G_k represents the generation of turbulence kinetic energy due to mean velocity gradients, G_ω represents the generation of *ω*, Γ_k and Γ_ω represent the effective diffusivity of *k* and *ω*, respectively. Y_k and Y_ω represent the dissipation of *k* and *ω*, respectively. S_k and S_ω represent the user defined functions for *k* and *ω*, respectively.

The effective diffusivities for the *k-ω* model are given by

$$\Gamma_k = \mu + \frac{\mu_t}{\sigma_k} \qquad \text{(A.16)}$$

and

$$\Gamma_{\omega} = \mu + \frac{\mu_t}{\sigma_{\omega}} \tag{A.17}$$

where, σ_k and σ_{ω} are the turbulent Prandtl numbers for k and ω, respectively. The turbulent viscosity, μ_t is computed by combining k and ω as follows:

$$\mu_t = \alpha^* \frac{\rho k}{\omega} \tag{A.18}$$

and

$$\alpha^* = \alpha^*_{\infty}\left(\frac{\alpha^*_0 + \mathrm{Re}_t/R_k}{1+\mathrm{Re}_t/R_k}\right) \tag{A.19}$$

where, $\mathrm{Re}_t = \frac{\rho k}{\mu\omega}$, $R_k = 6$, $\alpha^*_0 = \frac{\beta_i}{3} = \frac{0.072}{3}$, $\sigma_k = \sigma_{\omega} = 2$

D. Shear-stress transport (SST) *k-ω* model

The shear stress transport (SST) *k-ω* model was developed by Menter (1994) to effectively blend the robust and accurate formulation of the *k-ω* model in the near wall region with free-stream independence of the *k-ϵ* model in the far field. To achieve this, the *k-ϵ* model is converted into a *k-ω* formulation. The SST *k-ω* model is similar to standard *k-ω* model, however includes the following refinements:

- The standard *k-ω* model and transformed *k-ϵ* model are both multiplied by a blending function and both are added together. The blending function is designed to be one in the near wall region, which activates the standard *k-ω* model, and zero away from the surface, which activates the transformed *k-ϵ* model.
- The SST *k-ω* model incorporates a damped cross diffusion derivative term in the ω equation.
- The definition of the turbulent viscosity is modified to account for the transport of the turbulent shear stress.
- The modeling constants are different.

These features make the SST *k*-*ω* model more accurate and reliable for a wider class of flows (e.g., adverse pressure gradients, flow over airfoils, shock waves, rotating flows etc.) than the standard *k*-*ω* model.

Transport equations for the standard *k*-*ω* model

The SST *k*-*ω* model has a similar form to the standard *k*-*ω* model turbulence kinetic energy, *k*, and the specific dissipation rate, *ω*, are obtained from the following transport equations:

$$\frac{\partial}{\partial t}(\rho k)+\frac{\partial}{\partial x_i}(\rho k u_i)=\frac{\partial}{\partial x_j}\left(\Gamma_k \frac{\partial k}{\partial x_j}\right)+\tilde{G}_k-Y_k+S_k \tag{A.20}$$

and

$$\frac{\partial}{\partial t}(\rho \omega)+\frac{\partial}{\partial x_i}(\rho \omega u_i)=\frac{\partial}{\partial x_j}\left(\Gamma_\omega \frac{\partial \omega}{\partial x_j}\right)+G_\omega-Y_\omega+D_\omega+S_\omega \tag{A.21}$$

where, D_ω represents the cross-diffusion term.

The equations for Γ_k and Γ_ω are same as used in the standard *k*-*ω* model (Eqns. A.16 and A.17).

However, the turbulent viscosity, μ_t, the turbulent Prandtl numbers, σ_k and σ_ω are computed as follows:

$$\mu_t=\frac{\rho k}{\omega}\frac{1}{\max\left[\frac{1}{\alpha^*},\frac{SF_2}{\alpha_1 \omega}\right]} \tag{A.22}$$

Where, *S* is the strain rate magnitude and

$$\sigma_k=\frac{1}{(F_1/\sigma_{k,1})+((1-F_1)/\sigma_{k,2})} \tag{A.23}$$

$$\sigma_\omega=\frac{1}{(F_1/\sigma_{\omega,1})+((1-F_1)/\sigma_{\omega,2})} \tag{A.24}$$

The blending functions, F_1 and F_1 are given by:

$$F_1 = \tanh\left(\Phi_1^4\right) \tag{A.25}$$

$$\Phi_1 = \min\left[\max\left(\frac{\sqrt{k}}{0.09\omega y}, \frac{500\mu}{\rho y^2 \omega}\right), \frac{4\rho k}{\sigma_{\omega,2} D_\omega^+ y^2}\right] \tag{A.26}$$

$$D_\omega^+ = \max\left[2\rho \frac{1}{\sigma_{\omega,2}} \frac{1}{\omega} \frac{\partial k}{\partial x_j} \frac{\partial \omega}{\partial x_j}, 10^{-10}\right] \tag{A.27}$$

$$F_2 = \tanh\left(\Phi_2^2\right) \tag{A.28}$$

$$\Phi_2 = \max\left[2\frac{\sqrt{k}}{0.09\omega y}, \frac{500\mu}{\rho y^2 \omega}\right] \tag{A.29}$$

where, y is the distance to the next surface,

$\alpha_1 = 0.31$, $\sigma_{k,1} = 1.176$, $\sigma_{k,2} = 1$, $\sigma_{\omega,1} = 2$, $\sigma_{\omega,2} = 1.168$,

$$Y_k = \rho \beta_i \omega^2 \tag{A.30}$$

Instead of having a constant value of β_i, in this model it is given by:

$$\beta_i = F_1 \beta_{i,1} + (1 - F_1)\beta_{i,2} \tag{A.31}$$

where, $\beta_{i,1} = 0.075$, $\beta_{i,2} = 0.0828$

The cross-diffusion term D_ω is given by:

$$D_\omega = 2(1 - F_1)\rho \sigma_{\omega,2} \frac{1}{\omega} \frac{\partial k}{\partial x_j} \frac{\partial \omega}{\partial x_j} \tag{A.32}$$

List of Publications

Book Chapter

1. **Roy S**, and **Saha UK**, (2014), Design of Savonius-Style Wind Turbines, in *Small-Scale Wind Power – Design, Analysis, and Economic Impacts*, Chapter-4, pp. 65–91, Momentum Press, New York, USA, Print ISBN: 9781606504840.

Journals

2. **Roy S**, and **Saha UK**, (2015), Wind tunnel experiments of a newly developed two-bladed Savonius-style wind turbine. *Applied Energy*, Vol. 137, pp. 117–125.
3. **Roy S**, and **Saha UK**, (2014), An adapted blockage factor correlation approach in wind tunnel experiments of a Savonius-style wind turbine. *Energy Conversion and Management*, Vol. 86, pp. 418–427.
4. **Roy S**, and **Saha UK**, (2013), Review of experimental investigations into the design, performance and optimization of the Savonius rotor. *Proc. IMechE Part -A: Journal of Power and Energy*, Vol. 227, pp. 528–542.
5. **Roy S**, and **Saha UK**, (2013), Computational study to assess the influence of overlap ratio on static torque characteristics of a vertical axis wind turbine, *Procedia Engineering*, Vol. 51, pp. 694–702.
6. **Roy S**, and **Saha UK**, (2013), Review on the numerical investigations into the design and development of Savonius wind rotors. *Renewable and Sustainable Energy Reviews*, Vol. 24, pp. 73–83.

Conferences

7. **Roy S**, **Saha UK**, and **Mukherjee P**, (2014), Aerodynamic performance evaluation of a novel Savonius-style wind turbine under an oriented jet. *ASME 2014 Gas Turbine India Conference*, December 15–17, New Delhi, India.
8. **Roy S**, and **Saha UK**, (2014), Performance analysis of Savonius-style wind turbines under concentrated and oriented jets. *ASME Turbo Expo 2014*, June 16–20, Dusseldorf, Germany.
9. **Roy S**, and **Saha UK**, (2013), Investigations on the effect of aspect ratios into the performance of Savonius rotors. *ASME 2013 Gas Turbine India Conference*, December 5–6, Bangalore, India.
10. **Roy S**, and **Saha UK**, (2013), Numerical investigation to assess an optimal blade profile for the drag based vertical axis wind turbine. *ASME 2013 International Mechanical Engineering Congress & Exposition*, November 15–21, San Diego, USA.
11. **Roy S**, and **Saha UK**, (2012), Comparative analysis of turbulence models for flow simulation around a vertical axis wind turbine. *Indo-Danish International Conference on Wind Energy: Materials, Engineering, and Policies* (*WEMEP 2012*), November 22–23, Hyderabad, India.